

Evaluating Past Climate Variability and Modelling Its Impact on Tree Growth

by

Guangqi Li

M.Sc.

Biosphere and Climate Dynamics Group

Department of Biological Sciences

Macquarie University

July, 2015

Supervised by

Professor Sandy P. Harrison

This thesis is presented for the degree of Doctor of Philosophy

Table of Contents

ABSTRACT	i
Statement of Candidate	vi
ACKNOWLEDGEMENTS	vii
List of Publications	ix
Chapter 1 Introduction	1
1.1 Climate Models and Model Evaluation	3
1.2 The Palaeoclimate Modelling Intercomparison Project (PMIP)	6
1.3 Climate reconstruction: pollen records	11
1.4 Climate reconstruction from tree rings: the standard approach	13
1.5 Climate controls on tree growth	16
1.6 Modelling tree growth	19
1.7 Philosophy and Approach of this Thesis	22
1.8 References	27
Chapter 2: Precipitation scaling with temperature in warm and cold climates: An analysis of CMIP5 simulations	49
2.1 Introduction	50
2.2 Methods	51
2.3 Results: Simulated Changes	52
2.4 Results: Comparison With Observations	54
2.5 Discussion and Conclusions	55
2.6 References	55
Chapter 3: Evaluation of modern and mid-Holocene seasonal precipitation of the Mediterranean and northern Africa in the CMIP5 simulations	57
3.1 Introduction	58
3.2 Methods	60
3.2.1 Data sources: CMIP5 simulations	60
3.2.2 Data sources: modern and mid-Holocene climate data	60
3.2.3 Definition of climate regions	60
3.2.4 Analyses of the model simulations	61
3.3 Results	62

3.3.1 Modern observed climate	62
3.3.2 piControl simulations	62
3.3.3 Mid-Holocene simulation	65
3.3.4 Comparison of midHolocene simulations and mid-Holocene observations	65
3.3.5 Comparison between bias and anomaly	66
3.4 Discussion	68
3.5 Conclusions	71
3.6 References	71
3.7 Supplementary Information	76
Chapter 4: Evaluation of CMIP5 palaeosimulations to improve climate projections	79
4.1 Introduction	80
4.2 Robust features of past and future climates	81
4.3 Ability to simulate regional climate features	81
4.4 Multi-parameter evaluation of model skill	84
4.5 Improved ability to simulate climate change	84
4.6 Providing well-founded climate sensitivity constraints	85
4.7 Palaeosimulations and future projections	85
4.8 References	87
4.9 Supplementary Information	89
Chapter 5: Simulation of tree-ring widths with a model for primary production, carbon allocation, and growth	91
5.1 Introduction	92
5.2 Methods	93
5.2.1 Model structure and derivation	93
5.2.2 Model application	93
5.2.3 Model application	96
5.2.4 Statistical methods	97
5.3 Results	98
5.3.1 Simulated ring width versus observation	98
5.3.2 Parameter sensitivity analysis	98
5.3.3 Controls on tree growth	99
5.3.4 Simulated CO ₂ effect on tree growth	101
5.4 Discussion	101

5.5 References	102
Chapter 6: A model analysis of climate and CO₂ controls on tree growth in a semi-arid woodland	106
6.1 Introduction	108
6.2 Methods	110
6.2.1 The study area	110
6.2.2 Tree ring data	110
6.2.3 The tree growth model	111
6.2.4 Derivation of model parameter values	113
6.2.5 Climate inputs	114
6.2.6 Definition of the effective growing season.....	115
6.2.7 Application of the model	116
6.3 Results	117
6.3.1 Simulated ring width vs. observations	117
6.3.2 Simulations with varying [CO ₂]	118
6.4 Discussion and conclusions.....	119
6.5 References	121
Chapter 7: Allocation changes buffer CO₂ effect on tree growth since the last ice age	148
7.1 Introduction	150
7.2 Results	151
7.3 Discussion	154
7.4 Methods	155
7.4.1 The PT model.....	155
7.4.2 Climate and CO ₂ input: modern	158
7.4.3 Climate and CO ₂ input: LGM.....	158
7.4.4 Simulations.....	158
7.5 References	159
7.6 Supplementary Information.....	169
Conclusions and Directions for Future Work.....	171
References	172

List of Figures

- Figure 1-1 Pollen-based reconstructions of palaeo-climate. The plots show (a) mean annual temperature (MAT) and (b) mean annual precipitation (MAP) at the Last Glacial Maximum (LGM) and (c) mean temperature of the warmest month (MTWA) and (d) MAP for the mid-Holocene (MH). The data is from Bartlein et al., 2011. 14
- Figure 1-2 Sites from providing tree ring-width records for the historic period (post 1500 CE). The data are from the International Tree Ring Data Bank (ITRDB). 14
- Figure 1-3 Linkage between the thesis chapters, illustrating the philosophy and approach used. 24
- Figure 2-1 Theoretical limits on the rate of increase of precipitation with temperature, according to alternative hypotheses: (a) following the temperature dependence of the saturated vapor pressure of water, according to the Clausius-Clapeyron relationship (dotted line, CC); (b) following the temperature dependence of the fraction of net radiation that can be used for evaporation under equilibrium conditions (solid line, EF). The global ensemble mean temperature for each of the experiments is shown in order to place the simulated changes in context. 514
- Figure 2-2 The change in precipitation (%) as a function of the change in global temperature ($^{\circ}\text{C}$) as simulated by each of the six CMIP5 models (IPSL-CM5A-LR, MPI-ESM-P, MIROC-ESM, CCSM4, MRI-CGCM3, and GISS-E2-R) at the Last Glacial Maximum (LGM), from the historical run (average for period 1979–2005 CE), the 1% CO_2 run (1pct CO_2 , average for model years 86–115), and the 4x CO_2 run. The left-hand plot shows the global relationship, while the right-hand plots shows the change in global precipitation (%) over (red) land and (blue) ocean as a function of the change in global land and ocean temperature ($^{\circ}\text{C}$). 14
- Figure 2-3 Simulated changes in precipitation (%) in the wettest and driest areas of the tropical (30°N – 30°S) and extratropical ($>30^{\circ}\text{N}$ and $>30^{\circ}\text{S}$) land and ocean. The wettest and driest areas are defined separately for each individual model as those grid cells that fall in the top and bottom deciles of precipitation in the control simulation (piControl). Simulated changes in tropical precipitation (%)

during the wettest month (MPWE) and the driest month (MPDR) are shown in the bottom panels for comparison.....	53
Figure 2-4 Comparison between climate reconstructions and model simulations over the land. The comparison is based on the model grid cells where observations of both temperature and precipitation are available. The bars show the standard deviation of the spatial values for both observations and model simulations. The historical observations are differences between the 1979–2005 and 1941–1970 long-term means from the GHCN precipitation data set [Peterson and Vose, 1997] and the HadCRUT4 temperature data set [Morice et al., 2012]. The paleoclimate reconstructions are from Harrison et al. (submitted manuscript, 2013).....	54
Figure 3-1 Observed seasonal cycle of precipitation in each of the de- fined climate zones, using the CRU T3.1 data set (Harris et al., 2014). The mean precipitation each month (mm) is shown by the black line, with the standard deviation shown by the bars. The grey shading shows the maximum and minimum rainfall experienced within the observation period (1961–1990). Note that the scale for the desert region differs from that used for the other regions. Months are numbered consecutively from January (1) through to December (12).....	62
Figure 3-2 Observed and simulated modern and palaeoprecipitation patterns. The total summer and winter precipitation from the CRU T3.1 data set (Harris et al., 2014) are compared to ensemble averages of the piControl outputs of the 12 CMIP5 models. The simulated change in precipitation between the mid-Holocene and piControl simulations (midHolocene-piControl) is shown based on the ensemble average of the midHolocene outputs of the 12 CMIP5 models. The observed anomalies in mean annual precipitation (MAP) between the mid-Holocene and the present day are average values for $2^{\circ} \times 2^{\circ}$ grids from the Bartlein et al. (2011) data set.....	63
Figure 3-3 The location of the four precipitation zones in the CMIP5 I piControl simulations compared to the limits defined using the CRU TS3.1 data set (Harris et al., 2014). The precipitation regime was characterized using zonally averaged long-term means for 5° location of the four precipitation zones in the CMIP5 midHolocene simulations compared to the limits defined using the CRU TS3.1 data set (Harris et al., 2014). The precipitation regime was characterized	

- using zonally averaged long-term means for 5° latitude bands. The latitude bands. 63
- Figure 3-4 Comparison of simulated and observed mean annual and mean seasonal precipitation (mm) for each of the defined precipitation regimes (Mediterranean, desert, monsoon, double peak). The simulated precipitation (mean and standard deviation) is shown for both the climate zone as defined by the observations (solid line) and as defined in the piControl simulation itself (dotted line). The difference between these two lines for each model provides a measure of the degree to which incorrect placement of a given climate affects the zonal means. The grey bars represent one standard deviation of the mean annual and mean seasonal precipitation from observations. The seasons are defined as spring, summer, autumn and winter (as in Sect. 3.1)..... 64
- Figure 3-5 Simulated changes in total and seasonal precipitation in the midHolocene compared to the piControl for each of the four precipitation regimes (Mediterranean, desert, monsoon, double peak) for the region that is common between the two sets of simulations. The standard deviation of precipitation in the piControl control simulation of each model is shown (grey bars) to provide a visual measure of the significance of the simulated change in precipitation. The seasons are defined as spring, summer, autumn and winter (as in Sect. 3.1). 66
- Figure 3-6 Comparison of simulated and reconstructed changes in mean annual precipitation in the mid-Holocene for 5° latitude bands between 0 and 45° N. The reconstructions are from the Bartlein et al. (2011) data set. The mean, 25–75 % range and full range of the reconstructions are shown (for those latitude bands with sufficient data points). The model results are averages for the grid cells with observations. 67
- Figure 3-7 Relationship between biases in the piControl simulation of mean annual precipitation (mm) and mid-Holocene precipitation anomalies (midHolocene–piControl) as simulated by each of the CMIP5 models for each of the precipitation regimes (Double Peak, Monsoon, Desert, Mediterranean). The upper panels show biases and anomalies calculated for specific latitudinal bands as defined from the modern observed spatial extent of each regime (geographic region). The lower panels show biases and anomalies calculated for the region identified as characterized by a given regime in each model and simulation (model specific region). The regressions are calculated for all models

- (All: black), for the coupled ocean–atmosphere models (OA: blue) and for the carbon-cycle models (OAC: red)..... 68
- Figure 3-8 Comparison of simulated and observed summer and winter precipitation in each of the four precipitation regimes (Mediterranean, Desert, Monsoon, Double Peak). The observations (black) are the average for the period 1961–1990 from the CRU T3.1 data set (Harris et al., 2014). The simulated mean and standard deviation of precipitation from the CMIP5 models (blue) is based on the last 100 yr of the piControl. These simulations can be compared with results from coupled ocean–atmosphere simulations made during the second phase of the PMIP2 (Braconnot et al., 2012; shown in red). The PMIP2 results are the mean and standard deviation based on the last 100 yr of a piControl, except in three cases where only 50 yr of data were available. Model results are calculated for each precipitation regime based on the observed geographic extent characterized by these regimes, as defined using the CRU TS3.1 data set. Summer and winter as defined in Sect. 3.1. 69
- Figure 3-S1 Comparison of the mean annual and mean seasonal precipitation (mm) between the CRU data and historical simulations for each 5 latitude band. Because there is a very small amount of precipitation in some latitude band, the axis scale starts at 0 but differs in the maximum value depending on the total rainfall values. Only six models have historical simulations. For these models we also present the piControl simulations. The historical simulations are shown in color while the piControl simulations for each model are shown by a dashed line. The grey bars represent one standard deviation of the mean annual and mean seasonal precipitation from observations. The seasons are defined as spring (March, April, May), summer (June, July, August), autumn (September, October, November) and winter (December, January, February)..... 78
- Figure 4-1 Scatter plots showing temperature and precipitation changes in past, present and projected climates. The values shown are the simulated long-term mean differences (experiment minus piControl) for the seven models that have carried out all the experiments. a, Differences in the relative warming (or cooling) over global land and global ocean (land–ocean contrast) and b, over land in the northern extratropics and northern tropics (latitudinal amplification). SSTann: annual sea surface temperature. c, Comparisons of the simulated changes in land–ocean contrast and d, latitudinal amplification for the twentieth-century (historical) and LGM with observed changes. The reduced major axis

regression lines derived using all appropriate model grid cells are shown in magenta; the p-values test the null hypothesis that the slopes of the reduced major axis regression lines = 1.0. e, Percentage precipitation change relative to the change in global temperature and f, global temperature over land (green) and ocean (blue). The ordinary least-square regression with the intercept set at zero is shown in magenta; the p-values test the null hypothesis that the slope = 0. g, Comparisons of the simulated changes in precipitation scaling over land for the twentieth-century (historical) and LGM with observed changes. The ordinary least-square regression for absolute values of precipitation based on all model simulations is shown in magenta. In c, d and g, model output has been sampled only at the locations of respective observations. Bold crosses: area-weighted averages of twentieth-century observations and palaeoclimate reconstructions; finer lines: reconstruction uncertainties (standard deviation). 82

Figure 4-2 a, Comparison of simulated and reconstructed mid-Holocene changes in mean annual precipitation for 5° latitude bands (longitude 20° W to 40° E) between 0 and 45° N across northern Africa and the circum-Mediterranean region. b, Ratio of actual to equilibrium evapotranspiration and c, mean temperature of the warmest month for 5° latitude bands between 30 and 80° N across Eurasia (longitude 60° to 180° E). The reconstructions are from the data set in ref. 9, which provides a climate reconstruction for a 2 × 2° grid cell based on averaging the individual site-based reconstructions within that grid cell. The mean and standard error of the mean of the grid cell reconstructions are shown in each latitude band. The model results are averages of model output sampled at the location of the grid cells with observations. The number of grid cells contributing to the comparison for each variable is shown on the plots..... 83

Figure 4-3 Taylor diagram for the LGM and mid-Holocene precipitation and temperature anomalies. The distance of any model point from the origin indicates standard deviation of field, the distance of any model point from the green reference point indicates the centred root mean square (RMS) difference between model and data. Pattern correlation between model and observations is given by the azimuthal coordinate. Temperature is represented by MAT over land and SSTann at the LGM, and by MTWA for the mid-Holocene where the change in forcing is seasonal. Precipitation is always represented by MAP. Model statistics are corrected to account for observational uncertainties, by subtracting the estimated contributions made by observational errors as in ref.

62. Models from the CMIP5 ensemble are in red (temperature) and blue (precipitation), whereas models from the PMIP2 ensemble are in pink and pale blue, respectively.	85
Figure 4-4 Maps of the p-values of Hotelling's T2 test comparing the CMIP3 plus PMIP2 versus CMIP5 ensembles. The plots show the p-values for the test of the hypothesis of equality of the (multivariate) ensemble means of MAT, mean temperature of the coldest month, MTWA and MAP for the LGM (lgm), mid-Holocene (midHolocene) and the 1pctCO2 simulations in CMIP3 and CMIP5 (1pctto2x and 1pctCO2, respectively). The number of significant statistics (that is, $p < 0.05$, shown in pink) do not exceed that expected by chance. A previous study has shown that the results obtained using conventional meteorological variables are virtually identical.	86
Figure 5-1 Model application flow. We combined the simple light- use efficiency and photosynthesis model (P model) with a carbon allocation and functional geometric tree-growth model to simulate tree growth (e.g. ring width). The inputs to the P model are latitude, elevation, [CO2], monthly temperature, precipitation, and fractional cloud cover. Potential gross primary productivity (GPP) simulated by the P model drives the T model. The T model also requires a limited number of species-specific parameter values to be specified.	94
Figure 5-2 Estimation of parameter values for the application of the T model. Diameter at breast height (D), tree height (H), and crown area (Ac) of the 400 trees from the sample plots were used for the estimation of the initial slope of the height–diameter relationship (a) and (asymptotic) maximum tree height (Hm). Relationships among crown area (Ac), diameter at breast height (D), and height (H) (Eq. 7) are used to estimate the initial ratio of crown area to stem cross-sectional area (c).	97
Figure 5-3 Comparison between simulations and observations for the three age cohorts (young: 0–49 years; mature: 50–99 years; old > 100 years). Each tree was initialised at its actual diameter at 1958, calculated from the measured diameter in 2007, and measured radial growth between 1958 and 2007. The black line is the mean of observations within each age cohort, and grey bars are the standard deviation (SD) of individuals within each age cohort. The blue lines and bars are the mean and standard deviation from the simulations.	98

Figure 5-4 Parameter sensitivity analyses for the T model. A constant input of gross primary productivity (GPP) (mean during the period 1958–2006) was used to drive the T model to simulate tree growth for 500 years following establishment. The black line was obtained with the reference value of each parameter. The effects of an increase (150 % of reference value; blue line) and a decrease (50 % of reference value; red line) are also shown.....	99
Figure 5-5 Tree-growth response to climate and tree age: partial residual plots based on the GLM analysis (Table 5-2), obtained using the visreg package in R, are shown.....	100
Figure 6-1 An example of <i>Callitris collumellaris</i> sampled for tree-ring cores in the Great Western Woodlands, Western Australia.	136
Figure 6-2 Location of the Great Western Woodlands sampling site, Western Australia. The underlying map shows mean annual precipitation (MAP). We also show the location of other sites across Australia where <i>Callitris</i> have been sampled (data from International Tree-Ring Data Bank), and the locations of the nearest meteorological stations to the sampling site.	20
Figure 6-3 Interannual variability in tree-ring widths of <i>Callitris columellaris</i> from the Great Western Woodlands, Western Australia. In the top panel, the black line is the mean of the observations, and the grey bars show the standard deviation (SD) of the individual sampled trees. The blue line in the bottom panel shows the number of trees sampled for each interval.....	20
Figure 6-4 Prior (gray) and posterior (red) probability distribution function for fine-root turnover time (τ_r), fine-root specific respiration rate (r_r), sapwood-specific respiration rate (r_s); ratio of fine-root mass to foliage area (ζ).	20
Figure 6-5 Climate at the Great Western Woodlands site. The plot shows mean annual temperature, precipitation, total incident photosynthetically active radiation (PAR_0), and the ratio of actual to equilibrium evapotranspiration (α). The observed changes in $[CO_2]$ are shown for comparison.	20
Figure 6-6 Comparison between simulated and observed tree ring widths, for the period 1920 to the present, with $[CO_2]$ set at 360 ppm. The black line is the mean of the observations, and the grey bars are the standard deviation (SD) among the ten individual trees sampled. The blue line and bars are the mean and standard deviation for the ten simulated individual trees.	20

- Figure 6-7 Simulated and observed responses of tree growth to climate: partial residual plots based on the regression analysis, obtained using the visreg package in R, are shown. The predictor variables are (a) total incident photosynthetically active radiation (PAR_0), mean annual temperature (MAT), the ratio of actual to potential evapotranspiration (α) and vapour pressure deficit (VPD). 20
- Figure 6-8 Comparison of simulated ring width in simulations with fixed (blue line) and time-varying (red line) $[CO_2]$. The black line is the mean of the observed ring widths, and the grey bars are the standard deviation (SD) among the ten individual trees sampled. 21
- Figure 6-9 Simulated and observed response of tree radial growth to $[CO_2]$: partial residual plots based on the regression analysis, obtained using the visreg package in R, are shown. The dependent variable is mean ring width (from 1950 to 2012). The predictor variables are total incident photosynthetically active radiation (PAR_0), vapour pressure deficit (VPD), the ratio of actual to potential evapotranspiration (α), and monthly $[CO_2]$ 21
- Figure 6-10 Time variation of the values of parameters estimated by Bayesian optimization. The graph shows the percentage change to the mean value of fine-root turnover time (τ_r), fine-root specific respiration rate (r_r), sapwood specific respiration rate (r_s) and the ratio of fine-root mass to foliage area (ζ) for 30-year moving windows since 1920, using the appropriate $[CO_2]$ and α for each window. Values on the X-axis are plotted against the first year of each 30-year window. The uncertainty estimates (bars) for the ratio of fine-root mass to foliage area (ζ) are the standard deviation of six 5-year sub-windows within each 30-year window. 21
- Figure 6-11 Simulation of radial growth in response to changing climate and observed $[CO_2]$, allowing for the effect of changing allocation to fine roots. The black line is the mean of the observations, and the grey bars are the standard deviation (SD) among the ten individual trees sampled. The blue line and bars are the mean and standard deviation for the ten simulated individual trees. 21
- Figure 6-12 Simulated and observed response of tree radial growth to climate and $[CO_2]$ based on the simulations in which the ratio of fine-root mass to foliage area (ζ) is allowed to vary. Partial residual plots based on the regression analysis, obtained using the visreg package in R, are shown. The dependent

variable is mean ring width (from 1950 to 2012). The predictor variables are total incident photosynthetically active radiation (PAR_0), vapour pressure deficit (VPD), the ratio of actual to potential evapotranspiration (α), and monthly $[CO_2]$	21
Figure 7-1 Comparison between simulated and observed <i>Juniperus occidentalis</i> ring widths, for the period 1903 to 1987, from site CA640 (36.95°N, 118.92°W, 2630 m. a.s.l.). The black line is the mean of observations and the grey bars are the standard deviation (SD) between trees. The red line is the mean from the simulations.	22
Figure 7-2 Changes in c_i/c_a with elevation. The left panel show the simulated c_i/c_a at La Brea and the southern Californian sites under modern (red) and glacial (blue) conditions. The bar shows the two standard deviations for each site during the simulation period (50 years for modern, 100 years for glacial). Lower right panel shows the observed c_i/c_a from modern trees (all values for the period 1951-2000, red) and the 22 ka BP fossil sample from La Brea (blue). The red line shows the linear regression between observed modern c_i/c_a and elevation.....	22
Figure 7-3 Simulated impact of the separate effects of temperature and vapour pressure deficit (VPD) on c_i/c_a under glacial conditions.....	22
Figure 7-4 The impact of $[CO_2]$ on carbon allocation. The results show the impact of Bayesian tuning using glacial climate variables and different levels of $[CO_2]$ between 320 and 160 ppm. ζ is the ratio of fine-root mass to foliage area; L is leaf area index within the crown.....	22
Figure 7-5 Impact of individual climate variables on simulated glacial ring widths, where each experiment is run by imposing modern values for a variable or combination of variables and all other variables (including CO_2) are held at glacial values. The bars show the percentage change in simulated ring width between each experiment and the baseline glacial simulation. H has modern relative humidity; P has modern precipitation; T has modern temperature; TP has both modern temperature and precipitation; TPH has modern temperature, precipitation and relative humidity. In the final experiment (Full) all of the climate variables are modern and only CO_2 is set to glacial levels.	22
Figure 7-1s Simulated and observed response of tree radial growth to climate and $[CO_2]$: partial residual plots based on the regression analysis, obtained using	

the visreg package in R, are shown. The dependent variable is time series mean ring width of *Juniperus occidentalis* from site CA640 (36.95°N, 118.92°W, 2630 m a.s.l.) from 1903 to 1985. The predictor variables are total incident photosynthetically active radiation (PAR_0), mean annual temperature, vapour pressure deficit (VPD), the ratio of actual to potential evapotranspiration (α), and $[CO_2]$ during the growing season. 22

List of Tables

Table 3-1 Characteristics of the CMIP5 models used in these analyses.	61
Table 3-2 Summary of area-averaged climate anomalies (midHolocene minus piControl) for individual models for individual seasons and for mean annual precipitation. Bold font indicates values that are significantly different from the interannual variability of the modern observations. The seasons are spring, summer, autumn, and winter (as in Section 3.3.1).	67
Box 4-1 The relationship between the CMIP and the PMIP.	81
Table 4-S1 Description of past, present and future simulations.	89
Table 5-1 Parameter description and the derivation of parameter values.	96
Table 5-2 GLM analysis of tree-growth response to the climatic factors and age, based on simulations and observations. The dependent variable is mean ring width series (1958–2006) for each age cohort (young, mature, and old). The independent variables are the growing-season total annual photosynthetically active radiation (PAR_0), mean annual temperature (MAT), and the ratio of actual to potential evapotranspiration (α), with age cohort treated as a factor.	99
Table 6-1 Statistics for <i>Callitris columellaris</i> tree ring-width series sampled in the Great Western Woodlands, Western Australia	132
Table 6-2 Definition of T model parameters and derivation of parameter values. Most of the values were obtained from field measurements or are generic. For those values estimated using Bayesian calibration, we show the range of values given for <i>Callitris</i> (or related species) in the literature, the prior values used in the calibration, the posterior values and uncertainties, and the value used in the final model. The units are defined in the parameter column, except in the case of sapwood specific respiration where the measurements are in a different unit from the model parameter (and therefore specified explicitly).	133
Table 6-3 GLM analysis of relationship between ring width and climate parameters using different definitions of the effective growing season, based on the interval from 1950 to present. The dependent variable is mean ring width. The independent variables are the total annual photosynthetically active radiation	

(PAR), mean annual temperature (MAT), and the ratio of actual to potential evapotranspiration (α). The coefficients give the change in ring width (mm) per unit change in the climate parameter.....	134
Table 6-4 GLM analyses of simulated and observed response of tree growth to climate variables and CO ₂ . The dependent variable is mean ring width series (dates from 1950 and to 2012). The independent variables are annual photosynthetically active radiation (PAR), mean annual temperature (MAT), the ratio of actual to potential evapotranspiration (α), vapour pressure deficit (VPD) and monthly [CO ₂].....	135
Table 7-S1 Bayesian parameter optimisation for Juniperus in site CA640 (36.95°N, 118.92°W, 2630 m a.s.l.)	169

ABSTRACT

Past climates provide an opportunity to examine the response of the Earth System to large changes in external forcing. The changes in forcing over the last 21,000 years since the Last Glacial Maximum have been as large as those projected to occur over the 21st century as a result of anthropogenic changes in greenhouse gas concentrations and land-use changes. The fact that there have been equally large changes in forcing in the past as expected in the future, coupled with the availability of climate reconstructions of past climates, provides the motivation for using evaluations of simulations of past climates to evaluate how well the models that are used to project future climate changes perform.

Terrestrial vegetation is highly sensitive to changes in climate, and records of past vegetation changes are widely used to reconstruct past climate states. Statistical or model-inversion techniques have been used to reconstruct changes in seasonal temperature and water balance from pollen records from lakes and bogs. Most of these pollen records are at comparatively low resolution, and thus provide reconstructions of the long-term changes in mean climate state. Tree-ring series are the most abundant source of information used to reconstruct changes in short-term (interannual to decadal) climate variability. However, most of the available reconstructions focus on relationships with temperature and these relationships appear to break down in recent decades at many sites. An alternative approach is to use forward modelling to translate simulated climate variability into tree growth, which can then be directly compared to observations of tree-ring series.

In the first part of this thesis, I have used a global synthesis of pollen-based palaeoclimate reconstructions to evaluate how well state-of-the-art climate models from the fifth phase of the Coupled Model Intercomparison Project (CMIP5) capture large-scale (sub-continental to hemispheric) patterns of climate change. I initially examine the scaling of changes in precipitation with temperature at a hemispheric scale in warm and cold climate states (Chapter 2). I then examine how well models simulate large-scale changes in monsoon precipitation in response to changes in orbital forcing during the mid-Holocene, 6000 years ago, focusing on the northern Africa monsoon (Chapter 3). Both of these analyses, and an evaluation of simulated changes in precipitation and temperature in mid-continental Eurasia in the mid-Holocene, are included in Chapter 4 which provides a summary of all of the evaluations that have

been done of the CMIP5 palaeoclimate simulations. All of these papers focus on evaluation of changes in the long-term mean climate, but it is also important to evaluate how well the models simulate short-term (annual to decadal) climate variability. To do this, I developed a model to simulate tree growth driven by climate-driven changes in net primary production (Chapter 5). I tested this model using tree-ring data from the historical period in two contrasting climate settings, specifically in a cool climate in the Changbai Mountains, northeastern China (Paper 4) and in the semi-arid environment of the Great Western Woodlands, Western Australia (Chapter 6). The final paper (Chapter 7) uses the model to simulate tree growth during the Last Glacial Maximum (ca 21,000 years ago) in California, USA.

Changes in the hydrological cycle are expected to scale with temperature changes. However, both the observed changes in precipitation in recent decades and model simulations of precipitation changes during the historic period and the 21st century are smaller than would be predicted from the Clausius-Clapeyron relationship which describes the change in atmospheric water vapour content with temperature ($\sim 7\%/^{\circ}\text{C}$). It has been argued that this reflects energetic constraints on evaporation. To test this hypothesis, I analyzed the scaling of precipitation with temperature in warm (increased CO_2) and cold (Last Glacial Maximum, LGM) climates using six CMIP5 models that have simulated the response to both. Globally, precipitation increases in warm climates and decreases in cold climates. The estimate of the scaling across all the climate states and all models indicates a $2.06\% \pm 0.09\%$ change per degree temperature change at the global scale. The simulated scaling of precipitation to temperature is controlled by energetic constraints on evaporation rather than the atmospheric water-holding capacity, and is also affected by water availability. These constraints lead to a lower sensitivity of precipitation to temperature change over the land than that over the ocean, and a lower sensitivity over tropical land than over extratropical land. The simulated changes in precipitation per degree temperature change are comparable to the observed changes in both the historical period and the LGM, showing the models correctly predict the constraints on precipitation scaling.

Temperature-controlled precipitation change is a global large-scale phenomenon. However, regional precipitation change can also be influenced by changes in the large-scale circulation. Monsoon precipitation is one of the most typical circulation-controlled climate. To evaluate model performance of regional circulation changes, I

evaluated the spatial expression of seasonal climates of the Mediterranean and northern Africa in pre-industrial (piControl) and mid-Holocene (midHolocene, 6 yr BP) CMIP5 simulations using the observed regional pattern and amount of seasonal precipitation. Most of the piControl simulations reproduce the observed modern precipitation patterns in the Mediterranean and equatorial zone, but they overestimate the area influenced by the monsoon and underestimate the extent of desert. The models also fail to capture the observed amount of precipitation. The models simulated a stronger monsoon in response to orbital changes in seasonal insolation receipts in the mid-Holocene, including a northward expansion of the monsoon and an increase in summer and autumn rainfall. However, the mid-Holocene simulations underestimate the observed changes in annual precipitation, except in equatorial zone. The underestimation of precipitation in the latitude band from 15–30 °N is at least 50%. The failure to capture the observed monsoon expansion is unrelated to biases in the piControl simulations.

The failure to capture the observed changes in rainfall over northern Africa is an example of a long-standing modelling problem: current state-of-the-art models do not produce a better match to observations than previous generations of models. The mid-continent of Eurasia provides another example of a persistent problem in the simulation of regional climates during the mid-Holocene. The CMIP5 mid-Holocene simulations produce conditions drier than today in mid-continental Eurasia, particularly between 45° and 60° N, whereas observations systematically show that this region was wetter than today. In the models, dry conditions reduce evapotranspiration and result in an increase in surface temperature compared to today. However, the observations show that the mid-continent was cooler than today.

These three analyses form a major part of the evaluation of the CMIP5 palaeoclimate simulations described in Chapter 4. The main conclusion of this summary paper is that while models are able to reproduce the large-scale features (such as precipitation scaling with temperature) of past climates accurately they are poor at reproducing regional changes such as monsoon expansion or the water-balance of the mid-continental regions. This suggests that while we can have confidence in projections of large-scale features of projected future climates, such as the greater warming at high latitudes than in the tropics or enhanced land-sea contrast, predictions of regional climates are very uncertain.

Statistical reconstructions of past climate provide one source of information for model evaluation. An alternative approach is to use climate model outputs to drive simple forward models to predict the actual observations of vegetation changes. I have developed a tree growth model (the T model) that predicts carbon allocation to leaves, stem and roots, and thus can simulate tree-ring series. The tree-growth model is driven by a generic light-use efficiency model (the P model). The P model provides values for gross primary production (GPP) per unit of absorbed photosynthetically active radiation (PAR), which is estimated from leaf area. In the tree-growth model, GPP is allocated to foliage, transport tissue, and fine-root production and respiration in such a way as to satisfy well-understood dimensional and functional relationships. The T model represents both ontogenetic effects (the impact of ageing) and the effects of environmental variations and trends (climate and atmospheric CO₂ concentration [CO₂]) on growth.

I have tested the T model under modern climate conditions for three species in three different climate settings, including *Pinus koraiensis* in the cool and mild climate of the Changbai Mountains, northeastern China, *Callitris columellaris* in the semi-arid climate of the Great Western Woodlands, Western Australia, and *Juniperus occidentalis* in the montane climate of California, USA. In all three regions, when driven by the local climate and [CO₂], the T model produces realistic simulations of the interannual variability in ring width, and captures the effect of ontogenetic ageing on tree growth. The model correctly reproduces the effects of individual climate variables on tree growth, including the positive response of tree-ring width to growing season total photosynthetically active radiation (PAR₀), the positive response of ring-width to the ratio of actual to potential evapotranspiration (α), and the negative response of ring-width to annual mean vapour pressure deficit (VPD). Thus, the T model responds to climate in a realistic way in different regions and for different species.

I have also analysed the response of tree growth to changing [CO₂]. The impact of the recent increase in [CO₂] on tree growth in the Changbai Mountains is small compared to the influence of climate variability. *Callitris* trees in the Great Western Woodlands show no change in radial growth in response to increasing [CO₂]. By using a time-dependent calibration of the T model against increasing [CO₂], I have shown that this results from changes in carbon allocation strategy. As [CO₂] increases, *Callitris* allocates more carbon to below-ground growth such that the ratio of fine-root mass to foliage area increases by 14% with a 40 ppm increase in [CO₂]. Studies from

many parts of the world have shown that tree ring-widths are apparently insensitive to recent changes in $[\text{CO}_2]$; my analyses suggest that the absence of increased radial growth could be a consequence of a shift towards increased below-ground carbon allocation. Soil nutrient status and moisture availability may influence the sensitivity of carbon partitioning to changes in $[\text{CO}_2]$; these effects are not included in the current version of the T model.

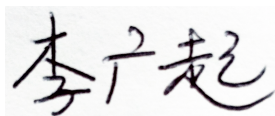
In my final analysis, I examine the impact of changes in climate and $[\text{CO}_2]$ on tree growth during the Last Glacial Maximum. An earlier study comparing fossil *Juniperus* wood from La Brea tar pits in California with modern *Juniperus* suggested that there was almost no change in ring width or the ratio of internal to external $[\text{CO}_2]$ at the LGM compared to present, despite the fact that the trees were growing in $[\text{CO}_2]$ levels of c_a 180 ppm. My model analyses show that: the c_i/c_a ratio was stable because both vapour pressure deficit and temperature were decreased with compensating effects; reduced photorespiration at lower temperatures partly mitigated the effect of low c_i on gross primary production, but maintenance of present-day radial growth required a ~25% reduction in below-ground carbon allocation.

Statement of Candidate

I certify that the work in this thesis entitled “Evaluating Past Climate Variability and Modelling Its Impact on Tree Growth” has not previously been submitted for a degree nor has it been submitted as part of requirements for a degree to any other university or institution other than Macquarie University.

I also certify that the thesis is an original piece of research and it has been written by me. Any help and assistance that I have received in my research work and the preparation of the thesis itself have been appropriately acknowledged.

In addition, I certify that all information sources and literature used are indicated in the thesis.

A handwritten signature in black ink, appearing to read '李广起' (Li Guangqi), is shown on a light gray background.

Guangqi Li (42764874)

23rd July 2015

ACKNOWLEDGEMENTS

First of all, I am grateful to my supervisor, Professor Sandy P. Harrison. Thank you for everything you've done for me. You are my academic mother. If it is not you, I would have no chance to take my PhD in such a beautiful city, Sydney; to develop my academic skills in the world-class research atmosphere; to assure myself to continue my career as a scientist. You guide me for my whole research path, from the very beginning data collection and analysis, to results interpretation, to writing down our cheering papers word by word and hand by hand. You are always telling me to keep passions on research, and encouraging me thinking independently. I do enjoy the exciting, refreshing, and full battery-charged feeling after each of our discussion. You lead me to communicate with other peers, to present our work, to involve into the collaborations with other scientists. I do really benefit so much from all of these, getting more confident, becoming more intelligent, and confirming my choice about continuing research. Now I am very proud to say, after 3.5-year PhD study, I have mentally grown up from a kid, who can only obey instructions, to a young scientist, who has personal unique ideas about our research. Thanks so much for guiding me all the way, and giving me opportunities to continue my research career as a postdoc in University of Reading. You are also like a mum for my life. Since the first day I arrived in Sydney, you let me stay in your place, took care for me, helped me to adapt the new environment. I still remember what you said to me at the very first few days when I came to Australia: "work hard, play hard", which I am always trying. And I really appreciate the education of wine, cheese and jazz music, which enriched my life and made it more meaningful. In my last two months of my PhD, you took care everything of my life, just to make sure I could put all of my strength onto the thesis. I cannot express my gratitude with my words, but I will never forget anything about this past three and half years.

I also want to thank Professor I. Colin Prentice. You also guide me and contribute to almost all of my papers during my PhD. I am so fortunate that I can have two best world-top class scientists supervising me, not only for my academic research, but also for my life. Your intelligence to science, your passion to research, and your attitude to life, all of these are my models. Thanks Colin so much for all of those great

meals when I stay with you and Sandy. And thanks so much for teaching me how to cook. In my mind, both you and Sandy are my supervisor.

I want to thank Bart and Kenji. Thank you very much for helping me with climate model data processing, choosing appropriate statistical methods, teaching me about Fortran subroutine and NCL, and supplying office space and other facilities when I visited University of Oregon. I do learn a lot from you, and do appreciate to have chance to be coauthor with you. And thanks to Ana. Your passion and focus on the research really encouraged me. Still missing those days when we worked together for our paper in Sydney. I am so happy to meet you there, my friend.

I also wish to thank Wang Han. You are like the elder sister for me, treating me so well. I really enjoy and gain a lot from our talks about research, life, and everything. I give all of my best wishes to you. And thanks Doug. You are the warmest and kindest guy on Earth. You are always such warmhearted and preparing to help me and everyone. I am so lucky to have you during my PhD, and looking forward to working with you again for our postdoc in Reading. And thanks to Sam, Anna, Henrique, Annika, Farzana, Zhiyong, Rhys, Trevor and all members of our BCD Group in Macquarie. It is my great pleasure to be a member of our big family, and I really enjoy the 3.5 years we spent together.

I do thank Macquarie University for supporting me with the scholarship and all of the other facilities and opportunities. I would never forget the 3.5 years I spent in Sydney, one of the happiest and most important periods in my life. This university, this city, and all of the people, did and will influence my life. I started my research career in Macquarie, where I have the best supervisors and the best colleagues helping me. I also started a new page of my life, meeting my wife here. This university and this city mean a lot to me.

At last, I'd like to say thank you to my wife and my parents. It is you who always accompany me, feed me, support me, and encourage me. You are the driving force in my life, forever.

List of Publications

Publications for thesis:

Six journal articles constitute Chapter 2-7 of my thesis. Five out of these six papers have been published, and one is submitted.

Chapter 2: **Li, G.**, Harrison, S. P., Bartlein, P. J., Izumi, K., and Prentice, I. C.:

Precipitation scaling with temperature in warm and cold climates: An analysis of CMIP5 simulations, *Geophysical Research Letters*, 40, 4018-4024, 2013.

Chapter 3: Pérez Sanz, A., **Li, G.**, González-Sampériz, P., and Harrison, S. P.:

Evaluation of modern and mid-Holocene seasonal precipitation of the Mediterranean and northern Africa in the CMIP5 simulations, *Climate of the Past*, 10, 551-568, 2014.

Chapter 4: Harrison, S. P., Bartlein, P. J., Izumi, K., **Li, G.**, Annan, J., Hargreaves, J.,

Braconnot, P., and Kageyama, M.: Implications of evaluation of CMIP5/PMIP3 palaeosimulations for climate projections, *Nature Climate Change*, 5: 735–743. doi:10.1038/nclimate2649, 2015.

Chapter 5: **Li, G.**, Harrison, S., Prentice, I., and Falster, D.: Simulation of tree-ring

widths with a model for primary production, carbon allocation, and growth, *Biogeosciences*, 11, 6711-6724, 2014.

Chapter 6: **Li, G.**, Harrison, S. P., and Prentice, I. C.: A model analysis of climate and

CO₂ controls on tree growth in a semi-arid woodland, *Biogeosciences Discussions*, 12, 4769-4800, 2015.

Chapter 7: **Li, G.**, Gerhart, L. M., Harrison, S. P., Ward, J., and Prentice, I. C.:

Allocation changes buffer CO₂ effect on tree growth since the last ice age, *Nature Communication*, (submitted), 2015.

Other publications obtained during candidature:

Zeppel, M., Harrison, S. P., Adams, H. D., Kelley, D. I., **Li, G.**, West, A., Dawson, T.,

Fensham, R., Medlyn, B. R., Palmer, A., Tissue, D. T., and McDowell, N.: Drought and resprouting plants, *New Phytologist*, 206, 583–589, 2015.

- Raihan, F., **Li, G.**, Harrison, S. P.: Detection of recent climate change in southeastern Bangladesh, *Journal of Climatology & Weather Forecasting* 3,127, doi:10.4172/2332-2594.1000127, 2015.
- Gallego-Sala, A., Charman, D., **Li, G.**, Harrison, S. P. and Prentice, I. C.: Climate driven expansion of blanket bogs in the British Isles during the Holocene, *Climate of the Past*, 12: 129-136, doi:10.5194/cp-12-129-2016, 2015.
- Harrison, S. P., Kelley, D. I., Wang, H., Herbert, A., **Li, G.**, Bradstock, R., Fontaine, J., Enright, N., Murphy, B. P., Pekin, B. K., Penman, T., Russell-Smith, J. and Wittkuhn, R. S., Patterns in the abundance of post-fire resprouting in Australia based on plot-level measurements. *Global Ecology and Biogeography*, (submitted), 2015

Conference Presentations:

- 2015.** "Palaeo-applications of a process-based tree-ring model" at International Union for Quaternary Research (INQUA) XIX Congress 2015: Nagoya Congress Centre, Nagoya, Japan . 26th July–2nd August 2015 (oral)
- 2014.** "Multiple climate factors control analysis of *Callitris columellaris* tree ring width in the last 150 years — application of T-model in Great Western Woodland, Western Australia" at ACCSP – 3rd PAGES Aus2k Workshop: Australian Bureau of Meteorology, Melbourne, Australia. 26th–27th June 2014 (poster)
- 2014.** "Simulation of tree ring-widths with a model for primary production, carbon allocation and growth" at second PMIP3 general meeting: Namur, Belgium. 25th–30th May 2014 (oral)
- 2014.** "Evaluation of seasonal climates of the Mediterranean and northern Africa in the CMIP5 simulations" at second PMIP3 general meeting: Namur, Belgium. 25th–30th May 2014 (poster)
- 2013.** "Simulation of tree ring-widths with a model for primary production, carbon allocation and growth" at AGU: San Francisco, USA. 9th–13th December 2013 (poster)
- 2012.** "Clausius-Clapeyron in a colder world: evaluation of the CMIP5 simulations" at PMIP3 2nd General Meeting: Crewe Hall, Crewe, Cheshire, UK. 6th–11th May 2012 (oral)

Seminar Presentations:

- 2015.** “The divergence problem and tree-growth modelling”. Invited presentation, Department of Life Sciences, Imperial College, London, UK, 29th June 2015 (oral)
- 2014.** “T model application in China and Australia - Simulation of tree ring-widths with a model for primary production, carbon allocation and growth”. Invited presentation in Centre for Past Climate Change (CPCC) seminar series, Reading, UK, 22nd October 2014 (oral)
- 2014.** “T model application in China and Australia - Simulation of tree ring-widths with a model for primary production, carbon allocation and growth” at Postgraduate Research Conference (HDR Annual Report): Macquarie University, Sydney, Australia. 1st-2nd December 2014 (oral)
- 2013.** “Interpretation of tree-ring data with a model for primary production, carbon allocation and grow” at Postgraduate Research Conference (HDR Annual Report): Macquarie University, Sydney, Australia. 18th-20th November 2013 (oral)
- 2013.** “Application of T model” at Brown Bag Seminar: Macquarie University, Sydney, Australia. 3rd May 2013 (oral)
- 2013.** “Precipitation scaling with temperature in warm and cold climates: an analysis of CMIP5 simulations” at Postgraduate supplementary conference (HDR Annual Report): Macquarie University, Sydney, Australia. 21th February 2013 (oral)
- 2013.** “Clausius–Clapeyron relationship test with CMIP5 simulations” at Brown Bag Seminar: Macquarie University, Sydney, Australia. 29rd June 2012 (oral)

Chapter 1

Introduction

INTRODUCTION

Past climate provide multiple realisations of the response of the climate system to changes in forcing. This provides the motivation to use palaeoclimate simulations to understand the mechanisms of climate change. It also provides the motivation to use past climate states to evaluate whether state-of-the-art models can reproduce such responses. The goal of my PhD is to develop and apply different tools to analyse and evaluate past climate variability, both in terms of long-term mean climate and short-term interannual variability.

Pollen records are widely used to reconstruct changes in the long-term mean climate. I use these reconstructions to examine how well state-of-the-art climate models simulate long-term and large-scale climate signals: specifically, the relationship between temperature and precipitation changes in past (Last Glacial Maximum, LGM: ca 21,000 years ago) and future (high CO₂ scenarios) climates (Chapter 2), the effect of circulation changes on monsoon precipitation over northern Africa during Middle Holocene (MH: ca 6000 years ago) (Chapter 3), and regional changes in temperature and precipitation in central Eurasia in the MH (Chapter 4). Chapter 4 also provides a summary of other analyses of the ability of the current generation of climate models to simulate large-scale and regional climate changes.

Tree ring-width data are widely used to provide climate reconstructions of annual climate variability, based on empirical statistical relationships between ring-width and specific climate variables at a given site. This approach cannot take account of non-analogue situations in the past, such as known changes in seasonality (as shown by Liu et al., 2004; Zhao et al., 2005; Braconnot et al., 2007b; Izumi et al., 2013) or the direct impacts of CO₂ on tree growth (Kienast and Luxmoore, 1988; Archer et al., 1995; Gedalof and Berg, 2010; van der Sleen et al., 2015). An alternative approach is to model tree growth under changing climate conditions. In the second part of my thesis, I develop (Chapter 5), test (Chapter 6) and apply (Chapter 7) a process-based forward tree growth model by combining a generic light-use-efficiency (LUE) gross primary productivity (GPP) model with a species-specific physiological carbon allocation tree growth model.

Here, as a background to my thesis, I first describe the development of climate models and the motivation for using palaeoclimate model-data comparison to evaluate climate models, and summarise previous work on climate-model evaluation. Then, I explain the motivation and basis for using forward-modelling method to simulate tree ring width.

1 Climate Models and Model Evaluation

1.1 Climate Model Construction and Evolution

Climate models are numerical representations of the interactions between atmosphere, ocean, land surface and ice, and can be used to simulate how the climate system responds to changes in external forcing. Climate models can range from simple energy-balance models (EBMs: Budyko, 1969; Sellers, 1969), which estimate the energy budget of the Earth either globally (zero-dimensional model) or with a single dimension of variability such as latitude (one-dimensional EBMs) through to more complex general circulation models (GCMs: Manabe et al., 1965; Arakawa and Lamb, 1977; Liang et al., 1994; Roeckner et al., 2003).

GCMs explicitly simulate the planetary circulation of the atmosphere and oceans on a rotating sphere based on the Navier-Stokes equations, with additional terms to describe the thermodynamics of energy fluxes between the land, ocean and atmosphere. GCMs operate on a 3-dimensional grid, with varying horizontal and vertical resolution. The horizontal resolution of the current generation of climate models varies between ca 80 to nearly 600 km, although most models have a resolution of between 1-2° in the atmosphere and ca 1° in the ocean (Flato et al., 2013). Vertical resolution varies between 30-40 layers in the atmosphere, and between 30-60 layers in the ocean. Resolution affects the representation of land-sea geography and topography, which is necessarily smoothed to the average for the whole grid cell. Processes that cannot be explicitly resolved at the grid cell resolution are parameterized, i.e. represented in a simplified way. Examples of such processes include cloud micro-physics, convection and cloud formation in the atmosphere, and meso-scale eddies in the ocean (Flato et al., 2013).

GCMs have evolved over time. The first models simulated only the atmospheric circulation (AGCMs: Arakawa and Lamb, 1977; Cess et al., 1990; Smith, 1990) and land-surface (e.g. albedo, surface roughness) and ocean (e.g. sea-surface temperature) characteristics were prescribed. Coupled models in which both the oceanic and atmospheric circulations are explicitly simulated (OAGCMs: Giorgi and Mearns, 2002; Sun and Hansen, 2003) simulate ocean temperature, the formation of sea ice and circulation, but again land-surface characteristics are prescribed. Models have been developed that explicitly simulate biospheric properties, including carbon-cycle models that simulate the terrestrial and ocean carbon cycle (Friedlingstein et al., 2006; Meinshausen et al., 2009) and models that include dynamic vegetation (OAVGCMs: Schurgers et al., 2008; Jungclaus et al., 2010; Zaehle and Dalmonech, 2011). Many state-of-the-art models incorporate treatments of multi-source aerosol, including dust, sea salt and biomass burning emissions (Bauer et al., 2008; Pechony and Shindell, 2009; Rostayn et al., 2010), and some include a fully-interactive treatment of atmospheric chemistry (Eyring et al., 2013). Increasing model sophistication increases the computational cost considerably, and for this reason most palaeoclimate simulations that have been made with the current generation of climate models do not incorporate dynamic vegetation, aerosol or atmospheric chemistry.

1.2 Model evaluation

The Coupled Model Intercomparison Project was set up in 1995 by the Working Group on Coupled Modelling (WGCM) of the World Climate Research Project (WCRP) to provide a community-based infrastructure in support of climate model diagnosis, validation, and intercomparison and a standard experimental protocol for studying climate changes using coupled OAGCMs. The current phase of CMIP (CMIP5: Taylor et al., 2012) was initiated in September 2008 and involves ca 20 climate modelling groups from around the world. The CMIP5 protocol includes a large range of experiments covering past, present and projected future climate, including projections of future climate changes under several Representative Concentration Pathway (RCP) forcing scenarios, with additional experiments to analyse the uncertainties in these projections. Palaeoclimate simulations, specifically of the Last Glacial Maximum (LGM: ca 21,000 years ago), the mid-Holocene (MH: ca 6000 years ago) and the Last Millennium (LM:

850-1850 CE), were included for the first time as part of the suite of CMIP simulations in CMIP5. Analyses of both past, present and future CMIP5 simulations have contributed to the recent IPCC Fifth Assessment Report (Flato et al., 2013; Masson-Delmotte et al., 2013).

Evaluation of the 20th century historical simulations against observations shows that the CMIP5/PMIP3 models reproduce continental-scale surface patterns and long-term trends in temperature and precipitation reasonably well (Flato et al., 2013). In most areas, the simulated multi-model mean temperature is <2 °C different from the observed temperatures. The simulated multi-model mean precipitation also reproduces the known large-scale features, with e.g. maximum precipitation just north of the equator in the central and eastern tropical Pacific, minimum precipitation in the Sahara, and dry conditions over the eastern subtropical ocean basins. Zonal radiation is also well simulated by the models (Flato et al., 2013).

However, the period of modern climate observations is short, rarely more than ca 200 years, and these records only sample a limited range of climate variability. While gridded global data sets of temperature are available from 1800 CE onwards (HadCRU: Morice et al., 2012), gridded precipitation data (e.g. GPCC: Becker et al., 2013) is only available since 1901. In both cases, the number of grid cells with observations is sparse prior to ca 1950 CE. The change in temperature between 1880 to 2012 has been estimated as 0.85 °C (Hartmann et al., 2013), whereas global mean temperature is projected to increase by between 0.3 °C and 1.7 °C (depending on the model) at the end of the 21st century under the RCP2.6 scenario, and between 2.6 °C and 4.8 °C by the end of the 21st century under the RCP8.5 scenario (Collins et al., 2013). Models that produce equally good simulations of the present day produce very different projections of future climate (Collins et al., 2013; Kirtman et al., 2013). The different responses of individual models to future forcing is the major cause of the uncertainty in climate projections, at least during the first half 21st century (Kirtman et al., 2013).

It is vital to evaluate whether climate model can reproduce large climate changes outside the range of historical climate observations. Past climates provide an opportunity to examine the response of the Earth System to large changes in external forcing. The

changes in forcing over the last 21,000 years since the Last Glacial Maximum have been as large as those projected to occur over the 21st century as a result of anthropogenic changes in greenhouse gas concentrations and land-use changes (Braconnot et al., 2012; Schmidt et al., 2014). The diversity of changes in forcing and resulting climates in the past provides many opportunities to evaluate different aspects of climate-model performance. Intervals when the atmospheric CO₂ concentration was as high or higher than today, exemplified by the mid-Pliocene (Sloan and Rea, 1996; Haywood et al., 2000; Haywood et al., 2009; Lunt et al., 2010; Haywood et al., 2011) or the Eocene (Greenwood and Wing, 1995; Sloan and Rea, 1996; Huber and Sloan, 2001; Lowenstein and Demicco, 2006) provide an opportunity to examine the impact of natural changes in atmospheric composition in the absence of anthropogenic land-use changes. Intervals characterized by orbitally-induced changes in the seasonality and latitudinal distribution of incoming solar radiation (insolation), as exemplified by the Last Interglacial (Allen et al., 1999; Blunier and Brook, 2001; Clark et al., 2009) or early- (Kutzbach, 1981; Marzin et al., 2013) and Mid-Holocene (Steig, 1999; Wanner et al., 2008) climates provides a good opportunity to examine circulation changes, and in particular the simulation of monsoon climates (Liu et al., 2004; Zhao et al., 2005; Braconnot et al., 2007b; Wang et al., 2008). Intervals characterized by rapid climate change, such as the Younger Dryas (~12800 to 11500 yr BP) or the intervals of rapid warming that form the first part of the Dansgaard–Oeschger (D-O) cycles characteristic of glacials (Harrison and Sanchez Goñi, 2010), provide examples to test whether models can capture abrupt climate events of large magnitude (Manabe and Stouffer, 1997; Mikolajewicz et al., 1997; Ganopolski and Rahmstorf, 2001; Renssen et al., 2001; Hopcroft et al., 2011; Menviel et al., 2014). Thus there are ample opportunities to use the palaeo-record for evaluating how well the models that are used to project future climate changes perform.

2. The Palaeoclimate Modelling Intercomparison Project (PMIP)

The first palaeoclimate simulations were made in the 1970's (e.g. Alsea, 1972; Gates, 1976; Manabe and Hahn, 1977). The Palaeoclimate Modelling Intercomparison Project (PMIP) was set up in the early 1990s (Joussaume and Taylor, 2000) to coordinate palaeo-experiments, multi-model analyses, evaluation of model results based on

palaeo-data; and supply a platform for discussion about palaeoclimatic models and data. The key aim of the project is to understand the mechanisms of climate change, to identify the different climatic factors that shape our environment, and to evaluate the capability of state-of-the-art models to reproduce different climates by comparing simulated climate with observations. The availability of results from many models makes it possible to evaluate the range of model responses and the robustness of the mechanisms leading to particular climate changes. There have been three generations of PMIP (PMIP1: Joussaume and Taylor, 2000; PMIP2: Crucifix et al., 2005; PMIP3: Braconnot et al., 2011; Braconnot et al., 2012), which have performed experiments with evolving state-of-the-art models: PMIP1 focused on atmosphere-only simulations, PMIP2 on coupled ocean-atmosphere or ocean-atmosphere-vegetation models, and PMIP3 on coupled ocean-atmosphere or earth-system models.

The LGM and the MH have been foci for simulations and data-model comparison since the first phase of the PMIP project. There are two reasons for this. First, the LGM and the MH represent substantially different climate states from the present day and from each other, and have large natural forcings that are relatively well known (Braconnot et al., 2012). Second, there are sufficient palaeo observations for both periods to be used for model evaluation (Waelbroeck et al., 2009; Leduc et al., 2010; Bartlein et al., 2011; Schmittner et al., 2011). Palaeoenvironmental data can be used to evaluate simulations qualitatively, and this has been done using e.g. changes in lake status from the Global Lake Status Data Base (GLSDB: Qin et al., 1998; Kohfeld and Harrison, 2000) and also broadscale vegetation types (biomes) reconstructed from pollen or plant-macrofossil data from the Palaeovegetation Mapping Project (known as BIOME 6000: Prentice and Webb III, 1998; Foley et al., 2000; Kohfeld and Harrison, 2000). However, there are also quantitative palaeoclimate reconstructions for most regions of the world (Waelbroeck et al., 2009; Leduc et al., 2010; Bartlein et al., 2011; Schmittner et al., 2011) that can be used for evaluation and benchmarking.

Orbital parameters at the LGM were nearly the same as they are today and the differences in incoming solar radiation (insolation) from today were therefore small. The major differences in forcing were caused by the large ice sheets over North America (Laurentide ice Sheet) and Europe (Eurasian Ice Sheet), changes in sea level and

palaeogeography caused by ice-sheet expansion, and the lower atmospheric concentration of greenhouse gases ($\text{CO}_2 \sim 185 \text{ ppm}$, $\text{CH}_4 \sim 350 \text{ ppb}$, $\text{N}_2\text{O} \sim 200 \text{ ppb}$). The change in orbital parameters and hence insolation is well known (Berger, 1978). The greenhouse gas concentrations at the LGM are also well known from ice core records (e.g. Augustin et al., 2004). The decrease in greenhouse gases at the LGM relative to pre-industrial levels results in a tropospheric radiative forcing of -2.8 W m^{-2} (Braconnot et al., 2007b; Braconnot et al., 2012). The expansion of the ice sheets at the LGM caused a sea-level lowering of ca 130m, and the change in albedo associated by the changes in palaeogeography had an important effect on northern hemisphere climate (Braconnot et al., 2012). In the PMIP3 simulations, the change in the ice sheets results in a forcing of between -1.85 and -3.49 W m^{-2} depending on the climate model while the overall change in forcing varied between -3.62 and -5.20 W m^{-2} (Abe-Ouchi et al., 2015). The change in forcing at the LGM is of a similar magnitude to that projected for the next century.

The seasonal and latitudinal distribution of MH insolation was different from today, because of the slow variations in Earth's orbital parameters, specifically climatic precession. Climatic precession varies with periodicities of 23,000 and 19,000 years (Berger, 1978), and causes opposite variations in insolation between the Northern and Southern Hemispheres. During the MH, seasonal contrast in the northern hemisphere was enhanced (by about 60 Wm^{-2}) and correspondingly reduced in the southern hemisphere. Greenhouse gas concentrations were similar to pre-industrial levels. These are the only global forcings of MH climate, although climate-induced changes in land-surface conditions would have influenced local forcings (Braconnot et al., 2012).

Simulations of the LGM and MH climates were compared to palaeo-observations during the first two phases of PMIP (Braconnot et al., 2007a; Braconnot et al., 2007b; Edwards et al., 2007; Schmidt et al., 2011). These comparisons established that models could reproduce the large-scale features of past climate changes, such as the global cooling at the LGM and the robust response of circulation to the presence of the northern hemisphere ice sheets, and the expansion of regional summer monsoons in the northern hemisphere during MH (PMIP, 2000). However, they also showed that AGCMs failed to reproduce the glacial cooling in the tropics shown by the palaeo-reconstructions

(Farrera et al., 1999; Pinot et al., 1999). These models also underestimated the latitudinal expansion of the summer monsoon over northern Africa (PMIP, 2000; Coe and Harrison, 2002) and the extent of mid-continental aridity in Eurasia (Yu and Harrison, 1996) during the MH. The OAGCMs and OAVGCMs used in PMIP2 produced a more realistic simulation of cooling in the tropical regions during LGM, and a more pronounced enhancement of the summer monsoons over western Africa and northern India (Braconnot et al., 2007a; Zhao and Harrison, 2012). However, the magnitude of the expansion of the northern African monsoon was still underestimated (Braconnot et al., 2004; Braconnot et al., 2007a); this underestimation of the monsoon response was also shown to be characteristic of other northern hemisphere monsoons (see e.g. Braconnot et al., 2012). The prediction of increased aridity in Eurasia was also a robust feature in the PMIP2 simulations (see e.g. Wohlfarth et al., 2004). Thus, these model-data comparisons helped to reveal the mechanisms of climate changes during both MH and LGM, but also indicated the need for improving climate models particularly with respect to the simulation of regional climate changes.

There have so far been only a limited number of multi-model analyses of the CMIP5/PMIP3 LGM and MH simulations (see e.g. Berger et al., 2013; Chavaillaz et al., 2013; DiNezio and Tierney, 2013; Izumi et al., 2013; Jiang et al., 2013; Li et al., 2013; Prado et al., 2013; Rojas, 2013; Harrison et al., 2014; Mauri et al., 2014; Pérez Sanz et al., 2014; Izumi et al., 2015; Harrison et al., 2015). Some studies have focused on regional patterns, while others have examined large-scale features of climate. Izumi et al. (2013), for example, showed that the simulated large-scale patterns of temperature changes at the LGM are remarkably similar (though of opposite sign) to those shown in raised CO₂ experiments. These signals include changes of comparable magnitude in the land-sea temperature contrast, in the magnitude of high-latitude amplification of temperature changes, and changes in seasonality in response to year-round forcing. The simulated patterns are consistent with those shown by palaeoclimatic or instrumental observations. Model analysis (Izumi et al., 2015) showed that the mechanisms governing land-sea contrast and high-latitude amplification are the same in cold and warm climate states, specifically they primarily reflect changes in surface downward clear-sky long-wave radiation. Changes in surface albedo play a role in strengthening the land-ocean contrast.

Changes in the hydrological cycle are expected to scale with temperature changes. Thus the large-scale precipitation changes would also be expected to show similar patterns of change (though of opposite sign) in both warm and cold climates. The water vapor holding capacity of the lower troposphere increases by $\sim 7\%$ per degree of warming, according to the Clausius-Clapeyron relationship (C-C). If atmospheric water availability were the only factor that affected precipitation, then precipitation could be expected to change at the same rate. However, the observed precipitation scaling with temperature is generally smaller than the ratio estimated by C-C (Adler et al., 2008), and this is also the case in simulations of the modern climate and of projected 21st century climates (Allan and Soden, 2007). Both the observed and simulated scaling of precipitation change with temperature are closer to the theoretical rate of evaporation (including transpiration) scaling with temperature change, which is $1\sim 3\%/^{\circ}\text{C}$ under normal conditions (Li et al., 2013). This suggests that the change in precipitation is constrained by energetic requirements for evaporation. The CMIP5/PMIP3 LGM experiments provide a good opportunity to examine how precipitation scales with temperature, whether factors such as moisture availability, or circulation changes induced by ice-sheet expansion influence this relationship, and whether the simulated scaling of precipitation with temperature at global and regional scales is consistent with palaeo-observations. This is the topic I explore in the first paper of this thesis.

The MH provides a good opportunity to test climate model performance in response to orbitally-induced changes in the seasonal and latitudinal distribution of insolation. Evaluation of the simulations in PMIP1 and PMIP2 identified two persistent problems in the simulation of regional climates: the failure to reproduce the observed expansion and strengthening of the northern Africa monsoon, and the simulation of aridity and warmer summers in central Eurasia where observations indicate cooler, wetter conditions. These regions provide a natural focus for testing whether the state-of-the-art CMIP5/PMIP3 climate models are able to simulate regional climates better than previous generations of models. This evaluation is the focus of Chapter 3 and Chapter 4 of this thesis.

3. Climate reconstruction: pollen records

There are many types of palaeo observation that can be used for model-data comparison including pollen (Guiot et al., 1989; Davis et al., 2003), tree rings (Esper et al., 2002; Fritts, 2012), coral (Dunbar et al., 1994; McGregor and Gagan, 2004), cave deposits (Hu et al., 2008; Zhang et al., 2008), lake levels (Street-Perrott and Harrison, 1985; Digerfeldt, 1988; Magny, 2004), and ice cores (Dansgaard et al., 1993; Petit et al., 1999). However, pollen-based climate reconstructions are the main source of information used in this thesis for the evaluation of mean climate changes. Terrestrial vegetation is highly sensitive to climate changes (Whitlock and Bartlein, 1997; Prentice and Webb III, 1998), and records of past vegetation changes, such as pollen or plant macrofossil records, therefore document past climate states. Statistical or model-inversion techniques are used to reconstruct quantitative changes in seasonal temperature and water balance from pollen records (Bartlein et al., 1984; Overpeck et al., 1985; Bartlein et al., 1986; Huntley and Prentice, 1988; Guiot, 1990; Peyron et al., 1998; Jackson and Williams, 2004). Pollen data are the major source of information used for model-data comparison for evaluating state-of-the-art climate model because the records are very widely distributed geographically and continuous records are available for much of the late Quaternary.

Most pollen records are at comparatively low resolution, and thus provide reconstructions of the long-term changes in mean climate state. Pollen data have been used to reconstruct several bioclimatic variables, which are related to growing-season warmth, winter cold, and plant-available moisture. Bartlein et al. (2011) have synthesized the available reconstructions and created a global data set of reconstructions of LGM and MH climate for model evaluation. This synthesis shows that LGM climate change is globally colder (Figure 1-a) and drier (Figure 1-b). The presence of large ice sheets led to circulation changes that resulted in distinctive regional patterns of climate, e.g., the southward displacement of the Westerlies by the Laurentide Ice Sheet resulted in colder but wetter conditions in southwestern North America while in contrast the eastern part of the continent was colder and drier during the LGM (Bartlein et al., 2011). The MH is characterized by large seasonal changes in temperature in the middle-to-high latitude regions (Figure 1-c). Circulation changes caused by enhanced

land-sea contrast led to changes in regional hydrology, which are reflected in both mean annual precipitation (Figure 1-d) and annual soil moisture. Thus, pollen reconstructions provide excellent targets for the evaluation of climate model performance.

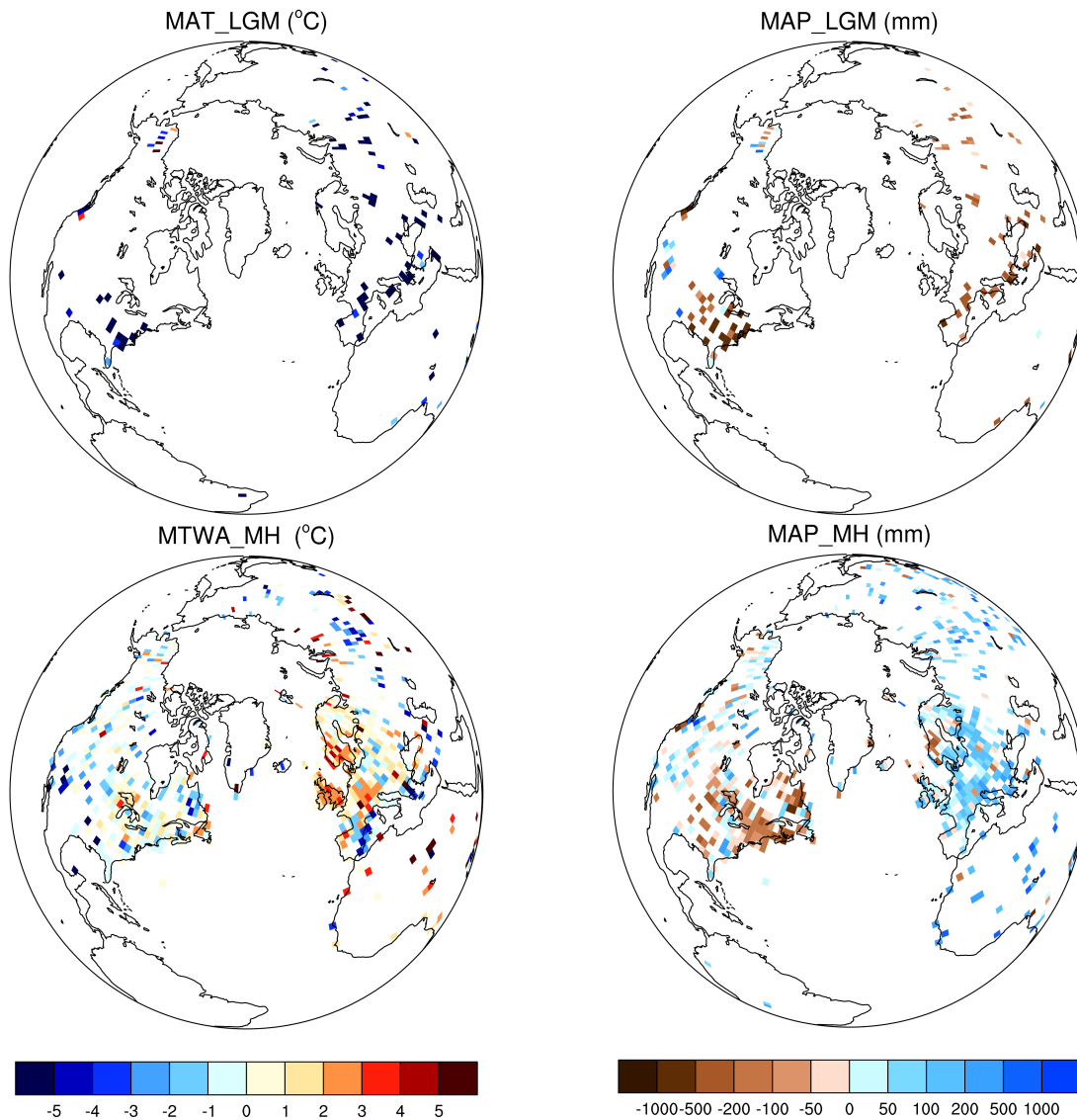


Figure 1 Pollen-based reconstructions of palaeoclimate. The plots show the anomalies of mean annual temperature (MAT) and mean annual precipitation (MAP) at the Last Glacial Maximum (LGM) and mean temperature of the warmest month (MTWA) and MAP for the mid-Holocene (MH). The data are from Bartlein et al. (2011).

4 Climate reconstruction from tree rings: the standard approach

Several different sources of data have been used to reconstruct interannual to interdecadal climate variability, including e.g. tree rings (Fritts, 2012); speleothems (McDermott, 2004), ice cores (Thompson et al., 2003) and lake sediments (Veski et al., 2004), but tree-ring data is the most abundant source (Figure 2) of such information especially for the historical period and the past 2000 years (Jacoby and D'Arrigo, 1989; Briffa et al., 2002; Esper et al., 2002; Mann and Jones, 2003; Briffa et al., 2004), and is the major contribution to the Past Global Changes (PAGES) 2K network (PAGES 2k Consortium, 2013). The annual increment of tree growth can be clearly identified, at least in seasonal climates, and this allows accurate dating (by layer-counting) of the rings back through time. Radiocarbon-dated tree-ring chronologies have also been used to reconstruct conditions during the Holocene (e.g. Briffa, 2000; Grudd et al., 2002; Naurzbaev et al., 2002) and there are also records covering the LGM (Becker et al., 1991; Friedrich et al., 1999; Gerhart et al., 2012).

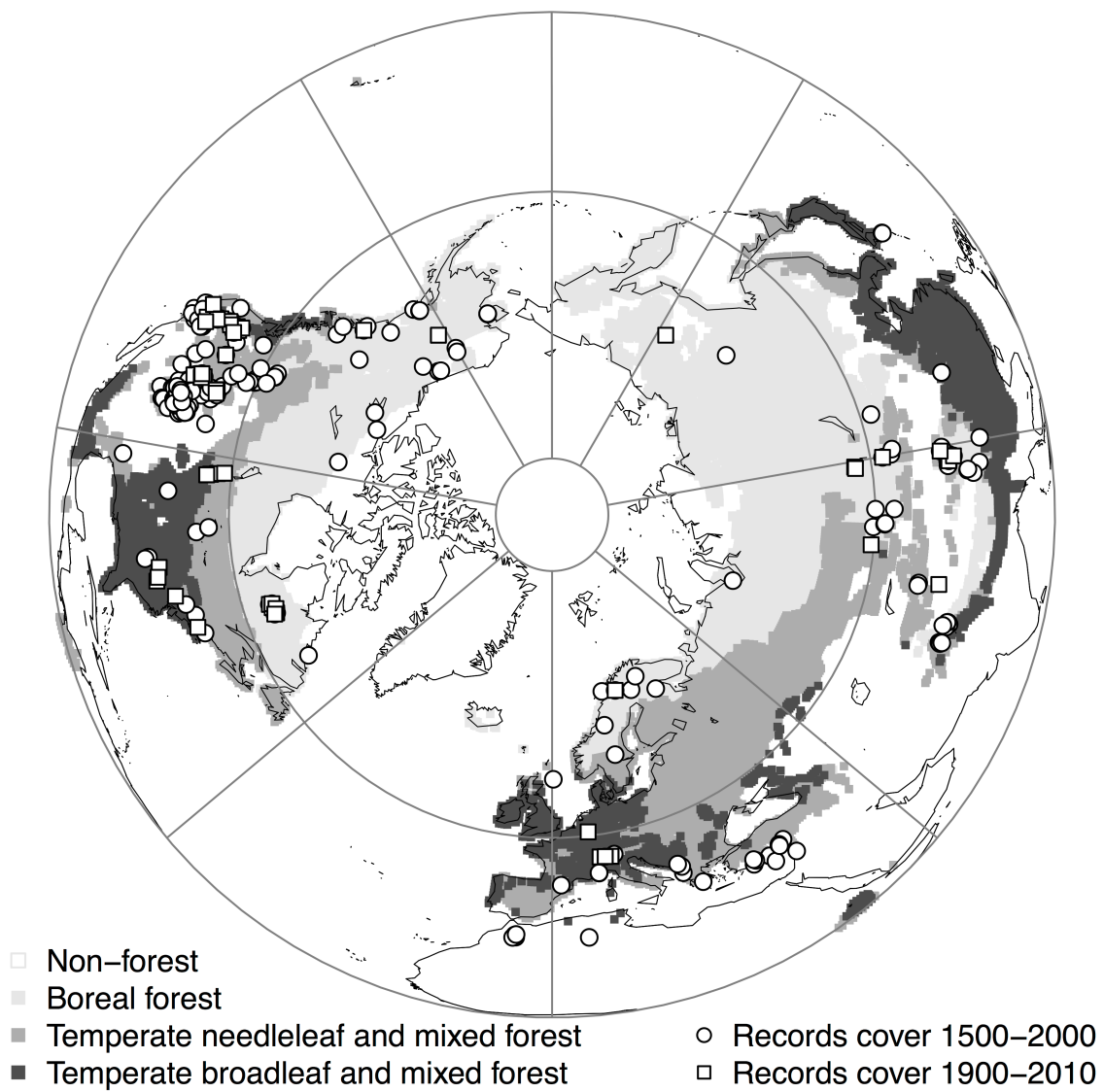


Figure 2 Sites from providing tree ring-width records for the historic period (post 1500 CE). The data are from the International Tree Ring Data Bank (ITRDB)

The general assumption is that tree growth is limited by whichever aspect of climate is the dominant stressor in a given environment (Limiting Factor Theory, Fritts, 2012). By selecting climatically-sensitive sites, it should be possible to provide a reconstruction of either temperature or precipitation changes through time. Reconstructions of climate from tree ring-widths are based on the statistical relationship established between tree radial growth and the key (limiting) climate variable during the period when instrumental measurements are available. This empirical relationship is then applied to the pre-instrumental record. Sufficiently good correlations between ring width and specific climate factors have been established for sites in many regions and this has allowed reconstructions of annual changes in the past 2,000 years climate to be made for many thousands of sites worldwide (Figure 2, e.g. Jacoby and D'Arrigo, 1989; Briffa et al., 2002; Esper et al., 2002; Mann and Jones, 2003; Briffa et al., 2004; Cullen and Grierson, 2009).

A number of recent studies, however, indicate that the relationships established from historical calibrations at specific sites break down in recent decades (post 1980 CE) such that climate predictions based on tree ring-width no longer accurately represent observed climate changes – a phenomenon known as the divergence problem (Briffa et al., 1998; Wilson et al., 2007; Büntgen et al., 2008; D'Arrigo et al., 2008; Esper and Frank, 2009). Explanations of the divergence problem invoke a variety of explanations for the breakdown of the relationship between climate and ring width, including e.g. the fact that critical climate thresholds have been exceeded in recent years, which means that reconstructed climate variable is no longer limiting to growth (Jacoby and D'Arrigo, 1995), changes in the partitioning between diffuse and direct radiation which affects photosynthesis (Stine and Huybers, 2014), or the increasing importance of other environmental factors on tree growth such as different responses from tree's growth to maximum and minimum temperature (Wilson and Luckman, 2002). The fundamental problem lies in the fact that tree growth is affected by multiple climate factors and any statistical single-factor relationship built using current climate data is unlikely to hold under all conditions. This suggests that it is necessary to understand how multiple climate factors control tree growth and to use this information to reconstruct climates from tree-ring data.

5 Climate controls on photosynthesis

The mean climate state is an important control on vegetation distribution and the type of plants that can grow in a particular region (Harrison et al., 2010). The northern limit of trees, for example, is controlled by the accumulated temperature during the growing season (growing degree days) which has to surpass a threshold for sufficient carbon to be accumulated to support the growth of woody tissue. The boundary between grasslands and woodlands or forests can also be determined by availability of soil moisture. The distribution of specific tree types, from deciduous needleleaved trees through boreal needleleaved trees into deciduous trees is determined by winter temperature which determines the type of frost tolerance strategy that is effective. The various climate controls on vegetation distribution are included in biogeography models (e.g. BIOME3: Haxeltine and Prentice, 1996) and are also built into dynamic vegetation models (DGVMs: e.g. Lund–Potsdam–Jena DGVM: Sitch et al., 2003). Shorter-term climate variability is not critical for vegetation distribution but is important for vegetation productivity, which in term is the major determinant of inter-annual variability in tree growth. Thus, an understanding of the climate controls on photosynthesis and carbon production is important in order to be able to build a model of tree growth.

Tree growth is jointly controlled by multiple factors, including light, CO₂, seasonal temperature and moisture, all of which affect metabolic process such as photosynthesis (Berry and Downton, 1982) and respiration (James, 1953). Here, I discuss the major controls of climate on tree growth, which forms the underpinning theory for the process-based model developed and applied in the second half of my thesis.

Photosynthesis is driven by the input of energy from solar radiation (Monteith, 1972). Only light of a specific wavelength spectrum (400 ~ 700 nanometers) can be absorbed by leaves and used for photosynthesis. This component is called the photosynthetically active radiation (PAR: McCree, 1981). Plants utilize PAR to fix carbon in the form of CO₂ from the atmosphere, and use this fixed carbon to produce carbohydrates. PAR is determined by latitude (solar altitude: Duffie and Beckman, 1980), elevation (air thickness dependence of atmosphere transmissivity: Allen, 1996), and cloud cover (Linacre, 1968), which affects the proportion of sunlight that reaches the ground surface.

Cloud cover changes spatially and temporally, and thus PAR, will also change through time and from site to site.

Moisture is an important factor controlling plant physiological functioning because water is the only solvent for most of chemical activities in the plant. There are two aspects to the moisture control on plant activity: availability of soil moisture and of air moisture. Both soil moisture and air moisture affect stomatal conductance via impacts on stomatal closure (Farquhar and Sharkey, 1982), which then impacts the uptake of CO_2 (and hence the CO_2 concentration inside the leaf) (Ball et al., 1987; Collatz et al., 1991). When the supply of water in the soil is limited, plants compensate by reducing stomatal opening or shutting down the stomata (Saliendra et al., 1995). Stomatal closure reduces the amount of incoming CO_2 , and thus restricts photosynthesis. Similarly, the amount of moisture in the atmosphere, as measured by the vapour pressure deficit (VPD, i.e. the difference between the saturated vapour pressure and the actual vapour pressure at a given temperature: Oren et al., 1999), determines the atmospheric demand for water and can also affect stomatal closure/openness (Saliendra et al., 1995; Oren et al., 1999). When the air is very dry, plants respond by shedding leaves. The amount of available soil moisture is largely controlled by inputs from precipitation (or other sources of water) and losses from evaporation as a function of solar radiation and temperature. Soil characteristics, such as soil texture, depth and organic content determine the water-holding capacity and percolation rates and hence the balance between soil moisture and runoff (Sykes and Prentice, 1995). VPD is largely determined by temperature: increased temperature increases the vapour holding capacity of the air, but does not affect the actual vapour pressure.

Temperature has both direct and indirect impacts on tree growth. Changes in temperature affect evaporation from the soil and evapotranspiration from the leaves, as well as the VPD. Thus, increasing temperature will increase drought stress. On the other hand, photorespiration (Kozaki and Takeba, 1996), which is the carbon loss that occurs during carbon fixation in order to reduce oxygenation reactions by the Rubisco enzyme, is a temperature-dependent process and increases as temperature increases (Bernacchi et al., 2003). While the effects of increasing temperature on tree growth through both drought and photorespiration are negative, most physiological processes

within the plant only operate above a threshold temperature and there are optimal temperature ranges for processes such as photosynthesis and respiration (Kobza and Edwards, 1987; Henkin et al., 1998). Thus, when temperatures are too low in winter, trees may adopt a deciduous habit or enter a state of dormancy. The positive effect of temperature on tree growth is exhibited through the relationship with the length of effective growing season (Henkin et al., 1998).

CO₂ is required for carbon fixation and thus the availability of CO₂ is a major determinant of tree growth. The positive impact of increased CO₂ (CO₂ fertilization) has been widely observed in experiments and in the field (Carlson and Bazzaz, 1980; Sage, 1994). To examine plant responses to elevated CO₂ on carbon cycling (Dickson et al., 2000), nitrogen cycling (Zak et al., 2003), water cycling (Leakey et al., 2009), Free-Air Carbon dioxide Enrichment (FACE) experiments have been made in different terrestrial ecosystems around the world, e.g. Duke Forest FACE (Herrick and Thomas, 2001), AspenFACE (Karnosky et al., 2003), Oak Ridge National Laboratory (ORNL) FACE (Norby et al., 2002). CO₂ fertilization can be expressed via increased water-use efficiency (Kimball and Idso, 1983; Peñuelas et al., 2011; Keenan et al., 2013). Increased water-use efficiency has been documented from the increased $\delta^{13}\text{C}$ in wood samples over the last 150 years (Andreu-Hayles et al., 2011; van der Sleen et al., 2015). However, the impact of CO₂ fertilization on tree growth may also be dependent on resource availability. Based on the least-cost hypothesis (Wright and Westoby, 2002; Prentice et al., 2014), increased water-use-efficiency due to the increasing CO₂ should be more obvious in dry areas, and thus the effect of CO₂ fertilization should be stronger in such areas. Similarly, in nutrient limited, especially nitrogen-limited, regions, the positive effects of CO₂ may be restricted by nutrient availability so that the impact of CO₂ fertilisation on growth is weak (Reich et al., 2006; Thornton et al., 2007). Results from the FACE experiments (DeLucia et al., 1999; King et al., 2001; Calfapietra et al., 2003; Lukac et al., 2003; Norby et al., 2004; Pritchard et al., 2008; Godbold et al., 2015) suggest that increasing CO₂ may result in a change in plant allocation strategies, and particularly an increase in underground carbon allocation at the expense of allocation to above-ground components such as trees or stems. This change in carbon allocation strategy may help to explain why some studies, particularly those based on remotely-sensed observations of the canopy or in-situ measurements of tree radial growth, have

not have detected the impact of CO₂ fertilization (e.g. Andreu-Hayles et al., 2011; Peñuelas et al., 2011; van der Sleen et al., 2015).

The complexity of the various controls on tree growth, and the fact that the relationships between these different controls will probably change in a radically changing climate, suggests that empirical approaches to reconstructing climate from tree rings may be of limited use in situations where climate is very different from present. This is the main driver for the development of physiology-based models of tree growth for predicting e.g. the response to future climate change (Collins et al., 2013). It is also the motivation for my development of a process-based tree growth model that could be used to evaluate the representation of short-term (interannual to decadal) climate variability in climate model simulations of the radically different climate of the past.

6 Modelling tree growth

Empirical models have been developed that take account of the influence of multiple climate factors on tree ring-widths. The iconic example is the Vaganov-Shashkin model (Evans et al., 2006; Vaganov et al., 2006). The model uses measurements of cambium activity and xylem cell formation and expansion, to construct statistical relationships between radial growth and climate variables which mimic the response of tree radial growth to climate, including daily temperature, soil moisture, precipitation, and solar radiation, and simulate tree ring-widths. A simplified version of the Vaganov–Shashkin model (VS-Lite, or VSL), driven by the monthly climate input, has also been developed and applied under different types of climate (Breitenmoser et al., 2014). Although empirical models such as V-S or VSL take account of the influence of multiple climate factors, they necessarily assume stationarity of the relationships between tree radial growth and the selected climate variables. They also ignore the effect of climate variables, such as PAR, CO₂, air moisture, which are equally important for tree growth.

MAIDEN (Misson, 2004; Misson et al., 2004; see also MAIDENiso: Danis et al., 2012) is a hybrid between statistical and process-based models, in that it explicitly simulates some physiological processes and used statistical relationships to mimic other processes. MAIDEN simulates net primary productivity (NPP) explicitly and then

allocates NPP to different carbon pools at the stand (rather than the individual tree) level, using a statistical parametrization derived from flux-tower observations. The allocation to stem wood is then standardized to yield a tree ring width-index. The model has been applied to a site in France (Fontainebleau Forest), and shown to reproduce the ring-width index derived from recent observations and the observed carbon flux (Misson, 2004; Misson et al., 2004). However, because MAIDEN uses a number of statistical parameterizations derived from calibration with flux-tower and ring width data, its applicability to other sites is limited to places where both daily climate data and carbon-flux measurements are available.

The advantage of a process-based model is that well-known processes of vegetation metabolism can be used to structure and define the process of tree growth. The impact of climate variables operates directly on key physiological processes. For example, temperature is used as the trigger for cambial activity such that changes in the length of effective growing season will result in an enhancement of tree growth. At the same time, temperature is also allowed to affect VPD and hence stomatal conductance, and photorespiration and hence the CO₂ compensation point. By explicitly modelling the influence of climate on key physiological processes, process-based models can take account of compensatory effects of changes in multiple variables. For example, soil drought generally has a negative effect on tree growth under moderate temperature and PAR conditions. CO₂ fertilization can compensate for the negative effect of soil drought when the ambient CO₂ is increasing.

Light-use efficiency (LUE) models are relatively simple models that predict net primary productivity (NPP) as a function of absorbed photosynthetically active radiation (APAR). LUE modeling was originally developed by Monteith (1972, 1979) and forms the basis for several diagnostic primary production models, including e.g. the Simple Diagnostic Biosphere Model (SDBM: Knorr and Heimann, 1995) and the Carnegie–Ames–Stanford Approach model (CASA: Potter et al., 1993; Field et al., 1995). It also underpins the widely used algorithms to estimate GPP and NPP from remotely-sensed “greenness” data (e.g. Running et al., 2004). LUE formulations are also used in complex, prognostic terrestrial vegetation and carbon-cycle models that originated from BIOME3 (Haxeltine and Prentice, 1996) and the Lund–Potsdam–Jena (LPJ) DGVM (Sitch et al., 2003).

Wang et al. (2014) have developed simple first-principles carbon cycle model based on the LUE formalism and the Farquhar model for C_3 photosynthesis (Farquhar et al., 1980). The model is driven by incident photosynthetically active radiation (PAR) and remotely sensed green-vegetation cover, with additional constraints imposed by low-temperature inhibition and CO_2 limitation. The ratio of leaf-internal to ambient CO_2 concentration in the model responds to growing-season mean temperature, atmospheric dryness and elevation, based on optimality theory (“least-cost hypothesis”: Wright et al., 2003; Prentice et al., 2014). The model is driven by monthly temperature, precipitation and cloud cover, and latitude and elevation are specified. This model (the P model) is fully consistent with observations of key physiological relationships (see e.g. Prentice et al., 2014) and has been shown to simulate both the geographic patterning and seasonal cycles GPP successfully (Wang et al., 2014). The P model therefore provides an efficient tool to simulate carbon inputs to tree growth by linking this model to a tree-specific carbon allocation model.

A number of models have been developed to represent the functional and geometric relationships describing carbon allocation by trees. Such models are built on measurable relationships, such as that between stem diameter and height (Thomas, 1996; Ishii et al., 2000; Falster and Westoby, 2005), and crown area and diameter or height (Duursma et al., 2010) that arise because of functional constraints on growth. The so-called “pipe” model represents the relationship between sapwood area and leaf area (Shinozaki et al., 1964; Yokozawa and Hara, 1995; Mäkelä et al., 2000). The ratio of fine-root mass to foliage area provides the linkage between above- and below-ground tissues (Falster et al., 2011). These functional relationships are expected to be stable through ontogeny, which implies that the fraction of new carbon allocated to different components is variable (Lloyd and Farquhar, 1996).

In the second half of my thesis, I couple a robust model that simulates of GPP (the P model: Wang et al., 2014) to a carbon-allocation model (the T model, Chapter 5) in order to produce a coupled model that can simulate the response of tree growth to climate, and explicitly simulates the annual increment of radial growth for comparison with

observed tree ring-widths. I then test the model in different climate settings (Chapters 5 and 6) before applying it to simulate tree growth at the LGM (Chapter 7).

The T model allocates carbon to the three major carbon stores: leaves, woody tissue and roots. It does not distinguish between stems and branches, nor does it distinguish between tap and fine roots. Even the allocation of carbon to these structural components is a simplification because carbon is also allocated to reproduction (Obeso, 2002; Hackett-Pain et al., 2015), is stored as non-structural carbohydrates for later use (Rosas et al., 2103; Simard et al., 2013), and can be released into the soil in the forms of exudates to support micorrhizal growth (Walker et al. 2003; Badri and Vivanco, 2009). All of these stores could represent a significant carbon cost in any one year (Hackett-Pain et al., 2015). However, there is currently insufficient information to be able to model these stores explicitly. Furthermore, the fact that our model reproduces the mean and interannual variability of ring widths in three different climate settings (Chapters 5, 6 and 7) confirms that the simple model represents the first-order carbon costs.

7. Philosophy and Approach of this Thesis

The initial goal of my PhD was to develop and apply different tools to analyse and evaluate past climate variability, both in terms of long-term mean climate and short-term interannual variability, using existing palaeoclimate reconstructions. The recognition that there might be problems in tree-ring reconstructions, the major source of quantitative palaeoclimate information on interannual climate variability, led me to develop a simple forward model of tree growth that could be used to translate climate model outputs into the something directly comparable with palaeo-record.

The first half of my thesis focuses on the evaluation of the CMIP5/PMIP3 palaeoclimate model simulations of long-term mean climate against the existing quantitative reconstructions from Bartlein et al. (2011). The goal of this is identify what aspects of past climate changes are simulated realistically and where there are mismatches between simulated and observed climates. Identifying the causes of mismatches between simulated and observed climates is a major task, which would necessitate considerable work on model parameterisation and running new simulations, and is

outside the scope of the thesis. Nevertheless, by identifying what aspects of past climate change are not simulated adequately, my research should contribute to the ongoing improvement of climate models.

The key questions addressed in the first part of the thesis are:

- can state-of-art models from CMIP5/PMIP3 capture the large-scale features of changing climate as determined by global energetics, and specifically the relationship between temperature and precipitation change at global and hemispheric scales?
- can state-of-art models from CMIP5/PMIP3 capture regional changes in the long-term mean climate, and specifically regional changes in the Mediterranean, northern Africa and central Eurasia during the mid-Holocene?

The second half of the thesis focuses on developing and testing the tree growth model, and then applying this in a palaeoclimate context. The key questions addressed in the second half of the thesis include:

- Can a simple generic growth and allocation model simulate interannual variability in tree ring widths realistically for different species in different climates over the recent and historical period?
- Does changing atmospheric CO₂ have an impact on carbon allocation and tree growth?
- How did low atmospheric CO₂ at the Last Glacial Maximum affect tree growth?

In the first half of the thesis, pollen reconstructed long-term mean climate was applied to evaluate the CMIP5/PMIP3 state-of-the-art of climate models' performance. Pollen-based climate reconstructions from Bartlein et al. (2011) provide the reconstructions I use of the long-term mean climate state. I use the climate of the LGM, as well as observations of the historical period, to test how well the CMIP5/PMIP3 models reproduce the scaling of precipitation with temperature at global and regional scales (Chapter 2). I then use reconstructions of MH climates for the northern Africa and Mediterranean regions, and from mid-continental Eurasia, to evaluate how well the CMIP5/PMIP3 models reproduce regional climate changes (Chapters 3 and 4). These three papers also allow me to investigate the mechanisms of climate change and to link

model performance under past climate states with features of the future climate simulations.

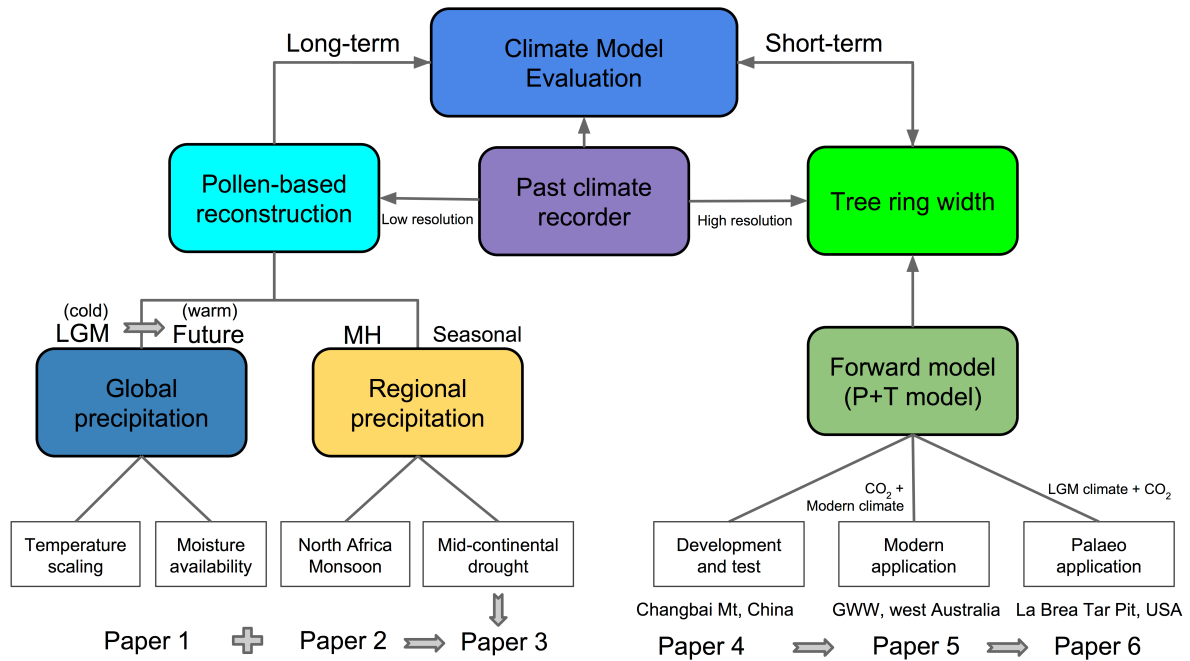


Figure 3 Linkage between the thesis chapters, illustrating the philosophy and approach used.

Thus, in Chapter 2 (Li, G., Harrison, S. P., Bartlein, P. J., Izumi, K., and Prentice, I. C: Precipitation scaling with temperature in warm and cold climates: An analysis of CMIP5/PMIP3 simulations. *Geophysical Research Letters*, 40, 4018-4024, 2013), I use simulations of LGM, historical (post-1850 CE), and increased CO₂ climates (specifically the CMIP5 1pctCO₂ experiment in which CO₂ is increased by 1% per year, and the CMIP5 abrupt4xCO₂ experiment, in which CO₂ is increased instantaneously to 1120 ppm; see Chapter 4: Harrison et al., 2015 for a description of these experiments) to examine precipitation scaling with temperature at global and hemispheric scales. I examine how far this scaling reflects the atmospheric water vapour holding capacity described by the Clausius-Clapeyron relationship, energy-controlled equilibrium evaporation, and moisture limitation. I also investigate whether the so-called “rich get richer” phenomenon that has been observed in recent decades and is seen in future

projections, where high precipitation regions get wetter and dry regions drier, applies in past climate states.

In Chapter 3 (Perez-Sanz, A., Li, G., González-Sampériz, P., and Harrison, S. P.: Evaluation of seasonal climates of the Mediterranean and northern Africa in the CMIP5/PMIP3 simulations. *Climate of the Past*, 10, 551-568, 2014), I examine the relationship between monsoon changes over northern Africa and seasonal climate changes in the Mediterranean region. I examine the impact of biases in the simulation of the pre-industrial control on how well the model simulates MH changes in monsoon precipitation. Model evaluation was conducted using both modern instrumental observations and palaeo-climate reconstructions.

In Chapter 4 (Harrison, S. P., Bartlein, P. J., Izumi, K., Li, G., Annan, J., Hargreaves, J., Braconnot, P., and Kageyama, M.: Implications of evaluation of CMIP5/PMIP3 palaeosimulations for climate projections. *Nature Climate Change*, in press, August 2015), I examine the mismatch between observed and simulated climates in central Eurasia (between 45° and 60° N), focusing on the relationship between biases in the simulation of soil moisture (as represented by reconstructions of actual to potential evapotranspiration, α) and biases in the simulation of summer temperature. This paper also summarises the results of other evaluations of the CMIP5/PMIP3 simulations of LGM and MH, including my own contributions to these evaluations.

Changes in mean climate state are likely to affect short-term, interannual to decadal, climate variability (e.g. Tudhope et al., 2001; Rimbu et al., 2004; Gladstone et al., 2005; Braconnot et al., 2012; Liu et al., 2014) and certainly are implicated in changes in short-term variability and climate extremes in projections of future climates (Timmermann et al., 1999; Boer, 2009; Kirtman et al., 2013; Collin et al., 2013). Tree radial growth, ring width, provides a way of reconstructing short-term climate variability. However, because of the failure of empirical tree-ring reconstructions to reproduce observed climate changes in recent decades (“divergence” problem: D’Arrigo et al., 2008) and because tree growth is influenced by many different aspects of climate, I have chosen to develop a simple process-based model which can simulate tree rings in response to climate change (Chapter 4). Forward modelling, in which a process-based model is driven by

climate-model outputs, provides an alternative approach to model evaluation, and has been developed for a number of other sensors of palaeoclimate (e.g. vegetation: Prentice et al., 2011; water balance: Coe and Harrison, 2002; Ward et al., 2007; fire: Martin Calvo et al., 2014; corals: Thompson et al., 2011). I test the tree growth model in two radically different modern climates: the cool, wet climate of the Changbai Mountains in China (Chapter 5) and the warm, dry climate of the Great Western Woodlands in Western Australia (Chapter 6). After approving model performance in the different climates of today, this tree growth model was applied in the Glacial *Juniperus* in La Brea tar pits in South California (Chapter 7).

In Chapter 5 (Li, G., Harrison, S. P., Colin Prentice, I., and Falster D.: Simulation of tree ring-widths with a model for primary production, carbon allocation and growth. *Biogeosciences*, 11, 6711–6724. 2014), I describe the development of the species-specific functional geometric carbon allocation model (the “T” model), and its coupling to a simple, generic light-use-efficiency carbon-cycle model (the “P” model: Wang et al., 2014). The P model provides values for GPP per unit of absorbed PAR. Absorbed PAR is estimated from the current leaf area. GPP is allocated to foliage, transport tissue, and fine root production and respiration in such a way as to satisfy well-understood dimensional and functional relationships. The T model represents both ontogenetic effects (i.e. the impact of ageing) and the effects of environmental variations and trends (climate and CO₂) on growth. I tested the PT model using tree-ring records from *Pinus koraiensis* that I had previously collected from the temperate, humid forests of the Changbai Mountain, China (Bai et al., 2008; Li et al., 2011).

Chapter 6 (Li, G., Harrison, S. P., and Prentice, I. C.: A model analysis of climate and CO₂ controls on tree growth in a semi-arid woodland. *Biogeosciences Discussion*, 12, 4769-4800, 2015), provides a further test of the performance of the coupled PT model based on tree-ring series on *Callitris columellaris* that I collected in the Great Western Woodland (GWW), Western Australia. The GWW occurs in a dry, Mediterranean climate region. The *Callitris* in this region is multi-stemmed and thus I developed a new algorithm to allow carbon allocation to be effectively distributed to several stems. I used Bayesian calibration to obtain values for poorly known parameters, especially parameters describing the underground components of the model. The tree-ring records

from the GWW do not show the expected positive response to the increase in CO₂ over recent decades, and I therefore used Bayesian optimization to investigate the reason for this. This analysis suggests that changes in carbon allocation strategy, and particularly an increase in carbon allocation to roots, may help to explain the apparent observed lack of response to CO₂.

Finally, I apply my tree growth model to simulate the growth of *Juniperus* during the LGM from La Brea Tar Pits, in coastal California (Chapter 7). The climate of the La Brea site was colder and wetter at the LGM (Bartlein et al., 2011) and the atmospheric CO₂ concentration was low (180 ppm: Augustin et al., 2004). Despite the low CO₂ and colder conditions, Ward et al., (2004) and Gerhart et al., (2012) found that the radial growth of the fossil *Juniperus* was similar to today. Furthermore, the c_i/c_a ratio measured on the fossil wood specimens was also similar to today. Thus, the leaf internal [CO₂] was close to close to the modern compensation point for C₃ plants, ~ 40-70 ppm and the trees were growing at close to carbon starvation levels.

In Chapter 7 (Li, G., Gerhart, L. M., Harrison, S. P., Ward, J., and Prentice, I. C.: Allocation changes buffer CO₂ effect on tree growth since the last ice age. (submitted to *Nature Communications*, 2015), I apply the PT model to investigate how *Juniperus* was able to grow at La Brea during the LGM. I showed that the model was able to simulate *Juniperus* growth under modern conditions, using data from site CA640 obtained from International Tree Ring Databank (36.95°N, 118.92°W, 2630 m a.s.l.; Graumlich, 1993), I then applied the model under LGM conditions, to investigate the contribution of climate changes and changes in allocation strategy to the maintenance of tree growth under low [CO₂] conditions.

References

- Abe-Ouchi, A., Saito, F., Kageyama, M., Braconnot, P.B., Harrison, S.P., Lambeck, K., Otto-Bleisner, B.L., Peltier, W.R., and Tarasov, L., Peterschmidt, J-Y., Takahashi, K., Ice-sheet configuration in the PMIP3/CMIP5 Last Glacial Maximum experiments. *Geoscientific Model Development Discussions* 8: 4293-4336.
- Adler, R. F., Gu, G., Wang, J. J., Huffman, G. J., Curtis, S., and Bolvin, D.: Relationships between global precipitation and surface temperature on interannual and longer

- timescales (1979–2006), *Journal of Geophysical Research: Atmospheres*, 113, D22104, doi:10.1029/2008JD010536, 2008.
- Allan, R. P., and Soden, B. J.: Large discrepancy between observed and simulated precipitation trends in the ascending and descending branches of the tropical circulation, *Geophysical Research Letters*, 34, L18705, doi:10.1029/2007GL031460, 2007.
- Allen, J. R., Brandt, U., Brauer, A., Hubberten, H.-W., Huntley, B., Keller, J., Kraml, M., Mackensen, A., Mingram, J., and Negendank, J. F.: Rapid environmental changes in southern Europe during the last glacial period, *Nature*, 400, 740-743, 1999.
- Allen, R. G.: Assessing integrity of weather data for reference evapotranspiration estimation, *Journal of Irrigation and Drainage Engineering*, 122, 97-106, 1996.
- Alyea, F. N.: Numerical Simulation of an Ice Age Paleoclimate, PhD thesis, Colorado State University, 1972.
- Andreu-Hayles, L., Planells, O., Gutierrez, E., Muntan, E., Helle, G., Anchukaitis, K. J., and Schleser, G. H.: Long tree-ring chronologies reveal 20th century increases in water-use efficiency but no enhancement of tree growth at five Iberian pine forests, *Global Change Biology*, 17, 2095-2112, 2011.
- Arakawa, A., and Lamb, V. R.: Computational design of the basic dynamical processes of the UCLA general circulation model, *Methods in Computational Physics*, 17, 173-265, 1977.
- Archer, S., Schimel, D. S., and Holland, E. A.: Mechanisms of shrubland expansion: land use, climate or CO₂? *Climatic Change*, 29, 91-99, 1995.
- Augustin, L., Barbante, C., Barnes, P. R., Barnola, J. M., Bigler, M., Castellano, E., Cattani, O., Chappellaz, J., Dahl-Jensen, D., and Delmonte, B.: Eight glacial cycles from an Antarctic ice core, *Nature*, 429, 623-628, 2004.
- Badri, D. V. and Vivanco, J.M.: Regulation and function of root exudates, *Plant, Cell and Environment*, 32, 666–681, 2009.
- Bai, F., Sang, W., Li, G., Liu, R., Chen, L., and Wang, K.: Long-term protection effects of national reserve to forest vegetation in 4 decades: biodiversity change analysis of major forest types in Changbai Mountain Nature Reserve, China, *Science in China series C: Life Sciences*, 51, 948-958, 2008.
- Ball, J. T., Woodrow, I. E., and Berry, J. A.: A model predicting stomatal conductance and its contribution to the control of photosynthesis under different environmental conditions, in: *Progress in Photosynthesis Research*, edited by: Biggins, J., Springer, 221-224, 1987.

- Bartlein, P. J., Harrison, S. P., Brewer, S., Connor, S., Davis, B. A. S., Gajewski, K., Guiot, J., Harrison-Prentice, T. I., Henderson, A., Peyron, O., Prentice, I. C., Scholze, M., Seppä, H., Shuman, B., Sugita, S., Thompson, R. S., Viau, A. E., Williams, J., and Wu, H.: Pollen-based continental climate reconstructions at 6 and 21 ka: a global synthesis, *Climate Dynamics*, 37, 775-802, 2011.
- Bartlein, P. J., Prentice, I. C., and Webb III, T.: Climatic response surfaces from pollen data for some eastern North American taxa, *Journal of Biogeography*, 13, 35-57, 1986.
- Bartlein, P. J., Webb, T., and Fleri, E.: Holocene climatic change in the northern Midwest: pollen-derived estimates, *Quaternary Research*, 22, 361-374, 1984.
- Bauer, S. E., Wright, D.L., Koch, D., Lewis, E. R., McGraw, R., Chang, L. S., Schwartz, S. E. and Ruedy, R.: MATRIX (Multiconfiguration Aerosol TRacker of mIXing state): An aerosol microphysical module for global atmospheric models, *Atmospheric Chemistry and Physics*, 8, 6003–6035, 2008.
- Becker, A., Finger, P., Meyer-Christoffer, A., Rudolf, B., Schamm, K., Schneider, U., and Ziese, M.: A description of the global land-surface precipitation data products of the Global Precipitation Climatology Centre with sample applications including centennial (trend) analysis from 1901-present, *Earth System Science Data*, 5, 71-99, 2013.
- Becker, B., Kromer, B., and Trimborn, P.: A stable-isotope tree-ring timescale of the Late Glacial/Holocene boundary, *Nature*, 353, 647 - 649, 1991.
- Berger, A.: Long-term variations of daily insolation and Quaternary climatic changes, *Journal of the Atmospheric Sciences*, 35, 2362-2367, 1978.
- Berger, M., Brandefelt, J., and Nilsson, J.: The sensitivity of the Arctic sea ice to orbitally induced insolation changes: a study of the mid-Holocene Paleoclimate Modelling Intercomparison Project 2 and 3 simulations, *Climate of the Past*, 9, 969-982, 2013.
- Bernacchi, C. J., Pimentel, C., and Long, S. P.: In vivo temperature response functions of parameters required to model RuBP-limited photosynthesis, *Plant, Cell & Environment*, 26, 1419-1430, 2003.
- Berry, J. A., and Downton, W. J. S.: Environmental regulation of photosynthesis, *Photosynthesis*, 2, 263-343, 1982.
- Blunier, T., and Brook, E. J.: Timing of millennial-scale climate change in Antarctica and Greenland during the last glacial period, *Science*, 291, 109-112, 2001.
- Boer, G. J.: Changes in interannual variability and decadal potential predictability under global warming, *Journal of Climate*, 22, 3098-3109, 2009.

- Braconnot, P., Harrison, S. P., Joussaume, S., Hewitt, C. D., Kitoch, A., Kutzbach, J. E., Liu, Z., Otto-Bliesner, B., Syktus, J., and Weber, S.: Evaluation of PMIP Coupled Ocean-Atmosphere Simulations of the Mid-Holocene, in: *Past Climate Variability through Europe and Africa*, edited by: Battarbee, R. W., Gasse, F., and Stickley, C. E., Springer, 515-533, 2004.
- Braconnot, P., Harrison, S. P., Kageyama, M., Bartlein, P. J., Masson-Delmotte, V., Abe-Ouchi, A., Otto-Bliesner, B., and Zhao, Y.: Evaluation of climate models using palaeoclimatic data, *Nature Climate Change*, 2, 417-424, 2012.
- Braconnot, P., Harrison, S. P., Otto-Bliesner, B., Abe-Ouchi, A., Jungclaus, J., and Peterschmitt, J.-Y.: The paleoclimate modeling intercomparison project contribution to CMIP5, *Clivar Exchanges*, 16, 15-19, 2011.
- Braconnot, P., Otto-Bliesner, B., Harrison, S., Joussaume, S., Peterchmitt, J.-Y., Abe-Ouchi, A., Crucifix, M., Driesschaert, E., Fichefet, T., and Hewitt, C. D.: Results of PMIP2 coupled simulations of the Mid-Holocene and Last Glacial Maximum—Part 2: feedbacks with emphasis on the location of the ITCZ and mid-and high latitudes heat budget, *Climate of the Past*, 3, 279-296, 2007a.
- Braconnot, P., Otto-Bliesner, B., Kageyama, M., Kitoh, A., Laîné, A., Loutre, M.-F., Marti, O., Merkel, U., Ramstein, G., and Valdes, P.: Results of PMIP2 coupled simulations of the Mid-Holocene and Last Glacial Maximum—Part 1: experiments and large-scale features, *Climate of the Past*, 3, 261–277, 2007b.
- Breitenmoser, P., Brönnimann, S., and Frank, D.: Forward modelling of tree-ring width and comparison with a global network of tree-ring chronologies, *Climate of the Past*, 10, 437-449, 2014.
- Briffa, K. R.: Annual climate variability in the Holocene: interpreting the message of ancient trees, *Quaternary Science Reviews*, 19, 87-105, 2000.
- Briffa, K. R., Osborn, T. J., and Schweingruber, F. H.: Large-scale temperature inferences from tree rings: a review, *Global and planetary change*, 40, 11-26, 2004.
- Briffa, K. R., Osborn, T. J., Schweingruber, F. H., Jones, P. D., Shiyatov, S. G., and Vaganov, E. A.: Tree-ring width and density data around the Northern Hemisphere: Part 1, local and regional climate signals, *The Holocene*, 12, 737-757, 2002.
- Briffa, K. R., Schweingruber, F. H., Jones, P. D., Osborn, T. J., Shiyatov, S. G., and Vaganov, E. A.: Reduced sensitivity of recent tree-growth to temperature at high northern latitudes, *Nature*, 391, 678-682, 1998.
- Budyko, M. I.: Effect of solar radiation variation on climate of Earth, *Tellus*, 21, 611–619, 1969.

- Büntgen, U. L. F., Frank, D., Wilson, R., Carrer, M., Urbinati, C., and Esper, J.: Testing for tree-ring divergence in the European Alps, *Global Change Biology*, 14, 2443-2453, 2008.
- Calfapietra, C., Gielen, B., Galema, A., Lukac, M., De Angelis, P., Moscatelli, M., Ceulemans, R., and Scarascia-Mugnozza, G.: Free-air CO₂ enrichment (FACE) enhances biomass production in a short-rotation poplar plantation, *Tree Physiology*, 23, 805-814, 2003.
- Carlson, R. W., and Bazzaz, F. A.: The effects of elevated CO₂ concentrations on growth, photosynthesis, transpiration, and water use efficiency of plants, *Environmental and climatic impact of coal utilization. Proceedings of a Symposium, Williamsburg, Virginia, USA, April 17-19, 1979.* edited by: Singh, J. J.; Deepak, A., 609-623, 1980,
- Cess, R. D., Potter, G., Blanchet, J., Boer, G., Del Genio, A., Deque, M., Dymnikov, V., Galin, V., Gates, W., and Ghan, S.: Intercomparison and interpretation of climate feedback processes in 19 atmospheric general circulation models, *Journal of Geophysical Research*, 95, 16601-16615, 1990.
- Chavaillaz, Y., Codron, F., and Kageyama, M.: Southern westerlies in LGM and future (RCP4. 5) climates, *Climate of the Past*, 9, 517-524, 2013.
- Clark, P. U., Dyke, A. S., Shakun, J. D., Carlson, A. E., Clark, J., Wohlfarth, B., Mitrovica, J. X., Hostetler, S. W., and McCabe, A. M.: The Last Glacial Maximum, *Science*, 325, 710-714, 2009.
- Coe, M., and Harrison, S.: The water balance of northern Africa during the mid-Holocene: an evaluation of the 6 ka BP PMIP simulations, *Climate Dynamics*, 19, 155-166, 2002.
- Collatz, G. J., Ball, J. T., Grivet, C., and Berry, J. A.: Physiological and environmental regulation of stomatal conductance, photosynthesis and transpiration: a model that includes a laminar boundary layer, *Agricultural and Forest Meteorology*, 54, 107-136, 1991.
- Collins, M., Knutti, R., Arblaster, J., Dufresne, J. L., Fichet, T., Friedlingstein, P., Gao, X., Gutowski, W. J., Johns, T., Krinner, G., Shongwe, M., Tebaldi, C., Weaver, A. J., and Wehner, M.: Long-term Climate Change: Projections, Commitments and Irreversibility, in: *Climate Change 2013: The Physical Science Basis. Contribution of Working Group I to the Fifth Assessment Report of the Intergovernmental Panel on Climate Change*, edited by: Stocker, T. F., Qin, D., Plattner, G. K., Tignor, M., Allen, S. K., Boschung, J., Nauels, A., Xia, Y., Bex, V., and Midgley, P. M., Cambridge University Press, Cambridge, United Kingdom and New York, NY, USA., 2013.
- Cramer, W., Bondeau, A., Woodward, F. I., Prentice, I. C., Betts, R. A., Brovkin, V., Cox, P. M., Fisher, V., Foley, J. A., and Friend, A. D.: Global response of terrestrial ecosystem

- structure and function to CO₂ and climate change: results from six dynamic global vegetation models, *Global Change Biology*, 7, 357-373, 2001.
- Crucifix, M., Braconnot, P., Harrison, S. P., and Otto-Bliesner, B.: Second phase of paleoclimate modelling intercomparison project, EOS, Transactions American Geophysical Union, 86, 264-264, 2005.
- Cullen, L. E., and Grierson, P. F.: Multi-decadal scale variability in autumn-winter rainfall in south-western Australia since 1655 AD as reconstructed from tree rings of *Callitris columellaris*, *Climate Dynamics*, 33, 433-444, 2009.
- D'Arrigo, R., Wilson, R., Liepert, B., and Cherubini, P.: On the 'divergence problem' in northern forests: a review of the tree-ring evidence and possible causes, *Global and Planetary Change*, 60, 289-305, 2008.
- Danis, P. A., Hatté, C., Misson, L., and Guiot, J.: MAIDENiso: a multiproxy biophysical model of tree-ring width and oxygen and carbon isotopes, *Canadian Journal of Forest Research*, 42, 1697-1713, 2012.
- Dansgaard, W., Johnsen, S., Clausen, H., Dahl-Jensen, D., Gundestrup, N., Hammer, C., Hvidberg, C., Steffensen, J., Sveinbjörnsdóttir, A., and Jouzel, J.: Evidence for general instability of past climate from a 250-kyr ice-core record, *Nature*, 364, 218-220, 1993.
- Davis, B. A., Brewer, S., Stevenson, A. C., and Guiot, J.: The temperature of Europe during the Holocene reconstructed from pollen data, *Quaternary Science Reviews*, 22, 1701-1716, 2003.
- DeLucia, E. H., Hamilton, J. G., Naidu, S. L., Thomas, R. B., Andrews, J. A., Finzi, A., Lavine, M., Matamala, R., Mohan, J. E., and Hendrey, G. R.: Net primary production of a forest ecosystem with experimental CO₂ enrichment, *Science*, 284, 1177-1179, 1999.
- Dickson, R. E., Lewin, K. F., Isebrands, J. G., Coleman, M. D., Heilman, W. E., Riemenschneider, D. E., Sober, J., Host, G. E., Zak, D. R., and Hendrey, G. R.: Forest atmosphere carbon transfer and storage (FACTS-II) the aspen Free-air CO₂ and O₃ Enrichment (FACE) project: an overview, General Technical Report-North Central Research Station, USDA Forest Service, 2000.
- Digerfeldt, G.: Reconstruction and regional correlation of Holocene lake-level fluctuations in Lake Bysjön, South Sweden, *Boreas*, 17, 165-182, 1988.
- DiNezio, P. N., and Tierney, J. E.: The effect of sea level on glacial Indo-Pacific climate, *Nature Geoscience*, 6, 485-491, 2013.

- Duffie, J. A., and Beckman, W. A.: Solar Engineering of Thermal Processes, Wiley, New York, 1980.
- Dunbar, R. B., Wellington, G. M., Colgan, M. W., and Glynn, P. W.: Eastern Pacific sea surface temperature since 1600 AD: The $\delta^{18}\text{O}$ record of climate variability in Galápagos corals, *Paleoceanography*, 9, 291-315, 1994.
- Duursma, R. A., Mäkelä, A., Reid, D. E., Jokela, E. J., Porte, A. J., and Roberts, S. D.: Self-shading affects allometric scaling in trees, *Functional Ecology*, 24, 723-730, 2010.
- Edwards, T. L., Crucifix, M., and Harrison, S. P.: Using the past to constrain the future: how the palaeorecord can improve estimates of global warming, *Progress in Physical Geography*, 31, 481-500, 2007.
- Esper, J., Cook, E. R., and Schweingruber, F. H.: Low-frequency signals in long tree-ring chronologies for reconstructing past temperature variability, *Science*, 295, 2250-2253, 2002.
- Esper, J., and Frank, D.: Divergence pitfalls in tree-ring research, *Climatic Change*, 94, 261-266, 2009.
- Evans, M. N., Reichert, B. K., Kaplan, A., Anchukaitis, K. J., Vaganov, E. A., Hughes, M. K., and Cane, M. A.: A forward modeling approach to paleoclimatic interpretation of tree-ring data, *Journal of Geophysical Research: Biogeosciences*, 111, G03008, 2006.
- Eyring, V., Arblaster, J.M., Cionni, I., Sedláček, J., Perlwitz, J., Young, P.J., Bekki, S., Bergmann, D., Cameron-Smith, P., Collins, W.J. and Faluvegi, G.: Long-term ozone changes and associated climate impacts in CMIP5 simulations, *Journal of Geophysical Research: Atmospheres*, doi:10.1002/jgrd.50316, 2013.
- Falster, D. S., Brännström, Å., Dieckmann, U., and Westoby, M.: Influence of four major plant traits on average height, leaf-area cover, net primary productivity, and biomass density in single-species forests: a theoretical investigation, *Journal of Ecology*, 99, 148-164, 2011.
- Falster, D. S., and Westoby, M.: Tradeoffs between height growth rate, stem persistence and maximum height among plant species in a post-fire succession, *Oikos*, 111, 57-66, 2005.
- Farquhar, G. D., and Sharkey, T. D.: Stomatal conductance and photosynthesis, *Annual Review of Plant Physiology*, 33, 317-345, 1982.
- Farquhar, G. D., von Caemmerer, S. v., and Berry, J. A.: A biochemical model of photosynthetic CO_2 assimilation in leaves of C_3 species, *Planta*, 149, 78-90, 1980.
- Farrera, I., Harrison, S. P., Prentice, I. C., Ramstein, G., Guiot, J., Bartlein, P. J., Bonnefille, R., Bush, M., Cramer, W., and Von Grafenstein, U.: Tropical climates at the Last Glacial

- Maximum: a new synthesis of terrestrial palaeoclimate data. I. Vegetation, lake-levels and geochemistry, *Climate Dynamics*, 15, 823-856, 1999.
- Field, C. B., Randerson, J. T., and Malmström, C. M.: Global net primary production: combining ecology and remote sensing, *Remote sensing of Environment*, 51, 74-88, 1995.
- Flato, G., Marotzke, J., Abiodun, B., Braconnot, P., Chou, S. C., Collins, W., Cox, P., Driouech, F., Emori, S., Eyring, V., Forest, C., Gleckler, P., Guilyardi, E., Jakob, C., Kattsov, V., Reason, C., and Rummukainen, M.: Evaluation of Climate Models, in: *Climate Change 2013: The Physical Science Basis. Contribution of Working Group I to the Fifth Assessment Report of the Intergovernmental Panel on Climate Change*, edited by: Stocker, T. F., Qin, D., Plattner, G.-K., Tignor, M., Allen, S. K., Boschung, J., Nauels, A., Xia, Y., Bex, V., and Midgley, P. M., Cambridge University Press, Cambridge, United Kingdom and New York, NY, USA., 2013.
- Foley, J. A., Levis, S., Costa, M. H., Cramer, W., and Pollard, D.: Incorporating dynamic vegetation cover within global climate models, *Ecological Applications*, 10, 1620-1632, 2000.
- Friedlingstein, P., Cox, P., Betts, R., Bopp, L., Von Bloh, W., Brovkin, V., Cadule, P., Doney, S., Eby, M., and Fung, I.: Climate-carbon cycle feedback analysis: Results from the C4MIP model intercomparison, *Journal of Climate*, 19, 3337-3353, 2006.
- Friedrich, M., Kromer, B., Spurk, M., Hofmann, J., and Kaiser, K. F.: Paleo-environment and radiocarbon calibration as derived from Lateglacial/Early Holocene tree-ring chronologies, *Quaternary International*, 61, 27-39, 1999.
- Fritts, H. C.: *Tree rings and climate*, Elsevier, London, New York, San Francisco, 2012.
- Ganopolski, A., and Rahmstorf, S.: Rapid changes of glacial climate simulated in a coupled climate model, *Nature*, 409, 153-158, 2001.
- Gates, W. L.: The numerical simulation of ice-age climate with a global general circulation model, *Journal of the Atmospheric Sciences*, 33, 1844-1873, 1976.
- Gedalof, Z., and Berg, A. A.: Tree ring evidence for limited direct CO₂ fertilization of forests over the 20th century, *Global Biogeochemical Cycles*, 24, GB3027, 2010.
- Gerhart, L. M., Harris, J. M., Nippert, J. B., Sandquist, D. R., and Ward, J. K.: Glacial trees from the La Brea tar pits show physiological constraints of low CO₂, *New Phytologist*, 194, 63-69, 2012.

- Giorgi, F., and Mearns, L. O.: Calculation of average, uncertainty range, and reliability of regional climate changes from AOGCM simulations via the “reliability ensemble averaging”(REA) method, *Journal of Climate*, 15, 1141-1158, 2002.
- Gladstone, R. M., Ross, I., Valdes, P. J., Abe-Ouchi, A., Braconnot, P., Brewer, S., Kageyama, M., Kitoh, A., Legrande, A., and Marti, O.: Mid-Holocene NAO: A PMIP2 model intercomparison, *Geophysical Research Letters*, 32, L16707, 2005.
- Godbold, D. L., Vašutová, M., Wilkinson, A., Edwards-Jonášová, M., Bambrick, M., Smith, A. R., Pavelka, M., and Cudlin, P.: Elevated atmospheric CO₂ affects ectomycorrhizal species abundance and increases sporocarp production under field conditions, *Forests*, 6, 1256-1273, 2015.
- Graumlich, L. J.: A 1000-year record of temperature and precipitation in the Sierra Nevada, *Quaternary Research*, 39, 249-255, 1993.
- Greenwood, D. R., and Wing, S. L.: Eocene continental climates and latitudinal temperature gradients, *Geology*, 23, 1044-1048, 1995.
- Grudd, H., Briffa, K. R., Karlén, W., Bartholin, T. S., Jones, P. D., and Kromer, B.: A 7400-year tree-ring chronology in northern Swedish Lapland: natural climatic variability expressed on annual to millennial timescales, *The Holocene*, 12, 657-665, 2002.
- Guiot, I., Pons, A., and Reille, M.: A 140,000-year continental climate reconstruction from two European pollen records, *Nature*, 338, 309-313, 1989.
- Guiot, J.: Methodology of the last climatic cycle reconstruction in France from pollen data, *Palaeogeography, Palaeoclimatology, Palaeoecology*, 80, 49-69, 1990.
- Hacket-Pain, A.J., Friend, A.D., Lageard, J.G. and Thomas, P.A.:The influence of masting phenomenon on growth-climate relationships in trees: explaining the influence of previous summers' climate on ring width, *Tree Physiology*, 35, 319-330, 2015.
- Harrison, S. P., Bartlein, P. J., Brewer, S., Prentice, I. C., Boyd, M., Hessler, I., Holmgren, K., Izumi, K., and Willis, K.: Climate model benchmarking with glacial and mid-Holocene climates, *Climate Dynamics*, 43, 671-688, 2014.
- Harrison, S. P., Prentice, I. C., Sutra J-P., Barboni, D., Kohfeld, K. E. and Ni. J.: Ecophysiological and bioclimatic foundations for a global plant functional classification, *Journal of Vegetation Science*, 21, 300-317, 2010.
- Harrison, S. P., and Sanchez Goñi, M. F.: Global patterns of vegetation response to millennial-scale variability and rapid climate change during the last glacial period, *Quaternary Science Reviews*, 29, 2957-2980, 2010.

- Hartmann, D. L., Tank, A. M. G. K., Rusticucci, M., Alexander, L. V., Brönnimann, S., Charabi, Y., Dentener, F. J., Dlugokencky, E. J., Easterling, D. R., Kaplan, A., Soden, B. J., Thorne, P. W., Wild, M., and Zhai, P. M.: Observations: Atmosphere and Surface., in: Climate Change 2013: The Physical Science Basis. Contribution of Working Group I to the Fifth Assessment Report of the Intergovernmental Panel on Climate Change, edited by: Stocker, T. F., Qin, D., Plattner, G.-K., Tignor, M., Allen, S. K., Boschung, J., Nauels, A., Xia, Y., Bex, V., and Midgley, P. M., Cambridge University Press, Cambridge, United Kingdom and New York, NY, USA, 2013.
- Haxeltine, A., and Prentice, I. C.: BIOME3: An equilibrium terrestrial biosphere model based on ecophysiological constraints, resource availability, and competition among plant functional types, *Global Biogeochemical Cycles*, 10, 693-709, 1996.
- Haywood, A. M., Dowsett, H. J., Robinson, M. M., Stoll, D. K., Dolan, A. M., Lunt, D. J., Otto-Bliesner, B., and Chandler, M. A.: Pliocene Model Intercomparison Project (PlioMIP): experimental design and boundary conditions (experiment 2), *Geoscientific Model Development*, 4, 571-577, 2011.
- Haywood, A. M., Dowsett, H. J., Valdes, P. J., Lunt, D. J., Francis, J. E., and Sellwood, B. W.: Introduction. Pliocene climate, processes and problems, *Philosophical Transactions of the Royal Society of London A: Mathematical, Physical and Engineering Sciences*, 367, 3-17, 2009.
- Haywood, A. M., Valdes, P. J., and Sellwood, B. W.: Global scale palaeoclimate reconstruction of the middle Pliocene climate using the UKMO GCM: initial results, *Global and Planetary Change*, 25, 239-256, 2000.
- Henkin, Z., Seligman, N., Kafkafi, U., and Noy-Meir, I.: 'Effective growing days': a simple predictive model of the response of herbaceous plant growth in a Mediterranean ecosystem to variation in rainfall and phosphorus availability, *Journal of Ecology*, 86, 137-148, 1998.
- Herrick, J. D., and Thomas, R. B.: No photosynthetic down-regulation in sweetgum trees (*Liquidambar styraciflua* L.) after three years of CO₂ enrichment at the Duke Forest FACE experiment, *Plant, Cell & Environment*, 24, 53-64, 2001.
- Hickler, T., Vohland, K., Feehan, J., Miller, P. A., Smith, B., Costa, L., Giesecke, T., Fronzek, S., Carter, T. R., and Cramer, W.: Projecting the future distribution of European potential natural vegetation zones with a generalized, tree species-based dynamic vegetation model, *Global Ecology and Biogeography*, 21, 50-63, 2012.

- Hopcroft, P. O., Valdes, P. J., and Beerling, D. J.: Simulating idealized Dansgaard-Oeschger events and their potential impacts on the global methane cycle, *Quaternary Science Reviews*, 30, 3258-3268, 2011.
- Hu, C., Henderson, G. M., Huang, J., Xie, S., Sun, Y., and Johnson, K. R.: Quantification of Holocene Asian monsoon rainfall from spatially separated cave records, *Earth and Planetary Science Letters*, 266, 221-232, 2008.
- Huber, M., and Sloan, L. C.: Heat transport, deep waters, and thermal gradients: Coupled simulation of an Eocene greenhouse climate, *Geophysical Research Letters*, 28, 3481-3484, 2001.
- Huntley, B., and Prentice, I. C.: July temperatures in Europe from pollen data, 6000 years before present, *Science*, 241, 687-690, 1988.
- Ishii, H., Reynolds, J. H., Ford, E. D., and Shaw, D. C.: Height growth and vertical development of an old-growth *Pseudotsuga-Tsuga* forest in southwestern Washington State, USA, *Canadian Journal of Forest Research*, 30, 17-24, 2000.
- Izumi, K., Bartlein, P. J., and Harrison, S. P.: Consistent large-scale temperature responses in warm and cold climates, *Geophysical Research Letters*, 40, 1817-1823, 2013.
- Izumi, K., Bartlein, P. J., and Harrison, S. P.: Energy-balance mechanisms underlying consistent large-scale temperature responses in warm and cold climates, *Climate Dynamics*, 44, 3111-3127, 2015.
- Jackson, S. T., and Williams, J. W.: Modern analogs in Quaternary paleoecology: here today, gone yesterday, gone tomorrow?, *Annual Review of Earth and Planetary Sciences*, 32, 495-537, 2004.
- Jacoby, G. C., and D'Arrigo, R. D.: Tree ring width and density evidence of climatic and potential forest change in Alaska, *Global Biogeochemical Cycles*, 9, 227-234, 1995.
- Jacoby Jr, G. C., and D'Arrigo, R.: Reconstructed Northern Hemisphere annual temperature since 1671 based on high-latitude tree-ring data from North America, *Climatic Change*, 14, 39-59, 1989.
- James, W. O.: *Plant Respiration*, Clarendon Press, Oxford, 1953.
- Jiang, X., Maloney, E. D., Li, J. F., and Waliser, D. E.: Simulations of the eastern North Pacific intraseasonal variability in CMIP5 GCMs, *Journal of Climate*, 26, 3489-3510, 2013.
- Joussaume, S., and Taylor, K.: The paleoclimate modeling intercomparison project, *World Meteorological Organization Publications-WMO TD*, 9-24, 2000.

- Joussaume, S., Taylor, K., Braconnot, P., Mitchell, J., Kutzbach, J., Harrison, S., Prentice, I., Broccoli, A., Abe-Ouchi, A., and Bartlein, P.: Monsoon changes for 6000 years ago: results of 18 simulations from the Paleoclimate Modeling Intercomparison Project (PMIP), *Geophysical Research Letters*, 26, 859-862, 1999.
- Jungclauss, J. H., Lorenz, S. J., Timmreck, C., Reick, C. H., Brovkin, V., Six, K. et al.: Climate and carbon-cycle variability over the last millennium, *Climate of the Past*, 6, 723–737, 2010.
- Karnosky, D. F., Zak, D. R., Pregitzer, K. S., Awmack, C. S., Bockheim, J. G., Dickson, R. E., Hendrey, G. R., Host, G. E., King, J. S., and Kopper, B. J.: Tropospheric O₃ moderates responses of temperate hardwood forests to elevated CO₂: a synthesis of molecular to ecosystem results from the Aspen FACE project, *Functional Ecology*, 17, 289-304, 2003.
- Keenan, T. F., Hollinger, D. Y., Bohrer, G., Dragoni, D., Munger, J. W., Schmid, H. P., and Richardson, A. D.: Increase in forest water-use efficiency as atmospheric carbon dioxide concentrations rise, *Nature*, 499, 324-327, 2013.
- Kienast, F., and Luxmoore, R. J.: Tree-ring analysis and conifer growth responses to increased atmospheric CO₂ levels, *Oecologia*, 76, 487-495, 1988.
- Kimball, B. A., and Idso, S. B.: Increasing atmospheric CO₂: effects on crop yield, water use and climate, *Agricultural Water Management*, 7, 55-72, 1983.
- King, J., Pregitzer, K., Zak, D., Sober, J., Isebrands, J., Dickson, R., Hendrey, G., and Karnosky, D.: Fine-root biomass and fluxes of soil carbon in young stands of paper birch and trembling aspen as affected by elevated atmospheric CO₂ and tropospheric O₃, *Oecologia*, 128, 237-250, 2001.
- Kirtman, B., Power, S. B., Adedoyin, J. A., Boer, G. J., Bojariu, R., Camilloni, I., Doblas-Reyes, F. J., Fiore, A. M., Kimoto, M., and Meehl, G. A.: Near-term climate change: Projections and predictability, in: *Climate Change 2013: The Physical Science Basis. Contribution of Working Group I to the Fifth Assessment Report of the Intergovernmental Panel on Climate Change*, edited by: Stocker, T. F., Qin, D., Plattner, G.-K., Tignor, M., Allen, S. K., Boschung, J., Nauels, A., Xia, Y., Bex, V., and Midgley, P. M., Cambridge University Press, Cambridge, UK, and New York, 953-1028, 2013.
- Knorr, W., and Heimann, M.: Impact of drought stress and other factors on seasonal land biosphere CO₂ exchange studied through an atmospheric tracer transport model, *Tellus B*, 47, 471-489, 1995.
- Kobza, J., and Edwards, G. E.: Influences of leaf temperature on photosynthetic carbon metabolism in wheat, *Plant Physiology*, 83, 69-74, 1987.

- Kohfeld, K. E., and Harrison, S. P.: How well can we simulate past climates? Evaluating the models using global palaeoenvironmental datasets, *Quaternary Science Reviews*, 19, 321-346, 2000.
- Kozaki, A., and Takeba, G.: Photorespiration protects C3 plants from photooxidation, *Nature*, 384, 557-560, 1996.
- Kutzbach, J. E.: Monsoon climate of the early Holocene: climate experiment with the earth's orbital parameters for 9000 years ago, *Science*, 214, 59-61, 1981.
- Landsberg, J. J., and Waring, R. H.: A generalised model of forest productivity using simplified concepts of radiation-use efficiency, carbon balance and partitioning, *Forest Ecology and Management*, 95, 209-228, 1997.
- Leakey, A. D., Ainsworth, E. A., Bernacchi, C. J., Rogers, A., Long, S. P., and Ort, D. R.: Elevated CO₂ effects on plant carbon, nitrogen, and water relations: six important lessons from FACE, *Journal of Experimental Botany*, 60, 2859-2876, 2009.
- Leduc, G., Schneider, R., Kim, J.-H., and Lohmann, G.: Holocene and Eemian sea surface temperature trends as revealed by alkenone and Mg/Ca paleothermometry, *Quaternary Science Reviews*, 29, 989-1004, 2010.
- Li, G., Bai, F., and Sang, W.: Different responses of radial growth to climate warming in *Pinus koraiensis* and *Picea jezoensis* var. *komarovii* at their upper elevational limits in Changbai Mountain, China, *Chinese Journal of Plant Ecology*, 35, 500-511, 2011.
- Li, G., Harrison, S. P., Bartlein, P. J., Izumi, K., and Prentice, I. C.: Precipitation scaling with temperature in warm and cold climates: An analysis of CMIP5 simulations, *Geophysical Research Letters*, 40, 4018-4024, 2013.
- Liang, X., Lettenmaier, D. P., Wood, E. F., and Burges, S. J.: A simple hydrologically based model of land surface water and energy fluxes for general circulation models, *Journal of Geophysical Research*, 99, 14,415-414,415, 1994.
- Linacre, E. T.: Estimating the net-radiation flux, *Agricultural Meteorology*, 5, 49-63, 1968.
- Liu, Z., Harrison, S. P., Kutzbach, J., and Otto-Bliesner, B.: Global monsoons in the mid-Holocene and oceanic feedback, *Climate Dynamics*, 22, 157-182, 2004.
- Liu, Z., Lu, Z., Wen, X., Otto-Bliesner, B. L., Timmermann, A., and Cobb, K. M.: Evolution and forcing mechanisms of El Nino over the past 21,000 years, *Nature*, 515, 550-553, 2014.
- Lloyd, J., and Farquhar, G. D.: The CO₂ dependence of photosynthesis, plant growth responses to elevated atmospheric CO₂ concentrations and their interaction with soil nutrient status. I. General principles and forest ecosystems, *Functional Ecology*, 10, 4-32, 1996.

- Lowenstein, T. K., and Demicco, R. V.: Elevated Eocene atmospheric CO₂ and its subsequent decline, *Science*, 313, 1928-1928, 2006.
- Lukac, M., Calfapietra, C., and Godbold, D. L.: Production, turnover and mycorrhizal colonization of root systems of three *Populus* species grown under elevated CO₂ (POPFACE), *Global Change Biology*, 9, 838-848, 2003.
- Lunt, D. J., Haywood, A. M., Schmidt, G. A., Salzmann, U., Valdes, P. J., and Dowsett, H. J.: Earth system sensitivity inferred from Pliocene modelling and data, *Nature Geoscience*, 3, 60-64, 2010.
- Magny, M.: Holocene climate variability as reflected by mid-European lake-level fluctuations and its probable impact on prehistoric human settlements, *Quaternary International*, 113, 65-79, 2004.
- Mäkelä, A., Landsberg, J., Ek, A. R., Burk, T. E., Ter-Mikaelian, M., Ågren, G. I., Oliver, C. D., and Puttonen, P.: Process-based models for forest ecosystem management: current state of the art and challenges for practical implementation, *Tree Physiology*, 20, 289-298, 2000.
- Manabe, S., and Hahn, D. G.: Simulation of the tropical climate of an ice age, *Journal of Geophysics Research*, 82, 3889-3911, 1977.
- Manabe, S., Smagorinsky, J., and Strickler, R. F.: Simulated climatology of a general circulation model with a hydrologic cycle 1, *Monthly Weather Review*, 93, 769-798, 1965.
- Manabe, S., and Stouffer, R. J.: Coupled ocean-atmosphere model response to freshwater input: Comparison to Younger Dryas event, *Paleoceanography*, 12, 321-336, 1997.
- Mann, M. E., and Jones, P. D.: Global surface temperatures over the past two millennia, *Geophysical Research Letters*, 30, 1820, 2003.
- Martin Calvo, M., Prentice, I. C., and Harrison, S. P.: Climate versus carbon dioxide controls on biomass burning: a model analysis of the glacial-interglacial contrast, 11, 6017-6027, 2014.
- Marzin, C., Braconnot, P., and Kageyama, M.: Relative impacts of insolation changes, meltwater fluxes and ice sheets on African and Asian monsoons during the Holocene. *Climate dynamics*, 41, 2267-2286, 2013.
- Masson-Delmotte, V., Schulz, M., Abe-Ouchi, A., Beer, J., Ganopolski, A., Rouco, J. F. G., Jansen, E., Lambeck, K., Luterbacher, J., Naish, T., Osborn, T., Otto-Bliesner, B., Quinn, T., Ramesh, R., Rojas, M., Shao, X., and Timmermann, A.: Information from Paleoclimate Archives, in: *Climate Change 2013: The Physical Science Basis. Contribution of Working Group I to the Fifth Assessment Report of the Intergovernmental Panel on Climate*

- Change, edited by: Stocker, T. F., Qin, D., Plattner, G.-K., Tignor, M., Allen, S. K., Boschung, J., Nauels, A., Xia, Y., Bex, V., and Midgley, P. M., Cambridge University Press, Cambridge University Press, Cambridge, United Kingdom and New York, NY, USA, 2013.
- Mauri, A., Davis, B. A. S., Collins, P. M., and Kaplan, J. O.: The influence of atmospheric circulation on the mid-Holocene climate of Europe: a data–model comparison, *Climate of the Past*, 10, 1925-1938, 2014.
- McCree, K. J.: Photosynthetically active radiation, in: *Physiological Plant Ecology I*, Springer, 41-55, 1981.
- McDermott, F.: Palaeo-climate reconstruction from stable isotope variations in speleothems: a review, *Quaternary Science Reviews*, 23, 901-918, 2004.
- McGregor, H. V., and Gagan, M. K.: Western Pacific coral $\delta^{18}\text{O}$ records of anomalous Holocene variability in the El Niño–Southern Oscillation, *Geophysical Research Letters*, 31, L11204, 2004.
- Medlyn, B. E.: Physiological basis of the light use efficiency model, *Tree Physiology*, 18, 167-176, 1998.
- Meinshausen, M., Meinshausen, N., Hare, W., Raper, S. C., Frieler, K., Knutti, R., Frame, D. J., and Allen, M. R.: Greenhouse-gas emission targets for limiting global warming to 2 °C, *Nature*, 458, 1158-1162, 2009.
- Menviel, L., Timmermann, A., Friedrich, T., and England, M.: Hindcasting the continuum of Dansgaard–Oeschger variability: mechanisms, patterns and timing, *Climate of the Past*, 10, 63-77, 2014.
- Mikolajewicz, U., Crowley, T. J., Schiller, A., and Voss, R.: Modelling teleconnections between the North Atlantic and North Pacific during the Younger Dryas, *Nature*, 387, 384-387, 1997.
- Misson, L.: MAIDEN: a model for analyzing ecosystem processes in dendroecology, *Canadian Journal of Forest Research*, 34, 874-887, 2004.
- Misson, L., Rathgeber, C., and Guiot, J.: Dendroecological analysis of climatic effects on *Quercus petraea* and *Pinus halepensis* radial growth using the process-based MAIDEN model, *Canadian Journal of Forest Research*, 34, 888-898, 2004.
- Monteith, J. L.: Solar radiation and productivity in tropical ecosystems, *Journal of Applied Ecology*, 9, 747-766, 1972.

- Morice, C. P., Kennedy, J. J., Rayner, N. A., and Jones, P. D.: Quantifying uncertainties in global and regional temperature change using an ensemble of observational estimates: The HadCRUT4 data set, *Journal of Geophysical Research: Atmospheres*, 117, D08101, 2012.
- Naurzbaev, M. M., Vaganov, E. A., Sidorova, O. V., and Schweingruber, F. H.: Summer temperatures in eastern Taimyr inferred from a 2427-year late-Holocene tree-ring chronology and earlier floating series, *The Holocene*, 12, 727-736, 2002.
- Norby, R. J., Hanson, P. J., O'Neill, E. G., Tschaplinski, T. J., Weltzin, J. F., Hansen, R. A., Cheng, W., Wullschleger, S. D., Gunderson, C. A., and Edwards, N. T.: Net primary productivity of a CO₂-enriched deciduous forest and the implications for carbon storage, *Ecological Applications*, 12, 1261-1266, 2002.
- Norby, R. J., Ledford, J., Reilly, C. D., Miller, N. E., and O'Neill, E. G.: Fine-root production dominates response of a deciduous forest to atmospheric CO₂ enrichment, *Proceedings of the National Academy of Sciences of the United States of America*, 101, 9689-9693, 2004.
- Obeso, J. R.: The costs of reproduction in plants, *New Phytologist*, 155, 321–348, 2002.
- Oren, R., Sperry, J. S., Katul, G. G., Pataki, D. E., Ewers, B. E., Phillips, N., and Schafer, K. V. R.: Survey and synthesis of intra-and interspecific variation in stomatal sensitivity to vapour pressure deficit, *Plant Cell and Environment*, 22, 1515-1526, 1999.
- Overpeck, J. T., Webb, T., and Prentice, I. C.: Quantitative interpretation of fossil pollen spectra: dissimilarity coefficients and the method of modern analogs, *Quaternary Research*, 23, 87-108, 1985.
- PAGES 2k Consortium: Continental-scale temperature variability during the past two millennia, *Nature Geoscience*, 6, 339-346, 2013.
- Pechony, O., and Shindell D. T.: Fire parameterization on a global scale, *Journal of Geophysical Research: Atmospheres*, 114, D16115, 2009.
- Peñuelas, J., Canadell, J. G., and Ogaya, R.: Increased water-use efficiency during the 20th century did not translate into enhanced tree growth, *Global Ecology and Biogeography*, 20, 597-608, 2011.
- Pérez Sanz, A., Li, G., González-Sampériz, P., and Harrison, S. P.: Evaluation of modern and mid-Holocene seasonal precipitation of the Mediterranean and northern Africa in the CMIP5 simulations, *Climate of the Past*, 10, 551-568, 2014.
- Petit, J.-R., Jouzel, J., Raynaud, D., Barkov, N. I., Barnola, J.-M., Basile, I., Bender, M., Chappellaz, J., Davis, M., and Delaygue, G.: Climate and atmospheric history of the past 420,000 years from the Vostok ice core, Antarctica, *Nature*, 399, 429-436, 1999.

- Peyron, O., Guiot, J., Cheddadi, R., Tarasov, P., Reille, M., de Beaulieu, J.-L., Bottema, S., and Andrieu, V.: Climatic reconstruction in Europe for 18,000 yr BP from pollen data, *Quaternary Research*, 49, 183-196, 1998.
- Pinot, S., Ramstein, G., Harrison, S. P., Prentice, I. C., Guiot, J., Stute, M., and Joussaume, S.: Tropical paleoclimates at the Last Glacial Maximum: comparison of Paleoclimate Modeling Intercomparison Project (PMIP) simulations and paleodata, *Climate Dynamics*, 15, 857-874, 1999.
- PMIP: Paleoclimate Modelling Intercomparison Project (PMIP): Proceedings of the Third PMIP Workshop (La Huardière, Canada, 4-8 October 1999), Joint Planning Staff for WCRP, World Meteorological Organization, 2000.
- Potter, C. S., Randerson, J. T., Field, C. B., Matson, P. A., Vitousek, P. M., Mooney, H. A., and Klooster, S. A.: Terrestrial ecosystem production: a process model based on global satellite and surface data, *Global Biogeochemical Cycles*, 7, 811-841, 1993.
- Prado, L. F., Wainer, I., and Chiessi, C. M.: Mid-Holocene PMIP3/CMIP5 model results: Intercomparison for the South American Monsoon System, *The Holocene*, 0959683613505336, doi: 10.1177/0959683613505336, 2013.
- Prentice, I. C., Dong, N., Gleason, S. M., Maire, V., and Wright, I. J.: Balancing the costs of carbon gain and water transport: testing a new theoretical framework for plant functional ecology, *Ecology Letters*, 17, 82-91, 2014.
- Prentice, I. C., Harrison, S. P., and Bartlein, P. J.: Global vegetation and terrestrial carbon cycle changes after the last ice age, *New Phytologist*, 189, 988-998, 2011.
- Prentice, I. C., and Webb III, T.: BIOME 6000: reconstructing global mid-Holocene vegetation patterns from palaeoecological records, *Journal of Biogeography*, 25, 997-1005, 1998.
- Pritchard, S. G., Strand, A. E., McCormack, M., Davis, M. A., Finzi, A. C., Jackson, R. B., Matamala, R., Rogers, H. H., and Oren, R.: Fine root dynamics in a loblolly pine forest are influenced by free-air-CO₂-enrichment: A six-year-minirhizotron study, *Global Change Biology*, 14, 588-602, 2008.
- Qin, B., Harrison, S. P., and Kutzbach, J. E.: Evaluation of modelled regional water balance using lake status data: a comparison of 6ka simulations with the NCAR CCM, *Quaternary Science Reviews*, 17, 535-548, 1998.
- Reich, P. B., Hobbie, S. E., Lee, T., Ellsworth, D. S., West, J. B., Tilman, D., Knops, J. M., Naeem, S., and Trost, J.: Nitrogen limitation constrains sustainability of ecosystem response to CO₂, *Nature*, 440, 922-925, 2006.

- Renssen, H., Isarin, R. F. B., Jacob, D., Podzun, R., and Vandenberghe, J.: Simulation of the Younger Dryas climate in Europe using a regional climate model nested in an AGCM: preliminary results, *Global and Planetary Change*, 30, 41-57, 2001.
- Rimbu, N., Lohmann, G., Lorenz, S. J., Kim, J.-H., and Schneider, R.: Holocene climate variability as derived from alkenone sea surface temperature and coupled ocean-atmosphere model experiments, *Climate Dynamics*, 23, 215-227, 2004.
- Roeckner, E., Bäuml, G., Bonaventura, L., Brokopf, R., Esch, M., Giorgetta, M., Hagemann, S., Kirchner, I., Kornblueh, L., and Manzini, E.: The atmospheric general circulation model ECHAM 5. PART I: Model description, Hamburg, Germany, 2003.
- Rojas, M.: Sensitivity of Southern Hemisphere circulation to LGM and 4×CO₂ climates, *Geophysical Research Letters*, 40, 965-970, 2013.
- Rosas T., Galiano L., Ogaya R., Peñuelas J., Martínez-Vilalta J: Dynamics of non-structural carbohydrates in three Mediterranean woody species following long-term experimental drought, *Frontiers in Plant Science*, 4, 400, doi:10.3389/fpls.2013.00400, 2013.
- Rotstayn, L.D., Collier, M.A., Dix, M.R., Feng, Y., Gordon, H.B., O'Farrell, S.P., Smith, I.N. and Syktus, J.: Improved simulation of Australian climate and ENSO related rainfall variability in a global climate model with an interactive aerosol treatment, *International Journal of Climatology*, 30, 1067–1088, 2010.
- Running, S. W., Nemani, R. R., Heinsch, F. A., Zhao, M., Reeves, M., and Hashimoto, H.: A continuous satellite-derived measure of global terrestrial primary production, *Bioscience*, 54, 547-560, 2004.
- Sage, R. F.: Acclimation of photosynthesis to increasing atmospheric CO₂: the gas exchange perspective, *Photosynthesis Research*, 39, 351-368, 1994.
- Saliendra, N. Z., Sperry, J. S., and Comstock, J. P.: Influence of leaf water status on stomatal response to humidity, hydraulic conductance, and soil drought in *Betula occidentalis*, *Planta*, 196, 357-366, 1995.
- Schmidt, G. A., Annan, J. D., Bartlein, P. J., Cook, B. I., Guilyardi, E., Hargreaves, J. C., Harrison, S. P., Kageyama, M., LeGrande, A. N., and Konecky, B.: Using palaeo-climate comparisons to constrain future projections in CMIP5, *Climate of the Past*, 10, 221-250, 2014.
- Schmidt, G. A., Jungclaus, J. H., Ammann, C. M., Bard, E., Braconnot, P., Crowley, T. J., Delaygue, G., Joos, F., Krivova, N. A., and Muscheler, R.: Climate forcing reconstructions for use in PMIP simulations of the last millennium (v1. 0), *Geoscientific Model Development*, 4, 33-45, 2011.

- Schmittner, A., Urban, N. M., Shakun, J. D., Mahowald, N. M., Clark, P. U., Bartlein, P. J., Mix, A. C., and Rosell-Mele, A.: Climate sensitivity estimated from temperature reconstructions of the Last Glacial Maximum, *Science*, 334, 1385-1388, 2011.
- Schurgers, G., U. Mikolajewicz, M. Groger, E. Maier-Reimer, M. Vizcaino, and A. Winguth,: Long-term effects of biogeophysical and biogeochemical interactions between terrestrial biosphere and climate under anthropogenic climate change. *Global Planet Change*, 64, 26–37, 2008.
- Sellers, W. D.: A global climatic model based on the energy balance of the earth-atmosphere system, *Journal of Applied Meteorology*, 8, 392-400, 1969.
- Shinozaki, K., Yoda, K., Hozumi, K., and Kira, T.: A quantitative analysis of plant form-the pipe model theory: I. Basic analyses, *Japan Journal of Ecology*, 14, 97-105, 1964.
- Simard S., Giovannelli A., Treydte K., Traversi M. L., King G. M., Frank D., and Fonti P.: Intra-annual dynamics of non-structural carbohydrates in the cambium of mature conifer trees reflects radial growth demands, *Tree Physiology*, 9, 913-923 doi:10.1093/treephys/tpt075, 2013.
- Sitch, S., Smith, B., Prentice, I. C., Arneth, A., Bondeau, A., Cramer, W., Kaplan, J., Levis, S., Lucht, W., and Sykes, M. T.: Evaluation of ecosystem dynamics, plant geography and terrestrial carbon cycling in the LPJ dynamic global vegetation model, *Global Change Biology*, 9, 161-185, 2003.
- Sloan, L. C., and Rea, D.: Atmospheric carbon dioxide and early Eocene climate: A general circulation modeling sensitivity study, *Palaeogeography, Palaeoclimatology, Palaeoecology*, 119, 275-292, 1996.
- Smith, R. N. B.: A scheme for predicting layer clouds and their water content in a general circulation model, *Quarterly Journal of the Royal Meteorological Society*, 116, 435-460, 1990.
- Steig, E. J.: Mid-Holocene climate change, *Science*, 286, 1485-1487, 1999.
- Stine, A. R., and Huybers, P.: Arctic tree rings as recorders of variations in light availability, *Nature Communications*, 5, 3836, doi: 10.1038/ncomms4836, 2014.
- Street-Perrott, F. A., and Harrison, S. P.: Lake levels and climate reconstruction, in: *Palaeoclimatic Analysis and Modelling*, edited by: Hecht, A. D., John Wiley, New York, 291-340, 1985.
- Sun, S., and Hansen, J. E.: Climate simulations for 1951-2050 with a coupled atmosphere-ocean model, *Journal of Climate*, 16, 2807-2826, 2003.

- Sykes, M. T., and Prentice, I. C.: Boreal forest futures: modelling the controls on tree species range limits and transient responses to climate change, in: *Boreal Forests and Global Change*, edited by: Apps, M. J., Price, D. T., and Wisniewski, J., Springer, 415-428, 1995.
- Taylor, K. E., Stouffer, R. J., and Meehl, G. A.: An overview of CMIP5 and the experiment design, *Bulletin of the American Meteorological Society*, 93, 485-498, 2012.
- Thomas, S. C.: Asymptotic height as a predictor of growth and allometric characteristics in Malaysian rain forest trees, *American Journal of Botany*, 83, 556-566, 1996.
- Thompson, D. M., Ault, T. R., Evans, M. N., Cole, J. E., and Emile-Geay, J.: Comparison of observed and simulated tropical climate trends using a forward model of coral $\delta^{18}\text{O}$, *Geophysical Research Letters*, 38, L14706, 2011.
- Thompson, L. G., Mosley-Thompson, E., Davis, M. E., Lin, P.-N., Henderson, K., and Mashiotta, T. A.: Tropical glacier and ice core evidence of climate change on annual to millennial time scales, in: *Climate Variability and Change in High Elevation Regions: Past, Present & Future*, edited by: Diaz, H. F., Springer, 137-155, 2003.
- Thompson, R. S., Whitlock, C., Bartlein, P. J., Harrison, S. P., and Spaulding, W. G.: Climatic changes in the western United States since 18,000 yr BP, in: *Global climates since the last glacial maximum*, University of Minnesota Press, Minneapolis, 468-513, 1993.
- Thonicke, K., Spessa, A., Prentice, I., Harrison, S. P., Dong, L., and Carmona-Moreno, C.: The influence of vegetation, fire spread and fire behaviour on biomass burning and trace gas emissions: results from a process-based model, *Biogeosciences*, 7, 1991-2011, 2010.
- Thornton, P. E., Lamarque, J. F., Rosenbloom, N. A., and Mahowald, N. M.: Influence of carbon-nitrogen cycle coupling on land model response to CO_2 fertilization and climate variability, *Global Biogeochemical Cycles*, 21, GB4018, 2007.
- Timmermann, A., Oberhuber, J., Bacher, A., Esch, M., Latif, M., and Roeckner, E.: Increased El Niño frequency in a climate model forced by future greenhouse warming, *Nature*, 398, 694-697, 1999.
- Tudhope, A. W., Chilcott, C. P., McCulloch, M. T., Cook, E. R., Chappell, J., Ellam, R. M., Lea, D. W., Lough, J. M., and Shimmield, G. B.: Variability in the El Niño-Southern Oscillation through a glacial-interglacial cycle, *Science*, 291, 1511-1517, 2001.
- Vaganov, E. A., Hughes, M. K., and Shashkin, A. V.: *Growth Dynamics of Conifer Tree Rings: Images of Past and Future Environments*, Springer, Berlin, Heidelberg, New York, 2006.

- van der Sleen, P., Groenendijk, P., Vlam, M., Anten, N. P., Boom, A., Bongers, F., Pons, T. L., Terburg, G., and Zuidema, P. A.: No growth stimulation of tropical trees by 150 years of CO₂ fertilization but water-use efficiency increased, *Nature Geoscience*, 8, 24-28, 2015.
- Veski, S., Seppä, H., and Ojala, A. E.: Cold event at 8200 yr BP recorded in annually laminated lake sediments in eastern Europe, *Geology*, 32, 681-684, 2004.
- Waelbroeck, C., Paul, A., Kucera, M., Rosell-Melé, A., Weinelt, M., Schneider, R., Mix, A., Abelmann, A., Armand, L., and Bard, E.: Constraints on the magnitude and patterns of ocean cooling at the Last Glacial Maximum, *Nature Geoscience*, 2, 127-132, 2009.
- Walker, T. S., Bais, H. P., Grotewold, E. and Vivanco, J. M.: Root Exudation and Rhizosphere Biology, *Plant Physiology*, 132, 44-51, 2003.
- Wang, H., Prentice, I., and Davis, T.: Biophysical constraints on gross primary production by the terrestrial biosphere, *Biogeosciences*, 11, 5987-6001, 2014.
- Wang, Y., Cheng, H., Edwards, R. L., Kong, X., Shao, X., Chen, S., Wu, J., Jiang, X., Wang, X., and An, Z.: Millennial-and orbital-scale changes in the East Asian monsoon over the past 224,000 years, *Nature*, 451, 1090-1093, 2008.
- Wannera, H., Beerb, J., Bütikofera, J., Crowleyc, T. J., Cubaschd, U., Flückigere, J., Goossef, H., Grosjeana, M., Joosg, F., Kaplanh, J. O., Küttela, M., Müllerg, S. A., Prenticei, I. C., Solominaj, O., Stockerg, T. F., Tarasovk, P., Wagnerl, M., and Widmannm, M.: Mid-to Late Holocene climate change: an overview, *Quaternary Science Reviews*, 27, 1791-1828, 2008.
- Ward, P. J., Aerts, J. C., de Moel, H., and Renssen, H.: Verification of a coupled climate-hydrological model against Holocene palaeohydrological records, *Global and Planetary Change*, 57, 283-300, 2007.
- Whitlock, C., and Bartlein, P. J.: Vegetation and climate change in northwest America during the past 125 kyr, *Nature*, 388, 57-61, 1997.
- Wilson, R., D'Arrigo, R., Buckley, B., Büntgen, U., Esper, J., Frank, D., Luckman, B., Payette, S., Vose, R., and Youngblut, D.: A matter of divergence: tracking recent warming at hemispheric scales using tree ring data, *Journal of Geophysical Research: Atmospheres*, 112, D17103, 2007.
- Wilson, R. J., and Luckman, B. H.: Tree-ring reconstruction of maximum and minimum temperatures and the diurnal temperature range in British Columbia, Canada, *Dendrochronologia*, 20, 257-268, 2002.

- Wohlfahrt, J., Harrison, S. P., and Braconnot, P.: Synergistic feedbacks between ocean and vegetation on mid-and high-latitude climates during the mid-Holocene, *Climate Dynamics*, 22, 223-238, 2004.
- Wright, I. J., and Westoby, M.: Leaves at low versus high rainfall: coordination of structure, lifespan and physiology, *New Phytologist*, 155, 403-416, 2002.
- Yokozawa, M., and Hara, T.: Foliage profile, size structure and stem diameter-plant height relationship in crowded plant populations, *Annals of Botany*, 76, 271-285, 1995.
- Yu, G., and Harrison, S. P.: An evaluation of the simulated water balance of Eurasia and northern Africa at 6000 y BP using lake status data, *Climate Dynamics*, 12, 723-735, 1996.
- Zak, D. R., Holmes, W. E., Finzi, A. C., Norby, R. J., and Schlesinger, W. H.: Soil nitrogen cycling under elevated CO₂: a synthesis of forest FACE experiments, *Ecological Applications*, 13, 1508-1514, 2003.
- Zaehle, S., and Dalmonech D.: Carbon-nitrogen interactions on land at global scales: Current understanding in modelling climate biosphere feedbacks, *Current Opinion in Environmental Sustainability*, 3, 311–320, 2011.
- Zhang, P., Cheng, H., Edwards, R. L., Chen, F., Wang, Y., Yang, X., Liu, J., Tan, M., Wang, X., and Liu, J.: A test of climate, sun, and culture relationships from an 1810-year Chinese cave record, *Science*, 322, 940-942, 2008.
- Zhao, Y., Braconnot, P., Marti, O., Harrison, S. P., Hewitt, C., Kitoh, A., Liu, Z., Mikolajewicz, U., Otto-Bliesner, B., and Weber, S. L.: A multi-model analysis of the role of the ocean on the African and Indian monsoon during the mid-Holocene, *Climate Dynamics*, 25, 777-800, 2005.
- Zhao, Y., and Harrison, S. P.: Mid-Holocene monsoons: a multi-model analysis of the inter-hemispheric differences in the responses to orbital forcing and ocean feedbacks, *Climate Dynamics*, 39, 1457-1487, 2012.

Chapter 2

Precipitation scaling with temperature in warm and cold climates: An analysis of CMIP5 simulations

Contribution by Co-Authors: G. L. was responsible for data analysis, figure and table generation; theoretical analysis of the energy-balance constraints was provided by I.C.P.; P.J.B., and K.I. performed the initial processing of CMIP5 model outputs; All authors were involved in interpretation of the data. G.L. and S.P.H. drafted the first version of the text, and all authors contributed to the final version.

Precipitation scaling with temperature in warm and cold climates: An analysis of CMIP5 simulations

Guangqi Li,¹ Sandy P. Harrison,^{1,2} Patrick J. Bartlein,³ Kenji Izumi,³
and I. Colin Prentice^{1,4}

Received 10 May 2013; revised 3 July 2013; accepted 9 July 2013; published 2 August 2013.

[1] We investigate the scaling between precipitation and temperature changes in warm and cold climates using six models that have simulated the response to both increased CO₂ and Last Glacial Maximum (LGM) boundary conditions. Globally, precipitation increases in warm climates and decreases in cold climates by between 1.5%/°C and 3%/°C. Precipitation sensitivity to temperature changes is lower over the land than over the ocean and lower over the tropical land than over the extratropical land, reflecting the constraint of water availability. The wet tropics get wetter in warm climates and drier in cold climates, but the changes in dry areas differ among models. Seasonal changes of tropical precipitation in a warmer world also reflect this “rich get richer” syndrome. Precipitation seasonality is decreased in the cold-climate state. The simulated changes in precipitation per degree temperature change are comparable to the observed changes in both the historical period and the LGM. **Citation:** Li, G., S. P. Harrison, P. J. Bartlein, K. Izumi, and I. Colin Prentice (2013), Precipitation scaling with temperature in warm and cold climates: An analysis of CMIP5 simulations, *Geophys. Res. Lett.*, 40, 4018–4024, doi:10.1002/grl.50730.

1. Introduction

[2] Changes in the hydrological cycle are expected to scale with temperature changes. Recent observations, as well as model simulations of the 20th century and the response to anthropogenic increases in CO₂, have shown that precipitation increases in a warming world [Meehl *et al.*, 2007]. The water vapor holding capacity of the lower troposphere increases by ~7% per degree of warming following the Clausius-Clapeyron relationship, which is well approximated by

$$e_s = 0.6108 e^{\frac{aT}{b+T}} \quad (1)$$

where e_s is the saturation vapor pressure (kPa), T is air temperature (°C), $a=17.27$, and $b=237.3$ °C. The observed and

simulated changes in precipitation, however, are consistently smaller than the changes in the saturation vapor pressure [Allan and Soden, 2007, 2008; Adler *et al.*, 2008; DiNezio *et al.*, 2011]. The difference between the two reflects energetic constraints on evaporation [Allan, 2009; Allen and Ingram, 2002; Previdi, 2010; Richter and Xie, 2008]. Equilibrium evaporation, which is the theoretical rate of evaporation (including transpiration) from a large, uniform, wet or well-watered surface, is given by

$$\lambda E_q = R_n \frac{de_s/dT}{de_s/dT + \gamma} \quad (2)$$

where λ is the latent heat of vaporization of water (≈ 2.45 MJ kg⁻¹), R_n is net radiation, and γ is the psychrometer constant (≈ 0.067 kPa K⁻¹ at sea level). The maximum evaporative fraction (the fraction of R_n that can be used for evaporation under equilibrium conditions) increases less steeply than the saturation vapor pressure, ~1%–4% per degree for temperatures in the range of 0°C–30°C (Figure 1). Equation (2) emphasizes the surface energy-balance constraint on evaporation. In contrast, vapor pressure deficit (a key predictor of evaporation in standard bulk formulae [e.g., Richter and Xie, 2008]) can be regarded as an outcome of rather than a constraint on evaporation [Raupach, 2000]. Indeed, Richter and Xie [2008] showed how key boundary layer properties influencing evaporation can change in response to large-scale changes in the surface energy balance. Water availability can place an additional constraint on evaporation from the land surface and hence further mute the increase of continental precipitation as temperature increases [Trenberth and Shea, 2005].

[3] Analyses of recent changes in tropical rainfall have shown that precipitation has increased markedly in wet regions and has decreased in subtropical dry regions [Adler *et al.*, 2008; Allan and Soden, 2007; Wentz *et al.*, 2007; Zhang *et al.*, 2007; Allan *et al.*, 2010]. This is also a feature of seasonal climates, with summer (monsoon) precipitation increasing more than winter (dry season) precipitation [Giorgi and Bi, 2005; Chou *et al.*, 2013]. This phenomenon has been referred to as “the rich get richer” syndrome [Trenberth, 2011] and can be explained either as a result of increasing the amount of atmospheric water vapor [Held and Soden, 2006] or from diversion of moisture into regions of atmospheric convergence associated with changes in atmospheric circulation [DiNezio *et al.*, 2011]. Trenberth and Shea [2005] suggested that a similar syndrome is also characteristic of extratropical regions, which is expected since these are regions of net moisture import from lower latitudes. Model simulations of the 20th and 21st centuries from the last round of the Coupled Model Intercomparison Project (CMIP3) show similar tendencies, with wetting in convergence regions and drying in the subtropics associated

Additional supporting information may be found in the online version of this article.

¹Department of Biological Sciences, Macquarie University, North Ryde, New South Wales, Australia.

²Department of Geography and Environmental Sciences, School of Human and Environmental Sciences, Reading University, Reading, UK.

³Department of Geography, University of Oregon, Eugene, Oregon, USA.

⁴AXA Chair of Biosphere and Climate Impacts, Department of Life Sciences and Grantham Institute for Climate Change, Imperial College, Ascot, UK.

Corresponding author: G. Li, Department of Biological Sciences, Macquarie University, North Ryde, NSW 2109, Australia. (guangqi.li@students.mq.edu.au)

©2013. American Geophysical Union. All Rights Reserved.
0094-8276/13/10.1002/grl.50730

LI ET AL.: CMIP5 PRECIPITATION: TEMPERATURE SCALING

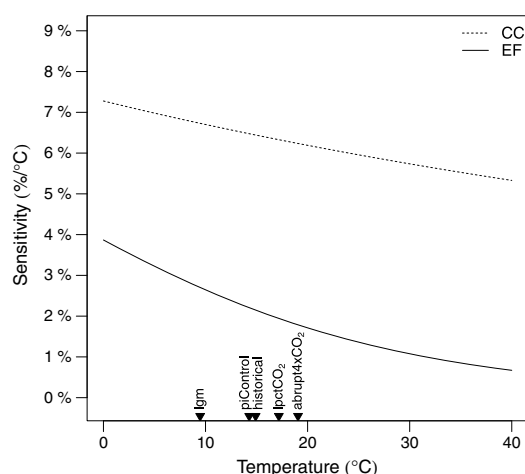


Figure 1. Theoretical limits on the rate of increase of precipitation with temperature, according to alternative hypotheses: (a) following the temperature dependence of the saturated vapor pressure of water, according to the Clausius-Clapeyron relationship (dotted line, CC); (b) following the temperature dependence of the fraction of net radiation that can be used for evaporation under equilibrium conditions (solid line, EF). The global ensemble mean temperature for each of the experiments is shown in order to place the simulated changes in context.

with a strengthening of the Walker circulation [DiNezio *et al.*, 2011]. However, the response of the tropical circulation is influenced by multiple processes operating on different time scales (e.g., water vapor [Bony *et al.*, 2013]), and the response of precipitation is weaker than that shown by the observational record and differs among different models [Allan and Soden, 2008].

[4] The observational record is short, and the strength of the precipitation response to temperature has been controversial [Wentz *et al.*, 2007; Adler *et al.*, 2008; Gu *et al.*, 2007; Huffman *et al.*, 2009; Trenberth, 2011]. Thus, it is still unclear whether the discrepancy between CMIP3 model results and observations is significant. Recent analyses [Izumi *et al.*, 2013] have shown that the simulated large-scale patterns of temperature changes at the Last Glacial Maximum (LGM) are remarkably similar (though of opposite sign) to those shown in raised CO_2 experiments. These signals include changes of comparable magnitude in the land-sea temperature contrast, in the magnitude of high-latitude amplification of temperature changes, and changes in seasonality in response to year-round forcing, and the simulated patterns are consistent with those in paleoclimatic or instrumental observations. Thus, the LGM experiments provide an opportunity to examine precipitation scaling with temperature and the regional patterns of precipitation changes and to determine whether these are consistent with paleo-observations.

[5] Here we analyze outputs from six models that have run both LGM and raised CO_2 experiments in CMIP5. We evaluate whether the raised CO_2 experiments show similar changes in precipitation to the earlier CMIP3 experiments and then examine whether consistent changes are also present in the cold-climate state of the LGM. The LGM is an equilibrium

experiment comparable to the CMIP5 $4\times\text{CO}_2$ experiment, but we also use the CMIP5 1% CO_2 per year transient experiment in our analyses. Finally, we examine the consistency between simulated and observed changes in precipitation scaling at the LGM and during the historic period to determine whether simulated changes in precipitation are realistic.

2. Methods

[6] Six CMIP5 models (IPSL-CM5A-LR, MPI-ESM-P, MIROC-ESM, CCSM4, MRI-CGCM3, and GISS-E2-R) have performed both the LGM and raised CO_2 experiments. In our analyses, we use five simulations. Following the CMIP5 naming conventions, these are the Last Glacial Maximum (*lgm*), a preindustrial control simulation (*piControl*), a 20th century simulation (*historical*), a transient 1% per year increase in CO_2 over the simulation (*1pctCO2*), and an abrupt change to $4\times\text{CO}_2$ (*abrupt4xCO2*). *lgm*, *piControl*, and *abrupt4xCO2* are equilibrium experiments, and *historical* and *1pctCO2* are transient experiments. The boundary conditions for each experiment are described in Taylor *et al.* [2012]. The *lgm* experiment represents a cold-climate state, in response to low greenhouse gas concentrations and expanded Northern Hemisphere ice sheets. The *1pctCO2* and *abrupt4xCO2* experiments represent warm-climate states, in response to increased greenhouse gas concentrations. The CO_2 concentration at the end of *1pctCO2* is similar to the CO_2 concentration used in the *abrupt4xCO2* experiment. To provide an alternative realization of a warm-climate state, we therefore sampled the middle part of the *1pctCO2* experiment (model years 86–115) when the CO_2 level was approximately 750 ppm. The total forcing in the *lgm* and $4\times\text{CO}_2$ experiments is similar but, although greenhouse gases are the dominant contributor to the tropical forcing at the *lgm* experiment, they contribute only about half (2.85 Wm^{-2}) of the total global forcing [Braconnot *et al.*, 2012].

[7] To compare the results from different models, with different spatial resolutions, the outputs of each model were regrided onto a common $2^\circ \times 2^\circ$ grid. Land grid-cells were defined as those $2^\circ \times 2^\circ$ cells with a land fraction of $>40\%$. The near-surface air temperature (*tas*) was used over the land and sea ice-covered sea surface (*sic* $\geq 40\%$), and the sea surface temperature (*tos*) was used over the ocean (*sic* $< 40\%$). (We use *tos* for ocean temperatures to facilitate comparisons with historical and paleoreconstructions of sea-surface temperatures; differences in *tos* and *tas* in ice-free areas are negligible.) The changes in precipitation and temperature for each experiment and model are expressed as anomalies from that model's *piControl* (experiment minus control), except in the case of the *historical* simulation, where the anomaly is calculated as the difference between the first and last 27 years of the simulation. We adopted this approach because the temperature at the beginning of the *historical* run is different from the corresponding PI simulation for most of the models (CCSM4, GISS-E2-R, IPSL-CM5A-LR, and MIROC-ESM); the 27 year interval is the length of the baseline period used for the calculation of anomalies in the HadCRUT4 data set. Area-averaged values are calculated for the globe, the tropics (here defined as 30°N – 30°S) and the extratropics ($>30^\circ\text{N}$ and $>30^\circ\text{S}$). We analyzed the seasonal climate changes in terms of changes in the wettest and driest month ((mean precipitation of the wettest month (MPWE) and mean precipitation of the driest month (MPDR)). The delimitation of wet and dry regions was made using precipitation deciles of the

LI ET AL.: CMIP5 PRECIPITATION: TEMPERATURE SCALING

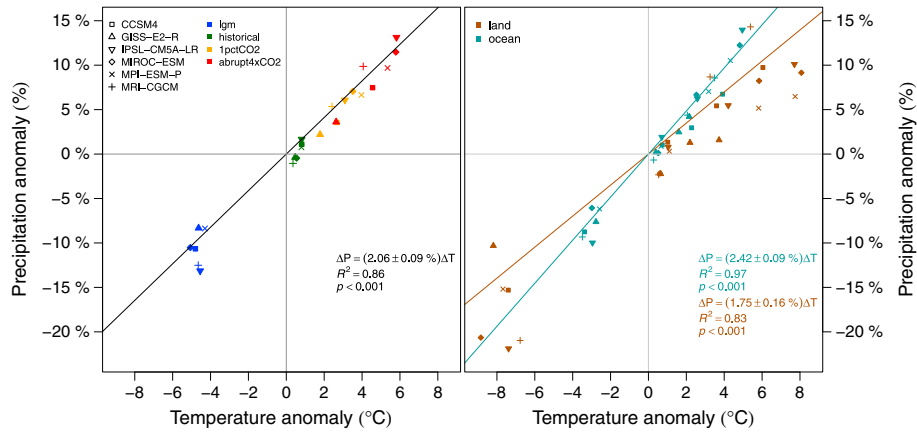


Figure 2. The change in precipitation (%) as a function of the change in global temperature (°C) as simulated by each of the six CMIP5 models (IPSL-CM5A-LR, MPI-ESM-P, MIROC-ESM, CCSM4, MRI-CGCM3, and GISS-E2-R) at the Last Glacial Maximum (LGM), from the historical run (average for period 1979–2005 CE), the 1% CO₂ run (*1pctCO₂*, average for model years 86–115), and the 4xCO₂ run. The left-hand plot shows the global relationship, while the right-hand plots shows the change in global precipitation (%) over (red) land and (blue) ocean as a function of the change in global land and ocean temperature (°C).

piControl for each model in order to capture the most extreme states (although similar results are obtained using, e.g., the upper and lower quartiles of precipitation). This results in different regions being defined as wet or dry in each model.

[8] We evaluate the realism of the *lgm* and *historical* simulations using paleoclimate reconstructions and historical observations over the land. (There are no reconstructions of precipitation over the ocean.) We use a data set of quantitative climate reconstructions for the LGM from S. P. Harrison et al. (Climate model benchmarking with glacial and mid-Holocene climates, submitted to *Climate Dynamics*, 2013). This data set provides reconstructions (including uncertainties) of several climate variables; here we use mean annual temperature over the land and ocean and mean annual precipitation over the land. The historical data are derived from two data sets: temperature data are from the HadCRUT4 combined land and ocean temperature data set [Morice et al., 2012], which covers the period from 1850 to 2009; precipitation data are from the GHCN (Global Historical Climatology Network, Version 2) product, which provides land precipitation data and covers the interval from 1900 to 2010 [Peterson and Vose, 1997]. The earliest part of the record is based on very few actual observations; the observed historical change is therefore taken as the difference between the mean for 1979–2005 and the mean for 1941–1970, and the simulated climate is the difference between the same years in the simulations.

3. Results: Simulated Changes

[9] The ensemble averages of the six models (see Figure S1 in the supporting information) illustrate the large changes in temperature and precipitation characteristic of the cold- and warm-climate states. The *lgm* simulations show changes of comparable magnitude (though opposite sign) to the 4xCO₂ simulations, consistent with the fact that the overall forcing is of comparable magnitude [Bracconnot et al., 2012], and *historical* and *1pctCO₂* show changes intermediate in magnitude. There are consistent patterns in the large-scale temperature response in warm- and cold-climate states [Izumi et al.,

2013]: the land warms/cools more than the oceans, and the high latitudes warm/cool more than the tropics. Izumi et al. [2013] also showed that there is a different seasonal response to year-round climate forcing in both warm and cold climates. These large-scale temperature patterns are broadly reflected in the changes in precipitation (Figure S1). In general, there are bigger changes in precipitation over the land than over the ocean in both warm- and cold-climate states. Changes in precipitation in the high latitudes (north of approximately 50°N) are larger than those in the midlatitudes (30°N–50°N), although the response of precipitation in the tropics does not scale straightforwardly with temperature.

[10] There is a strong relationship between changes in global temperature and precipitation, with increased precipitation in a warm climate and decreased precipitation in a cold-climate state (Figure 2). The estimate of the scaling across all the climate states and all models indicates a 2.06% ± 0.09% change per degree (Figure 2); estimates based on individual models across the climate states vary between 1.63% and 2.51% per degree. The range of values (Table S1) obtained for the *lgm* experiment (1.80%–2.89%) is similar to that obtained for the 4xCO₂ experiment (1.37%–2.43%). The values for an individual model are always larger in the *lgm* experiment than in the 4xCO₂ experiment, however, consistent with the fact that the energetic limitation on evaporation is smaller in the colder state (Figure 1). The values from the *1pctCO₂* experiment are not consistently larger than those from the 4xCO₂ experiment, but the differences in scaling between the two experiments are small.

[11] The *historical* simulation is the only experiment to include volcanic and solar forcing and changes in aerosols and land use. The simulated changes in temperature over the historic period are small (<1°C), as is the magnitude of the forcing (relative to the *lgm* or 4xCO₂ simulations), though consistent with the magnitude of changes shown by the HadCRUT4 data (Figure S2). The results obtained for the *historical* simulations are anomalous: while some models show an increase in precipitation over the course of the simulation, three models (GISS-E2-R, MIROC-ESM, and

LI ET AL.: CMIP5 PRECIPITATION: TEMPERATURE SCALING

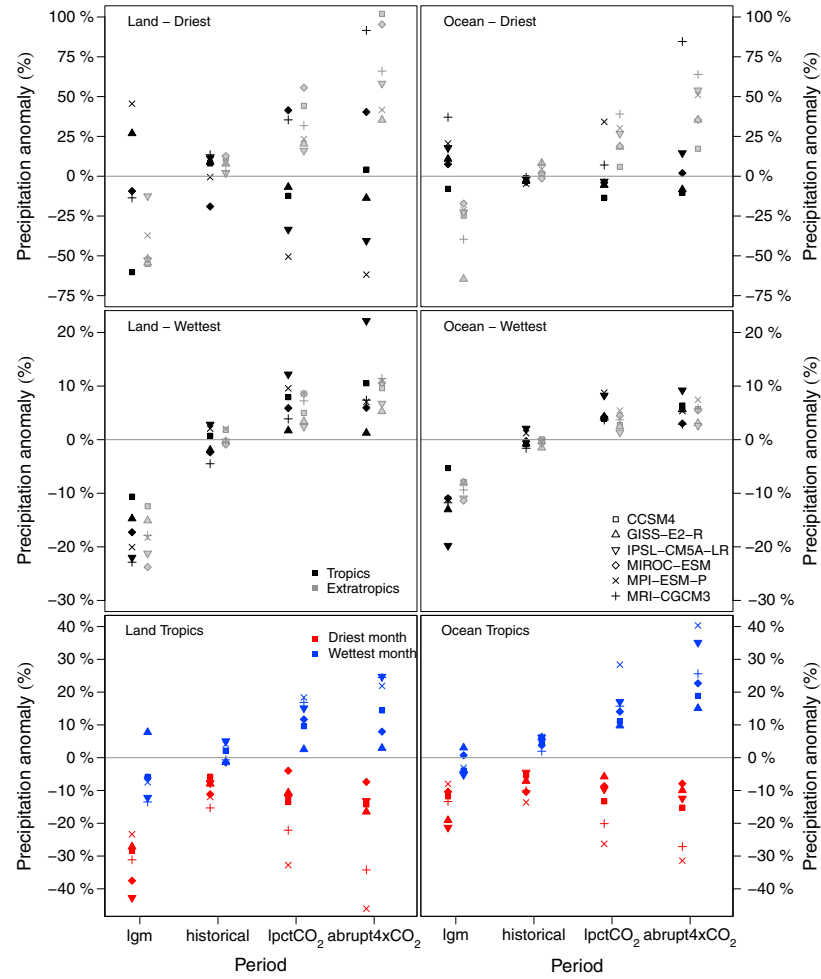


Figure 3. Simulated changes in precipitation (%) in the wettest and driest areas of the tropical (30°N – 30°S) and extratropical ($>30^{\circ}\text{N}$ and $>30^{\circ}\text{S}$) land and ocean. The wettest and driest areas are defined separately for each individual model as those grid cells that fall in the top and bottom deciles of precipitation in the control simulation (*piControl*). Simulated changes in tropical precipitation (%) during the wettest month (MPWE) and the driest month (MPDR) are shown in the bottom panels for comparison.

MRI-CGCM3) show a negative relationship between temperature and precipitation.

[12] To quantify the impact of water availability as a constraint in the *lgm* and raised CO_2 experiments, we estimated the precipitation scaling over the land and ocean separately. The estimate of the scaling across all climate states and all models (Figure 2) indicates a $2.42 \pm 0.09\%$ change per degree over the ocean and a $1.75 \pm 0.16\%$ change over the land. This finding suggests that the change in global precipitation with temperature is slightly reduced because of the additional constraint of water supply on evaporation over land areas. Estimates of the relationship between temperature and precipitation obtained from individual models and experiments generally show that the scaling over the ocean is greater than that over the land (Table S2). Thus, the values obtained for the model ensemble mean for ocean and land, respectively, are 2.64% and 2.28% for the *lgm*

experiment, 2.04% and 1.39% for the *1pctCO2* experiment, and 2.32% and 1.33% for the *4xCO2* experiment. Model responses over the ocean are more consistent than those over the land (Figure 2). The variability over the land probably reflects larger differences in treatment of the land among the different models (e.g., number of vegetation types, treatment of soil moisture, effective rooting depth, and inclusion of carbon cycle).

[13] The role of water limitation can also be examined by comparing the scaling over the tropical and extratropical land areas, with the expectation that water supply constraints might be less prominent in extratropical regions. In warm-climate states, the scaling of precipitation with temperature over the extratropical land (mean value, *1pctCO2*: $2.61\%/^{\circ}\text{C}$ and *4xCO2*: $2.77\%/^{\circ}\text{C}$) is indeed greater than over tropical land areas (mean value, *1pctCO2*: $1.00\%/^{\circ}\text{C}$ and *4xCO2*: $0.72\%/^{\circ}\text{C}$). This is also generally the case for individual

LI ET AL.: CMIP5 PRECIPITATION: TEMPERATURE SCALING

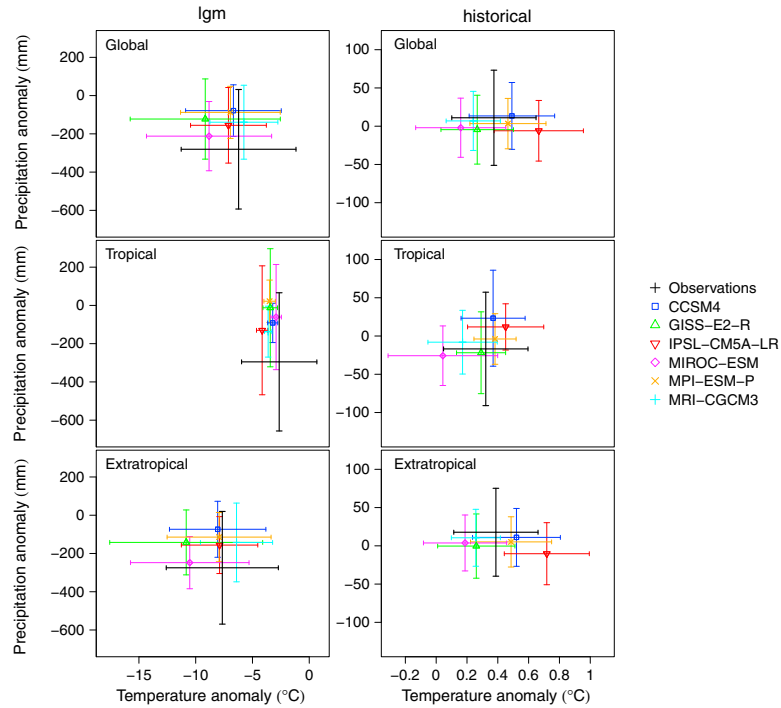


Figure 4. Comparison between climate reconstructions and model simulations over the land. The comparison is based on the model grid cells where observations of both temperature and precipitation are available. The bars show the standard deviation of the spatial values for both observations and model simulations. The historical observations are differences between the 1979–2005 and 1941–1970 long-term means from the GHCN precipitation data set [Peterson and Vose, 1997] and the HadCRUT4 temperature data set [Morice *et al.*, 2012]. The paleoclimate reconstructions are from Harrison *et al.* (submitted manuscript, 2013).

models (Table S2). However, the scaling between temperature and precipitation in the *lgm* experiment is greater over tropical ($3.67\%/^{\circ}\text{C}$) than extratropical ($2.87\%/^{\circ}\text{C}$) land areas (Table S2).

[14] Tropical areas that are wet in the preindustrial period, as defined by the top decile of precipitation, get wetter in warm-climate states and drier in cold-climate states (Figure 3). This is true for both land and ocean regions. The behavior of dry tropical regions, as defined by the lowest decile of precipitation in the preindustrial control state, is less coherent. Half of the models show these regions becoming wetter in the $4x\text{CO}_2$ simulation both over the land and over the ocean. At the *lgm* experiment, most of the models show these regions of the ocean getting wetter (five out of six models), as expected, but the models show both wetting (three models) and drying (three models) over the land. Thus, the models show a robust response of wet environments to temperature changes, but the nature of the precipitation changes in dry regions, particularly dry land regions, is model dependent. These findings are not sensitive to the definition of wet and dry regions: similar numbers of models show wetting/drying, for example, when the regions are defined using the top/bottom quartile of preindustrial precipitation. Extratropical areas that are wet in the preindustrial period get wetter in warm climates and drier in cold climates (Figure 3). However, this is also true for extratropical areas that are dry in the preindustrial period. Thus, the “rich get richer” syndrome is a characteristic of tropical climates but has no parallel in the extratropics.

[15] Precipitation is highly seasonal over most of the tropics, with summer (monsoon) rain and drier conditions in winter. Summer precipitation (as indexed by MPWE) increases while winter precipitation (as indexed by MPDR) decreases over both the land and the ocean in warm-climate states (Figure 3), leading to a significant increase in precipitation seasonality. In a cold world (Figure 3), there are precipitation decreases in both MPDR and MPWE; although the changes are proportionally larger in MPDR, the absolute changes are large in summer, and thus, these changes result in an overall decrease in precipitation seasonality. Thus, the change in tropical precipitation in both warm- and cold-climate states is consistent with the rich get richer syndrome and consistent with the idea [Chou *et al.*, 2007] that changes in precipitation are associated with strengthening (in warm-climate states) and weakening (in cold-climate states) of the monsoons. The Afro-Asian monsoon is weaker in the *lgm* experiments (see also Braconnot *et al.*, 2007), a feature which is also shown by palaeoenvironmental evidence [Harrison and Bartlein, 2012].

4. Results: Comparison With Observations

[16] Paleoclimate reconstructions show generally colder and drier conditions over the land at the LGM. The simulated changes in temperature (at grid cells where there are paleoclimate reconstructions) are colder than observed (Figure 4). Nevertheless, the simulated change in precipitation is systematically less than observed, both in the tropics and

extratropics. Thus, the scaling between temperature and precipitation changes in the models appears to be somewhat weaker than observed. However, the comparison for the historical period (Figure 4) does not show a marked discrepancy between the observed and simulated changes in precipitation scaling with temperature. In the tropics, the models showing greater warming over the land than the observations are also wetter, and those that show cooler conditions are drier. In the extratropics, most models show increased temperatures and little or no change in precipitation, whereas the observations show modest increases in both temperature and precipitation. Given the failure to identify a systematic bias in the historical simulations, it seems likely that differences between simulated and observed changes at the LGM are within the range of observational uncertainty.

5. Discussion and Conclusions

[17] Global precipitation increases with warming and decreases with cooling. The relationship, as estimated here from the individual models and simulations, varies between 1.5 and 3% per degree. This range is consistent with previous model-based estimates of precipitation changes during the 20th century [Held and Soden, 2006], using future scenarios [Allen and Ingram, 2002; Held and Soden, 2006], and based on PMIP2 LGM experiments [Boos, 2012].

[18] There are consistent patterns in the nature of the scaling of large-scale precipitation changes with temperature in warm- and cold-climate states. Thus, the change in precipitation with temperature is greater over the ocean than over the land in both warm and cold climates. Similarly, over land areas, the change in precipitation per degree temperature change is larger in the extratropics than the tropics. Changes in tropical precipitation are greatest in areas that are currently wet, resulting in increased precipitation in warm-climate states and decreased precipitation in cold-climate states. The seasonality of precipitation in the tropics also changes in a consistent way, with increased seasonality in warm-climate states and decreased seasonality in cold-climate states.

[19] At global and regional scales, the scaling of precipitation change with temperature is consistently much less than the 7% per degree change in atmospheric water vapor predicted by the Clausius-Clapeyron relationship, but consistent with the values expected taking into account energetic constraints on evaporation (~1%–4% per degree for temperatures in the range of 0°C–30°C). The steeper scaling over the ocean compared to the land, and over the extratropical land compared to the generally more arid tropical land, suggests that water limitations reduce modeled precipitation/temperature scaling by about a quarter.

[20] Both the spatial patterns and the scaling relationships are broadly consistent with earlier analyses [see, e.g., Held and Soden, 2006; Liu et al., 2009; Previdi, 2010; Boos, 2012]. The response of precipitation in 20th century simulations is generally weaker than that shown by the observational record [Allan and Soden, 2008]. The results presented here show that the same applies to the response of precipitation differences between *lgm* and present. However, evaluation using *historical* observations suggests that differences between the observed and simulated precipitation scaling do not exceed the reconstruction uncertainty. Broadly speaking, the evaluations suggest that models are able to capture the large-scale constraints on precipitation scaling in a realistic way.

[21] The inclusion of paleosimulations in the CMIP5 suite of model experiments makes it possible to demonstrate the robustness of simulated behavior across a wider range of climates. More importantly, it offers additional possibilities for model evaluation. Our analyses show that the energetic constraints on evaporation (and water limitation over the land) constrain the simulated changes in precipitation scaling with temperature in a realistic way. While improvements in the availability of paleoclimate reconstructions, and analysis of precipitation scaling over a wider range of paleoclimates, would be useful, these analyses demonstrate the utility of inclusion of paleoclimate simulations as CMIP5 experiments.

[22] **Acknowledgments.** We acknowledge the World Climate Research Programme's Working Group on Coupled Modelling, which is responsible for CMIP, and the climate modeling groups for producing and making available their model output. (For CMIP, the U.S. Department of Energy's Program for Climate Model Diagnosis and Intercomparison provided coordinating support and led the development of the software infrastructure in partnership with the Global Organization for Earth System Science Portals.) The analyses and figures are based on data archived at CMIP5 on 15 August 2012. G.L. is supported by an International Postgraduate Research Scholarship at Macquarie University. This research was supported by the Australian Research Council under grant DP1201100343 (S.P.H.) and by the U.S. National Science Foundation under grant ATM-0602409 (P.J.B. and K.I.).

[23] The Editor thanks two anonymous reviewers for their assistance in evaluating this paper.

References

- Adler, R. F., G. Gu, J. J. Wang, G. J. Huffman, S. Curtis, and D. Bolvin (2008), Relationships between global precipitation and surface temperature on interannual and longer timescales (1979–2006), *J. Geophys. Res.*, **113**, D22104, doi:10.1029/2008JD010536.
- Allan, R. P. (2009), Examination of relationships between clear-sky longwave radiation and aspects of the atmospheric hydrological cycle in climate models, reanalyses, and observations, *J. Clim.*, **22**(11), 3127–3145, doi:10.1175/2008JCLI2616.1.
- Allan, R. P., and B. J. Soden (2007), Large discrepancy between observed and simulated precipitation trends in the ascending and descending branches of the tropical circulation, *Geophys. Res. Lett.*, **34**, L18705, doi:10.1029/2007GL031460.
- Allan, R. P., and B. J. Soden (2008), Atmospheric warming and the amplification of precipitation extremes, *Science*, **321**(5895), 1481–1484, doi:10.1126/science.1160787.
- Allan, R. P., B. J. Soden, V. O. John, W. Ingram, and P. Good (2010), Current changes in tropical precipitation, *Environ. Res. Lett.*, **5**(2), 025205, doi:10.1088/1748-9326/5/2/025205.
- Allen, M. R., and W. J. Ingram (2002), Constraints on future changes in climate and the hydrologic cycle, *Nature*, **419**(6903), 224–232, doi:10.1038/nature01092.
- Bony, S., G. Bellon, D. Klocke, S. Sherwood, S. Fernepin, and S. Denvil (2013), Robust direct effect of carbon dioxide on tropical circulation and regional precipitation, *Nat. Geosci.*, doi:10.1038/NGEO1799.
- Boos, W. R. (2012), Thermodynamic scaling of the hydrological cycle of the last glacial maximum, *J. Clim.*, **25**(3), 992–1006, doi:10.1175/JCLI-D-11-00010.1.
- Braconnot, P., et al. (2007), Results of PMIP2 coupled simulations of the mid-Holocene and Last Glacial Maximum, Part 1: Experiments and large-scale features, *Clim. Past*, **3**, 261–277.
- Braconnot, P., S. P. Harrison, M. Kageyama, P. J. Bartlein, V. Masson-Delmotte, A. Abe-Ouchi, B. Otto-Bliesner, and Y. Zhao (2012), Evaluation of climate models using paleoclimatic data, *Nat. Clim. Change*, **2**, 417–424, doi:10.1038/nclimate1456.
- Chou, C., J.-Y. Tu, P.-H. Tan (2007), Asymmetry of tropical precipitation change under global warming, *Geophys. Res. Lett.*, **34**, L17708, doi:10.1029/2007GL030327.
- Chou, C., J. C. H. Chiang, C.-W. Lan, C.-H. Chung, Y.-C. Liao, and C.-J. Lee (2013), Increase in the range between wet and dry season precipitation, *Nat. Geosci.*, doi:10.1038/NGEO1744.
- DiNezio, P., A. Clement, G. Vecchi, B. Soden, A. Broccoli, B. Otto-Bliesner, and P. Braconnot (2011), The response of the Walker circulation to Last Glacial Maximum forcing: Implications for detection in proxies, *Paleoceanography*, **26**, PA3217, doi:10.1029/2010PA002083.
- Giorgi, F., and X. Bi (2005), Updated regional precipitation and temperature changes for the 21st century from ensembles of recent

LI ET AL.: CMIP5 PRECIPITATION: TEMPERATURE SCALING

- AOGCM simulations, *Geophys. Res. Lett.*, **32**, L21715, doi:10.1029/2005GL024288.
- Gu, G., R. F. Adler, G. J. Huffman, and S. Curtis (2007), Tropical rainfall variability on interannual-to-interdecadal and longer time scales derived from the GPCP monthly product, *J. Clim.*, **20**(15), 4033–4046, doi:10.1175/JCLI4227.1.
- Harrison, S. P., and P. J. Bartlein (2012), Records from the past, lessons for the future: what the palaeo-record implies about mechanisms of global change, in *The Future of the World's Climates*, edited by A. Henderson-Sellers, and K. McGuffie, pp. 403–436, Elsevier, Oxford, UK.
- Held, I. M., and B. J. Soden (2006), Robust responses of the hydrological cycle to global warming, *J. Clim.*, **19**(21), 5686–5699, doi:10.1175/JCLI3990.1.
- Huffman, G. J., R. F. Adler, D. T. Bolvin, and G. Gu (2009), Improving the global precipitation record: GPCP version 2.1, *Geophys. Res. Lett.*, **36**, L17808, doi:10.1029/2009GL040000.
- Izumi, K., P. J. Bartlein, and S. P. Harrison (2013), Consistent behaviour of the climate system in response to past and future forcing, *Geophys. Res. Lett.*, **40**, 1817–1823, doi:10.1002/grl.50350.
- Liu, S. C., C. Fu, C.-J. Shiu, J.-P. Chen, and F. Wu (2009), Temperature dependence of global precipitation extremes, *Geophys. Res. Lett.*, **36**, L17702, doi:10.1029/2009GL040218.
- Meehl, G. A., et al. (2007), Global climate projections, in *Climate Change 2007: The Physical Science Basis, Contribution of Working Group I to the Fourth Assessment Report of the Intergovernmental Panel on Climate Change*, edited by S. Solomon et al., pp. 749–845, Cambridge Univ. Press, Cambridge, United Kingdom and New York, NY, USA.
- Morice, C. P., J. J. Kennedy, N. A. Rayner, and P. D. Jones (2012), Quantifying uncertainties in global and regional temperature change using an ensemble of observational estimates: The HadCRUT4 dataset, *J. Geophys. Res.*, **117**, D08101, doi:10.1029/2011JD017187.
- Peterson, T. C., and R. S. Vose (1997), An overview of the Global Historical Climatology Network temperature database, *Bull. Am. Meteorol. Soc.*, **78**(12), 2837–2849, doi:10.1175/1520-0477(1997)078<2837:A00TGH>2.0.CO;2.
- Previdi, M. (2010), Radiative feedbacks on global precipitation, *Environ. Res. Lett.*, **5**, 025211, doi:10.1088/1748-9326/5/2/025211.
- Raupach, M. (2000), Equilibrium evaporation and the convective boundary layer, *Boundary Layer Meteorol.*, **96**, 107–142.
- Richter, I., and S. P. Xie (2008), Muted precipitation increase in global warming simulations: A surface evaporation perspective, *J. Geophys. Res.*, **113**, D24118, doi:10.1029/2008JD010561.
- Taylor, K. E., R. J. Stouffer, and G. A. Meehl (2012), An overview of CMIP5 and the experiment design, *Bull. Am. Meteorol. Soc.*, **93**(4), 485, doi:10.1175/BAMS-D-11-00094.1.
- Trenberth, K. E. (2011), Changes in precipitation with climate change, *Clim. Res.*, **47**(1), 123, doi:10.3354/cr00953.
- Trenberth, K. E., and D. J. Shea (2005), Relationships between precipitation and surface temperature, *Geophys. Res. Lett.*, **32**, L14703, doi:10.1029/2005GL022760.
- Wentz, F. J., L. Ricciardulli, K. Hilburn, and C. Mears (2007), How much more rain will global warming bring?, *Science*, **317**(5835), 233–235, doi:10.1126/science.1140746.
- Zhang, X., F. W. Zwiers, G. C. Hegerl, F. H. Lambert, N. P. Gillett, S. Solomon, P. A. Stott, and T. Nozawa (2007), Detection of human influence on twentieth-century precipitation trends, *Nature*, **448**(7152), 461–465, doi:10.1038/nature06025.

Chapter 3

Evaluation of modern and mid-Holocene seasonal precipitation of the Mediterranean and northern Africa in the CMIP5 simulations

Contribution by Co-Authors: G. L. and A.P. were responsible for data analysis, figure and table generation; all authors were responsible for interpretation of the data; A.P. drafted the first version of the manuscript and all authors contributed to the final version.

Clim. Past, 10, 551–568, 2014
www.clim-past.net/10/551/2014/
doi:10.5194/cp-10-551-2014
© Author(s) 2014. CC Attribution 3.0 License.



Evaluation of modern and mid-Holocene seasonal precipitation of the Mediterranean and northern Africa in the CMIP5 simulations

A. Perez-Sanz^{1,2}, G. Li², P. González-Sampériz¹, and S. P. Harrison^{2,3}

¹Pyrenean Institute of Ecology, (IPE)-CSIC, Avda Montañana 1005, 50059 Zaragoza, Spain

²Department of Biological Sciences, Macquarie University, North Ryde, NSW 2109, Australia

³Centre for Past Climates and Department of Geography & Environmental Sciences, School of Archaeology, Geography and Environmental Sciences, (SAGES) University of Reading, Whiteknights, Reading, RG6 6AB, UK

Correspondence to: A. Perez-Sanz (anaperez@ipe.csic.es; anpsanz@gmail.com)

Received: 7 August 2013 – Published in Clim. Past Discuss.: 17 September 2013

Revised: 4 February 2014 – Accepted: 6 February 2014 – Published: 20 March 2014

Abstract. We analyse the spatial expression of seasonal climates of the Mediterranean and northern Africa in pre-industrial (*piControl*) and mid-Holocene (*midHolocene*, 6 yr BP) simulations from the fifth phase of the Coupled Model Intercomparison Project (CMIP5). Modern observations show four distinct precipitation regimes characterized by differences in the seasonal distribution and total amount of precipitation: an equatorial band characterized by a double peak in rainfall, the monsoon zone characterized by summer rainfall, the desert characterized by low seasonality and total precipitation, and the Mediterranean zone characterized by summer drought. Most models correctly simulate the position of the Mediterranean and the equatorial climates in the *piControl* simulations, but overestimate the extent of monsoon influence and underestimate the extent of desert. However, most models fail to reproduce the amount of precipitation in each zone. Model biases in the simulated magnitude of precipitation are unrelated to whether the models reproduce the correct spatial patterns of each regime. In the *midHolocene*, the models simulate a reduction in winter rainfall in the equatorial zone, and a northward expansion of the monsoon with a significant increase in summer and autumn rainfall. Precipitation is slightly increased in the desert, mainly in summer and autumn, with northward expansion of the monsoon. Changes in the Mediterranean are small, although there is an increase in spring precipitation consistent with palaeo-observations of increased growing-season rainfall. Comparison with reconstructions shows most models underestimate the mid-Holocene changes in annual precipitation, except in the equatorial zone. Biases in the *piControl*

have only a limited influence on *midHolocene* anomalies in ocean–atmosphere models; carbon-cycle models show no relationship between *piControl* bias and *midHolocene* anomalies. Biases in the prediction of the *midHolocene* monsoon expansion are unrelated to how well the models simulate changes in Mediterranean climate.

1 Introduction

The Mediterranean area, including southern Europe and northern Africa, is characterized today by a highly seasonal climate with summer drought and a wet season between October and March (Mehta and Yang, 2008). The generally low precipitation and marked seasonality gives rise to drought-adapted, sclerophyllous vegetation that is highly susceptible to wildfire during the dry season (Moreira et al., 2011). The Mediterranean region has experienced warming and increased drought in recent years (Camuffo et al., 2010; Hoerling et al., 2012; European Environment Agency, 2012) and has been identified as highly vulnerable to future climate changes (Giorgi, 2006). Model projections indicate large increases in temperatures and a reduction in mean annual precipitation (e.g. Meehl et al., 2007; Giorgi and Lionello, 2008; Nikulin et al., 2011), both of which would lead to large changes in vegetation cover and exacerbate wildfires (Amatulli et al., 2013). Given the high socio-economic costs of such changes, it is important to assess the reliability of model projections. Measures of how well the models simulate modern climate do not provide a measure of whether

the simulation of climate changes is realistic. However, the evaluation of model performance in the geologic past does provide a way of making such an assessment (Braconnot et al., 2012; Schmidt et al., 2014a).

The mid-Holocene (MH, 6000 yr BP) provides an opportunity to examine climate-model performance in the Mediterranean region. Palaeoenvironmental evidence suggests that the Mediterranean was wetter than today during the mid-Holocene. Lake levels across the region were higher than present (Kohfeld and Harrison, 2000; Magny et al., 2002; Roberts et al., 2008), indicating a more positive balance between precipitation and evaporation. Speleothem records also indicate increased precipitation compared to present (Roberts et al., 2011). The observed expansion of deciduous trees (Prentice et al., 1996; Roberts et al., 2004; Carrión et al., 2010) across the region indicates that there was a change in rainfall seasonality with increased summer rainfall (Prentice et al., 1996). The observed decrease of fires in lowland areas, coupled with an increase in fires at higher elevations, is consistent with more humid conditions – which would suppress fires in already forested lowland regions but allow them to increase as forests expanded into higher elevation areas (Vannière et al., 2011). The changes in climate were spatially complex (Roberts et al., 2011), but pollen-based climate reconstructions (e.g. Cheddadi et al., 1997; Davis et al., 2003; Bartlein et al., 2011) show that most of the Mediterranean region was characterized by a year-round decrease in temperature and an increase in plant-available moisture.

Systematic comparisons with observations have shown that global climate models are unable to reproduce the observed MH patterns of rainfall changes in the Mediterranean. In particular, they do not show a sufficiently large increase in summer rainfall to explain the shift towards deciduous vegetation. This was identified as a problem in atmosphere-only simulations of the mid-Holocene made during the first phase of the Palaeoclimate Modelling Intercomparison Project (PMIP1; see e.g. Masson et al., 1999; Guiot et al., 1999; Bonfils et al., 2004). Coupled ocean–atmosphere simulations made during PMIP2 were able to simulate the types of climate changes seen in the Mediterranean, but the geographic placement of these climate types, the spatial extent and the magnitude of the changes were not well captured (Brewer et al., 2007). In particular, the simulated changes in precipitation are small and insufficient to explain the observed expansion of deciduous forests in the region.

The Mediterranean climate involves a complex interaction between different processes acting at several different spatio-temporal scales (Xoplaki et al., 2003; Luterbacher et al., 2006; CLIVAR, 2010; Lionello, 2012). However, inter-annual variability in Mediterranean summer precipitation is linked to variability in the strength of the Afro–Asian monsoon system (Rodwell and Hoskins, 2001; Raicich et al., 2003; Gaetani et al., 2011). Analyses of climate model simulations of the present day suggest that Mediterranean summer precipitation is suppressed during years when the Afro–

Asian monsoon system is strong. This results from intensification of the Hadley cell and enhanced subsidence in the subtropics (i.e. strengthening of the Azores High), leading to high pressure over the eastern Mediterranean which results in decreased rainfall (Gaetani et al., 2011). However, when monsoon intensification is accompanied by northward movement of the intertropical convergence zone, as model simulations indicate occurred in the mid-Holocene (Braconnot et al., 2007a; Marzin and Braconnot, 2009), the Azores High is also displaced northeastward and weakened (e.g. Harrison et al., 1992). This has been shown to have a significant impact on precipitation in eastern North America (Forman et al., 1995; van Soelen et al., 2012) and could potentially lead to increased summer rainfall in the Mediterranean region.

The PMIP2 simulations show a significant enhancement and northward expansion of the African monsoon during the mid-Holocene in response to changes in insolation forcing (Braconnot et al., 2007a). However, comparisons with pollen-based estimates of the change in mean annual precipitation (Joussaume et al., 1999; Bartlein et al., 2011) show that the models underestimate the increase in precipitation by between 20 and 50 % (Braconnot et al., 2007a, 2012). Most models fail to produce a sufficient northward expansion of the monsoon. This underestimation of monsoon expansion is also present in the CMIP5 (Coupled Model Intercomparison Project) MH simulations (see e.g. Harrison et al., 2013). It is possible that this bias in the simulation of the African monsoon is linked to the failure to simulate the MH Mediterranean climate accurately, since larger shifts in the position of the monsoon are produced by models incorporating land-surface feedbacks and/or with higher spatial resolution (Levis et al., 2004; Wohlfahrt et al., 2004; Bosmans et al., 2012).

MH model simulations, made with the same models that are used for future projections, have been made as part of the fifth phase of the CMIP5 (Taylor et al., 2012) and are being analysed as part of the third phase of the Palaeoclimate Modelling Intercomparison Project (PMIP3; Braconnot et al., 2012).

Kelley et al. (2012) have shown that the simulation of the seasonal cycle of precipitation in the Mediterranean region under modern conditions is reasonable, although as in earlier versions of the models the amplitude of the cycle is more muted than observed with too little rain in winter and too much rain in summer (Brands et al., 2013). However, evaluation of CMIP5 model performance against modern observations suggests that some aspects of the simulation of the Afro–Asian monsoons (see e.g. Monerie et al., 2012; Roehrig et al., 2013; Sperber et al., 2013) are improved compared to earlier versions of the models, although preliminary assessments of the CMIP5 model indicate that improvements in the modern simulations do not translate into improvements in the simulation of the MH monsoon climate (Harrison et al., 2013), and thus, given the dynamic links between the

monsoon and Mediterranean precipitation, in MH Mediterranean climate changes.

In this study, we examine the performance of the CMIP5 models for modern and MH climates, and compare the simulated climates with modern and palaeo-observations. This allows us to assess whether biases in the control simulations influence the MH simulations and to investigate whether regional biases in the simulation of MH monsoon changes influence model performance in the Mediterranean.

2 Methods

We present analyses of the pre-industrial (*piControl*) and MH (*midHolocene*) made by 12 coupled ocean–atmosphere models from the fifth phase of the CMIP5. In order to investigate whether biases in the control simulation influence the realism of the *midHolocene* climates, we first evaluate the *piControl* simulation. We use modern observations from the CRU TS3.1 data set, in the absence of climate reconstructions from northern Africa for the *piControl* interval. The *piControl* simulation is driven by boundary conditions appropriate for 1850 AD, but comparisons with a subset of transient historical simulations show that the spatial patterns and magnitudes of seasonal climates are very similar. In order to evaluate whether models capture the spatial expression of specific seasonal patterns, we define a number of climate types using the modern observations and apply these definitions to delimit these climate types in the *piControl* and *midHolocene* simulations. We evaluate the *midHolocene* simulations using quantitative climate reconstructions derived from pollen records. Although there are many kinds of palaeo-records that indicate that northern Africa and the circum-Mediterranean region were wetter during the mid-Holocene, including e.g. lake-level and archaeological records, these other sources of information do not provide quantitative estimates of the change in precipitation. Comparisons of simulated and observed climates are based on the simulated precipitation both within climate zones and within geographic zones.

2.1 Data sources: CMIP5 simulations

We examine precipitation changes between a mid-Holocene (*midHolocene*, 6000 yr BP) equilibrium simulation and a control simulation representing pre-industrial conditions (*piControl*) using 12 models from the fifth phase of the CMIP5. Both the *midHolocene* and *piControl* are equilibrium simulations. We use the *midHolocene* and *piControl* simulations in the CMIP5 (<http://cmip-pcmdi.llnl.gov/cmip5/dataportal.html>) archive as of 15 August 2012 (Table 1). Seven of these simulations are made with ocean–atmosphere (OA) models, and the other 5 models include an interactive carbon cycle (OAC). The *piControl* simulation has boundary conditions (insolation, greenhouse gas concentrations) appropriate for

1850 CE (common era). The *midHolocene* experiment shows the response to changes in the seasonal and latitudinal distribution in insolation 6000 yr ago; greenhouse gas concentrations are set at *piControl* levels (for details of the experimental protocol see Taylor et al., 2012, and Braconnot et al., 2012). To assess whether the *piControl* state differs from recent observed climates, we used outputs from a historical simulation (*historical*: 1850–2005 CE) available for six of the models. The *historical* simulation is forced by time-varying changes in solar, volcanic, and greenhouse gases (Taylor et al., 2012; Braconnot et al., 2012).

The output from each model was interpolated to a common grid (0.5°) using bilinear interpolation to facilitate comparisons and the calculation of zonal averages. Long-term mean monthly, seasonal, and annual precipitation values were obtained by averaging the last 100 yr of the *piControl* and *midHolocene* simulations, except in the case of HADGEM2-CC where only 35 yr of *midHolocene* simulated outputs are available. Long-term means of the six *historical* simulations were obtained by averaging the last 30 yr of each simulation. All averages were areally weighted (by the area of the model grid cells).

2.2 Data sources: modern and mid-Holocene climate data

Observations of the modern climate are taken from the CRU TS3.1 data set (Harris et al., 2014), which provides monthly precipitation values on a 0.5° grid for the interval 1850–2006. We have created a monthly precipitation climatology using data from January 1961 through to December 1990. Zonal averages are constructed by areally weighting the gridded values.

Bartlein et al. (2011) provide quantitative reconstructions of mean annual precipitation (MAP), expressed as anomalies from the present, from pollen and plant macrofossil records. The original site-based reconstructions were averaged to provide gridded values on a 2° × 2° grid, and differences between the site reconstructions within each grid were used to provide an estimate of reconstruction uncertainty (as a pooled estimate of the standard error). The data set provides mid-Holocene estimates of MAP anomalies for 62 cells (out of a possible 397 cells) within the area of interest (latitude: 0–45° N, longitude: 20° W–30° E).

2.3 Definition of climate regions

Precipitation regimes can be characterized by a combination of the form of the seasonal cycle, seasonal concentration, and magnitude. We determined these characteristics of modern precipitation (using the CRU TS3.1 data set) for zonally averaged 5° latitude bands between 0 and 45° N. The seasonal cycle of precipitation in each 5° latitude band was characterized according to the number of distinct rainfall peaks present in the 12 month precipitation climatology, using the R package

Table 1. Characteristics of the CMIP5 models used in these analyses.

Model name	Type	Resolution (number of grid cells: latitude, longitude)			Year length	Simulations			Reference
		Atmosphere	Ocean	Sea ice		<i>midHolocene</i>	<i>piControl</i>	<i>historical</i>	
BCC-CSM1-1	OAC	64, 128	232, 360	232, 360	365	X	X		Wu et al. (2013)
CCSM4	OA	192, 288	320, 384	320, 384	365	X	X	X	Gent et al. (2011)
CNRM-CM5	OA	128, 256	292, 362	292, 362	365–366	X	X		Volodro et al. (2013)
CSIRO-Mk3-6-0	OA	96, 192	189, 192	96, 192	365	X	X		Rotstayn et al. (2010)
CSIRO-Mk3L-1-2	OA	56, 64	128, 225	56, 64	365	X	X		Phipps et al. (2011)
GISS-E2-R	OA	90, 144	90, 144	90, 144	365	X	X	X	Schmidt et al. (2014b)
HadGEM2-CC	OAC	145, 192	216, 360	216, 360	360	X	X		Collins et al. (2011)
HadGEM2-ES	OAC	145, 192	216, 360	216, 360	360	X	X		Collins et al. (2011)
IPSL-CM5A-LR	OAC	96, 96	149, 182	149, 182	365	X	X	X	Dufresne et al. (2013)
MIROC-ESM	OAC	64, 128	192, 256	192, 256	365	X	X	X	Watanabe et al. (2011)
MPI-ESM-P	OA	96, 192	220, 256	220, 256	365–366	X	X	X	Raddatz et al. (2007)
MRI-CGCM3	OA	160, 320	360, 368	360, 368	365	X	X	X	Yukimoto et al. (2011)

“pastecs” to determine whether there was a significant “pit” or “peak” in any month. A pit or peak is considered significant if the probability of turning points occurring in a random series is < 0.05 , given by

$$(P(t) = 2/n(t-1)!(n-1)!)$$

where n is the number of observations at time t (Ibanez, 1982).

We calculated the total precipitation in each season (spring: March, April, May; summer: June, July, August; autumn: September, October, November; winter: December, January, February) and for the whole year. A measure of seasonal concentration was calculated following Kelley et al. (2013), where the magnitude of precipitation in each month is represented by the length of a vector in the complex plane and the direction of the vector represents the timing (with January set to 0°). The length of the mean vector divided by the annual precipitation provides an index of seasonal concentration (C), where C is 1 when the precipitation is concentrated in a single month and 0 when it is evenly distributed throughout the year.

We applied these definitions to determine the position of different precipitation regimes in the *piControl* and *mid-Holocene* simulations. Comparison of the observed limits and those identified in the *piControl* allows us to examine (a) whether the models produce these distinctive precipitation regimes and (b) how well they simulate their placement independently of whether they simulate the correct magnitude of precipitation. Comparison of the *piControl* and *mid-Holocene* limits allows us to characterize shifts in precipitation regimes, again, independent of changes in precipitation magnitude.

2.4 Analyses of the model simulations

We evaluate model performance for the *piControl* simulation in two steps. First we examine whether the models reproduce

the spatial extent of different precipitation regimes, and then we examine whether they reproduce the magnitude of total annual and of seasonal precipitation. Long-term means for the period 1961–1990 from the CRU TS3.1 data set (Harris et al., 2014) are compared with long-term averages for the last 100 yr of the *piControl*. The standard deviation (SD) of the observations provides a measure of the significance of the difference between observations and simulations. We examine the differences between simulated and observed climate for the latitude band corresponding to a given precipitation regime in the observations. We also compare the differences in the amount of precipitation for the geographic region identified as falling within a specific precipitation regime in each model, which may be less/more extensive than the region identified in the observations.

We also examine the change in precipitation in the mid-Holocene in two steps. First we identify the spatial extent of each precipitation regime in the *midHolocene* simulations and compare this with the spatial extent shown in the *piControl* simulation of the same model. This allows us to identify whether there have been shifts in the precipitation regimes. We then examine the magnitude of the precipitation change in the latitude band characterized by a specific regime in both the *piControl* and the *midHolocene* simulations for each model. This allows us to identify whether there has been a change in precipitation in situ. We use the standard deviation of the *piControl* simulation for each model to determine whether the change between *midHolocene* and *piControl* is significant.

We examine whether the biases in simulated precipitation (both the bias in spatial extent of a given precipitation regime and the bias in the magnitude of the simulated precipitation) influence the simulated change in precipitation between *piControl* and *midHolocene*. The bias and anomaly values have been obtained firstly for discrete geographical zones (the zones characterized by different rainfall regimes today, as defined from the CRU data set) and secondly for

the model-defined regions of these different rainfall regimes (e.g. the region where the simulated rainfall is of the monsoon type). We use linear regression to examine the relationship between precipitation biases and anomalies for all models, and for the OA and OAC classes of models.

The realism of the simulated change in precipitation (*mid-Holocene – piControl*) is assessed by comparing with reconstructions of mean annual precipitation (MAP) from the Bartlein et al. (2011) data set. Comparisons are made by averaging the simulated precipitation for the grid cells where there are observations within each 5° latitude band. There are sufficient data in most of the 5° latitude bands to make robust comparisons.

3 Results

3.1 Modern observed climate

The modern climate of the region can be divided into four distinct latitudinal zones, differentiated by marked differences in the seasonal distribution and amount of rainfall (Fig. 1). In the south, the equatorial band is characterized by high rainfall (~1800 mm) throughout the year (Fig. 2) but with peaks in precipitation in spring (~460 mm) and autumn (~600 mm) and less rainfall in summer. This pattern reflects the seasonal migration north and south of the intertropical convergence zone. The “double-peak” rainfall pattern (hereafter DP) occurs between 0 and 5° N. The region further north (5–20° N) is characterized by summer monsoonal rainfall and dry winters. The amount of rainfall declines progressively from ca. 650 mm in summer (June, July, August) in the south to less than 100 mm in the north. The desert area (20–30° N) is characterized by low rainfall (< 100 mm yr⁻¹). There is no pronounced seasonal differentiation of rainfall in the desert, although southern regions tend to have slightly more rain in summer than winter and northern regions slightly more rainfall in winter than summer. The Mediterranean zone (30–45° N) is characterized by higher rainfall, increasing from 200 mm yr⁻¹ in the south band to 780 mm yr⁻¹ in the north. The rainfall is concentrated in the winter half-year, with a pronounced summer drought.

3.2 *piControl* simulations

These four rainfall regimes can generally be identified in the *piControl* simulations, although two of the models (CNRM-CM5, MRI-CGCM3) fail to reproduce the DP pattern in the equatorial zone. However, several models represent the spatial extent of the regimes poorly. Thus 5 out of the 12 models show monsoon penetration further north than observed (Fig. 3a). Most models place the northern limit of the desert correctly, but two models (CSIRO-Mk3L-1-2, IPSL-CM5A-LR) show the area of low rainfall and low rainfall seasonality extending further north than observed.

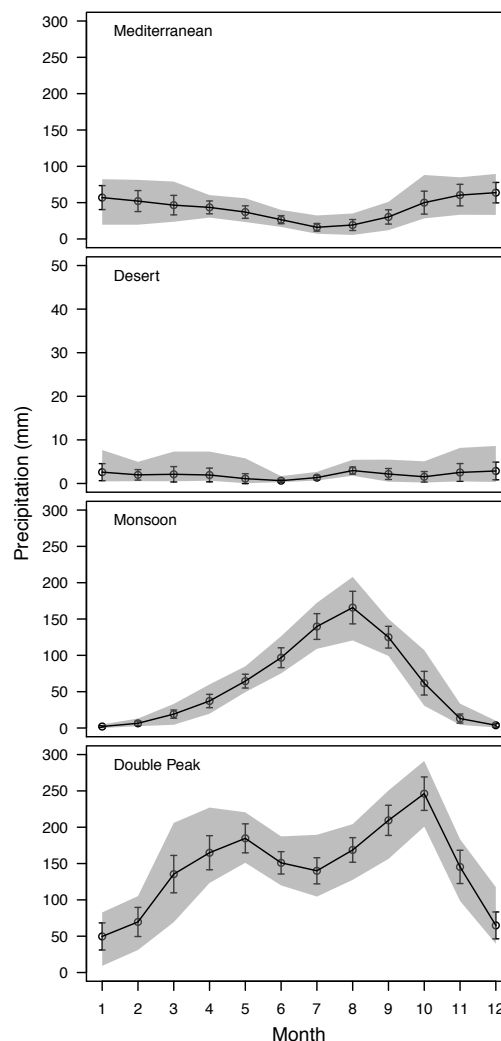


Fig. 1. Observed seasonal cycle of precipitation in each of the defined climate zones, using the CRU T3.1 data set (Harris et al., 2014). The mean precipitation each month (mm) is shown by the black line, with the standard deviation shown by the bars. The grey shading shows the maximum and minimum rainfall experienced within the observation period (1961–1990). Note that the scale for the desert region differs from that used for the other regions. Months are numbered consecutively from January (1) through to December (12).

Since there are no reconstructions of pre-industrial climate, we evaluate how well the models reproduce the magnitude of seasonal precipitation within each precipitation regime by comparing to observations for the period 1961–1990. Comparison of the *piControl* and *historical* simulations (Fig. S1, Supplement), for the six models where both runs are available, shows that differences in the simulated patterns and amount of precipitation between the two simulations are small. Differences between the two simulations

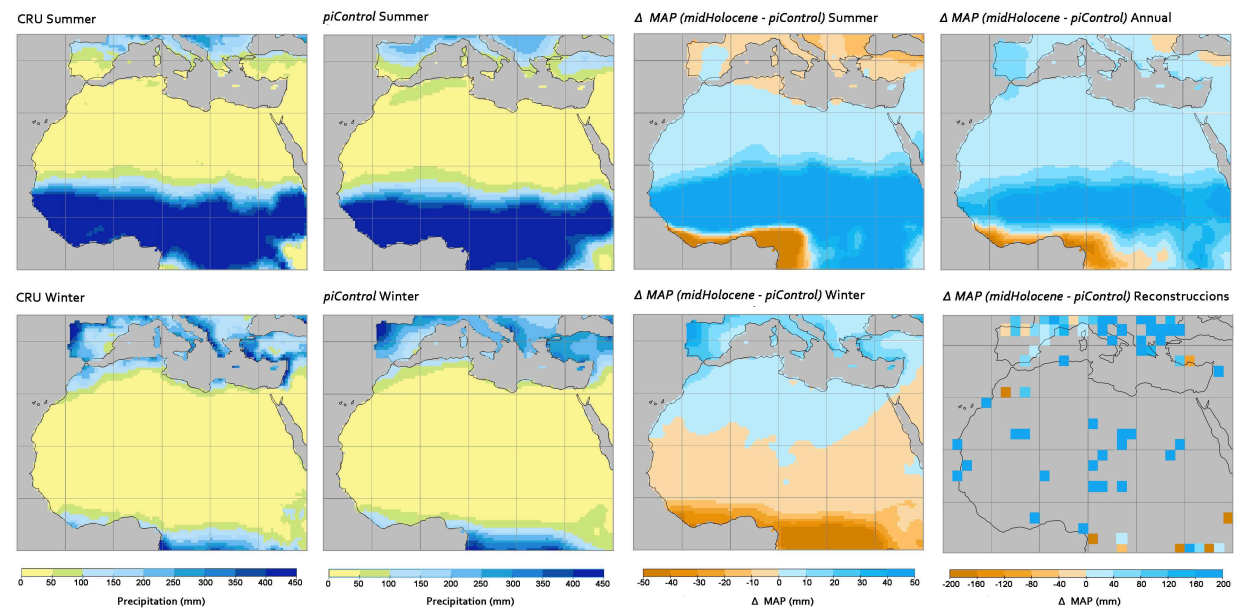


Fig. 2. Observed and simulated modern and palaeoprecipitation patterns. The total summer and winter precipitation from the CRU T3.1 data set (Harris et al., 2014) are compared to ensemble averages of the *piControl* outputs of the 12 CMIP5 models. The simulated change in precipitation between the mid-Holocene and *piControl* simulations (*midHolocene-piControl*) is shown based on the ensemble average of the *midHolocene* outputs of the 12 CMIP5 models. The observed anomalies in mean annual precipitation (MAP) between the mid-Holocene and the present day are average values for $2^{\circ} \times 2^{\circ}$ grids from the Bartlein et al. (2011) data set.

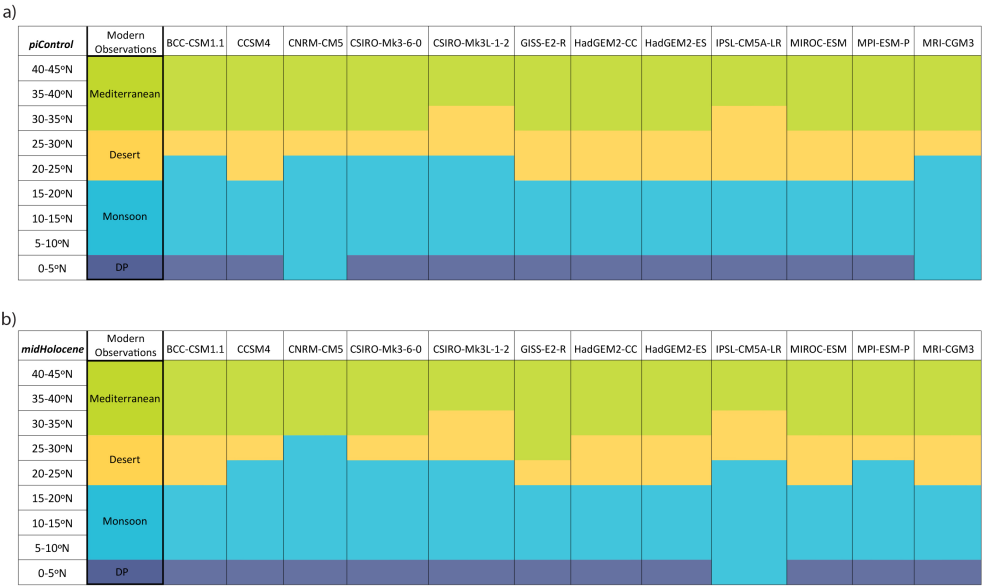


Fig. 3. The location of the four precipitation zones in the CMIP5 *piControl* simulations compared to the limits defined using the CRU TS3.1 data set (Harris et al., 2014). The precipitation regime was characterized using zonally averaged long-term means for 5° latitude bands. The location of the four precipitation zones in the CMIP5 *midHolocene* simulations compared to the limits defined using the CRU TS3.1 data set (Harris et al., 2014). The precipitation regime was characterized using zonally averaged long-term means for 5° latitude bands.

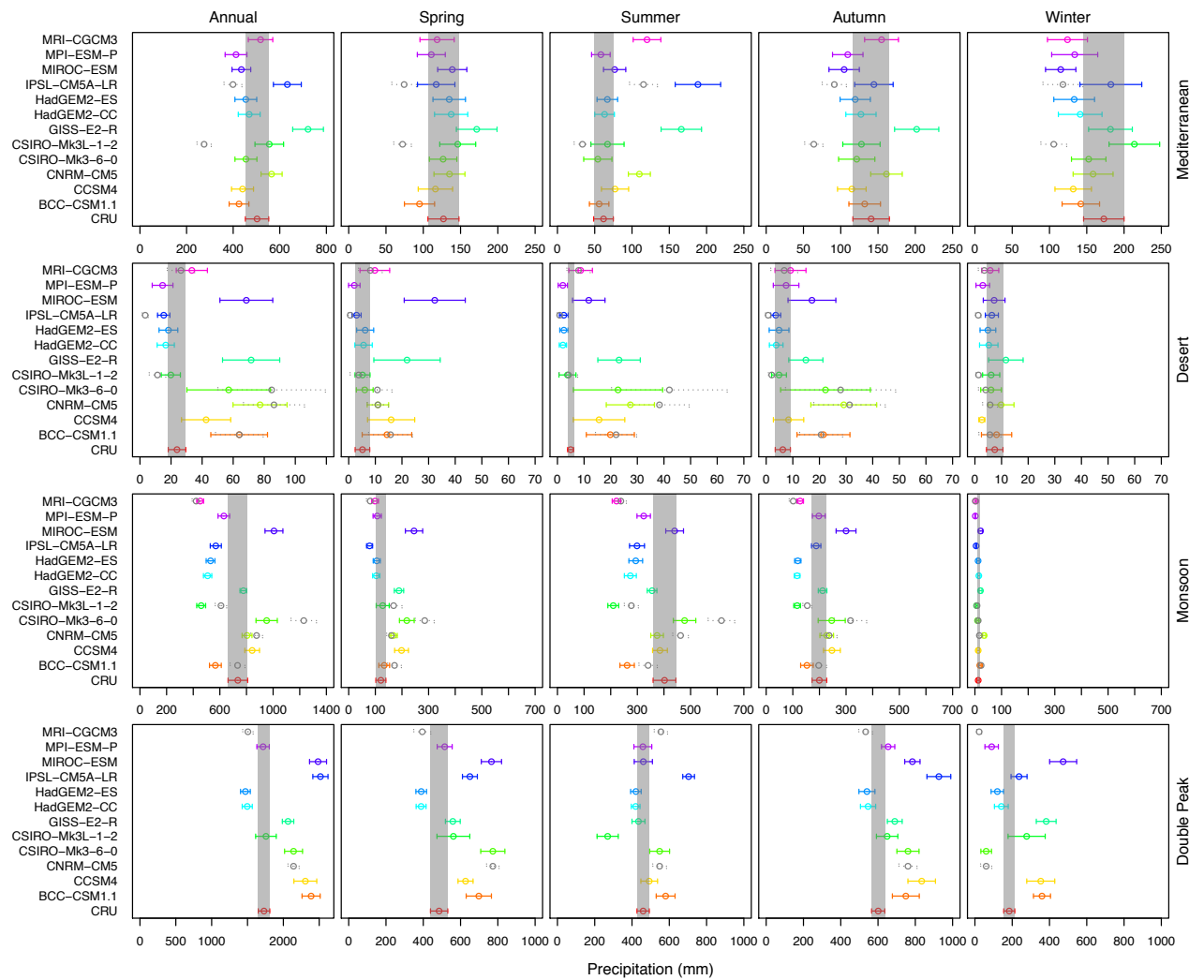


Fig. 4. Comparison of simulated and observed mean annual and mean seasonal precipitation (mm) for each of the defined precipitation regimes (Mediterranean, desert, monsoon, double peak). The simulated precipitation (mean and standard deviation) is shown for both the climate zone as defined by the observations (solid line) and as defined in the *piControl* simulation itself (dotted line). The difference between these two lines for each model provides a measure of the degree to which incorrect placement of a given climate affects the zonal means. The grey bars represent one standard deviation of the mean annual and mean seasonal precipitation from observations. The seasons are defined as spring, summer, autumn and winter (as in Sect. 3.1).

are generally much smaller than the difference between the simulated and observed climate.

Comparison of the *piControl* with modern observations shows that most models fail to reproduce the magnitude of the precipitation (Fig. 4). Only two models (CSIRO-Mk3L-1-2, MPI-ESM-P) correctly reproduce the amount of rainfall in the DP band, while six models overestimate the rainfall by between 350 and 790 mm yr⁻¹. Although some models overestimate the amount of precipitation in every season, the positive biases are largest in spring (75–290 mm), autumn (90–325 mm) and winter (50–290 mm). Only two models (GISS-E2-R, CNRM-CM5) simulate the correct magnitude

of mean annual precipitation in the monsoon zone. Seven models underestimate, and three models overestimate, the mean annual rainfall in the monsoon zone. The bias ranges from 280 mm less than observed to 270 mm more than observed. Models that underestimate the total amount of rainfall in the monsoon zone (e.g. BCC-CSM1.1, CSIRO-Mk3L-1-2, HadGEM2-CC, HadGEM2-ES, IPSL-CM5A-LR, MPI-ESM-P and MRI-CGCM3) do so because of simulating too little precipitation in summer and autumn, i.e. because the simulation of the monsoon is too weak. However, models that overestimate the total precipitation in this zone (e.g. CCSM4, CNRM-CM5, CSIRO-Mk3-6 and MIROC-ESM) generally

overestimate the rainfall in all seasons of the year. Seven models simulate too much precipitation in the desert zone ($10\text{--}55\text{ mm yr}^{-1}$), with too much rainfall in spring, summer and autumn. Given that the desert zone is by definition confined to regions with $< 100\text{ mm}$ precipitation, the overestimation of rainfall in this zone is large. Four models underestimate the Mediterranean precipitation (by between 35 and 90 mm yr^{-1}), because of underestimation of the autumn and winter rainfall, although they overestimate the summer rainfall. However, the IPSL-CM5A-LR and GISS-E2-R models overestimate total precipitation in this region: GISS produces too much rainfall in spring (45 mm), summer (100 mm) and autumn (60 mm), while IPSL-CM5A-LR simulates too much rainfall (130 mm) in summer only. Comparison of results from models that correctly simulate the location of each regime (compared to the observations) and those in which the area characterized by a given regime is too extensive or too small show that the biases in simulated precipitation are not related to whether models reproduce the spatial location of each regime correctly.

3.3 Mid-Holocene simulation

The location of the DP regime does not change between the *piControl* and *midHolocene* simulations of most (9) of the models (Fig. 3b). The two models (CNRM-CM5, MRI-CGCM3) that failed to simulate a DP pattern in the equatorial zone in the *piControl* nevertheless simulate this pattern in the *midHolocene* experiment. However, in the IPSL-CM5A-LR *midHolocene* simulation, the precipitation in the equatorial zone is more monsoon-like than in the model's *piControl* simulation. Most of the models (6) show no change in the northern limit of the monsoon; four models (CCSM4, IPSL-CM5A-LR, MRI-CGCM3, CNRM-CM5) show a northward displacement of the northern limit of the monsoon, while two models (BCC-CSM1.1, MRI-CGCM3) show a southward displacement of the northern limit of the monsoon as a result of southward expansion of the desert regime. Only two models (BBC-CSM1.1, MRI-CGCM3) show a northward displacement of the northern limit of the desert zone. Thus, in most of the *midHolocene* simulations, the desert regime occupies either a similar (5 models) or a slightly contracted area (4 models) compared to the *piControl*. Only one model (GISS-E2-R) shows a southward expansion of the Mediterranean precipitation regime; otherwise, this zone occupies the same position as in the *piControl* simulations.

We necessarily confine our comparisons of the magnitude of changes within each precipitation regime to those models that simulate a given regime in both the *piControl* and *midHolocene* simulations. The changes in the DP regime are not consistent and in general do not exceed the variability shown by the *piControl*. Only two models (CSIRO-Mk3-6-0, MIROC-ESM) show a significant reduction in precipitation (of 200 and 250 mm , respectively) in the *midHolocene* compared to the *piControl* (Fig. 5; Table 2). In the case of

the CSIRO-Mk3-6-0 model, this is the result of a large decrease in autumn precipitation but in the case of the MIROC-ESM the decrease is concentrated in the spring. The monsoon zone is characterized by a significant increase in precipitation, except in the case of the CSIRO-Mk3-6-0 model. The anomalies range from $+50$ to $+200\text{ mm yr}^{-1}$, reflecting large increases in summer ($15\text{--}140\text{ mm}$) and autumn ($20\text{--}250\text{ mm}$) rainfall. Changes in winter and spring precipitation in winter and spring are not significant. Most models show an increase in mean annual precipitation in the desert regime ($5\text{--}35\text{ mm}$) as a result of increased summer and autumn rainfall, but the change only exceeds *piControl* variability in three cases (CCSM4, GISS-E2-R and MIROC-ESM). Most of the models (11) show an increase in mean annual precipitation ($10\text{--}75\text{ mm}$) in the Mediterranean regime, although this increase only exceeds the *piControl* variability in the case of the GISS-E2-R model. The simulated increase in mean annual precipitation in the GISS-E2-R model results from an increase in spring, summer and autumn and a negligible change in winter. All of the models show an increase in spring precipitation, and two models (IPSL-CM5A-LR, HADGEM2-CC) show an increase in summer rainfall accompanied by either a small increase or no change in winter.

3.4 Comparison of *midHolocene* simulations and mid-Holocene observations

Reconstructions of the change in mean annual precipitation in the mid-Holocene (Fig. 6) show somewhat drier conditions (ca. 40 mm yr^{-1}) in the equatorial zone ($0\text{--}5^\circ\text{ N}$), an increase in precipitation of between 300 and 400 mm yr^{-1} between 10 and 30° N , and an increase of between 100 and 150 mm yr^{-1} in the Mediterranean ($35\text{--}45^\circ\text{ N}$). The simulated changes lie within the observed range between 0 and 5° N , with only three of the models lying outside the $25\text{--}75\%$ range. Several models simulate changes within the range of the observed increase in precipitation between 10 and 15° N (e.g. MRI-CGCM3, HADGEM2-CC, HADGEM2-ES, MIROC-ESM, IPSL-CM5a_LR and CCSM4). However, none of the models simulate the observed increase in precipitation (mean of ca. 390 mm yr^{-1}) between 15 and 30° N or indeed simulate changes within the range of the observations (Fig. 6). This is true even in the southernmost zone ($15\text{--}20^\circ\text{ N}$), although in this zone some of the models (e.g. MIROC-ESM) simulate a change of ca. 50% of the observed mean change in precipitation. Models underestimate the reconstructed change in precipitation in the Mediterranean zone ($35\text{--}45^\circ\text{ N}$), although most models lie within the extremes of the observational range. The highest simulated change in precipitation is ca. 50 mm yr^{-1} (GISS-E2-R) compared to the reconstructed mean change of between 100 and 150 mm yr^{-1} .

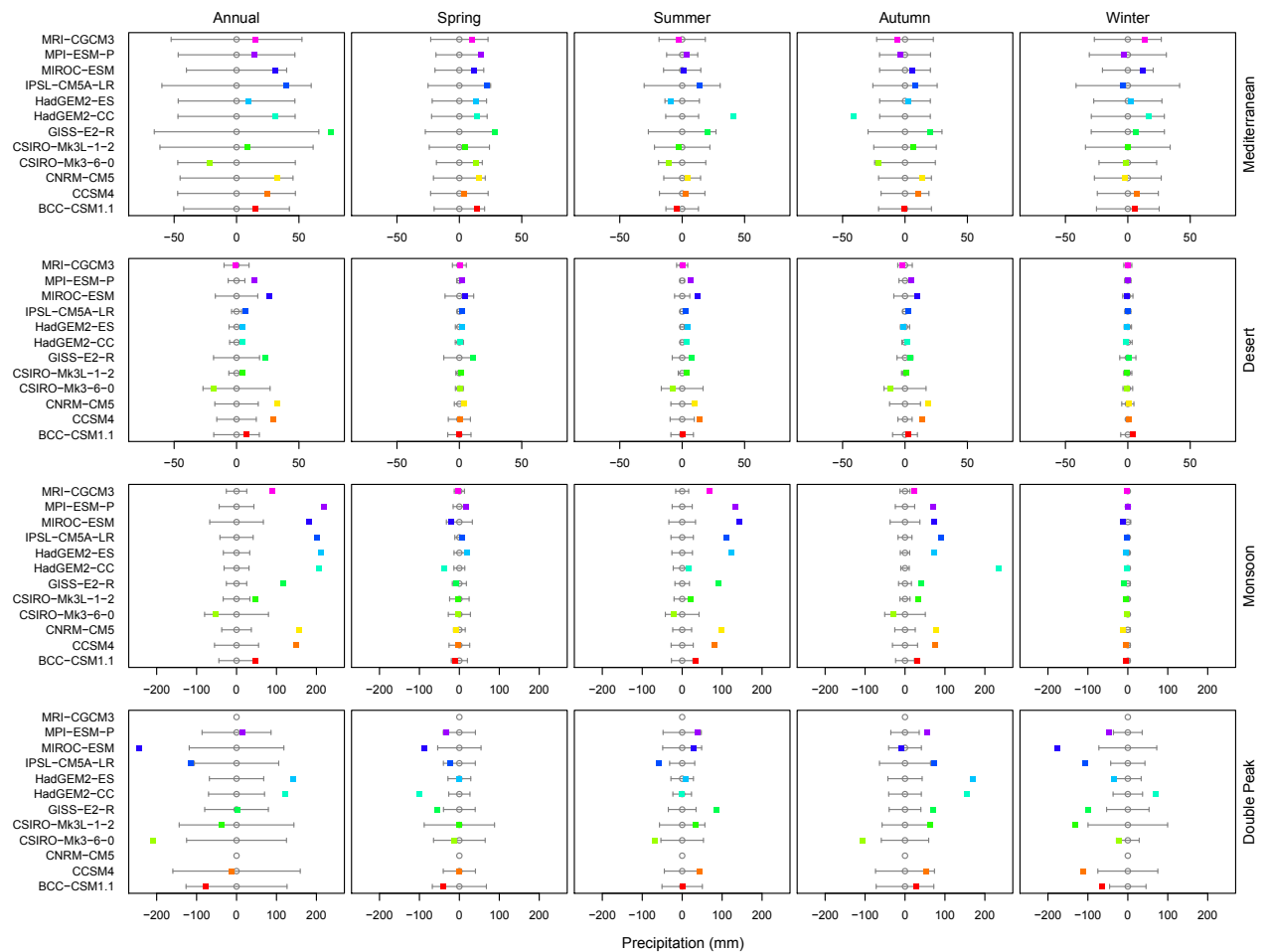


Fig. 5. Simulated changes in total and seasonal precipitation in the *midHolocene* compared to the *piControl* for each of the four precipitation regimes (Mediterranean, desert, monsoon, double peak) for the region that is common between the two sets of simulations. The standard deviation of precipitation in the *piControl* control simulation of each model is shown (grey bars) to provide a visual measure of the significance of the simulated change in precipitation. The seasons are defined as spring, summer, autumn and winter (as in Sect. 3.1).

3.5 Comparison between bias and anomaly

Comparison of the *piControl* bias and *midHolocene* anomaly suggests that model performance in the control simulations directly affects model performance in the *midHolocene* simulations in the DP, desert and Mediterranean regions (Fig. 7). In the DP region, there is a significant negative correlation (Fig. 7, all models, black line: slope = -0.23 , $R^2 = 0.74$, $p = 0.0$) between the bias and the anomaly: models that overestimate precipitation in the *piControl* show the largest reductions in precipitation in the *midHolocene* simulations (e.g. BCC-CSM1.1, CSIRO-Mk3-6-0 and MIROC-ESM). The overall relationship is driven by the OAC simulations (red line: $R^2 = 0.88$, $p = 0.02$); the slope for the OA models is not significant (blue line: $R^2 = 0.37$, $p = 0.2$). Indeed, as examination of these relationships in model-defined DP regions shows, the negative relationship shown by the

OA models in the $0-5^\circ$ N is driven by the two models that simulate monsoon-like regimes in this zone in the *piControl*.

There is no relationship between the *piControl* bias and the *midHolocene* anomaly in the monsoon zone (Fig. 7), whether this is defined geographically (slope = 0.00 , $R^2 = 0.0$, $p = 0.98$) or using the model-based regimes (slope = 0.08 , $R^2 = 0.05$, $p = 0.49$). Thus, the ability to simulate the correct magnitude of modern precipitation appears to have no influence on the magnitude of the response of the monsoon to changed forcing. However, the OA and OAC models appear to show opposite tendencies: the OA models show a weakly positive relationship between the bias and the anomaly (models that simulate less rainfall than observed in the *piControl* produce smaller MH anomalies) whereas the OAC models show a (very) weakly negative relationship.

Table 2. Summary of area-averaged climate anomalies (*midHolocene* minus *piControl*) for individual models for individual seasons and for mean annual precipitation. Bold font indicates values that are significantly different from the interannual variability of the modern observations. The seasons are spring, summer, autumn, and winter (as in Sect. 3.1).

Season anomaly	BCC-CSM1.1	CCSM4	CNRM-CM5	CSIRO-Mk3-6-0	CSIRO-Mk3L-1-2	GISS-E2-R	HadGEM2-CC	HadGEM2-ES	IPSL-CM5A-LR	MIROC-ESM	MPI-ESM-P	MRI-CGCM3
Mediterranean												
Annual	15.0	24.4	32.6	−21.2	8.4	75.7	30.9	9.2	40.1	30.8	14.3	15.4
Spring	13.9	3.7	16.1	13.0	4.2	28.4	14.5	13.0	22.2	11.6	17.6	10.4
Summer	−4.3	2.7	4.7	−10.7	−2.4	20.5	40.6	−8.8	14.0	0.8	3.5	−2.8
Autumn	−0.4	10.5	14.0	−21.6	6.6	20.3	−40.9	2.9	8.0	6.0	−3.9	−5.9
Winter	5.8	7.4	−2.3	−1.9	0.0	6.5	16.7	2.1	−4.1	12.4	−2.9	13.8
Desert												
Annual	7.7	29.5	32.7	−18.5	4.6	22.8	4.5	4.4	6.8	26.1	14.3	7.7
Spring	0.1	0.6	3.6	0.8	1.3	10.6	0.6	2.1	1.8	4.2	2.1	0.1
Summer	0.8	14.3	9.6	−7.4	3.2	7.7	3.4	4.2	2.8	12.3	6.7	0.8
Autumn	2.8	13.9	18.5	−11.5	0.9	3.9	2.1	−1.3	2.3	10.1	5.1	2.8
Winter	4.1	0.6	1.0	−0.5	−0.8	0.7	−1.7	−0.5	−0.1	−0.4	0.4	4.1
Monsoon												
Annual	47.4	148.6	155.8	−53.5	47.2	116.1	207.6	210.4	202.4	182.1	219.9	88.5
Spring	−11.2	−2.6	−7.4	−2.6	−2.7	−7.5	−39.1	19.3	6.0	−19.7	17.5	−1.9
Summer	33.6	80.4	97.2	−20.3	21.5	91.6	15.4	122.8	110.0	142.4	132.8	68.3
Autumn	29.8	76.6	78.7	−28.3	32.9	41.4	233.6	72.5	89.6	72.2	70.2	23.7
Winter	−4.7	−5.9	−12.6	−2.3	−4.5	−9.4	−2.2	−4.3	−3.2	−12.7	−0.7	−1.5
DP												
Annual	−76.7	−13.3	−	−208.8	−36.4	2.8	123.0	142.0	−	−244.4	14.3	−
Spring	−41.3	0.5	−	−12.7	−0.6	−56.2	−100.9	−1.7	−	−87.2	−32.0	−
Summer	1.1	43.8	−	−68.1	33.9	87.1	−1.8	8.6	−	29.3	38.7	−
Autumn	29.1	53.1	−	−106.8	63.2	71.0	154.9	168.9	−	−9.6	55.6	−
Winter	−65.5	−110.7	−	−21.1	−132.9	−99.1	70.7	−33.9	−	−176.9	−48.1	−

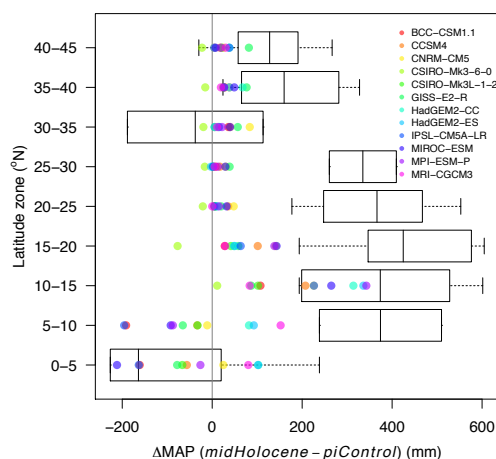


Fig. 6. Comparison of simulated and reconstructed changes in mean annual precipitation in the mid-Holocene for 5° latitude bands between 0 and 45° N. The reconstructions are from the Bartlein et al. (2011) data set. The mean, 25–75 % range and full range of the reconstructions are shown (for those latitude bands with sufficient data points). The model results are averages for the grid cells with observations.

There is a significant positive correlation between the *piControl* bias and *midHolocene* anomaly in the desert region (Fig. 7). This is true whether the region is defined geographically (slope = 0.32, $R^2 = 0.58$, $p = 0.01$) or using the model-defined desert regimes (slope = 0.32, $R^2 = 0.48$, $p = 0.02$). Models that produce a reasonable simulation of modern rainfall in this region fail to produce a significant enhancement in the *midHolocene* simulation (CSIRO-Mk3L-1-2, HadGEM2-CC, IPSL-CM5A-LR) whereas models that are too wet in the *piControl* produce large changes in the *midHolocene* (CCSM4, GISS-E2-R and MIROC-ESM). However, these relationships are driven by the OA simulations; the OAC simulations do not show any significant relationship between the *piControl* bias and the *midHolocene* anomaly.

There is also a significant positive correlation between bias and anomaly in the Mediterranean region (Fig. 7), whether the region is defined geographically (slope = 0.14, $R^2 = 0.58$, $p = 0.01$) or using the model-defined regimes (slope = 0.15, $R^2 = 0.48$, $p = 0.02$). Models that underestimate precipitation in this zone in the *piControl* show only small increases in the *midHolocene* (BCC-CSM1.1, CCSM4 and MPI-ESM) while models with positive bias (GISS-E2-R and IPSL-CM5A-LR) produce larger changes in precipitation. However, the relationship for the OAC simulations is again non-significant.

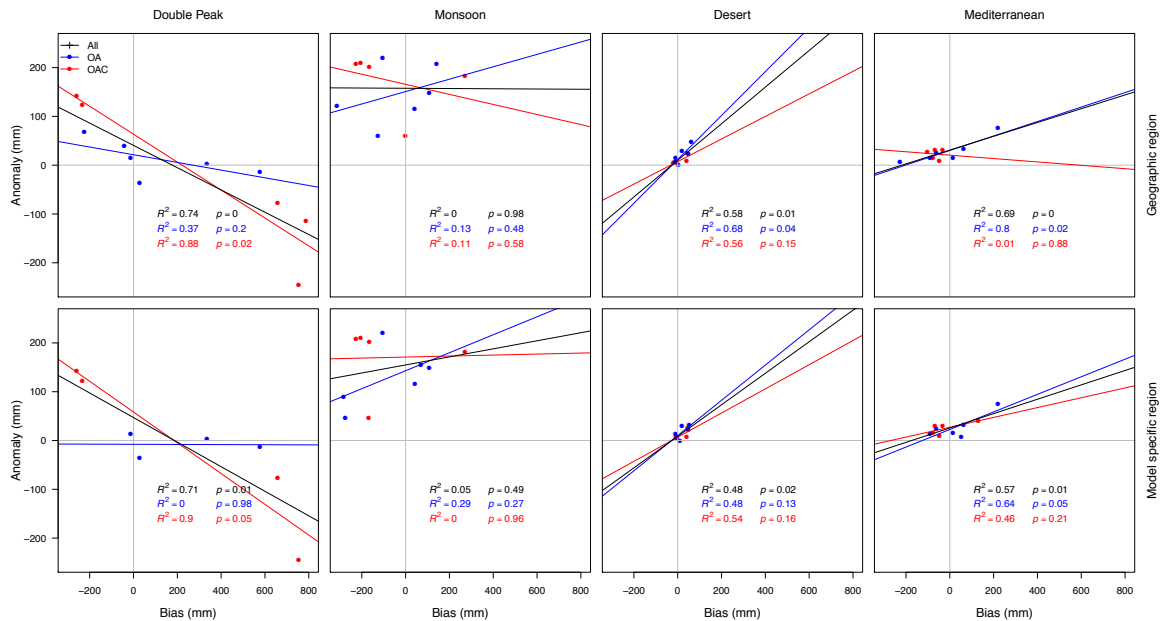


Fig. 7. Relationship between biases in the *piControl* simulation of mean annual precipitation (mm) and mid-Holocene precipitation anomalies (*midHolocene* – *piControl*) as simulated by each of the CMIP5 models for each of the precipitation regimes (Double Peak, Monsoon, Desert, Mediterranean). The upper panels show biases and anomalies calculated for specific latitudinal bands as defined from the modern observed spatial extent of each regime (geographic region). The lower panels show biases and anomalies calculated for the region identified as characterized by a given regime in each model and simulation (model specific region). The regressions are calculated for all models (All: black), for the coupled ocean–atmosphere models (OA: blue) and for the carbon-cycle models (OAC: red).

Even in those regions where there are significant relationships between *piControl* bias and the *midHolocene* anomaly, the R^2 value ranges from 0.48 to 0.75. Thus, the bias in the *piControl* is not the only factor that determines whether the simulated magnitude of the MH climate change is correct. Furthermore, biases in the *piControl* appear to have less (or no) influence on the simulated *midHolocene* anomaly in the OAC simulations, except in the DP zone.

4 Discussion

Our analyses suggest that the CMIP5 models fail to reproduce key aspects of both the modern and MH climate of the northern Africa and Mediterranean region. Although the models generally reproduce the four characteristic seasonal patterns of precipitation, they do not always simulate these patterns in the correct place. They also tend to underestimate the magnitude of seasonal changes in precipitation. For example, they underestimate the amount of winter rainfall and overestimate the summer rainfall in the Mediterranean region. This is consistent with previous analyses of Mediterranean climates in both the CMIP3 (Giorgi and Lionello, 2008) and CMIP5 (Kelley et al., 2012) simulations. The models overestimate the precipitation in the DP zone, again a feature identified from previous analyses (Roehrig et al.,

2013). Previous analyses of the CMIP5 models (e.g. Roehrig et al., 2013; Brands et al., 2013) have suggested that there is a tendency for models to underestimate precipitation in the Sahel zone. While our analyses confirm this, with 8 out of 12 models showing less summer precipitation than observed, some of the models (e.g. CSIRO-Mk3L-1-2, BCC-CSM1.1) show a distinct improvement when the comparison is made between regions defined by precipitation regimes rather than geographically (Fig. 4). Furthermore, the temporal interval used for comparison also plays a role: MIROC-ESM, for example, simulates summer precipitation correctly but annual rainfall is too large because the simulated monsoon season is too long. Our evaluations are based on the assumption that the difference in climate between the *piControl* (1850 AD) and the 1961–1990 modern climatology is small. Comparisons of the *piControl* and *historical* simulations (Fig. S1, Supplement) for a sub-set of the models appear to support this assumption: the differences between the simulations are smaller than the difference between the simulated and observed climates. There is no synthesis of data for the pre-industrial era from northern Africa, but data from the Mediterranean region does not suggest substantial differences (e.g. Davis et al., 2003).

The models produce a northward shift and amplification of monsoon precipitation in the MH in response to insolation forcing. While the broad-scale patterns of change are

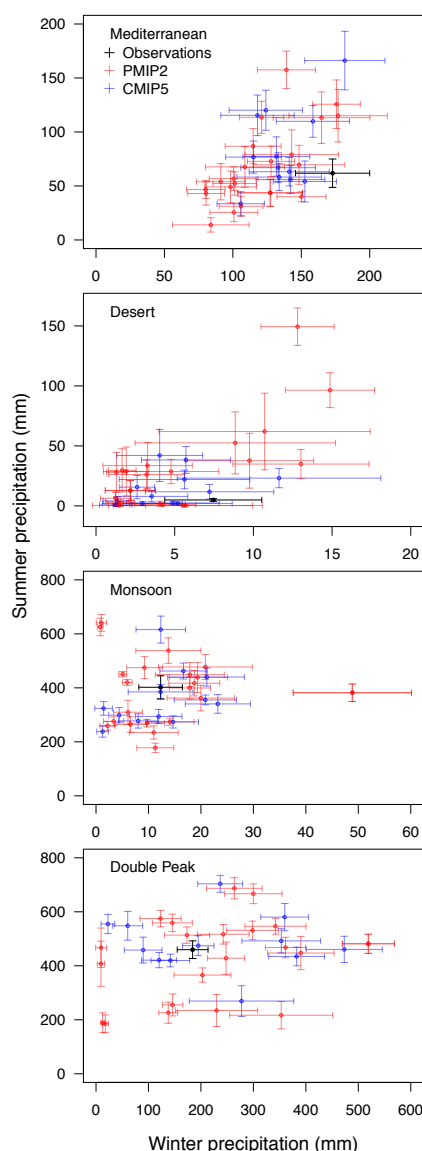


Fig. 8. Comparison of simulated and observed summer and winter precipitation in each of the four precipitation regimes (Mediterranean, Desert, Monsoon, Double Peak). The observations (black) are the average for the period 1961–1990 from the CRU T3.1 data set (Harris et al., 2014). The simulated mean and standard deviation of precipitation from the CMIP5 models (blue) is based on the last 100 yr of the *piControl*. These simulations can be compared with results from coupled ocean–atmosphere simulations made during the second phase of the PMIP2 (Braconnot et al., 2012; shown in red). The PMIP2 results are the mean and standard deviation based on the last 100 yr of a *piControl*, except in three cases where only 50 yr of data were available. Model results are calculated for each precipitation regime based on the observed geographic extent characterized by these regimes, as defined using the CRU TS3.1 data set. Summer and winter as defined in Sect. 3.1.

consistent with the observations, the magnitude of these changes is significantly underestimated (Fig. 6). The failure to simulate a sufficiently large expansion of the African monsoon has been a major criticism of previous generations of climate models (Joussaume et al., 1999; Coe and Harrison, 2002; Braconnot et al., 2007a, 2012; Brayshaw et al., 2011; Zhao and Harrison, 2011). Comparisons between CMIP5 and PMIP2 models (Fig. 8) show that the two ensembles are indistinguishable in terms of simulated changes over this study region. Global comparisons of these two sets of simulations (e.g. Harrison et al., 2013) appear to confirm that the CMIP5 models are no better at simulating climate changes than previous generations of models. It was originally suggested that the underestimation of monsoon expansion reflected the failure to include feedbacks associated with climate-induced changes in land-surface characteristics, including wetter and more organic soils, the replacement of desert by grassland and shrubland, and the expansion of lakes and wetlands. Indeed, simulations in which the impacts of changes in land-surface characteristics were prescribed through changing albedo produced much larger monsoons (Street-Perrott et al., 1990; Kutzbach et al., 1996; Coe and Bonan, 1997; Broström et al., 1998). However, this effect is not as pronounced in asynchronously-coupled climate–vegetation simulations (Claussen and Gaylor, 1997; Texier et al., 1997; Braconnot et al., 1999), models with dynamic vegetation from PMIP2 (Braconnot et al., 2012), or indeed coupled carbon–climate models in CMIP5 (Harrison et al., 2013). In general, these models produce a strengthening of the monsoon in situ and only a minor northward expansion of the zone of monsoon rainfall. If we assume that the coupled models are behaving reasonably, this shows that the changes to the energy budget produced by the prescribed changes in albedo are compensated by changes in the partitioning between latent and sensible heating through increased evapotranspiration. This implies that some other mechanism, for example associated with changes in circulation, is required to produce the observed expansion of rainfall in the Sahara.

Our MH model evaluation is based on pollen-based reconstructions of mean annual precipitation. Although the increase in monsoon precipitation is large (300–400 mm between 5 and 30° N) and spatially coherent, there are some zonal bands where the number of reconstructions is limited (see Fig. 6). However, other sources of palaeoenvironmental data, including vegetation (Hoelzmann et al., 1998; Prentice and Jolly, 2000; Watrin et al., 2009; Niedermeyer et al., 2010), lake-level reconstructions (Kohfeld and Harrison, 2000; Tierney et al., 2011), and archaeological evidence (Kuper and Kröpelin, 2006; Dunne et al., 2012), show that the magnitude of the reconstructed precipitation changes in these zones is plausible. Furthermore, the reconstructions of climate conditions in the Mediterranean region are based on a much larger number of individual data points (Bartlein et al., 2011). Thus, the discrepancies between the model

simulations and the observations are not simply a result of lack of information.

It would be possible to use the qualitative information about changes in water balance provided by lake-level records to constrain pollen-based climate reconstructions (see e.g. Cheddadi et al., 1997). While this could provide more robust reconstructions of the observed change in precipitation for northern Africa, the number of observations would still necessarily be limited to sites where both pollen and lake-level records are available. Model inversion provides an alternative approach to use of lake-level data for climate reconstruction (see e.g. Vassiljev et al., 1998), and one that has already been successfully used with pollen data (Wu et al., 2007). However, changes in lake-water balance can be brought about by changes in multiple climate parameters (temperature, precipitation, seasonality of precipitation, cloudiness, vapour pressure, wind speed) and the magnitude of the lake-level changes that occur in response to changes in catchment-water balance are influenced by morphometric factors (lake depth and shape, lake size relative to catchment size) (Harrison et al., 2002), and the methodology for taking account of all these factors has not yet been developed.

The simulated increase in mean annual precipitation in the Mediterranean region is small and, in comparison with the variability already present in the *piControl*, is not significant. However, although just half of the models show an increase in summer, all of them show an increase in precipitation in spring and some of them also show an increase in autumn. Thus, some of the models produce an increase in growing season moisture that, although too small, is consistent with the expansion of deciduous forest in this region during the mid-Holocene. Temperate deciduous forests occur in midlatitude regions with > 700 mm of annual precipitation spread throughout the year (see Harrison et al., 2010). Temperate deciduous forest occurs, for example, around Lake Banyoles in eastern Spain, where mean annual precipitation is ca. 800 mm and nearly half of this falls in spring and summer (Soler et al., 2007). According to the mid-Holocene simulations for the Mediterranean area, the largest increase in growing-season precipitation is ca. 30 mm in spring and 40 in summer (GISS-E2-R and HadGEM2-CC respectively), and the overall change in mean annual precipitation is < 75 mm (GISS-E2-R). This is less than the increase required for deciduous trees to grow. Nevertheless, these simulations point to mechanisms that could help to explain the observed vegetation changes in the Mediterranean. Furthermore, if the absence of a significant increase in summer rainfall in the Mediterranean is linked to underestimation of the northward migration of the African monsoon, then improvements in the simulation of monsoonal changes should also lead to a more realistic simulation of Mediterranean climate.

We have shown that there is a significant relationship between the bias in the control simulation and the magnitude of the simulated MH changes in precipitation for the DP, desert and Mediterranean zones, although no such relationship is

present in the monsoon zone. However, the relationship in the desert and Mediterranean zones is only apparent in the OA models; the *piControl* bias does not seem to affect the *midHolocene* anomaly in the OAC models. The OA models also show a weakly positive (though non-significant) relationship between *piControl* bias and *midHolocene* anomaly in the monsoon region. Thus, the apparently significant relationships between bias and anomaly found when considering all the models are not a consistent feature of these simulations. Even in the DP, desert and Mediterranean zones, the bias in the OA *piControl* simulations only explains part of the variability in simulated climate changes. Previous studies have also had difficulties in finding consistent relationships between control biases and MH changes in precipitation. Comparison of control and MH atmosphere-only simulations made in the first phase of the PMIP1 showed that intermodel differences in the position of the intertropical convergence zone in the control simulation was reflected in the intermodel differences of its position in the MH simulation (Joussaume et al., 1999). However, there was no clear relationship between the amount of precipitation in the control and the increase in precipitation in the MH (Braconnot et al., 2002). Braconnot et al. (2007b), analysing OA simulations from PMIP2, showed that the relationship between the simulated precipitation in the control to the ratio of the change in precipitation between MH and control was negative: models that simulated very little rainfall tended to produce larger changes at the MH. However, this relationship was clearly driven by only three models, and the remaining models show no trend between the precipitation in the control simulation and the ratio of change in the MH. Thus, this seems to be consistent with our analyses. It is hard to escape the conclusion that improvements to the simulation of modern climate (see e.g. Haerter et al., 2011) will not guarantee that climate changes will be correctly simulated.

In this study, we have analysed the realism of simulated climates both in terms of climate regimes and by comparing specific geographic bands. The use of climate regimes places less stringent requirements on model performance, allowing an assessment, for example, of whether a model can simulate changes in seasonality independent of location. One reason for adopting this approach is the concern that model resolution, particularly in regions of complex topography, could affect geographic patterning (see e.g. Brewer et al., 2007). However, it can be difficult to find objective criteria for the definition of these climate regimes. Although we have been able to distinguish DP from monsoon, and monsoon from desert, climates solely on the basis of precipitation seasonality, it is not possible to use this type of criterion to distinguish desert and Mediterranean climates. Brewer et al. (2007) used *k*-means clustering to define climate regimes in Europe. Although this is an approach that needs to be further explored, it involves some arbitrary decisions about the climate variables used for clustering as well as the number of clusters considered.

Many of the large-scale features characteristic of projected climate changes are a feature of past climate changes, and comparison with palaeo-observations shows that current models reproduce these features in a realistic way (e.g. Braconnot et al., 2012; Izumi et al., 2013; Schmidt et al., 2014a; Li et al., 2013). Models, as we confirm here for northern Africa and the Mediterranean region, are also able to simulate precipitation regimes and shifts in these regimes in a realistic way (Joussaume et al., 1999; Braconnot et al., 2007a; Brewer et al., 2007). However, there are still important discrepancies between the simulated and observed magnitude of changes in precipitation, despite the increasing complexity and resolution of the CMIP5 models compared to earlier generations of models. Given that the ability to simulate the magnitude of MH changes in seasonal climates does not appear to be systematically related to biases in the control simulations, focusing on improving the simulation of modern climate will not ensure that future projections or retrodictions of the climate of the Mediterranean and northern Africa will be more reliable. This is of concern given the environmental problems associated with recent climate changes in the Mediterranean and the importance of monsoonal rainfall for agriculture in northern Africa.

5 Conclusions

The CMIP5 models fail to reproduce key aspects of both the modern and MH climate of the northern Africa and Mediterranean region, including the correct geographical location of zonal precipitation regimes in the pre-industrial simulation and the magnitude of MH changes in these regimes.

Although biases in the OA simulations explain part of the variability in simulated climate changes, a similar relationship is not found for the OAC simulations. Thus, overall, biases in the control simulations cannot explain the failure to reproduce MH changes in precipitation.

As in previous generations of model simulations, the CMIP5 simulations underestimate the northward shift and the magnitude of observed changes in the north African monsoon.

In the Mediterranean region, the simulations show a tendency for increased growing-season precipitation. Such a shift is required to explain observed vegetation changes in this region in the MH, but the simulated shift is much too small. We speculate that this is linked to the underestimation of changes in the north African monsoon, suggesting that improved simulation of Mediterranean climates is linked to improvements in simulating the climate of northern Africa.

The failure to simulate observed mid-Holocene changes in the north African monsoon and the potentially linked failure to simulate the observed shift in rainfall seasonality in the Mediterranean raises concerns about the reliability of model projections of future climates in these regions.

Supplementary material related to this article is available online at <http://www.clim-past.net/10/551/2014/cp-10-551-2014-supplement.pdf>.

Acknowledgements. This work was initiated when A. Perez-Sanz was a guest scientist at Macquarie University; we thank the Department of Biology for providing funds to facilitate this visit. G. Li is supported by an International Postgraduate Research Scholarship at Macquarie University. This research was supported by the Australian Research Council, grant number DP1201100343 (SPH) and the CGL2012-33063 (PGS) by the Spanish CICYT. We acknowledge the World Climate Research Programme's Working Group on Coupled Modelling, which is responsible for CMIP, and the climate modelling groups for producing and making available their model output. (For CMIP the US Department of Energy's Program for Climate Model Diagnosis and Intercomparison provides coordinating support and led development of software infrastructure in partnership with the Global Organization for Earth System Science Portals.) The analyses and figures are based on data archived at CMIP5 on 15 August 2012.

Edited by: A. Paul

References

- Amatulli, G., Camia, A., and San-Miguel-Ayanz, J.: Estimating future burned areas under changing climate in the EU-Mediterranean countries, *Sci. Total Environ.*, 450–451, 209–222, doi:10.1016/j.scitotenv.2013.02.014, 2013.
- Bartlein, P. J., Harrison, S. P., Brewer, S., Connor, S., Davis, B. A. S., Gajewski, K., Guiot, J., Harrison-Prentice, T. I., HENDERSON, A., Peyron, O., Prentice, I. C., Scholze, M., Seppä, H., Shuman, B., Sugita, S., Thompson, R. S., Vial, A. E., Williams, J., and Wu, H.: Pollen-based continental climate reconstructions at 6 and 21 ka: a global synthesis, *Clim. Dynam.*, 37, 775–802, doi:10.1007/s00382-010-0904-1, 2011.
- Bonfils, C., de Noblet-Ducoudré, N., Guiot, J., and Bartlein, P.: Some mechanisms of mid-Holocene climate change in Europe, inferred from comparing PMIP models to data, *Clim. Dynam.*, 23, 79–98, doi:10.1007/s00382-004-0425-x, 2004.
- Bosmans, J. H. C., Drijfhout, S. S., Tuenter, E., Lourens, L. J., Hilgen, F. J., and Weber, S. L.: Monsoonal response to mid-holocene orbital forcing in a high resolution GCM, *Clim. Past*, 8, 723–740, doi:10.5194/cp-8-723-2012, 2012.
- Braconnot, P., Joussaume, S., Marti, O., and de Noblet, N.: Synergistic feedbacks from ocean and vegetation on the African monsoon response to mid-Holocene insolation, *Geophys. Res. Lett.*, 26, 2481–2484, doi:10.1029/1999GL006047, 1999.
- Braconnot, P., Harrison, S. P., Kageyama, M., Bartlein, P. J., Masson-Delmotte, V., Abe-Ouchi, A., Otto-Bliesner, B., and Zhao, Y.: Evaluation of climate models using palaeoclimatic data, *Nat. Clim. Change*, 2, 417–424, doi:10.1038/nclimate1456, 2012.
- Braconnot, P., Loutre, M., Dong, B., Joussaume, S., and Valdes, P.: How the simulated change in monsoon at 6 ka BP is related to the simulation of the modern climate: results from the Paleoclimate Modeling Intercomparison Project, *Clim. Dynam.*, 19, 107–121, doi:10.1007/s00382-001-0217-5, 2002.

- Braconnot, P., Otto-Bliesner, B., Harrison, S., Joussaume, S., Peterchmitt, J.-Y., Abe-Ouchi, A., Crucifix, M., Driesschaert, E., Fichefet, Th., Hewitt, C. D., Kageyama, M., Kitoh, A., Laîné, A., Loutre, M.-F., Marti, O., Merkel, U., Ramstein, G., Valdes, P., Weber, S. L., Yu, Y., and Zhao, Y.: Results of PMIP2 coupled simulations of the Mid-Holocene and Last Glacial Maximum – Part 1: experiments and large-scale features, *Clim. Past*, 3, 261–277, doi:10.5194/cp-3-261-2007, 2007a.
- Braconnot, P., Otto-Bliesner, B., Harrison, S., Joussaume, S., Peterchmitt, J.-Y., Abe-Ouchi, A., Crucifix, M., Driesschaert, E., Fichefet, Th., Hewitt, C. D., Kageyama, M., Kitoh, A., Loutre, M.-F., Marti, O., Merkel, U., Ramstein, G., Valdes, P., Weber, L., Yu, Y., and Zhao, Y.: Results of PMIP2 coupled simulations of the Mid-Holocene and Last Glacial Maximum – Part 2: feedbacks with emphasis on the location of the ITCZ and mid- and high latitudes heat budget, *Clim. Past*, 3, 279–296, doi:10.5194/cp-3-279-2007, 2007b.
- Brands, S., Herrera, S., Fernández, J., and Gutiérrez, J. M.: How well do CMIP5 Earth System Models simulate present climate conditions in Europe and Africa?: A performance comparison for the downscaling community, *Clim. Dynam.*, 41, 803–817, doi:10.1007/s00382-013-1742-8, 2013.
- Brayshaw, D. J., Rambeau, C. M. C., and Smith, S. J.: Changes in Mediterranean climate during the Holocene: Insights from global and regional climate modelling, *Holocene*, 21, 15–31, doi:10.1177/0959683610377528, 2011.
- Brewer, S., Guiot, J., and Torre, F.: Mid-Holocene climate change in Europe: a data-model comparison, *Clim. Past*, 3, 499–512, doi:10.5194/cp-3-499-2007, 2007.
- Broström, A., Coe, M., Harrison, S. P., Gallimore, R., Kutzbach, J. E., Foley, J., Prentice, I. C., and Behling, P.: Land surface feedbacks and palaeomonsoons in northern Africa, *Geophys. Res. Lett.*, 25, 3615–3618, doi:10.1029/98GL02804, 1998.
- Camuffo, D., Bertolin, C., Barriendos, M., Dominguez-Castro, F., Cocheo, C., Enzi, S., Sghedoni, M., Valle, A., Garnier, E., Alcorado, M. J., Xoplaki, E., Luterbacher, J., Diodato, N., Maugeri, M. Nunes, M. F., and Rodriguez, R.: 500-years temperature reconstruction in the Mediterranean Basin by means of documentary data and instrumental observations, *Climatic Change*, 101, 169–199, 2010.
- Carrión, J. S., Fernández, S., González-Sampériz, P., Gil-Romera, G., Badal, E., Carrión-Marco, Y., López-Merino, L., López-Sáez, J. A., Fierro, E., and Burjachs, F.: Expected trends and surprises in the Lateglacial and Holocene vegetation history of the Iberian Peninsula and Balearic Islands, *Rev. Palaeobot. Palynol.*, 162, 458–475, doi:10.1016/j.revpalbo.2009.12.007, 2010.
- Cheddadi, R., Yu, G., Guiot, J., Harrison, S. P., and Prentice, I. C.: The climate of Europe 6000 years ago, *Clim. Dynam.*, 13, 1–9, doi:10.1007/s003820050148, 1997.
- Claussen, M. and Gaylor, V.: The greening of the Sahara during the mid-Holocene: results of an interactive atmosphere-biosphere model, *Global Ecol. Biogeogr.*, 6, 369–377, 1997.
- CLIVAR: Climate in Spain: Past, Present and Future. Regional climate change assessment report, edited by: Pérez, F. F. and Boscolo, R., Ministerio de Ciencia e Innovación, Madrid, 83 pp., 2010.
- Coe, M. T. and Bonan, G.: Feedbacks between climate and surface water in northern Africa during the middle Holocene, *J. Geophys. Res.*, 102, 11087–11101, doi:10.1029/97JD00343, 1997.
- Coe, M. T. and Harrison, S. P.: The water balance of northern Africa during the mid-Holocene: an evaluation of the 6 kaBP PMIP simulations, *Clim. Dynam.*, 19, 155–166, doi:10.1007/s00382-001-0219-3, 2002.
- Collins, W. J., Bellouin, N., Doutriaux-Boucher, M., Gedney, N., Halloran, P., Hinton, T., Hughes, J., Jones, C. D., Joshi, M., Liddicoat, S., Martin, G., O'Connor, F., Rae, J., Senior, C., Sitch, S., Totterdell, I., Wiltshire, A., and Woodward, S.: Development and evaluation of an Earth-System model – HadGEM2, *Geosci. Model Dev.*, 4, 1051–1075, doi:10.5194/gmd-4-1051-2011, 2011.
- Davis, B. A. S., Brewer, S., Stevenson, A. C., and Guiot, J.: The temperature of Europe during the Holocene reconstructed from pollen data, *Quaternary Sci. Rev.*, 22, 1701–1716, doi:10.1016/S0277-3791(03)00173-2, 2003.
- Dufresne, J.-L., Foujols, M.-A., Denvil, S., Caubel, A., Marti, O., Aumont, O., Balkanski, Y., Bekki, S., Bellenger, H., and Benshila, R.: Climate change projections using the IPSL-CM5 Earth System Model: from CMIP3 to CMIP5, *Clim. Dynam.*, 9–10, 2123–2165, doi:10.1007/s00382-012-1636-1, 2013.
- Dunne, J., Evershed, R. P., Salque, M., Cramp, L., Bruni, S., Ryan, K., Biagetti, S., and di Lernia, S.: First dairying in green Saharan Africa in the fifth millennium bc, *Nature*, 486, 390–394, doi:10.1038/nature11186, 2012.
- European Environment Agency: Climate change, impacts and vulnerability in Europe 2012: an indicator-based report, European Environment Agency, Copenhagen, 2012.
- Forman, S. L., Oglesby, R., Markgraf, V., and Stafford, T.: Paleoclimatic significance of Late Quaternary eolian deposition on the Piedmont and High Plains, Central United States, *Global Planet. Change*, 11, 35–55, doi:10.1016/0921-8181(94)00015-6, 1995.
- Gaetani, M., Pohl, B., Douville, H., and Fontaine, B.: West African Monsoon influence on the summer Euro-Atlantic circulation, *Geophys. Res. Lett.*, 38, L09705, doi:10.1029/2011GL047150, 2011.
- Gent, P. R., Danabasoglu, G., Donner, L. J., Holland, M. M., Hunke, E. C., Jayne, S. R., Lawrence, D. M., Neale, R. B., Rasch, P. J., and Vertenstein, M.: The community climate system model version 4, *J. Climate*, 24, 4973–4991, doi:10.1175/2011JCLI4083.1, 2011.
- Giorgi, F.: Climate change hot-spots, *Geophys. Res. Lett.*, 33, L08707, doi:10.1029/2006GL025734, 2006.
- Giorgi, F. and Lionello, P.: Climate change projections for the Mediterranean region, *Global Planet. Change*, 63, 90–104, doi:10.1016/j.gloplacha.2007.09.005, 2008.
- Guiot, J., Boreux, J. J., Braconnot, P., and Torre, F.: Data-model comparison using fuzzy logic in paleoclimatology, *Clim. Dynam.*, 15, 569–581, doi:10.1007/s003820050301, 1999.
- Haerter, J. O., Hagemann, S., Moseley, C., and Piani, C.: Climate model bias correction and the role of timescales, *Hydrol. Earth Syst. Sci.*, 15, 1065–1079, doi:10.5194/hess-15-1065-2011, 2011.
- Harris, I., Jones, P. D., Osborn, T. J., and Lister, D. H.: Updated high-resolution grids of monthly climatic observations – the CRU TS3.10 Dataset, *Int. J. Climatol.*, 34, 623–642, doi:10.1002/joc.3711, 2014.

- Harrison, S. P., Prentice, I. C., and Bartlein, P. J.: Influence of insolation and glaciation on atmospheric circulation in the North Atlantic sector: Implications of general circulation model experiments for the Late Quaternary climatology of Europe, *Quaternary Sci. Rev.*, 11, 283–299, doi:10.1016/0277-3791(92)90002-P, 1992.
- Harrison, S. P., Yu, G., and Vassiljev, J.: Climate changes during the Holocene recorded by lakes from Europe, in: *Climate Development and History of the North Atlantic Realm*, edited by: Wefer, G., Berger, W., Behre, K.-E., and Jansen, E., Springer-Verlag, Berlin, Heidelberg, 191–204, 2002.
- Harrison, S. P., Prentice, I. C., Barboni, D., Kohfeld, K. E., Ni, J., and Sutra, J.-P.: Ecophysiological and bioclimatic foundations for a global plant functional classification, *J. Veg. Sci.*, 21, 300–317, doi:10.1111/j.1654-1103.2009.01144.x, 2010.
- Harrison, S. P., Bartlein, P. J., Brewer, S., Prentice, I. C., Boyd, M., Hessler, I., Holmgren, K., Izumi, K., and Willis, K.: Model benchmarking with glacial and mid-Holocene climates, *Clim. Dynam.*, 1432–0894, doi:10.1007/s00382-013-1922-6, 2013.
- Hoelzmann, P., Jolly, D., Harrison, S. P., Laarif, F., Bonnefille, R., and Pachur, H.-J.: Mid-Holocene land-surface conditions in northern Africa and the Arabian Peninsula: A data set for the analysis of biogeophysical feedbacks in the climate system, *Global Biogeochem. Cy.*, 12, 35–51, doi:10.1029/97GB02733, 1998.
- Hoerling, M., Eischeid, J., Perlwitz, J., Quan, X., Zhang, T., and Pegion, P.: On the increased frequency of Mediterranean drought, *J. Climate*, 25, 2146–2161, 2012.
- Ibanez, F.: Sur une nouvelle application de la théorie de l'information à la description des séries chronologiques planctoniques, *J. Plankton Res.*, 4, 619–632, doi:10.1093/plankt/4.3.619, 1982.
- Izumi, K., Bartlein, P. J., and Harrison, S. P.: Consistent large-scale temperature responses in warm and cold climates, *Geophys. Res. Lett.*, 40, 1817–1823, doi:10.1002/grl.50350, 2013.
- Joussaume, S., Taylor, K. E., Braconnot, P., Mitchell, J. F. B., Kutzbach, J. E., Harrison, S. P., Prentice, I. C., Broccoli, A. J., Abe-Ouchi, A., Bartlein, P. J., Bonfils, C., Dong, B., Guiot, J., Herterich, K., Hewitt, C. D., Jolly, D., Kim, J. W., Kislov, A., Kitoh, A., Loutre, M. F., Masson, V., McAvaney, B., McFarlane, N., de Noblet, N., Peltier, W. R., Peterschmitt, J. Y., Pollard, D., Rind, D., Royer, J. F., Schlesinger, M. E., Syktus, J., Thompson, S., Valdes, P., Vettoretti, G., Webb, R. S., and Wyputta, U.: Monsoon changes for 6000 years ago: Results of 18 simulations from the Paleoclimate Modeling Intercomparison Project (PMIP), *Geophys. Res. Lett.*, 26, 859–862, doi:10.1029/1999GL000126, 1999.
- Kelley, C., Ting, M., Seager, R., and Kushnir, Y.: Mediterranean precipitation climatology, seasonal cycle, and trend as simulated by CMIP5, *Geophys. Res. Lett.*, 39, L21703, doi:10.1029/2012GL053416, 2012.
- Kelley, D. I., Prentice, I. C., Harrison, S. P., Wang, H., Simard, M., Fisher, J. B., and Willis, K. O.: A comprehensive benchmarking system for evaluating global vegetation models, *Biogeosciences*, 10, 3313–3340, doi:10.5194/bg-10-3313-2013, 2013.
- Kohfeld, K. E. and Harrison, S. P.: How well can we simulate past climates? Evaluating the models using global palaeoenvironmental datasets, *Quaternary Sci. Rev.*, 19, 321–346, doi:10.1016/S0277-3791(99)00068-2, 2000.
- Kuper, R. and Kröpelin, S.: Climate-Controlled Holocene Occupation in the Sahara: Motor of Africa's Evolution, *Science*, 313, 803–807, doi:10.1126/science.1130989, 2006.
- Kutzbach, J. E., Bonan, G. B., Foley, J. A., and Harrison, S. P.: Vegetation and soils feedbacks on the response of the African monsoon response to orbital forcing in early to middle Holocene, *Nature*, 384, 623–626, doi:10.1038/384623a0, 1996.
- Levis, S., Bonan, G. B., and Bonfils, C.: Soil feedback drives the mid-Holocene North African monsoon northward in fully coupled CCSM2 simulations with a dynamic vegetation model, *Clim. Dynam.*, 23, 791–802, doi:10.1007/s00382-004-0477-y, 2004.
- Li, G., Harrison, S. P., Bartlein, P. J., Izumi, K., and Colin Prentice, I.: Precipitation scaling with temperature in warm and cold climates: An analysis of CMIP5 simulations, *Geophys. Res. Lett.*, 40, 4018–4024, doi:10.1002/grl.50730, 2013.
- Lionello, P.: *The climate of the Mediterranean Region from the past to the future*, Elsevier Science, Burlington, 2012.
- Luterbacher, J., Xoplaki, E., Casty, C., Wanner, H., Pauling, A., Kuttel, M., Rutishauser, T., Bronnimann, S., Fischer, E., and Fleitmann, D.: Mediterranean climate variability over the last centuries: a review, in: *Mediterranean climate variability*, Elsevier, Amsterdam, Oxford, 2006.
- Magny, M., Miramont, C., and Sivan, O.: Assessment of the impact of climate and anthropogenic factors on Holocene Mediterranean vegetation in Europe on the basis of palaeohydrological records, *Palaeogeogr. Palaeoclimatol.*, 186, 47–59, doi:10.1016/S0031-0182(02)00442-X, 2002.
- Marzin, C. and Braconnot, P.: Variations of Indian and African monsoons induced by insolation changes at 6 and 9.5 kyr BP, *Clim. Dynam.*, 33, 215–231, doi:10.1007/s00382-009-0538-3, 2009.
- Masson, V., Cheddadi, R., Braconnot, P., Joussaume, S., and Texier, D.: Mid-Holocene climate in Europe: what can we infer from PMIP model-data comparisons?, *Clim. Dynam.*, 15, 163–182, doi:10.1007/s003820050275, 1999.
- Meehl, G. A., Stocker, T. F., Collins, W. D., Friedlingstein, P., Gaye, A. T., Gregory, J. M., Kitoh, A., Knutti, R., Murphy, J. M., Nodas, A., Raper, S. C. B., Watterson, I. G., Weaver, A. J., and Zhao, Z. C.: *Global Climate Projections, in Climate Change 2007: The Physical Science Basis. Contribution of Working Group I to the Fourth Assessment Report of the Intergovernmental Panel on Climate Change*, edited by: Solomon, S., Quin, D., Manning, M., Chen, Z., Marquis, M., Averyt, K. B., Tignor, M., and Miller, H. L., Cambridge University Press, Cambridge, UK and New York, USA, 2007.
- Mehta, A. V. and Yang, S.: Precipitation climatology over Mediterranean Basin from ten years of TRMM measurements, *Adv. Geosci.*, 17, 87–91, doi:10.5194/adgeo-17-87-2008, 2008.
- Monerie, P.-A., Fontaine, B., and Roucou, P.: Expected future changes in the African monsoon between 2030 and 2070 using some CMIP3 and CMIP5 models under a medium-low RCP scenario, *J. Geophys. Res.*, 117, D16111, doi:10.1029/2012JD0017510, 2012.
- Moreira, F., Viedma, O., Arianoutsou, M., Curt, T., Koutsias, N., Rigolot, E., Barbat, A., Corona, P., Vaz, P., Xanthopoulos, G., Mouillot, F., and Bilgili, E.: Landscape – wild-fire interactions in southern Europe: Implications for landscape management, *J. Environ. Manage.*, 92, 2389–2402, doi:10.1016/j.jenvman.2011.06.028, 2011.

- Niedermeyer, E. M., Schefuß, E., Sessions, A. L., Mulitza, S., Mollenhauer, G., Schulz, M., and Wefer, G.: Orbital- and millennial-scale changes in the hydrologic cycle and vegetation in the western African Sahel: insights from individual plant wax δD and $\delta^{13}C$, *Quaternary Sci. Rev.*, 29, 2996–3005, doi:10.1016/j.quascirev.2010.06.039, 2010.
- Nikulin, G., Kjellström, E., Hansson, U., Strandberg, G., and Ullerstig, A.: Evaluation and future projections of temperature, precipitation and wind extremes over Europe in an ensemble of regional climate simulations, *Tellus*, 63, 41–55, doi:10.1111/j.1600-0870.2010.00466.x, 2011.
- Phipps, S. J., Rotstayn, L. D., Gordon, H. B., Roberts, J. L., Hirst, A. C., and Budd, W. F.: The CSIRO Mk3L climate system model version 1.0 – Part 1: Description and evaluation, *Geosci. Model Dev.*, 4, 483–509, doi:10.5194/gmd-4-483-2011, 2011.
- Prentice, C., Guiot, J., Huntley, B., Jolly, D., and Cheddadi, R.: Reconstructing biomes from palaeoecological data: a general method and its application to European pollen data at 0 and 6 ka, *Clim. Dynam.*, 12, 185–194, doi:10.1007/BF00211617, 1996.
- Prentice, I. C. and Jolly, D.: Mid-Holocene and glacial-maximum vegetation geography of the northern continents and Africa, *J. Biogeogr.*, 27, 507–519, doi:10.1046/j.1365-2699.2000.00425.x, 2000.
- Raddatz, T., Reick, C., Knorr, W., Kattge, J., Roeckner, E., Schnur, R., Schnitzler, K.-G., Wetzel, P., and Jungclaus, J.: Will the tropical land biosphere dominate the climate–carbon cycle feedback during the twenty-first century?, *Clim. Dynam.*, 29, 565–574, doi:10.1007/s00382-007-0247-8, 2007.
- Raichich, F., Pinardi, N. and Navarra, A.: Teleconnections between Indian monsoon and Sahel rainfall and the Mediterranean, *Int. J. Climatol.*, 23, 173–186, doi:10.1002/joc.862, 2003.
- Roberts, N., Stevenson, T., Davis, B., Cheddadi, R., Brewster, S., and Rosen, A.: Holocene climate, environment and cultural change in the circum-Mediterranean region, in: *Past Climate Variability through Europe and Africa*, vol. 6, edited by: Battarbee, R. W., Gasse, F., and Stickley, C. E., Springer Netherlands, Dordrecht, 343–362, 2004.
- Roberts, N., Jones, M. D., Benkaddour, A., Eastwood, W. J., Filippi, M. L., Frogley, M. R., Lamb, H. F., Leng, M. J., Reed, J. M., Stein, M., Stevens, L., Valero-Garcés, B., and Zanchetta, G.: Stable isotope records of Late Quaternary climate and hydrology from Mediterranean lakes: the ISOMED synthesis, *Quaternary Sci. Rev.*, 27, 2426–2441, doi:10.1016/j.quascirev.2008.09.005, 2008.
- Roberts, N., Eastwood, W. J., Kuzucuoglu, C., Fiorentino, G., and Caracuta, V.: Climatic, vegetation and cultural change in the eastern Mediterranean during the mid-Holocene environmental transition, *Holocene*, 21, 147–162, doi:10.1177/0959683610386819, 2011.
- Rodwell, M. J. and Hoskins, B. J.: Subtropical Anticyclones and Summer Monsoons, *J. Climate*, 14, 3192–3211, doi:10.1175/1520-0442(2001)014<3192:SAASM>2.0.CO;2, 2001.
- Roehrig, R., Bouniol, D., Guichard, F., Hourdin, F., and Redelsperger, J.-L.: The present and future of the West African monsoon: a process-oriented assessment of CMIP5 simulations along the AMMA transect, *J. Climate*, 26, 6471–6505, doi:10.1175/JCLI-D-12-00505.1, 2013.
- Rotstayn, L. D., Collier, M. A., Dix, M. R., Feng, Y., Gordon, H. B., O’Farrell, S. P., Smith, I. N., and Syktus, J.: Improved simulation of Australian climate and ENSO-related rainfall variability in a global climate model with an interactive aerosol treatment, *Int. J. Climatol.*, 30, 1067–1088, doi:10.1002/joc.1952, 2010.
- Schmidt, G. A., Annan, J. D., Bartlein, P. J., Cook, B. I., Guilyardi, E., Hargreaves, J. C., Harrison, S. P., Kageyama, M., LeGrande, A. N., Konecky, B., Lovejoy, S., Mann, M. E., Masson-Delmotte, V., Risi, C., Thompson, D., Timmermann, A., Tremblay, L.-B., and Yiou, P.: Using palaeo-climate comparisons to constrain future projections in CMIP5, *Clim. Past*, 10, 221–250, doi:10.5194/cp-10-221-2014, 2014a.
- Schmidt, G. A., Kelley, M., Nazarenko, L., Ruedy, R., Russell, G. L., Aleinov, I., Bauer, M., Bauer, S. E., Bhat, M. K., Bleck, R., Canuto, V., Chen, Y.-H., Cheng, Y., Clune, T. L., Del Genio, A., de Fainchtein, R., Faluvegi, G., Hansen, J. E., Healy, R. J., Kiang, N. Y., Koch, D., Lacis, A. A., LeGrande, A. N., Lerner, J., Lo, K. K., Matthews, E. E., Menon, S., Miller, R. L., Oinas, V., Olosio, A. O., Perlwitz, J. P., Puma, M. J., Putman, W. M., Rind, D., Romanou, A., Sato, M., Shindell, D. T., Sun, S., Syed, R. A., Tausnev, N., Tsigaridis, K., Unger, N., Voulgarakis, A., Yao, M.-S., and Zhang, J.: Configuration and assessment of the GISS ModelE2 contributions to the CMIP5 archive, *J. Adv. Model. Earth Syst.*, 6, 1–44, doi:10.1002/2013MS000265, 2014b.
- Soler, M., Serra, T., Colomer, J., and Romero, R.: Anomalous rainfall and associated atmospheric circulation in the northeast Spanish Mediterranean area and its relationship to sediment fluidization events in a lake, *Water Resour. Res.*, 43, W01404, doi:10.1029/2005WR004810, 2007.
- Sperber, K. R., Annamalai, H., Kang, I.-S., Kitoh, A., Moise, A., Turner, A., Wang, B., and Zhou, T.: The Asian summer monsoon: an intercomparison of CMIP5 vs. CMIP3 simulations of the late 20th century, *Clim. Dynam.*, 41, 27–2744, doi:10.1007/s00382-012-1607-6, 2013.
- Street-Perrot, F. A., Mitchell, J. F. B., Marchand, D. S., and Brunner, J. S.: Milankovitch and albedo forcing of the tropical monsoon: a comparison of geological evidence and numerical simulations for 9000 y BP, *T. Roy. Soc. Edinb.*, 81, 407–427, 1990.
- Taylor, K. E., Stouffer, R. J., and Meehl, G. A.: An Overview of CMIP5 and the Experiment Design, *B. Am. Meteorol. Soc.*, 93, 485–498, doi:10.1175/BAMS-D-11-00094.1, 2012.
- Texier, D. de Noblet, N., Harrison, S. P., Haxeltine, A., Joussaume, S., Jolly, D., Laarif, F., Prentice, I. C., and Tarasov, P. E.: Quantifying the role of biosphere-atmosphere feedbacks in climate change: coupled model simulation for 6000 years B.P. and comparison with palaeodata for northern Eurasia and northern Africa, *Clim. Dynam.*, 13, 865–882, 1997.
- Tierney, J. E., Lewis, S. C., Cook, B. I., LeGrande, A. N., and Schmidt, G. A.: Model, proxy and isotopic perspectives on the East African Humid Period, *Earth Planet. Sc. Lett.*, 307, 103–112, doi:10.1016/j.epsl.2011.04.038, 2011.
- Vanniere, B., Power, M. J., Roberts, N., Tinner, W., Carrión, J., Magny, M., Bartlein, P., Colombaroli, D., Daniau, A. L., Finsinger, W., Gil-Romera, G., Kaltenrieder, P., Pini, R., Sadori, L., Turner, R., Valsecchi, V., and Vescovi, E.: Circum-Mediterranean fire activity and climate changes during the mid-Holocene environmental transition (8500–2500 cal. BP), *Holocene*, 21, 53–73, doi:10.1177/0959683610384164, 2011.

- van Soelen, E., Brooks, G., Larson, R., Sinninghe Damste, J., and Reichert, G.: Mid- to late-Holocene coastal environmental changes in southwest Florida, USA, *Holocene*, 22, 929–938, doi:10.1177/0959683611434226, 2012.
- Vassiljev, J., Harrison, S. P., and Guiot, J.: Simulating the Holocene lake-level record of Lake Bysjön, southern Sweden, *Quatern. Res.* 49, 62–71, doi:10.1006/qres.1997.1942, 1998.
- Voldoire, A., Sanchez-Gomez, E., y Méliá, D. S., Decharme, B., Cassou, C., Sénéci, S., Valcke, S., Beau, I., Alias, A., and Chevallier, M.: The CNRM-CM5, 1 global climate model: description and basic evaluation, *Clim. Dynam.*, 9–10, 2091–2121, doi:10.1007/s00382-011-1259-y, 2013.
- Watanabe, S., Hajima, T., Sudo, K., Nagashima, T., Takemura, T., Okajima, H., Nozawa, T., Kawase, H., Abe, M., Yokohata, T., Ise, T., Sato, H., Kato, E., Takata, K., Emori, S., and Kawamiya, M.: MIROC-ESM 2010: model description and basic results of CMIP5-20c3m experiments, *Geosci. Model Dev.*, 4, 845–872, doi:10.5194/gmd-4-845-2011, 2011.
- Watrin, J., Lézine, A.-M., and Hély, C.: Plant migration and plant communities at the time of the “green Sahara”, *C. R. Geosci.*, 341, 656–670, doi:10.1016/j.crte.2009.06.007, 2009.
- Wohlfahrt, J., Harrison, S. P., and Braconnot, P.: Synergistic feedbacks between ocean and vegetation on mid- and high-latitude climates during the mid-Holocene, *Clim. Dynam.*, 22, 223–238, doi:10.1007/s00382-003-0379-4, 2004.
- Wu, H., Guiot, J., Brewer, S., and Guo, Z.: Climatic changes in Eurasia and Africa at the last glacial maximum and mid-Holocene: reconstruction from pollen data using inverse vegetation modeling, *Clim. Dynam.*, 29, 211–229, doi:10.1007/s00382-007-0231-3, 2007.
- Wu, T., Li, W., Ji, J., Xin, X., Li, L., Wang, Z., Zhang, Y., Li, J., Zhang, F., and Wei, M.: Global carbon budgets simulated by the Beijing Climate Center Climate System Model for the last century, *J. Geophys. Res.-Atmos.*, 118, 4326–4347, doi:10.1002/jgrd.50320, 2013.
- Xoplaki, E., González-Rouco, F., Luter, J., and Wanner, H.: Mediterranean summer air temperature variability and its connection to the large-scale atmospheric circulation and SSTs, *Clim. Dynam.*, 20, 723–739, 2003.
- Yukimoto, S., Yoshimura, H., Hosaka, M., Sakami, T., Tsujino, H., Hirabara, M., Tanaka, T. Y., Deushi, M., Obata, A., Nakano, H., Adachi, Y., Shindo, E., Yabu, S., Ose, T., and Kitoh, A.: Meteorological Research Institute Earth System Model Version 1 (MRI-ESM1): Model Description – Technical reports of the meteorological research institute No. 64, Meteorological Research Institute, Japan, 88 pp., 2011.
- Zhao, Y. and Harrison, S. P.: Mid-Holocene monsoons: a multi-model analysis of the inter-hemispheric differences in the responses to orbital forcing and ocean feedbacks, *Clim. Dynam.*, 39, 1457–1487, doi:10.1007/s00382-011-1193-z, 2011.

Supplementary Material

Evaluation of seasonal climates of Mediterranean and Northern Africa in the CMIP5 simulations

Ana Perez-Sanz^{1,2}, Guangqi Li², Penélope González-Sampériz¹, Sandy P. Harrison^{2,3}

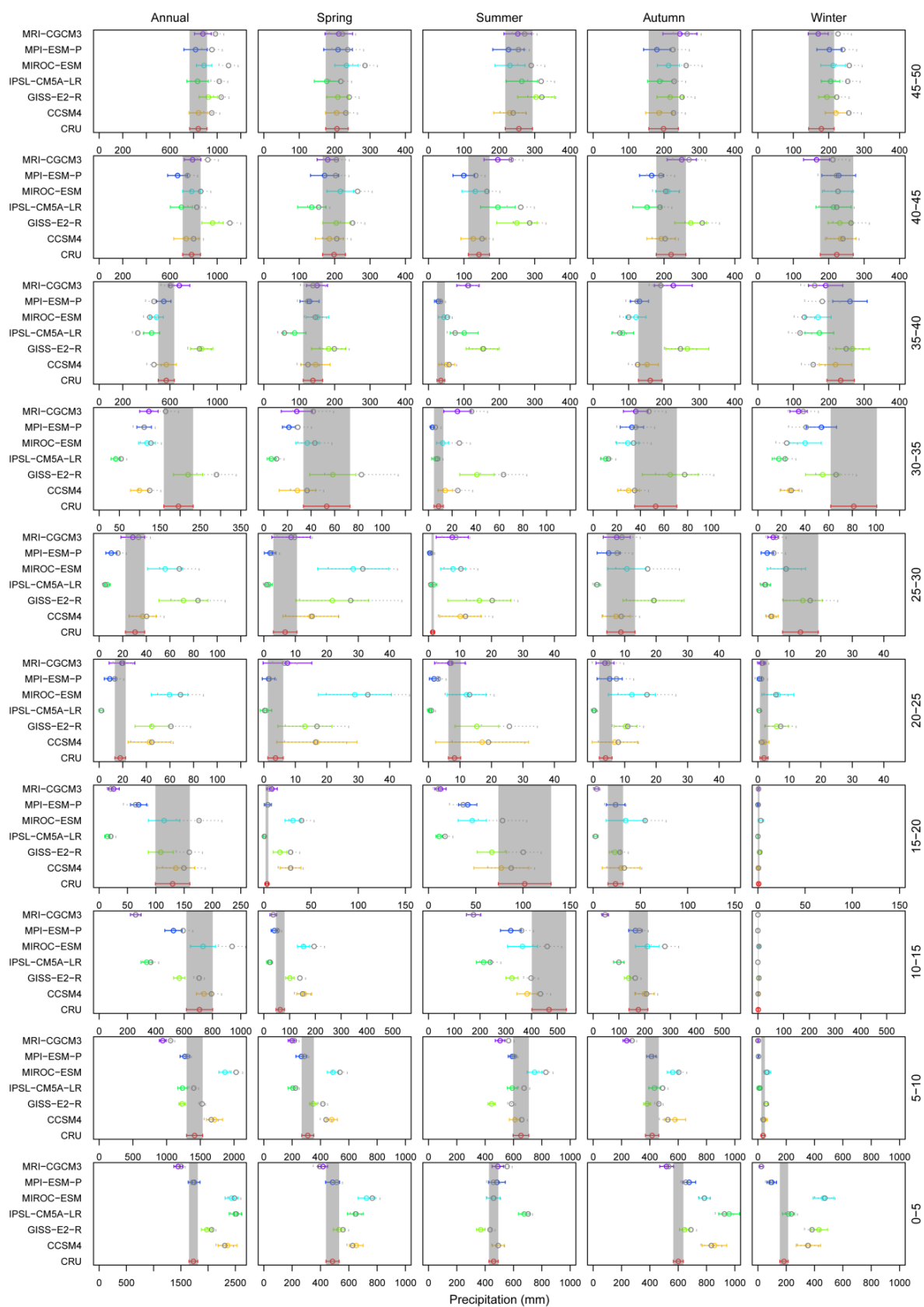
1: Pyrenean Institute of Ecology, (IPE)-CSIC, Avda. Montañana 1005, 50059 Zaragoza, Spain.

2: Department of Biological Sciences, Macquarie University, North Ryde, NSW 2109, Australia.

3: Department of Geography & Environmental Sciences, School of Human and Environmental Sciences, Reading University, Whiteknights, Reading RG6 6AB, UK.

This auxiliary material contains (a) figures showing comparisons between CRU dataset and *historical* simulations of the seasonal and annual precipitation for each 5°-latitudinal band of the study area.

Figure S1. Comparison of the mean annual and mean seasonal precipitation (mm) between the CRU data and *historical* simulations for each 5 latitude band. Because there is a very small amount of precipitation in some latitude band, the axis scale starts at 0 but differs in the maximum value depending on the total rainfall values. Only six models have *historical* simulations. For these models we also present the *piControl* simulations. The historical simulations are shown in color while the *piControl* simulations for each model are shown by a dash line. The grey bars represent one standard deviation of the mean annual and mean seasonal precipitation from observations. The seasons are defined as spring (March, April, May), summer (June, July, August), autumn (September, October, November) and winter (December, January, February).



Chapter 4

Evaluation of CMIP5 palaeo simulations to improve climate projections

Contribution by Co-Authors: G.L. contributed the analyses used in Figure 1 (e, f, g) and Figure 2; K.I. contributed the analyses used in Figure 1 (a-d); J.A. and J.H. provided the analyses used in Figure 3; P.J.B. contributed the analyses used in Figure 4; S.P.H. planned the paper and was responsible for drafting the text; all authors contributed to the final version.

Evaluation of CMIP5 palaeo-simulations to improve climate projections

S. P. Harrison^{1,2*}, P. J. Bartlein³, K. Izumi^{3,4,5}, G. Li², J. Annan⁶, J. Hargreaves⁶, P. Braconnot⁴ and M. Kageyama⁴

Structural differences among models account for much of the uncertainty in projected climate changes, at least until the mid-twenty-first century. Recent observations encompass too limited a range of climate variability to provide a robust test of the ability to simulate climate changes. Past climate changes provide a unique opportunity for out-of-sample evaluation of model performance. Palaeo-evaluation has shown that the large-scale changes seen in twenty-first-century projections, including enhanced land-sea temperature contrast, latitudinal amplification, changes in temperature seasonality and scaling of precipitation with temperature, are likely to be realistic. Although models generally simulate changes in large-scale circulation sufficiently well to shift regional climates in the right direction, they often do not predict the correct magnitude of these changes. Differences in performance are only weakly related to modern-day biases or climate sensitivity, and more sophisticated models are not better at simulating climate changes. Although models correctly capture the broad patterns of climate change, improvements are required to produce reliable regional projections.

State-of-the-art climate models were used during the fifth phase of the Coupled Model Intercomparison Project (CMIP5, see Box 1) to provide information about the likely evolution of climate over the twenty-first century, with additional experiments to analyse the uncertainties inherent in these projections¹. Evaluation of the CMIP5 historical (that is, twentieth-century; Supplementary Table 1) experiments shows that the simulation of modern climate has improved compared with simulations made as part of CMIP3. In particular, the current generation of models reproduces continental-scale surface patterns and long-term trends in temperature, and shows an improved ability to capture continental-scale precipitation patterns and reproduce the statistics of leading modes of climate variability such as the North Atlantic Oscillation, El Niño–Southern Oscillation and Quasi-Biennial Oscillation². Nevertheless, models that perform equally well for present-day climate produce very different responses to anthropogenic forcing (that is, in Representative Concentration Pathway (RCP) scenario simulations; Supplementary Table 1). The largest component of the uncertainty in model projections in the first part of the twenty-first century stems from differences between the response of individual models to the same forcing rather than internal variability or differences between the forcing scenarios themselves³. Differences between the climate forcing scenarios become more important by the end of the century⁴, but intermodel differences still play a role in amplifying the scenario-related uncertainties and, indeed, still play a dominant role in explaining regional differences^{3,5,6}.

Past climates provide an opportunity to evaluate model performance outside the range of recent observed climate variability. Palaeoclimate simulations of the Last Glacial Maximum (LGM, 21 kyr ago) and mid-Holocene (6 kyr ago) were included in the CMIP5 simulations for this reason (Supplementary Table 1). Neither

of these periods provides an analogue for the future evolution of climate — indeed, no past climate state provides a direct analogue for the future — but the change in forcing at the LGM was of similar magnitude (of the order of $3\text{--}6\text{ W m}^{-2}$) to that projected for the next century⁷, whereas the mid-Holocene provides an opportunity to evaluate simulations at a time of radically changed seasonality. Both periods have been foci for synthesis of palaeoclimate reconstructions^{8,9}. Palaeoclimate evaluation using mid-Holocene and LGM climate reconstructions can help both to explain why the simulated mean response differs between models and to determine whether the upper or lower part of the range of response to future changes in forcing is inherently more likely to be realistic.

In a review of the potential of the CMIP5 palaeoclimate experiments to quantify uncertainties in model projections, six objectives were identified for the palaeoclimate simulations, including: (1) identification of robust features of past and future climates; (2) evaluation of model ability to simulate regional climate changes; (3) multi-parameter evaluation of overall model skill; (4) improvements in model performance between CMIP3 and CMIP5 in the simulation of large climate changes; (5) provision of well-founded constraints on climate sensitivity; and (6) evaluation of the role and magnitude of feedbacks. Analyses of many aspects of the CMIP5 palaeosimulations have now been completed and considerable progress has been made in addressing these six tasks. Our goal here is to synthesize and update these results, and to discuss their implications for the reliability (or otherwise) of future projections. We focus on the mid-Holocene and LGM simulations because these are the time periods for which there are global data sets of quantitative climate reconstructions^{8,9} and because they have been examined with several generations of models^{10–13}, allowing us to assess the evolution of model performance. However, we also draw on

¹Centre for Past Climate Change, School of Archaeology, Geography and Environmental Sciences (SAGES), University of Reading, Whiteknights, Reading RG6 6AH, UK. ²Department of Biological Sciences, Macquarie University, North Ryde, NSW 2109, Australia. ³Department of Geography, University of Oregon, Eugene, Oregon 97403-1251, USA. ⁴Laboratoire des Sciences du Climat et de l'Environnement/Institut Pierre Simon Laplace, unité mixte de recherches CEA-CNRS-UVSQ, Orme des Merisiers, bât 712, 91191 Gif sur Yvette Cedex, France. ⁵Laboratoire de Meteorologie Dynamique (LMD/IPSL), CNRS/UPMC, Tour 45-55, 3eme etage, 4 place Jussieu, boîte 99, 75252 Paris cedex 05, France. ⁶BlueSkiesResearch.org.uk, The Old Chapel, Albert Hill, Settle BD24 9HE, UK. *email: s.p.harrison@reading.ac.uk

Box 1 | The relationship between the CMIP and the PMIP.

The CMIP was set up in 1995 by the Working Group on Coupled Modelling of the World Climate Research Programme to provide a standard experimental protocol for studying climate changes using coupled atmosphere–ocean general circulation models. CMIP provides a community-based infrastructure in support of climate model diagnosis, validation and intercomparison. Initially, CMIP archived and analysed outputs from model ‘control runs’ in which climate forcing was constant, and idealized simulations in which atmospheric CO₂ concentration was increased either abruptly or in a transient fashion. Phase 3 of CMIP (CMIP3) included ‘realistic’ scenarios for historic, present and future climate. These simulations provided the basis for analyses underpinning the IPCC fourth assessment report. The current phase of CMIP (CMIP5)¹, which was initiated at the end of 2008, involves a large range of experiments for past, present and projected future climate, as well as more idealized experiments designed to explore model behaviour. Analysis of these simulations has already been used as input to the recent IPCC fifth assessment report and continues to be exploited for improved understanding of the mechanisms of climate change.

Palaeoclimate simulations were not included in CMIP prior to CMIP5. Nevertheless, the modelling community has been involved in a parallel effort to use past climate states to understand the mechanisms of climate change since the 1980s. These efforts have been coordinated by the PMIP^{7,10,12,93}. The first round of

PMIP intercomparisons (PMIP1) focused on atmospheric general circulation model simulations of the mid-Holocene and LGM, and was broadly parallel to the concurrent efforts of the Atmospheric Modelling Intercomparison Project⁹⁴. PMIP2 focused on comparison of coupled atmosphere–ocean model simulations of the mid-Holocene and LGM. Although PMIP2 was broadly concurrent with CMIP3, and many of the same modelling groups were involved in both intercomparison projects, the palaeosimulations were generally run with either lower resolution or older versions of the models. The inclusion of palaeo-experiments in CMIP5 means that we now have simulations of past and future climate made with exactly the same version and at exactly the same resolution. As PMIP coordinates the analysis of the CMIP5 palaeo-experiments, these are often referred to as PMIP3 experiments (or PMIP3/CMIP5) experiments (although here, for simplicity, we refer to them as CMIP5 experiments).

The evaluation of the CMIP5 simulations is only one component of the ongoing work during PMIP3. PMIP3 is also running experiments for non-CMIP5 time periods and is coordinating the analysis and exploitation of transient simulations across intervals of rapid climate change in the past. PMIP also provides an umbrella for model intercomparison projects focusing on specific times in the past, such as the Pliocene Modelling Intercomparison Project⁹⁹, or on specific aspects of the palaeoclimate system, such as the Palaeo Carbon Modelling Intercomparison Project⁹⁵.

other Palaeoclimate Modelling Intercomparison Project (PMIP) experiments where appropriate.

Robust features of past and future climates

There are several features of the temperature changes in future projections (and the more idealized 1pctCO₂ and abrupt4xCO₂ warming scenarios) that are remarkably consistent, including stronger warming over land than ocean (enhanced land–ocean contrast), stronger responses at higher than lower latitudes (latitudinal amplification) and differential responses in summer and winter leading to changes in seasonal contrast^{3,14,15}. These large-scale temperature responses, which emerged in the first Intergovernmental Panel on Climate Change (IPCC) assessment 25 years ago, are present in palaeoclimate simulations as well, not only of the LGM and mid-Holocene^{16–18}, but also of other intervals such as the last interglaciation¹⁹ and the mid-Pliocene^{20,21}. The variations in response are proportional and nearly linear across simulations of both warm (1pctCO₂, abrupt4xCO₂) and cold (LGM) climate states (Fig. 1a,b), and the simulated magnitude of the relative changes between land and ocean, higher and lower latitudes, and summer and winter temperature is supported by historical and palaeoclimate observations¹⁶ (Fig. 1c,d). Although this agreement between the simulated and observed responses is apparent on the large (hemispheric) scale, there is some evidence that it may not hold on a more regional level. It has been suggested, for example, that the CMIP5 models underestimate mid-Holocene warming in the eastern Canadian Arctic by >1 °C (ref. 22).

Several components of the surface energy balance are involved in the temperature responses in the LGM, historical and idealized warming scenario simulations, but surface downward clear-sky longwave radiation, which includes the effect of changes in CO₂, water vapour and atmospheric energy transport, is the most important component driving land–ocean contrast and high-latitude amplification in both warm (abrupt4xCO₂) and cold (LGM) climates²³. Surface albedo plays a significant but secondary role in promoting high-latitude amplification in both cold and warm

climates¹⁵, and in intensifying the land–ocean contrast in the warm climate case. Surface albedo has also been shown to contribute to latitudinal amplification in mid-Pliocene simulations²⁰. Changes in seasonality are consistent in pattern but, in contrast to the relative simplicity of the mechanisms underpinning land–ocean contrast or latitudinal amplification, the genesis of the seasonality changes is different in warm and cold climates²³.

Precipitation increases as temperature increases, although at a rate that is consistently smaller than the rate of change in saturation vapour pressure, partly because of energetic constraints on evaporation and partly because of constraints in water availability over land^{24,25}. Precipitation increases are characteristic of the CMIP5 future (RCP) and idealized warming (1pctCO₂, abrupt4xCO₂) simulations²⁶. The scaling between the change in temperature and precipitation is remarkably consistent in palaeoclimate (LGM), historical and idealized warming (1pctCO₂, abrupt4xCO₂) simulations (Fig. 1e), both over land and ocean (Fig. 1f), and is also consistent with palaeoclimate and historical observations²⁷ (Fig. 1g). Analyses of precipitation changes in idealized warm (1pctCO₂, abrupt4xCO₂) climate states²⁷ also show other robust large-scale responses, including larger changes in precipitation per degree temperature change in extratropical than tropical land areas. Changes in tropical precipitation are greatest in areas that are currently wet, resulting in increased precipitation in warm climate states and decreased precipitation in cold climate states. The seasonality of precipitation in the tropics also changes in a consistent way, with increased seasonality in warm climate states and decreased seasonality in cold climate states²⁷. All of these features are consistent with palaeoclimate and historical observations of large-scale precipitation changes.

Ability to simulate regional climate features

The regional response to changes in forcing has been a major focus in the evaluation of the CMIP5 mid-Holocene and LGM simulations. There can be three types of mismatch: cases where the models simulate the same robust response to a forcing but the response is

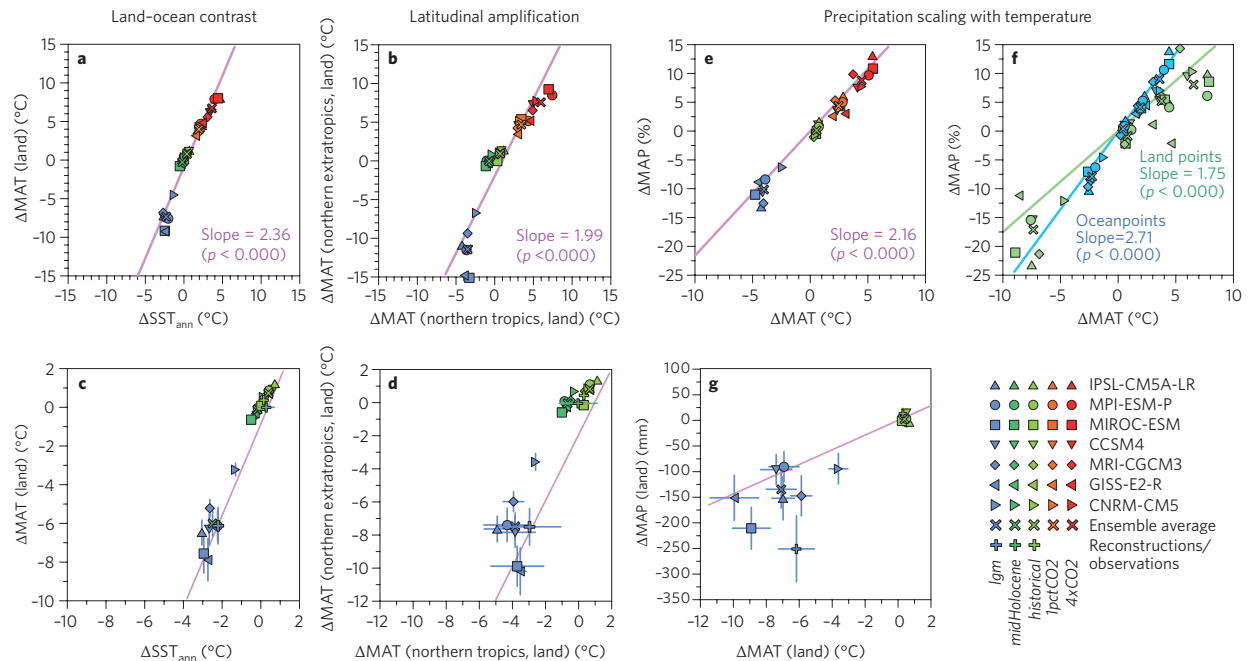


Figure 1 | Scatter plots showing temperature and precipitation changes in past, present and projected climates. The values shown are the simulated long-term mean differences (experiment minus piControl) for the seven models that have carried out all the experiments. **a**, Differences in the relative warming (or cooling) over global land and global ocean (land-ocean contrast) and **b**, over land in the northern extratropics and northern tropics (latitudinal amplification). SST_{ann} : annual sea surface temperature. **c**, Comparisons of the simulated changes in land-ocean contrast and **d**, latitudinal amplification for the twentieth-century (historical) and LGM with observed changes. The reduced major axis regression lines derived using all appropriate model grid cells are shown in magenta; the p -values test the null hypothesis that the slopes of the reduced major axis regression lines = 1.0. **e**, Percentage precipitation change relative to the change in global temperature and **f**, global temperature over land (green) and ocean (blue). The ordinary least-square regression with the intercept set at zero is shown in magenta; the p -values test the null hypothesis that the slope = 0. **g**, Comparisons of the simulated changes in precipitation scaling over land for the twentieth-century (historical) and LGM with observed changes. The ordinary least-square regression for absolute values of precipitation based on all model simulations is shown in magenta. In **c**, **d** and **g**, model output has been sampled only at the locations of respective observations. Bold crosses: area-weighted averages of twentieth-century observations and palaeoclimate reconstructions; finer lines: reconstruction uncertainties (standard deviation).

of the wrong magnitude; cases where the models simulate the same robust response to a forcing but the response is of the wrong sign; and cases where different models give different responses to the same forcing. Here we provide examples of each of these cases.

The insolation-induced amplification of Northern Hemisphere monsoons during the early to mid-Holocene provides the classic example of the use of model simulations to provide a mechanistic explanation of past climate changes²⁸. Monsoon amplification, expressed through an increase in both the geographic area receiving monsoon rain and the overall amount of precipitation, is a feature of atmosphere-only simulations^{10,29}. Simulations show that ocean feedback increases the length of the monsoon season and amplifies the magnitude of the overall response^{30–32}. The CMIP5 mid-Holocene simulations show both a substantial expansion of the Asian (Pacific) and northern Africa monsoons with an increase in total precipitation^{33–35}, and a corresponding reduction in area and decrease in total precipitation in the Southern Hemisphere monsoons³⁶. A previous study⁷ showed that the PMIP Phase II (PMIP2) mid-Holocene simulations consistently underestimated the magnitude of change in the Northern Hemisphere monsoons. The CMIP5 mid-Holocene simulations show less amplification than the PMIP2 simulations over Asia, with strengthening of the meridional wind of only 32% compared with 40% in PMIP2 (ref. 33). The discrepancy between observed and CMIP5 simulated changes in the amount of mid-Holocene precipitation over northern Africa is at least 50% in the latitude band from 15–30° N (Fig. 2)³⁵. Land-surface feedbacks,

associated with the climate-induced change in vegetation cover and surface water storage, have been invoked as one way to reconcile these discrepancies^{37–42}. Although some vegetation-enabled models show amplification of the northern Africa monsoon in the mid-Holocene^{43,44}, the PMIP2 models with dynamic vegetation did not produce greater amplification of any of the Northern Hemisphere monsoons during that time⁷. Furthermore, mid-Holocene simulations with the (CMIP5) CCSM4 model⁴⁵ show that vegetation feedback produces only very small changes in seasonal temperature and has no impact on precipitation over the Pacific monsoon region. The contrast between these PMIP2/CMIP5 results and earlier studies that prescribed vegetation changes or used simpler models suggests that significant improvements to the modelling of vegetation and its coupling with the atmosphere are required to address the role of land-surface feedbacks properly⁴⁶.

The intertropical convergence zone is located too far south in the Atlantic sector in most of the CMIP5 historical and pre-industrial control (piControl) simulations, reflecting a damped meridional temperature gradient that has been related to biases in radiation and heat fluxes⁴⁷. Analyses of the West African monsoon in a subset of the PMIP2 mid-Holocene simulations show this bias affects the meridional temperature gradient and limits the northward movement of the intertropical convergence zone⁴⁸, which is also true for some of the CMIP5 mid-Holocene experiments. Differences in the amplification of the mid-Holocene monsoon over northern Africa in the CMIP5 experiments are not consistently related

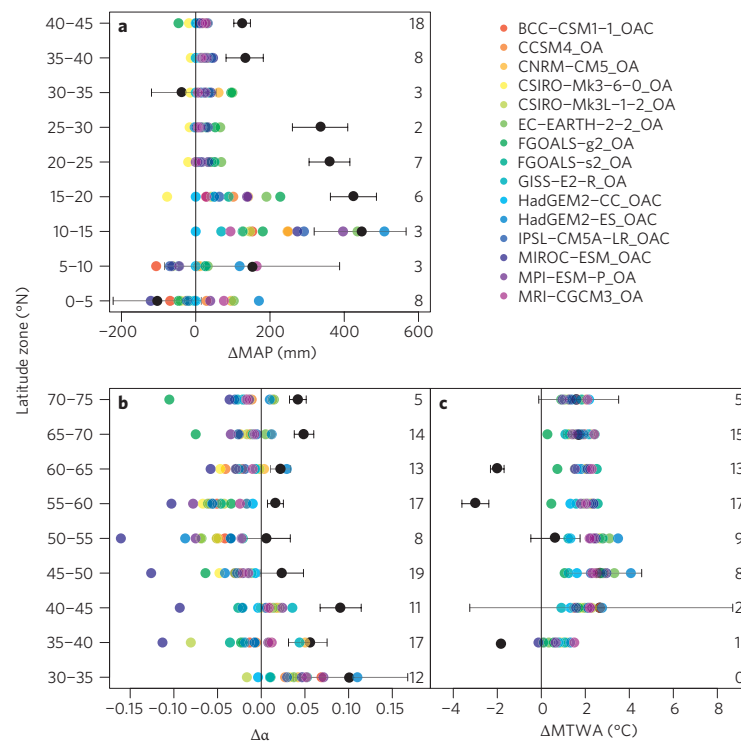


Figure 2 | Comparison of observed and simulated regional climate. **a**, Comparison of simulated and reconstructed mid-Holocene changes in mean annual precipitation for 5° latitude bands (longitude 20° W to 40° E) between 0 and 45° N across northern Africa and the circum-Mediterranean region. **b**, Ratio of actual to equilibrium evapotranspiration and **c**, mean temperature of the warmest month for 5° latitude bands between 30 and 80° N across Eurasia (longitude 60° to 180° E). The reconstructions are from the data set in ref. 9, which provides a climate reconstruction for a $2 \times 2^\circ$ grid cell based on averaging the individual site-based reconstructions within that grid cell. The mean and standard error of the mean of the grid cell reconstructions are shown in each latitude band. The model results are averages of model output sampled at the location of the grid cells with observations. The number of grid cells contributing to the comparison for each variable is shown on the plots.

to precipitation biases in the piControl simulations³⁵ because the mid-Holocene change in precipitation is driven by an increase in deep convection, so differences are largely linked to the way each model represents different convective regimes⁴⁸.

The extent of mid-continental drying in Eurasia during the mid-Holocene is another example of a persistent regional mismatch between models and observations^{29,49,50}. The CMIP5 mid-Holocene simulations (Fig. 2) show drier conditions in Eurasia, particularly between 45° and 60° N, whereas observations systematically show that the mid-continental extratropics were wetter than today. At the same time, the models show a significant increase in summer temperature, whereas observations suggest cooler summers (Fig. 2). Temperature biases in the CMIP5 historical (twentieth-century) simulations are linked to systematic biases in evapotranspiration⁵¹, with oversimulation of precipitation (and hence evapotranspiration) leading to cold temperature biases, and undersimulation of precipitation leading to warm biases. A similar mechanism seems to explain the mismatch in Eurasia in the mid-Holocene: the models do not produce a sufficient increase in regional precipitation and therefore underestimate evapotranspiration (and hence the ratio of actual to equilibrium evaporation, α) compared with observations, causing simulated summer temperatures of up to 4° warmer than observed.

The mid-Holocene climate of Europe provides a third example of a persistent mismatch between models and observations. CMIP5 mid-Holocene simulations show generalized warming over Europe in summer and fail to reproduce the observed summer cooling

in southern Europe⁵². Winter temperature anomalies are not as consistent between models, but the CMIP5 mid-Holocene simulations do not show the strong winter warming in northern Europe shown by observations. These same discrepancies were present in mid-Holocene simulations with previous generations of models^{53–55}. A previous study⁵² suggests that these persistent discrepancies are related to the failure to simulate atmospheric circulation patterns correctly, specifically anticyclonic blocking in summer and increased dominance of the positive phase of the NAO in winter during the mid-Holocene. This study argues that atmospheric circulation patterns over Europe are also poorly simulated in modern (twentieth-century) simulations, which could explain why Europe is warming faster than projected⁵⁶.

Not all features of regional climates show a robust response to past changes in forcing, even when there is a consistent response in the future RCP simulations. For example, there is a consistent year-round reduction in the extent of Arctic sea ice in CMIP5 RCP simulations³. There is also a consistent reduction of summer sea-ice cover in response to increases in summer insolation in the CMIP5 mid-Holocene simulations⁵⁷, with the largest changes shown by those models with thicker sea ice in the piControl simulation. However, some models show increased and some decreased ice thickness in winter. An analysis of two models with similar sea-ice sensitivity in RCP scenario and abrupt4xCO₂ simulations, but very different responses to mid-Holocene forcing, suggests that differences in the sign of the mid-Holocene changes in winter sea-ice extent may be related to cloud feedback. HADGEM2-ES shows a year-round

decrease in sea-ice extent, whereas MIROC-ESM shows a smaller decrease in summer and a slight increase in winter. The difference in summer is attributed to differences in cloud cover between the two simulations⁵⁷. Cloud-mediated differences in the summer response help to explain the different winter responses when the direct forcing is weak: a large reduction in summer sea-ice extent offsets the growth of sea ice in autumn and winter such that the overall extent of winter sea ice remains less than in the piControl simulation, whereas when the change in summer sea-ice extent is small it is insufficient to offset any orbitally induced winter increase. Similar analyses of the CMIP5 LGM simulations⁵⁸ confirm the relationship between sea-ice thickness in the piControl simulations and the magnitude of the change in summer sea-ice extent during the LGM, and also show that models have different responses to the change in forcing. The responses seem to be most different in the Southern Ocean, where there are also large discrepancies between simulated and observed sea-ice patterns.

The behaviour of the Southern Hemisphere westerly jet provides a second example of inconsistency in model simulations of the past that is not characteristic of future projections. The position of the Southern Hemisphere westerly jet is consistently shifted poleward in future simulations compared with the pre-industrial state because the tropospheric meridional temperature gradient is weakened. The CMIP5 models show diametrically opposed changes in the location of the Southern Hemisphere westerlies during the LGM, with half showing a equatorward shift and half showing a poleward shift in mean position compared with the piControl state^{59,60}. The equatorward shift is consistent with the expected strengthening of the upper tropospheric temperature gradient. However, the models that unexpectedly simulate a poleward shift of the jet stream during the LGM compared with the pre-industrial state in fact show a strong LGM lower tropospheric cooling at high latitudes. This implicates different sensitivity to prescribed changes in the Antarctic ice sheet and to the simulated sea-ice extent in influencing the location of the Southern Hemisphere westerlies during the LGM⁵⁹. Situations in which there is a consistent response in the future but different responses in the past thus provide an opportunity to explore model sensitivity to a wider diversity of feedbacks, such as the evolution of the ice sheets, than are currently included in simulations of the future.

A final example of inconsistent behaviour among models is provided by an analysis of hydroclimate in the tropical Pacific during the LGM⁶¹. This study provides an analysis of seven PMIP2 and five CMIP5 simulations, and shows contrasting responses of change in precipitation over the maritime continent (Southeast Asia, Indonesia, New Guinea and the Philippines): some models show widespread drying whereas others show a modest increase in precipitation. These different behaviours are, at least in part, due to simulated differences in the Walker circulation. The model (HadCM3) that most accurately reflects the pattern of the observed change in precipitation and ocean salinity, with strong and widespread drying over the maritime continent associated with freshening of the Arabian Sea and the western Pacific, is the sole model to produce a sufficiently weakened Walker circulation over the Indian Ocean. Only one of the CMIP5 models (MPI-ESM-P) shows weakening of the Walker circulation, but the change is not large enough to reproduce the observations.

Multi-parameter evaluation of model skill

Multi-parameter evaluation of simulations using global data sets is a routine measure of model performance under modern conditions². Evaluations of the CMIP5 mid-Holocene and LGM simulations based on ten different seasonal or annual climate variables show that no model performs equally well for all variables^{2,13}. In general, models are better at simulating mean (or median) values of any climate variable than at simulating the spatial variability or the geographic

patterning in that variable. Although the CMIP5 models seem to have some skill in predicting mean annual temperature (MAT) and mean annual precipitation (MAP) during the LGM (Fig. 3), they have no skill in predicting summer temperature (mean temperature of the warmest month, MTWA) in the mid-Holocene, a result that confirms earlier analyses of the PMIP2 models⁶². Precipitation (as represented by MAP) is somewhat better simulated than temperature (as represented by MTWA) in the mid-Holocene but the reverse is true in the LGM simulations, where temperature (as represented by MAT) is better simulated than MAP (Fig. 3). Nevertheless, some models are better than others at capturing mid-Holocene and LGM climate change, and indeed perform better than the ensemble mean model¹³. The ensemble mean model usually provides the best estimate of the modern climate⁶³. This may be because the ensemble mean filters out the impact of outliers in a collection of models that essentially have been 'tuned' to modern climate, but could also reflect the fact that the ensemble is too small and, physically speaking, the models are too closely related to characterize the underlying distribution effectively⁶⁴. The fact that this is not the case in palaeo-experiments challenges the prevailing approach of using future projections to examine climate impacts — in which all available simulations are averaged to derive an ensemble response, with the spread of the experiments considered as a measure of uncertainty.

The spatial coverage of palaeoclimate reconstructions is more limited than modern observations and some key regions are undersampled⁹. Model evaluation has therefore often focused on data-rich regions and/or a limited number of climate parameters. Nevertheless, even taking account of the limited data and occasionally large uncertainties of palaeoclimate reconstructions, it is clear that the LGM and mid-Holocene simulations provide a rigorous test of model performance. Although there is reasonable agreement in the overall magnitude of the cooling during the LGM, primarily because the large-scale changes are dominated by land–ocean contrast and latitudinal gradients, the CMIP5 models show only limited skill in capturing sub-continental-scale patterns of temperature change. The mid-Holocene lacks the strong annual mean forcing that is present during the LGM and in future simulations, so the poor performance with respect to mean annual signals (Fig. 3) is therefore unsurprising. Our ability to evaluate these simulations is somewhat compromised by uncertainties about the seasonal attribution of sea-surface temperature reconstructions⁶⁵. However, comparisons of continental seasonal climates confirm that the mid-Holocene still presents a challenge for the models. Some of the discrepancy between simulated and reconstructed mid-Holocene and LGM climate may reflect the simplified design of the experiments and, in particular, the omission of known feedbacks (for example, dust forcing during the LGM, land-surface characteristics in both simulations¹⁸). However, these feedbacks are also not included in future projections.

Improvement in ability to simulate climate change

The evidence of modest overall model skill during the mid-Holocene and LGM, and for substantial misrepresentation of past regional climates, clearly raises serious questions about state-of-the-art models. The current generation of models has been shown to be better at simulating some aspects of the modern climate². Individual models are incorporating more complex treatments of key processes and feedbacks, and for individual models these improvements translate into better simulations of key aspects of past climate^{66,67}. However, relative to previous generations of models, these developments apparently do not translate into an improved ability to simulate climate change. At the ensemble level, the differences between the CMIP5 simulations and earlier CMIP3/PMIP2 simulations are small and statistically unimportant, both for the past and for the future (Fig. 4). There is growing feeling that future analyses of climate change and its impacts should be based on cross-generational

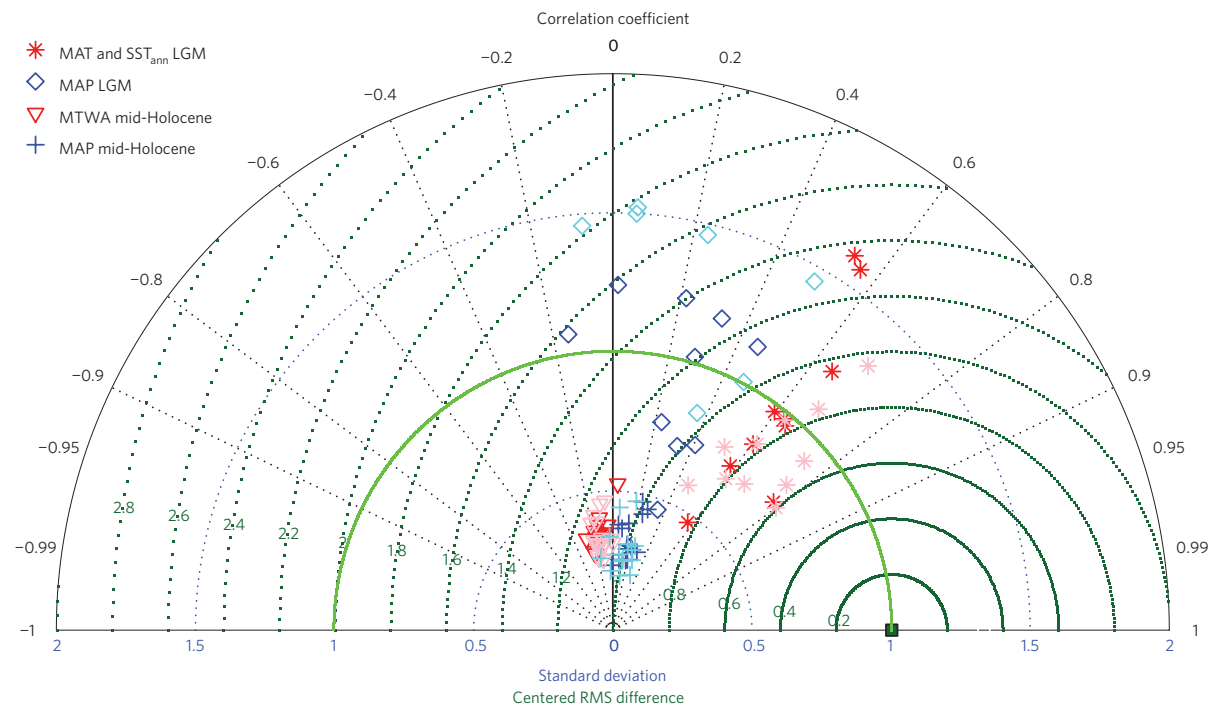


Figure 3 | Taylor diagram⁹⁰ for the LGM and mid-Holocene precipitation and temperature anomalies. The distance of any model point from the origin indicates standard deviation of field, the distance of any model point from the green reference point indicates the centred root mean square (RMS) difference between model and data. Pattern correlation between model and observations is given by the azimuthal coordinate. Temperature is represented by MAT over land and SST_{ann} at the LGM, and by MTWA for the mid-Holocene where the change in forcing is seasonal. Precipitation is always represented by MAP. Model statistics are corrected to account for observational uncertainties, by subtracting the estimated contributions made by observational errors as in ref. 62. Models from the CMIP5 ensemble are in red (temperature) and blue (precipitation), whereas models from the PMIP2 ensemble are in pink and pale blue, respectively.

ensembles of model output constrained by observations^{68,69}, and palaeo-evaluations support this approach, not only because there seems to be little improvement between different generations of models, but also because some models are better than others at reproducing the magnitude and patterns of large climate changes.

Providing well-founded climate sensitivity constraints

Differences in climate sensitivity, conventionally defined as the change in global average temperature for a doubling of CO₂, are realized as intermodel differences in the projections of future global warming. It has proved difficult to evaluate model sensitivity using historical observations, and this has motivated attempts to use past climate states as a constraint⁷⁰. The LGM has been a focus for such attempts because of the large difference in climate from present^{71–75}. Many (though not all) energy-balance mechanisms operate similarly in simulations of the LGM and of future (warm) climates across the ensemble of CMIP5 models²³, although there is asymmetry in the strengths of different feedbacks⁷⁶. One study⁷⁴ found a significant correlation in the previous generation of climate models (PMIP2) between tropical temperature change during the LGM and equilibrium sensitivity, but this relationship is not evident in the CMIP5 LGM simulations. We have re-examined this finding by combining the CMIP5 and PMIP2 ensembles (following the approach suggested in ref. 69), taking the mean of the outputs where more than one integration was carried out by closely related models. This gives a total of 11 simulations and a weak correlation between tropical temperature during the LGM and equilibrium climate sensitivity, which is barely significant at the 90%

level. This provides an estimate of climate sensitivity in the range of 1.4–4.4 °C, but the tenuous nature of the correlation cannot be ignored when assessing the credibility of this result. The presence of strong and consistent spatial patterns in temperature changes, as evidenced by land–ocean contrast and high-latitude amplification, suggest that tropical temperature may be an insufficient constraint on climate sensitivity. Another study¹³ adopted an alternative approach, by comparing the CMIP5 and PMIP2 model ensemble with all available LGM temperature reconstructions and estimating climate sensitivity from the regression as the temperature at which global bias is zero. They obtained an estimate of 2.7 °C, but again argued that the result was only barely significant ($p = 0.12$) even after the removal of a marked warm-bias outlier. Thus, although the LGM provides a useful check on model performance, it remains a challenge to generate well-founded quantitative constraints on climate sensitivity from these simulations.

Palaeosimulations and future projections

Evaluation of the CMIP5 palaeosimulations demonstrates the value of including past climate states as targets for model intercomparison. Systematic examination of features that are characteristic of future climate simulations in palaeoclimate experiments and palaeoclimate reconstructions provides an opportunity to determine whether these features are robust characteristics of the climate system, and whether they are features of the actual response of the climate system to changes in forcing rather than model artefacts^{7,16,18}. The broad-scale temperature and precipitation responses seen in future simulations are present in palaeosimulations and correctly

represented in both LGM and historical simulations. This gives us confidence that the projected changes in land–sea temperature contrast, high-latitude amplification, temperature seasonality, the scaling of precipitation with temperature and the differential precipitation–temperature scaling over land and ocean are reliable. Similarly, the fact that models produce large-scale changes in climate consistent with palaeo-reconstructions for multiple different climate states enhances our confidence in the simulated changes shown in future projections. The palaeo-record has the ability to discriminate between models where they show differences in the response to forcing, and again this provides a way of determining which models are more reliable.

Nevertheless, the modest overall skill of the CMIP5 models for the mid-Holocene and LGM shows the limitations of the current generation of models. Specifically, the models are unable to reproduce the magnitude of changes in regional climates, even when taking into account the uncertainties inherent in the palaeo-reconstructions. The amplification of the Northern Hemisphere monsoons is a robust feature of future (RCP) climate simulations^{3,4}. Although the underlying cause differs (increased greenhouse gases rather than a change in insolation), the antecedent condition of continental warming in the subtropics leading to increased land–ocean contrast is the same in future and mid-Holocene simulations. Thus, the fact that models persistently underestimate the magnitude of regional precipitation changes over Africa and Asia during the mid-Holocene suggests that the future predictions could be similarly affected. Given that these monsoon systems influence the livelihood of more than half of the world's population, this is a situation that needs to be rectified. Addressing the causes of persistent mismatches, both for the monsoon regions and for other regions identified by palaeo-comparison, should be a research priority.

It is possible that discrepancies between simulated and observed regional climates in the mid-Holocene and LGM are due to uncertainties in the specification of prescribed boundary conditions or the failure to include additional potential forcings⁷. Simulated LGM climates are indeed sensitive to the form of the prescribed ice sheet^{7,77}. However, the latest reconstructions of the size and form of the LGM ice sheets are more similar to one another than to previous attempts at reconstruction. Furthermore, the impact of uncertainties in ice-sheet prescription is small and highly localized compared with the other, well-constrained forcings. Similarly, some of the model simulations prescribe vegetation to be the same as present in both the mid-Holocene and the LGM. However, inclusion of dynamic vegetation does not seem to improve the simulation of mid-Holocene regional climates. Furthermore, Earth system models do not seem to perform better overall than models that do not include a dynamic carbon cycle and/or dynamic vegetation. Inclusion of dust forcing has been shown to improve the simulations of LGM climate⁷⁸, for example, but again the impact of dust is small compared with the impact of the changes in the ice sheet or atmospheric composition^{78,79}. Thus, although uncertainties in the experimental protocol could contribute somewhat to the poor performance of the CMIP5 models, the large discrepancies between observations and simulations cannot be explained away by invoking the experimental design.

It is of concern that the current generation of climate models does not perform better overall than previous generations of models, in terms of either modern climate or palaeoclimate changes^{13,69}. On the positive side, this opens up the possibility of using cross-generational ensembles for projections of climate and climate impacts, which would provide a larger ensemble and more robust measurements of uncertainties. However, there is a need to screen the models used in constructing such ensembles, because palaeo-evaluation shows that some models are consistently better than others at reproducing the magnitude and patterns of large climate changes.

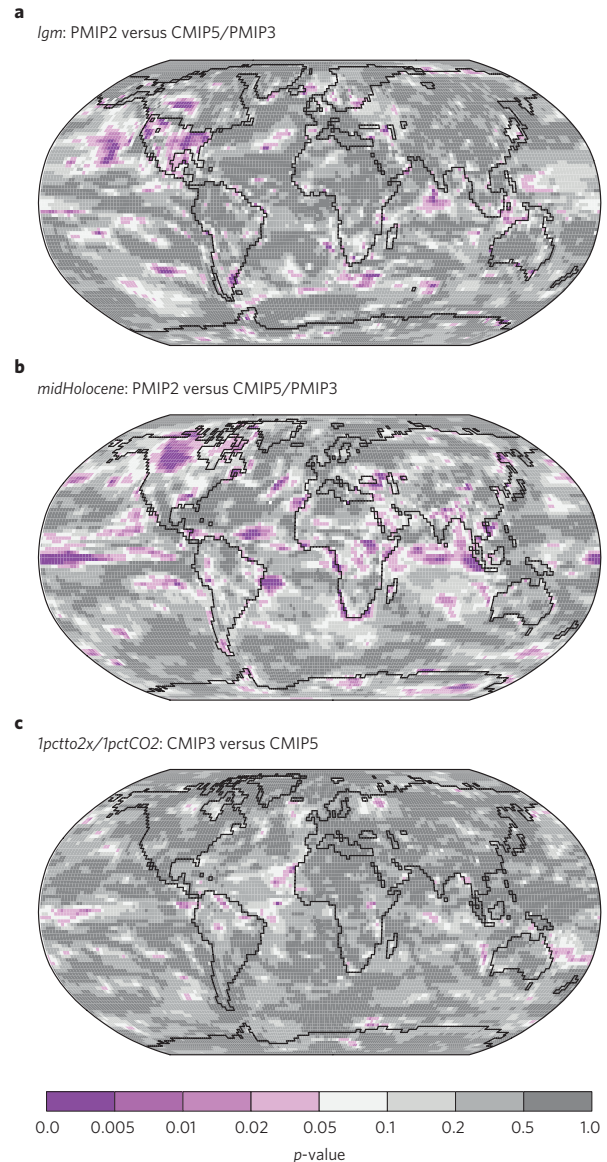


Figure 4 | Maps of the p-values of Hotelling's T2 test⁹¹ comparing the CMIP3 plus PMIP2 versus CMIP5 ensembles. The plots show the p-values for the test of the hypothesis of equality of the (multivariate) ensemble means of MAT, mean temperature of the coldest month, MTWA and MAP for the LGM (*lgm*), mid-Holocene (*midHolocene*) and the 1pctCO2 simulations in CMIP3 and CMIP5 (*1pctto2x* and *1pctCO2*, respectively). The number of significant statistics (that is, $p < 0.05$, shown in pink) do not exceed that expected by chance⁹². A previous study¹³ has shown that the results obtained using conventional meteorological variables are virtually identical.

Palaeo-simulations have not delivered on the promise to provide a well-founded additional constraint on climate sensitivity. This is partly because of the limited size of the ensemble, even when including LGM experiments with the previous CMIP3/PMIP2 generation of models. However, a second issue is associated with the limited amount of palaeoclimate data, and particularly quantitative reconstructions, from the Southern Hemisphere. It is difficult to constrain a global average based on unevenly distributed

data points. The continued expansion of palaeoclimate data sets will also allow evaluation of other regional climate changes. However, the robust nature of the spatial variations of climate change in the past (and future) calls into question whether a focus on global average responses is sensible.

Much of our knowledge about regional climate changes is based on qualitative inferences from geologic, biological or archaeological records, which provide a more detailed picture of the geographic areas affected than currently possible using quantitative climate reconstructions. Qualitative records are useful because they confirm that the more limited quantitative information is realistic. For example, although there are only 58 grid cells with quantitative reconstructions of mid-Holocene MAP for northern Africa, we are confident that the reconstructed increase in monsoon precipitation is reasonable because of the extensive information on the widespread occurrence of lakes^{80,81}, profound changes in vegetation cover^{82,83} and abundant human settlements^{84,85}. However, qualitative data of this sort cannot be used explicitly in model evaluation. Although some of these records could be used for quantitative reconstruction using statistical techniques, generally the exploitation of most of these data relies on the use of forward models, for example, of vegetation⁸⁶ or lake water balance^{87,88}. We suggest that increased emphasis on climate reconstruction and greater exploitation of forward modelling is urgently required to improve climate model evaluation.

The CMIP community is currently defining the suite of experiments that will constitute the basis for the next IPCC assessment report. CMIP5 was the first explicit inclusion of palaeo-experiments in the CMIP suite of simulations but they have already shown their usefulness. We urge all members of the CMIP community to run palaeosimulations and to use them in model diagnosis. Demonstrating which features of the simulated climate change are likely to be realistic, and which are not, will do much to increase confidence in future projections.

Received 24 December 2014; accepted 10 April 2015;
published online 24 July 2015

References

- Taylor, K. E., Stouffer, R. J. & Meehl, G. A. An overview of CMIP5 and the experiment design. *Bull. Am. Meteorol. Soc.* **93**, 485–498 (2012).
- Flato, G. *et al.* in *Climate Change 2013: The Physical Science Basis* (eds Stocker, T. F. *et al.*) 741–866 (IPCC, Cambridge Univ. Press, 2013).
- Kirtman, B. *et al.* in *Climate Change 2013: The Physical Science Basis* (eds Stocker, T. F. *et al.*) 953–1028 (IPCC, Cambridge Univ. Press, 2013).
- Collins, M. *et al.* in *Climate Change 2013: The Physical Science Basis* (eds Stocker, T. F. *et al.*) 1029–1136 (IPCC, Cambridge Univ. Press, 2013).
- Hawkins, E. & Sutton, R. The potential to narrow uncertainty in regional climate predictions. *Bull. Am. Meteorol. Soc.* **90**, 1095–1107 (2009).
- Hawkins, E. & Sutton, R. The potential to narrow uncertainty in projections of regional precipitation change. *Clim. Dynam.* **37**, 407–418 (2011).
- Braconnot, P. *et al.* Evaluation of climate models using palaeoclimatic data. *Nature Clim. Change* **2**, 417–424 (2012).
- MARGO Project Members Constraints on the magnitude and patterns of ocean cooling at the Last Glacial Maximum. *Nature Geosci.* **2**, 127–132 (2009).
- Bartlein, P. J. *et al.* Pollen-based continental climate reconstructions at 6 and 21 ka: A global synthesis. *Clim. Dynam.* **37**, 775–802 (2011).
- Joussaume, S. *et al.* Monsoon changes for 6000 years ago: Results of 18 simulations from the Paleoclimate Modelling Intercomparison Project (PMIP). *Geophys. Res. Lett.* **26**, 859–862 (1999).
- Pinot, S. *et al.* Tropical palaeoclimates at the Last Glacial Maximum: Comparison of Paleoclimate Modelling Intercomparison Project (PMIP) simulations and paleodata. *Clim. Dynam.* **15**, 857–874 (1999).
- Braconnot, P. *et al.* Results of MIP2 coupled simulations of the mid-Holocene and Last Glacial Maximum—Part 1: Experiments and large-scale features. *Clim. Past* **3**, 261–277 (2007).
- Harrison, S. P. *et al.* Model benchmarking with glacial and mid-Holocene climates. *Clim. Dynam.* **43**, 671–688 (2014).
- Joshi, M. M., Lambert, F. H. & Webb, M. J. An explanation for the difference between twentieth and twenty-first century land–sea warming ratio in climate models. *Clim. Dynam.* **41**, 1853–1869 (2013).
- Pithan, F. & Mauritsen, T. Arctic amplification dominated by temperature feedbacks in contemporary climate models. *Nature Geosci.* **7**, 181–184 (2014).
- Izumi, K., Bartlein, P. J. & Harrison, S. P. Consistent behaviour of the climate system in response to past and future forcing. *Geophys. Res. Lett.* **40**, 1–7 (2013).
- Hargreaves, J. C. & Annan, J. D. Can we trust climate models? *WIREs Clim. Change* **5**, 435–440 (2014).
- Schmidt, G. A. *et al.* Using paleo-climate comparisons to constrain future projections in CMIP5. *Clim. Past* **10**, 221–250 (2014).
- Lunt, D. J. *et al.* A multi-model assessment of last interglacial temperatures. *Clim. Past* **9**, 699–717 (2013).
- Hill, D. J. *et al.* Evaluating the dominant components of warming in Pliocene climate simulations. *Clim. Past* **10**, 79–90 (2014).
- Salzmann, U. *et al.* Challenges in quantifying Pliocene terrestrial warming revealed by data–model discord. *Nature Clim. Change* **3**, 969–974 (2013).
- Miller, G. H., Lehman, S. J., Refsnider, K. A., Southon, J. R. & Zhong, Y. Unprecedented recent summer warmth in Arctic Canada. *Geophys. Res. Lett.* **40**, 5745–5751 (2013).
- Izumi, K., Bartlein, P. J. & Harrison, S. P. Energy-balance mechanisms underlying consistent large-scale temperature responses in warm and cold climates. *Clim. Dynam.* **44**, 3111–3127 (2015).
- Allan, R. P. Examination of relationships between clear-sky longwave radiation and aspects of the atmospheric hydrological cycle in climate models, reanalysis, and observations. *J. Climate* **22**, 3127–3145 (2009).
- Trenberth, K. E. & Shea, D. J. Relationships between precipitation and surface temperature. *Geophys. Res. Lett.* **32**, L14703 (2005).
- Lau, W. K. M., Wu, H.-T. & Kim, K.-M. A canonical response of precipitation characteristics to global warming from CMIP5 models. *Geophys. Res. Lett.* **40**, 3163–3169 (2013).
- Li, G., Harrison, S. P., Bartlein, P. J., Izumi, K. & Prentice, I. C. Precipitation scaling with temperature in warm and cold climates: An analysis of CMIP5 simulations. *Geophys. Res. Lett.* **40**, 4018–4024 (2013).
- Kutzbach, J. E. & Street-Perrott, F. A. Milankovitch forcing of fluctuations in the level of tropical lakes from 18 to 0 kyr BP. *Nature* **317**, 130–134 (1985).
- Wohlfahrt, J., Harrison, S. P. & Braconnot, P. Synergistic feedbacks between ocean and vegetation on mid- and high-latitude climates during the mid-Holocene. *Clim. Dynam.* **22**, 223–238 (2004).
- Marzin, C. & Braconnot, P. The role of the ocean feedback on Asian and African monsoon variations at 6 kyr and 9.5 kyr BP. *C. R. Geosci.* **341**, 643–655 (2009).
- Wang, T., Wang, H. J. & Jiang, D. B. Mid-Holocene East Asian summer climate as simulated by the PMIP2 models. *Paleogeogr. Palaeoclimatol. Palaeoecol.* **288**, 93–102 (2010).
- Zhao, Y. & Harrison, S. P. Mid-Holocene monsoons: A multi-model analysis of the inter-hemispheric differences in the responses to orbital forcing and ocean feedbacks. *Clim. Dynam.* **39**, 1457–1487 (2012).
- Jiang, D., Lang, X., Tian, Z. & Ju, L. Mid-Holocene East Asian summer monsoon strengthening: Insights from Paleoclimate Modeling Intercomparison Project (PMIP) simulations. *Paleogeogr. Palaeoclimatol. Palaeoecol.* **369**, 422–429 (2013).
- Jiang, D., Tian, Z. & Land, X. Mid-Holocene net precipitation changes over China: Model–data comparison. *Quat. Sci. Rev.* **82**, 104–120 (2013).
- Perez-Sanz, A., Li, G., Gonzalez, P. & Harrison, S. P. Evaluation of seasonal climates of northern Africa and the Mediterranean in the CMIP5 simulations. *Clim. Past* **10**, 551–568 (2014).
- Prado, L. F., Wainer, I. & Chiessi, C. M. Mid-Holocene PMIP3/CMIP5 model results: Intercomparison for the South American monsoon system. *Holocene* **21**, 1915–1920 (2013).
- Kutzbach, J. E., Bonan, G. B., Foley, J. A. & Harrison, S. P. Vegetation and soils feedbacks on the response of the African monsoon to orbital forcing in the early to middle Holocene. *Nature* **384**, 623–626 (1996).
- Claussen, M. & Gayler, V. The greening of the Sahara during the mid-Holocene: Results of an interactive atmosphere–biome model. *Glob. Ecol. Biogeogr. Lett.* **6**, 369–377 (1997).
- Broström, A. *et al.* Land surface feedbacks and palaeomonsoons in northern Africa. *Geophys. Res. Lett.* **25**, 3615–3618 (1998).
- Braconnot, P., Joussaume, S., Marti, O. & de Noblet, N. Synergistic feedbacks from ocean and vegetation on the African monsoon response to mid-Holocene insolation. *Geophys. Res. Lett.* **26**, 2481–2484 (1999).
- Otto, J., Raddatz, T., Claussen, M., Brovkin, V. & Gayler, V. Separation of atmosphere–ocean–vegetation feedbacks and synergies for mid-Holocene climate. *Glob. Biogeochem. Cycles* **23**, L09701 (2009).
- Claussen, M., Bathiany, S., Brovkin, V. & Kleinen, T. Simulated climate–vegetation interaction in semi-arid regions affected by plant diversity. *Nature Geosci.* **6**, 954–958 (2013).
- Levis, S., Bonan, G. B. & Bonfils, C. Soil feedback drives the mid-Holocene North African monsoon northward in fully coupled CCSM2 simulations with a dynamic vegetation model. *Clim. Dynam.* **23**, 791–802 (2004).

44. Wang, Y. *et al.* Detecting vegetation–precipitation feedbacks in mid-Holocene North Africa from two climate models. *Clim. Past* **4**, 59–67 (2008).
45. Tian, Z. & Jiang, D. Mid-Holocene ocean and vegetation feedbacks over East Asia. *Clim. Past* **9**, 2153–2171 (2013).
46. Prentice, I. C., Liang, X., Medlyn, B. & Wang, Y. Reliable, robust and realistic: The three R's of next-generation land-surface modelling. *Atmos. Chem. Phys. Discuss.* **14**, 24811–24861 (2014).
47. Roehrig, R., Bouniol, D., Guichard, F., Hourdin, F. & Redelsperger, J.-L. The present and future of the West African monsoon: A process-oriented assessment of CMIP5 simulations along the AMMA transect. *J. Climate* **26**, 6471–6505 (2013).
48. Zheng, W. & Braconnot, P. Characterization of model spread in PMIP2 mid-Holocene simulations of the African monsoon. *J. Climate* **26**, 1192–1210 (2013).
49. Yu, G. & Harrison, S. P. An evaluation of the simulated water balance of Eurasia and northern Africa at 6000 yr BP using lake status data. *Clim. Dynam.* **12**, 723–735 (1996).
50. Wohlfahrt, J. *et al.* Evaluation of coupled ocean–atmosphere simulations of Northern Hemisphere extratropical climates in the mid-Holocene. *Clim. Dynam.* **31**, 871–890 (2008).
51. Mueller, B. & Seneviratne, S. I. Systematic land climate and evapotranspiration biases in CMIP5 simulations. *Geophys. Res. Lett.* **41**, 128–134 (2014).
52. Mauri, A., Davis, B. A. S., Collins, P. M. & Kaplan, J. O. The influence of atmospheric circulation on the mid-Holocene climate of Europe: A data–model comparison. *Clim. Past* **10**, 1925–1938 (2014).
53. Masson, V. *et al.* Mid-Holocene climate in Europe: What can we infer from PMIP model data comparisons? *Clim. Dynam.* **15**, 163–182 (1999).
54. Brewer, S., Guiot, J. & Torre, F. Mid-Holocene climate change in Europe: A data–model comparison. *Clim. Past* **3**, 499–512 (2007).
55. Davis, B. A. S. & Brewer, S. Orbital forcing and the role of the latitudinal temperature/insolation gradient. *Clim. Dynam.* **32**, 143–165 (2009).
56. van Oldenborgh, G. J. *et al.* Western Europe is warming much faster than expected. *Clim. Past* **5**, 1–12 (2009).
57. Berger, A., Brandefelt, J. & Nilsson, J. The sensitivity of the Arctic sea ice to orbitally induced insolation changes: A study of the mid-Holocene Paleoclimate Modelling Intercomparison Project 2 and 3 simulations. *Clim. Past* **9**, 969–982 (2013).
58. Goosse, H., Roche, D. M., Mairesse, A. & Berger, M. Modelling past sea ice changes. *Quat. Sci. Rev.* **79**, 191–206 (2013).
59. Chavaillaz, Y., Codron, F. & Kageyama, M. Southern westerlies in LGM and future (RCP4.5) climates. *Clim. Past* **9**, 517–524 (2013).
60. Rojas, M. Sensitivity of Southern Hemisphere circulation to LGM and 4 × CO₂ climates. *Geophys. Res. Lett.* **40**, 965–970 (2013).
61. DiNezio, P. N. & Tierney, J. E. The effect of sea level on glacial Indo-Pacific climate. *Nature Geosci.* **6**, 485–491 (2013).
62. Hargreaves, J. C., Annan, J. D., Ohgaito, R., Paul, A. & Abe-Ouchi, A. Skill and reliability of climate model ensembles at the Last Glacial Maximum and mid-Holocene. *Clim. Past* **9**, 811–823 (2013).
63. Gleckler, P. J., Taylor, K. E. & Doutriaux, C. Performance metrics for climate models. *J. Geophys. Res.* **113**, D06104 (2008).
64. Annan, J. D. & Hargreaves, J. C. Understanding the CMIP3 multimodel ensemble. *J. Climate* **24**, 4529–4538 (2011).
65. Hessler, I. *et al.* Implication of methodological uncertainties for mid-Holocene sea surface temperature reconstructions. *Clim. Past* **10**, 2237–2252 (2014).
66. Kageyama, M. *et al.* Mid-Holocene and Last Glacial Maximum climate simulations with the IPSL model – Part I: Comparing IPSL CM5A to IPSL CM4. *Clim. Dynam.* **40**, 2447–2468 (2013).
67. Kageyama, M. *et al.* Mid-Holocene and Last Glacial Maximum climate simulations with the IPSL model: Part II: Model–data comparisons. *Clim. Dynam.* **40**, 2469–2495 (2013).
68. Knutti, R. The end of model democracy? *Clim. Change* **102**, 395–404 (2010).
69. Rauser, F., Gleckler, P. & Marotzke, J. Rethinking the default construction of multi-model climate ensembles. *Bull. Am. Meteorol. Soc.* <http://dx.doi.org/10.1175/BAMS-D-13-00181.1> (2014).
70. PALAEOSSENS project members Making sense of palaeoclimate sensitivity. *Nature* **491**, 683–691 (2012).
71. Annan, J. D., Hargreaves, J. C., Ohgaito, R., Abe-Ouchi, A. & Emori, S. Efficiently constraining climate sensitivity with ensembles of paleoclimate simulations. *SOLA* **1**, 181–184 (2005).
72. Crucifix, M. Does the Last Glacial Maximum constrain climate sensitivity? *Geophys. Res. Lett.* **33**, L18701 (2006).
73. Schneider von Deimling, T., Held, H., Ganolpolski, A. & Rahmstorf, S. Climate sensitivity estimated from ensemble simulations of glacial climate. *Clim. Dynam.* **27**, 149–163 (2006).
74. Hargreaves, J. C., Annan, J. D., Yoshimori, M. & Abe-Ouchi, A. Can the Last Glacial Maximum constrain climate sensitivity? *Geophys. Res. Lett.* **39**, L24702 (2012).
75. Tripati, A. K. *et al.* Modern and glacial tropical snowlines controlled by sea surface temperature and atmospheric mixing. *Nature Geosci.* **7**, 205–209 (2014).
76. Yoshimori, M., Hargreaves, J. C., Annan, J. D., Yokohata, T. & Abe-Ouchi, A. Dependency of feedbacks on forcing and climate state in physics parameter ensembles. *J. Climate* **24**, 6440–6455 (2011).
77. Otto-Bliesner, B. L. *et al.* Last Glacial Maximum and Holocene climate in CCSM3. *J. Climate* **19**, 2526–2544 (2006).
78. Schmittner, A. *et al.* Climate sensitivity estimated from temperature reconstructions of the Last Glacial Maximum. *Science* **334**, 1385–1388 (2011).
79. Claquin, T. *et al.* Radiative forcing effect of ice-age dust. *Clim. Dynam.* **20**, 193–202 (2003).
80. Hoelzmann, P. *et al.* Mid-Holocene land-surface conditions in northern Africa and the Arabian peninsula: A data set for the analysis of biogeophysical feedbacks in the climate system. *Glob. Biogeochem. Cycles* **12**, 35–51 (1998).
81. Lézine, A.-M., Hély, C., Grenier, C., Braconnot, P. & Krinner, G. Sahara and Sahel vulnerability to climate changes, lessons from Holocene hydrological data. *Quat. Sci. Rev.* **30**, 3001–3012 (2011).
82. Elenga, H. *et al.* Pollen-based reconstruction for Southern Europe and Africa 18,000 years ago. *J. Biogeogr.* **27**, 621–634 (2000).
83. Watrin, J., Lézine, A.-M. & Hély, C. Plant migration and ecosystems at the time of the “green Sahara”. *C. R. Geosci.* **341**, 656–670 (2009).
84. Kuper, R. & Kropelin, S. Climate-controlled Holocene occupation in the Sahara: Motor of Africa's evolution. *Science* **313**, 803–807 (2006).
85. Manning, K. & Timpson, A. The demographic response to Holocene climate change in the Sahara. *Quat. Sci. Rev.* **101**, 28–35 (2014).
86. Prentice, I. C., Harrison, S. P. & Bartlein, P. J. Global vegetation and terrestrial carbon cycle changes after the last ice age. *New Phytol.* **189**, 988–998 (2011).
87. Coe, M. T. & Harrison, S. P. The water balance of northern Africa during the mid-Holocene: An evaluation of the 6ka BP PMIP experiments. *Clim. Dynam.* **19**, 155–166 (2002).
88. Ward, P. J., Aerts, J. C. J. H., de Moel, H. & Renssen, H. Verification of a coupled climate–hydrological model against Holocene palaeohydrological records. *Glob. Planet. Change* **57**, 283–300 (2007).
89. Haywood, A. M. *et al.* Pliocene Model Intercomparison Project (PlioMIP): Experimental design and boundary conditions (Experiment 1). *Geosci. Model Dev.* **3**, 227–242 (2010).
90. Taylor, K. E. Summarizing multiple aspects of model performance in a single diagram. *J. Geophys. Res.* **106**, 7183–7192 (2001).
91. Wilks, D. S. *Statistical Methods in the Atmospheric Sciences* 3rd edn (International Geophysics Series 100, Academic, 2011).
92. Wilks, D. S. On “field significance” and the false discovery rate. *J. Appl. Meteorol. Climatol.* **45**, 1181–1189 (2006).
93. Joussaume, S. & Taylor, K. E. in *Proc. 1st Int. AMIP Sci. Conf.* 425–430 (WCRP Series Report 92, WMO, 1995).
94. Gates, W. L. AMIP: The Atmospheric Model Intercomparison Project. *Bull. Am. Meteorol. Soc.* **73**, 1962–1970 (1992).
95. Abe-Ouchi, A. & Harrison, S. P. Constraining the carbon-cycle feedback using palaeodata: The PalaeoCarbon Modelling Intercomparison Project. *Eos* **90**, 140 (2009).

Acknowledgements

This paper is a contribution to the ongoing work on the PMIP. We thank all of the modelling groups who have contributed to the CMIP5 archive. We acknowledge financial support from the Centre for Past Climate Change, University of Reading. G.L. was supported by an international postgraduate research scholarship at Macquarie University. P.J.B. and K.I. were supported by the US National Science Foundation paleoclimatology programme. M.K., P.B. and K.I. acknowledge financial support from Labex L-IPSL.

Author contributions

S.P.H. planned the paper and was responsible for drafting the text; all authors were involved in analysis and interpretation of the data, and contributed to the final version.

Additional information

Reprints and permissions information is available online at www.nature.com/reprints. Correspondence should be addressed to S.P.H.

Competing financial interests

The authors declare no competing financial interests.

Evaluation of CMIP5 palaeosimulations to improve climate projections

S. P. Harrison^{1,2*}, P. J. Bartlein³, K. Izumi^{3,4,5}, G. Li², J. Annan⁶, J. Hargreaves⁶, P. Braconnot⁴ and M. Kageyama⁴

Table 1 | Description of past, present and future simulations.

Abbreviation (in this Review)	Name of experiment(s) (in ESGF or PMIP databases)	Description	Boundary conditions
RCP	rcp2.6, rcp4.5, rcp6, rcp8.5	Transient simulations from 2006 to 2100	Forced with RCP scenarios of changes in atmospheric composition and land use that produce radiative forcing of 2.6, 4.5, 6 and 8.5 W m ⁻² by 2100
1pctCO2	1pctCO2	CMIP5 transient simulation with a 1% yr ⁻¹ change in CO ₂ from a pre-industrial control to quadrupled CO ₂	Trace gases: CO ₂ changes from, for example, 280 to 1,120 ppm in 140 yr Other boundary conditions: as in CMIP5 piControl
1pctto2xCO2	1pctto2x	CMIP3 transient simulation	Trace gases: 1% increase in CO ₂ from either a pre-industrial or present-day control simulation (70 yr), then hold constant for an additional 150 yr. Other boundary conditions as in the CMIP3 pre-industrial or present-day simulations.
abrupt4xCO2	abrupt4xCO2	CMIP5 equilibrium simulation with instantaneous quadrupling of CO ₂ relative to pre-industrial	Trace gases: for example, CO ₂ = 1,120 ppm Other boundary conditions: as in CMIP5 piControl
historical (twentieth century)	historical	CMIP5 transient simulation 1850–2005	For this experiment, each modelling group defined the forcings appropriately for their model to be consistent with observations. These could include time-varying: Atmospheric composition (including CO ₂), due to both anthropogenic and volcanic influences Solar forcing Emissions or concentrations of short-lived species and natural and anthropogenic aerosols or their precursors Land use
piControl	piControl	Equilibrium simulation of 1850, used as control for abrupt4xCO2, mid- Holocene and LGM simulations, and as baseline for the historical (twentieth century) simulation	Non-evolving, pre-industrial conditions, which could include: Prescribed atmospheric concentrations of all well-mixed gases (including CO ₂) and of some short-lived (reactive) species Prescribed non-evolving emissions or concentrations of natural aerosols or their precursors and of some short-lived (reactive) species Unperturbed land use For comparison with past climate experiments, the following conditions were typically used: Orbital parameters: eccentricity = 0.016724, obliquity = 23.446°, perihelion – 180° = 102.04° Trace gases: CO ₂ = 280 ppm, CH ₄ = 650 ppb, N ₂ O = 270 ppb, CFC = 0, O ₃ = modern – 10 DU Ice sheet: modern Land surface: modern or computed with dynamical vegetation model Carbon cycle: interactive, with atmospheric concentration prescribed and ocean and land carbon fluxes diagnosed as recommended in CMIP5 Note: modelling groups that did not run palaeosimulations may have used a slightly different configuration for the piControl (see documentation of individual models)

SUPPLEMENTARY INFORMATION

DOI: 10.1038/NCLIMATE2649

continued...

mid-Holocene	<i>midHolocene</i> (CMIP5/PMIP3)	Equilibrium simulation of 6,000 yr BP	<p>Orbital parameters: eccentricity = 0.018682, obliquity = 24.105°, perihelion – 180° = 0.87°</p> <p>Trace gases: CO₂ = 280 ppm, CH₄ = 760 ppb, N₂O = 270 ppb, CFC = 0, O₃ = same as in CMIP5 PI</p> <p>Ice sheet: as in CMIP5 piControl</p> <p>Land surface: computed using a dynamical vegetation module or prescribed as in piControl, with phenology computed for models with active carbon cycle or prescribed from data</p> <p>Carbon cycle: interactive, with atmospheric concentration prescribed and ocean and land carbon fluxes diagnosed as recommended in CMIP5</p>
	<i>PMIP_6k</i> (PMIP2)	Equilibrium simulation of 6,000 yr BP	<p>Orbital parameters: eccentricity = 0.018682, obliquity = 24.105°, perihelion – 180° = 0.87°</p> <p>Trace gases: CO₂ = 280 ppm, CH₄ = 650 ppb, N₂O = 270 ppb, CFC = 0, O₃ = same as in PMIP_0k control run</p> <p>Ice sheet: as in PMIP_0k control run</p> <p>Land surface: same as control simulation, except in models with interactive vegetation</p> <p>Carbon cycle: fixed</p>
LGM	<i>lgm</i> (CMIP5/PMIP3)	Equilibrium simulation of the LGM, 21,000 yr BP	<p>Orbital parameters: eccentricity = 0.018994, obliquity = 22.949°, perihelion – 180° = 114.42°</p> <p>Trace gases: CO₂ = 185 ppm, CH₄ = 350 ppb, N₂O = 200 ppb, CFC = 0, O₃ = as in CMIP5 PI</p> <p>Ice sheet: prescribed consensus ice sheet as described on PMIP3 website, with consistent changes to land-sea mask and sea level</p> <p>Land surface: computed using a dynamical vegetation module or prescribed as in piControl, with phenology computed for models with active carbon cycle or prescribed from data</p> <p>Carbon cycle: interactive, with atmospheric concentration prescribed and ocean and land carbon fluxes diagnosed as recommended in CMIP5</p>
	<i>PMIP_21k</i> (PMIP2)	Equilibrium simulation of the LGM, 21,000 yr BP	<p>Orbital parameters: eccentricity = 0.018994, obliquity = 22.949°, perihelion – 180° = 114.42°</p> <p>Trace gases: CO₂ = 185 ppm, CH₄ = 350 ppb, N₂O = 200 ppb, CFC = 0, O₃ = as in CMIP5 PI</p> <p>Ice sheet: prescribed consensus ice sheet as described on PMIP3 website, with consistent changes to land-sea mask and sea level</p> <p>Land surface: same as control simulation, except in models with interactive vegetation</p> <p>Carbon cycle: fixed</p>
last interglaciation	No systematic naming convention	Equilibrium simulation of one interval during the last interglaciation (for example, 130,000, 128,000, 127,000, 126,000 or 125,000 yr BP)	<p>Orbital parameters: appropriate orbital parameters for time period chosen</p> <p>Trace gases: either specified according to PMIP3 protocol, or independently derived but for the specified time period, or kept the same as in piControl (see ref. 19 for details)</p> <p>Other boundary conditions: as in piControl</p>
mid-Pliocene	mid-Pliocene warm period <i>PlioExp2a</i>	Equilibrium, atmosphere- only simulation of the warm period between 3.29 and 2.97 Myr BP	<p>Orbital parameters: as in piControl</p> <p>Trace gases: CO₂ = 405 ppm, otherwise as in piControl</p> <p>Ice sheet: PRISM3D, with consistent land-sea geography and sea level</p> <p>Land surface: PRISM3D</p> <p>Ocean: PRISM3D</p>

The future simulations are either scenario-driven (RCP) or idealized simulations of warm climate states caused by enhanced CO₂ (1pctCO₂, abrupt4xCO₂). The present day is represented either by a twentieth-century climate extracted from a historical simulation or by a piControl simulation. The palaeosimulations include both the mid-Holocene and LGM simulations analysed in detail in this Review, and the last interglaciation and mid-Pliocene experiments. More details of the last interglaciation and mid-Pliocene experiments can be found in refs 19 and 89, respectively. ppm: parts per million; ppb: parts per billion; CFC: chlorofluorocarbon.

Chapter 5

Simulation of tree-ring widths with a model for primary production, carbon allocation, and growth

Contribution by Co-Authors: G. L. was responsible for model coding, model parameterisation, field data collection, measurement and analysis, figure and table generation; the theoretical basis for the model was established by I. C. P. in consultation with D. F.; G. L., S. P. H., and I. C. P. were jointly responsible for development of the model and interpretation of the results; G.L. and S.P.H. made the first draft of the text and all authors were involved in the final version of the manuscript.

Biogeosciences, 11, 6711–6724, 2014
 www.biogeosciences.net/11/6711/2014/
 doi:10.5194/bg-11-6711-2014
 © Author(s) 2014. CC Attribution 3.0 License.



Simulation of tree-ring widths with a model for primary production, carbon allocation, and growth

G. Li¹, S. P. Harrison^{1,2}, I. C. Prentice^{1,3}, and D. Falster¹

¹Department of Biological Sciences, Macquarie University, North Ryde, NSW 2109, Australia

²School of Archaeology, Geography and Environmental Sciences (SAGES), Reading University, Reading, UK

³AXA Chair of Biosphere and Climate Impacts, Grand Challenges in Ecosystem and the Environment, Department of Life Sciences and Grantham Institute for Climate Change, Imperial College London, Ascot, UK

Correspondence to: G. Li (guangqi.li@students.mq.edu.au)

Received: 27 February 2014 – Published in Biogeosciences Discuss.: 4 July 2014

Revised: 20 October 2014 – Accepted: 22 October 2014 – Published: 4 December 2014

Abstract. We present a simple, generic model of annual tree growth, called “*T*”. This model accepts input from a first-principles light-use efficiency model (the “*P*” model). The *P* model provides values for gross primary production (GPP) per unit of absorbed photosynthetically active radiation (PAR). Absorbed PAR is estimated from the current leaf area. GPP is allocated to foliage, transport tissue, and fine-root production and respiration in such a way as to satisfy well-understood dimensional and functional relationships. Our approach thereby integrates two modelling approaches separately developed in the global carbon-cycle and forest-science literature. The *T* model can represent both ontogenetic effects (the impact of ageing) and the effects of environmental variations and trends (climate and CO₂) on growth. Driven by local climate records, the model was applied to simulate ring widths during the period 1958–2006 for multiple trees of *Pinus koraiensis* from the Changbai Mountains in northeastern China. Each tree was initialised at its actual diameter at the time when local climate records started. The model produces realistic simulations of the interannual variability in ring width for different age cohorts (young, mature, and old). Both the simulations and observations show a significant positive response of tree-ring width to growing-season total photosynthetically active radiation (PAR₀) and the ratio of actual to potential evapotranspiration (α), and a significant negative response to mean annual temperature (MAT). The slopes of the simulated and observed relationships with PAR₀ and α are similar; the negative response to MAT is underestimated by the model. Comparison of simulations with fixed and changing atmospheric CO₂ concen-

tration shows that CO₂ fertilisation over the past 50 years is too small to be distinguished in the ring-width data, given ontogenetic trends and interannual variability in climate.

1 Introduction

Forests cover about 30 % of the land surface (Bonan, 2008) and are estimated to contain 861 ± 66 PgC (Pan et al., 2011). Inventory-based estimates show that forests have been a persistent carbon sink in recent decades, with a gross uptake of 4.0 ± 0.5 PgC year⁻¹ and a net uptake of 1.1 ± 0.8 PgC year⁻¹ between 1990 and 2007 (Pan et al., 2011). This is a significant amount in comparison to the amounts of carbon released from fossil fuel burning, cement production, and deforestation (9.5 ± 0.8 PgC year⁻¹ in 2011: Ciais et al., 2013), and thus forest growth has a substantial effect on atmospheric CO₂ concentration and climate (Shevliakova et al., 2013). However, there is considerable geographic variability in the trends in the carbon sink, as well as the factors controlling regional trends, and uncertainty about how forest growth and carbon sequestration will be affected by climate change, and climate-driven changes in wildfire (Ciais et al., 2013; Moritz et al., 2013). The changing importance of disturbance, and its influence on forest age, is likely to have a significant impact on the ability of forests to act as carbon sinks. It is generally assumed that stand-level productivity stabilises or declines with age (Ryan and Yodar, 1997; Caspersen et al., 2011). However, recent analyses have shown that mass growth rate (and hence

carbon accumulation) by individual trees increases continuously with tree size (Stephenson et al., 2014), pointing to a need to understand the relationship between individual and stand-growth rates. Predictions of future changes in the terrestrial carbon cycle (e.g. Friedlingstein and Prentice, 2010) rely on ecosystem models that explicitly represent leaf-level processes, such as photosynthesis, but in most cases do not incorporate the response of individual trees. In models that do consider individual tree growth (e.g. ED: Moorcroft et al., 2001; Medvigy et al., 2012; LPJ-GUESS: Smith et al., 2001; Claesson and Nycander, 2013), little attention has been paid to evaluating the realism of simulated radial growth. Incorporating the response of individual trees to climate and environmental change within such modelling frameworks should help to provide more realistic estimates of the role of forests in the global carbon cycle.

Climate factors, such as temperature and moisture availability during the growing season, are important drivers of tree growth (Harrison et al., 2010). This forms the basis for reconstructing historical climate changes from tree-ring records of annual growth (Fritts, 2012). However, photosynthetically active radiation (PAR) is the principal driver of photosynthesis. Models for primary production that use temperature, not PAR, implicitly rely on the far-from-perfect correlation between temperature and PAR (Wang et al., 2014). PAR can change independently from temperature (through changes in cloudiness affecting PAR or atmospheric circulation changes affecting temperature) and this may help to explain why statistical relationships between tree growth and temperature at some high-latitude and high-elevation sites appear to break down in recent decades (D'Arrigo et al., 2008). CO₂ concentration also has an impact on tree growth, although its magnitude is still controversial; trends in tree growth have been attributed to increasing atmospheric CO₂ concentration in some studies (Wullschlegel et al., 2002; Körner, 2006; Huang et al., 2007; Koutavas, 2013) and not others (Miller, 1986; Luo et al., 2004; Reich et al., 2006). To resolve these apparent conflicts, and to understand tree-growth processes better, it is necessary to analyse the response of tree growth to multiple factors acting simultaneously, including solar radiation, climate, CO₂, and ontogenetic stage.

Modelling is needed for this purpose. Empirical models of annual tree-growth and climate variables (temperature and precipitation) have been used to simulate tree radial growth (Fritts, 2012). Process-based bioclimatic models might be preferable, however, because this allows other factors to be taken into account (e.g. the direct impact of CO₂ concentration on photosynthesis) and for non-stationarity in the response to specific climate variables. Vaganov et al. (2006) and Rathgeber et al. (2005) have used bioclimatic variables (temperature and soil-moisture availability) chosen to reflect physiological processes to simulate radial tree growth. The MAIDEN model (Misson, 2004; Misson et al., 2004; see also MAIDENiso: Danis et al., 2012) models the pheno-

logical and meteorological controls on net primary production (NPP) and explicitly allocates carbon to different carbon pools (including the stem) on a daily basis using phenological stage-dependent rules. Nevertheless, MAIDEN still requires the tuning of several parameters.

Simple equations representing functional and geometric relationships can describe carbon allocation by trees and make it possible to model individual tree growth (Yokozawa and Hara, 1995; Givnish, 1988; Falster et al., 2011; King, 2011). Such models are built on measurable relationships, such as that between stem diameter and height (Thomas, 1996; Ishii et al., 2000; Falster and Westoby, 2005), and crown area and diameter or height (Duursma et al., 2010) that arise because of functional constraints on growth. The pipe model represents the relationship between sapwood area and leaf area (Shinozaki et al., 1964; Yokozawa and Hara, 1995; Mäkelä et al., 2000). The ratio of fine-root mass to foliage area provides the linkage between above- and below-ground tissues (Falster et al., 2011). These functional relationships are expected to be stable through ontogeny, which implies that the fraction of new carbon allocated to different compartments is variable (Lloyd, 1999). In this paper, we combine the two modelling approaches previously developed in the global carbon-cycle (ecophysiology) and forest-science (geometric and carbon allocation) literature to simulate individual tree growth.

2 Methods

2.1 Model structure and derivation

We use a light-use efficiency model (the *P* model: Wang et al., 2014), driven by growing-season PAR, climate, and ambient CO₂ concentration inputs, to simulate gross primary production (GPP). The simulated GPP is used as input to a species-based carbon allocation and functional geometric tree-growth model (the *T* model) to simulate individual tree growth (Fig. 1).

2.1.1 The *P* model

The *P* model is a simple but powerful light-use efficiency and photosynthesis model, which simulates GPP per unit of absorbed PAR from latitude, elevation, temperature, precipitation, and fractional cloud cover (Wang et al., 2014). The climate observations used here are monthly temperature, precipitation, and fractional cloud cover, which are interpolated to a daily time step for subsequent calculations of the variables that determine annual GPP.

Potential annual GPP is the product of the PAR incident on vegetation canopies during the growing season (PAR₀), with the maximum quantum efficiency of photosynthesis (Φ_0), the fraction of absorbed PAR (fAPAR), and the effect of photorespiration and substrate limitation at subsaturating [CO₂], represented as a function of the leaf-internal [CO₂] (c_i) and

the photorespiratory compensation point (Γ^*), as shown in Eq. (1).

$$\text{GPP} = \Phi_0 (\text{PAR}_0 \times \text{fAPAR}) (c_i - \Gamma^*) / (c_i + 2\Gamma^*), \quad (1)$$

where Φ_0 is set to $0.48 \text{ g C mol}^{-1} \text{ photon}$, based on a quantum efficiency of $0.05 \text{ mol C mol}^{-1} \text{ photon}$ and a leaf absorptance of 0.8. Daily PAR at the top of the atmosphere is calculated based on solar geometry and is subsequently modified by transmission through the atmosphere, which is dependent on elevation and cloud cover. Annual effective PAR (PAR_0) is calculated as the annual sum of daily PAR, taking into account the low-temperature inhibition of photosynthesis and growth, using a linear ramp function to downweight PAR on days with temperatures below 10°C . Days with temperatures below 0°C do not contribute to PAR_0 . See Wang et al. (2014) for details. In this application, we first calculated potential GPP with fAPAR set to 1. fAPAR is not an input to the model, but is calculated implicitly, from the foliage cover simulated by the *T* model.

Leaf-internal $[\text{CO}_2]$ is obtained from the ambient $[\text{CO}_2]$ via the “least-cost hypothesis” (Wright et al., 2003; Prentice et al., 2014). Wang et al. (2014) provide a continuous prediction of the c_i / c_a ratio as a function of environmental aridity, temperature and elevation based on the following hypothesis:

$$c_i / c_a = 1 / (1 + C \sqrt{(\eta \sqrt{D}) / K}), \quad (2)$$

where D is the cumulative water deficit over a year (proportional to an annual “effective value” of the vapour pressure deficit: VPD), η is the dynamic viscosity of water, K is the effective Michaelis–Menten coefficient for Rubisco-limited photosynthesis, and C is a constant. The difference between the annual actual and equilibrium evapotranspiration is used as a proxy for D (see Prentice et al., 2013). D is calculated using the daily interpolated temperature, precipitation, and cloudiness data. Annual actual evapotranspiration is derived from equilibrium evapotranspiration and precipitation using a simple soil-moisture accounting scheme with a daily time step, as described in Gallego-Sala et al. (2010). The temperature dependences of η and K follow Prentice et al. (2014). Both K and η change steeply with temperature: K changes from 196 ppm at 10°C to 1094 ppm at 30°C ; η decreases from 1.31 mPa s at 10°C to only 0.798 mPa s at 30°C .

The temperature dependence of Γ^* is described by an exponential closely approximating an Arrhenius function (Bernacchi et al., 2003):

$$\Gamma^* = \Gamma_{25}^* \exp(0.0512 \Delta T), \quad (3)$$

where Γ_{25}^* is the value of Γ^* at 25°C (4.331 Pa), and ΔT is the monthly temperature difference from 25°C .

The *P* model has been shown to simulate well many of the global patterns of annual and maximum monthly terrestrial GPP by C_3 plants. The simulated seasonal cycle of GPP at different latitudes is supported by analyses of CO_2 flux measurements (Wang et al., 2014).

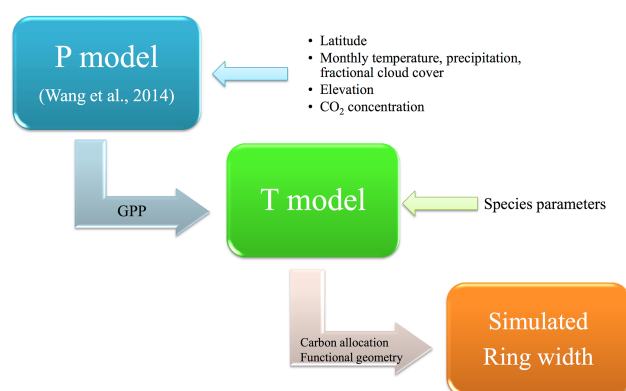


Figure 1. Model application flow. We combined the simple light-use efficiency and photosynthesis model (*P* model) with a carbon allocation and functional geometric tree-growth model to simulate tree growth (e.g. ring width). The inputs to the *P* model are latitude, elevation, $[\text{CO}_2]$, monthly temperature, precipitation, and fractional cloud cover. Potential gross primary productivity (GPP) simulated by the *P* model drives the *T* model. The *T* model also requires a limited number of species-specific parameter values to be specified.

2.1.2 The *T* model

We assume that potential GPP is the first-order driver of tree growth both at stand and individual level. The *T* model translates potential GPP, as simulated by the *P* model into individual tree growth, which depends on foliage cover within the canopy and the respiration of non-green tissues, carbon allocation to different tissues, and relationships between different dimensions of the tree. Although these relationships are often loosely called “allometries”, true allometries (power functions) have the undesirable mathematical property for growth modelling that, if the power is greater than 1, the derivative evaluated at the start of growth is 0; if the power is between 0 and 1, the derivative is infinite. We have therefore avoided the use of power functions, except for geometric relationships, in which they are unambiguously correct.

Functional geometric relationship

Carbon is allocated to different tissues within the constraint of the basic functional or geometric relationships between different dimensions of the tree.

Asymptotic height–diameter trajectories (Thomas, 1996; Ishii et al., 2000; Falster and Westoby, 2005) are modelled as

$$H = H_m [1 - \exp(-aD/H_m)], \quad (4)$$

where H is the tree height, D is the basal diameter, H_m is the (asymptotic) maximum height, and a is the initial slope of the relationship between height and diameter.

The model also requires the derivative of this relationship:

$$dH/dD = a \exp(-aD/H_m) = a(1 - H/H_m). \quad (5)$$

The form of the stem is assumed to be paraboloid (Jonson, 1910; Larson, 1963). It can be shown (assuming the pipe model) that this form is uniquely consistent with a uniform vertical distribution of foliage area during early growth; i.e. in the absence of heartwood. Here, the total stem mass (W_s) is expressed as a function of D and H :

$$W_s = (\pi/8)\rho_s D^2 H, \quad (6)$$

where ρ_s is the density of the wood, and $(\pi/8) D^2 H$ is the volume of a paraboloid stem.

The relationship of diameter increment to stem increment is then given by:

$$dW_s/dt = (\pi/8)\rho_s [D^2 (dH/dD) + 2DH] dD/dt. \quad (7)$$

The projected crown area (A_c) is estimated from D and H using an empirical relationship:

$$A_c = (\pi c/4a)DH, \quad (8)$$

where c is the initial ratio of crown area to stem cross-sectional area. This relationship was chosen as an intermediate between previously published expressions that relate A_c either to D^2 or H . It is consistent with reported allometric coefficients typically between 1 and 2 for the relationship between A_c and D .

Crown fraction (f_c) is also derived from H and D . As we assumed the stem to be paraboloid, the stem cross-sectional area at height z is

$$A_s(z) = A_s(1 - z/H), \quad (9)$$

where A_s is the basal area: $A_s = (\pi/4)D^2$. We find the height (z^*) at which the ratio of foliage area (A_f) to stem area at height z^* ($A_s(z^*)$) is the same as the initial ratio of crown area to stem cross-sectional area (c). We obtain crown area (A_c) from:

$$A_c = cA_s(z^*) = cA_s(1 - z^*/H). \quad (10)$$

Combining this with Eq. (8), we obtain $(\pi c/4a)DH = cA_s(1 - z^*/H)$, which reduces to

$$f_c = (1 - z^*/H) = H/aD. \quad (11)$$

The initial slope (a) is, in principle, dependent both on species growth form and ambient conditions, including light availability. Here, it is determined directly from observations.

Carbon allocation

Actual GPP (P) is obtained from potential GPP (P_0) using Beer's law (Jarvis and Leverenz, 1983):

$$P = P_0 A_c (1 - \exp(-kL)), \quad (12)$$

where k is the extinction coefficient for PAR, and L is the leaf area index within the crown.

NPP is derived from annual GPP, corrected for foliage respiration (which is set at 10 % of total GPP, an approximation based on the theory developed by Prentice et al., 2014 and Wang et al., 2014) by further deducting growth respiration and the maintenance respiration of sapwood and fine roots. Growth respiration is assumed to be proportional to NPP, following:

$$P_{\text{net}} = y(P - R_m) = y(P - W_s r_s - \zeta \sigma W_f r_r), \quad (13)$$

where P_{net} is NPP, R_m is the maintenance respiration of stem and fine roots, and y is the “yield factor” accounting for growth respiration. Total maintenance respiration of non-green parts comprises fine-root respiration ($\zeta \sigma W_f r_r$, where ζ is the ratio of fine-root mass to foliage area, σ is the specific leaf area, W_f is the mass of carbon in foliage ($(1/\sigma)LA_c$), and r_r is the specific respiration rate of fine roots), and stem (sapwood) respiration ($W_s r_s$, where W_s is the mass of carbon in sapwood, and r_s is the specific respiration rate of sapwood). W_s can be estimated from A_c through the pipe model:

$$W_s = LA_c v_H \rho_s H_f, \quad (14)$$

where v_H is the Huber value (ratio of sapwood to leaf area; Cruiziat et al., 2002), and H_f is the mean foliage height $H(1 - f_c/2)$. The constraint that the initial sapwood area must be equal to the stem cross-sectional area leads to the following identity: $Lcv_H = 1$.

NPP is allocated to stem increment (dW_s/dt), foliage increment (dW_f/dt), fine-root increment ($\zeta \sigma dW_f/dt$), foliage turnover (W_f/τ_f , where τ_f is the turnover time of foliage), and fine-root turnover ($\zeta \sigma W_f/\tau_r$, where τ_r is the turnover time of fine roots). For simplicity, in common with many models, we do not consider allocation to branches and coarse roots separately from allocation to stem:

$$P_{\text{net}} = dW_s/dt + (1 + \zeta \sigma)dW_f/dt + (1/\tau_f + \zeta \sigma/\tau_r)W_f. \quad (15)$$

From Eqs. (13) and (15), the stem increment (dW_s/dt) can now be expressed as:

$$dW_s/dt = yA_c [P_0(1 - \exp(-kL)) - \rho_s(1 - f_c/2)Hr_s/c - L\zeta r_r] - L(\pi c/4a)[aD(1 - H/H_m) + H](1/\sigma + \zeta)dD/dt - LA_c(1/\sigma\tau_f + \zeta/\tau_r). \quad (16)$$

The annual increment in (dD/dt) and all the other diameter-related indices are simulated by combining Eqs. (7) and (16).

2.1.3 Definition of the growing season

The season over which GPP is accumulated (i.e. the effective growing season) is defined as running from July in the previous year through to the end of June in the current year. This definition is consistent with the fact that photosynthesis peaks around the time of the summer solstice (Bauerle et al., 2012) and that maximum leaf area occurs shortly after this

Table 1. Parameter description and the derivation of parameter values.

Parameter	Code	Value	Uncertainty or range of value from literature	Value source: observation or published literature
Initial slope of height–diameter relationship (–)	<i>a</i>	116	±4.35	Observation (Fig. 2)
Initial ratio of crown area to stem cross-sectional area (–)	<i>c</i>	390.43	±11.84	Observation (Fig. 2)
Maximum tree height (m)	<i>H_m</i>	25.33	±0.71	Observation (Fig. 2)
Sapwood density (kg C m ^{–3})	<i>ρ_s</i>	200	±25	Observation
Leaf area index within the crown (–)	<i>L</i>	1.8	1.5–1.96	Chen et al. (2004)
Specific leaf area (m ² kg ^{–1} C)	<i>σ</i>	14	13.22–16.82	Huo and Wang (2007)
Foliage turnover time (years)	<i>τ_f</i>	4	–	Luo (1996)
Fine-root turnover time (years)	<i>τ_r</i>	1.04	–	Shan et al. (1993)
PAR extinction coefficient (–)	<i>k</i>	0.5	–	Pierce and Running (1988)
Yield factor (–)	<i>y</i>	0.6	0.5–0.7	Zhang et al. (2009)
Ratio of fine-root mass to foliage area (kg C m ^{–2})	<i>ζ</i>	0.17	–	White et al. (2000)
Fine-root specific respiration rate (year ^{–1})	<i>r_r</i>	0.913	–	Yan and Zhao (2007)
Sapwood-specific respiration rate (year ^{–1})	<i>r_s</i>	0.044 (1.4 nmol mol ^{–1} s ^{–1})	0.5–10, 20 nmol mol ^{–1} s ^{–1}	Landsberg and Sands (2010)

(Rautiainen et al., 2012). Carbon fixed during the later half of the year (July to December) is therefore either stored or allocated for purposes other than foliage expansion. Observations of tree radial growth show that it can occur before leaf-out (in broadleaved trees) or leaf expansion (in needle-leaved trees), thus confirming that some part of this growth is based on starch reserves from the previous year (Michelet et al., 2012). This definition of the effective growing season is also supported by analyses of our data, which showed that correlations between simulated and observed tree-ring widths are poorer when the model is driven by GPP from the current calendar year rather than an effective growing season from July through to June.

2.2 Model application

2.2.1 Observations

We use site-specific information on climate and tree growth from a relatively low-elevation site (ca. 128°02' E, 42°20' E; 800 m a.s.l.) in mixed conifer and broadleaf virgin forest in the Changbai Mountains in northeastern China (Bai et al., 2008). This region was chosen because there is no evidence of human influence on the vegetation, and the forests are maintained by natural regeneration. Data on tree height, diameter, and crown area were collected for 400 individual *Pinus koraiensis* trees from 35 20 m × 20 m sample plots. The 400 trees included all individuals of this species in the 35 plots, representing a complete sampling of the variability in growth. Tree height and diameter were measured directly, and crown area measured as the area of projected ground coverage. Tree-ring cores were obtained from 46 of these individuals in 2007. The selected trees were either from the canopy layer or from natural gaps in the forest, and, in both cases, not overshadowed by nearby indi-

viduals in order to minimise the possible effects of competition. An attempt was made to select individuals of different diameters (the diameter at breast height was from 10 to 70 cm at the time of sampling), broadly corresponding to the range of diameters recorded in the original sampling. The 46 trees were of different ages (ranging from < 50 to ca. 200 years at the time of sampling in 2006); subsequent analyses show there is little relationship between age and diameter at breast height. Environmental conditions (e.g. soil depth and light availability) were relatively uniform across the sampling plot. Monthly temperature, precipitation, and fractional cloud cover data from 1958 onwards were obtained from the Songjiang meteorological station (128°15' E, 42°32' E; 591.4 m a.s.l.), which is representative of the regional climate at low elevations in the Changbai Mountains.

2.2.2 Derivation of *T* model parameter values

T model parameter values were derived from measurements made at the sampling site or from the literature (Table 1). We estimated the initial slope of the height–diameter relationship (*a*: 116), the initial ratio of crown area to stem cross-sectional area (*c*: 390.43), and maximum tree height (*H_m*: 25.33 m) using non-linear regression applied to the diameter at breast height (*D*), tree height (*H*), and crown area (*A_c*) measurements on all the 400 trees from the sample plots (Fig. 2). We used a value of sapwood density derived from three measurements at the sampling site (Table 1). We used values of leaf area index within the crown (*L*), specific leaf area (*σ*), foliage turnover time (*τ_f*), and fine-root turnover time (*τ_r*) for *Pinus koraiensis* from field studies conducted in northeastern China (Table 1). No species-specific information was available for the PAR extinction coefficient (*k*), yield factor (*y*), ratio of fine-root mass to foliage area (*ζ*), fine-root specific respiration rate (*r_r*), or sapwood-specific respiration rate (*r_s*).

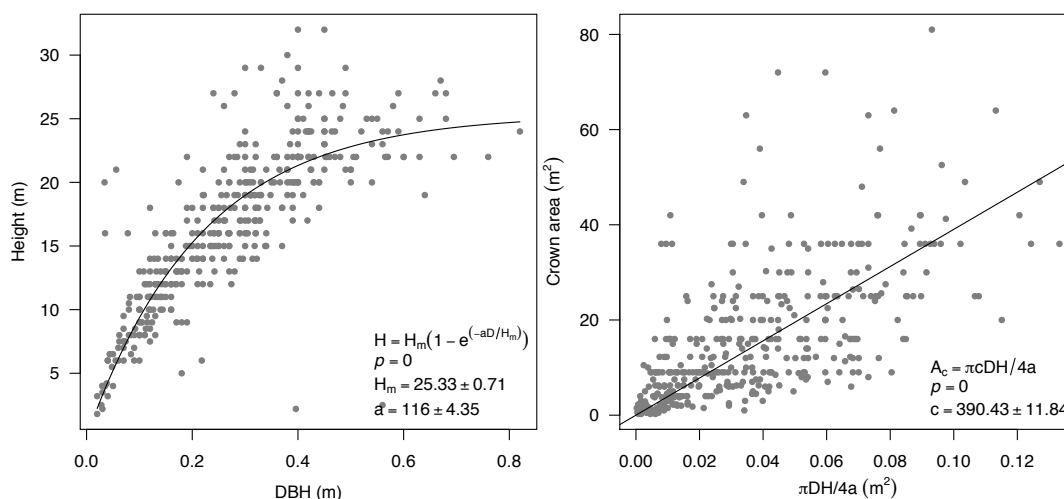


Figure 2. Estimation of parameter values for the application of the T model. Diameter at breast height (D), tree height (H), and crown area (A_c) of the 400 trees from the sample plots were used for the estimation of the initial slope of the height–diameter relationship (a) and (asymptotic) maximum tree height (H_m). Relationships among crown area (A_c), diameter at breast height (D), and height (H) (Eq. 7) are used to estimate the initial ratio of crown area to stem cross-sectional area (c).

We therefore used published values for other species of evergreen needleleaf trees, taken from papers that summarise results from a range of field measurements. Most of the published values for these parameters fall in a relatively narrow range (Table 1). The uncertainty in fine-root specific respiration rate is not given in the original source paper (Yan and Zhao, 2007), but the average value is consistent with other studies (e.g. Zogg et al., 1996). The published values for sapwood-specific respiration rate in pines show considerable variability, ranging from 0.5 to 10 or even 20 nmol mol^{−1} s^{−1} (Landsberg and Sands, 2010). Analyses (see Sect. 3.1) show that the model is sensitive to the specification of sapwood respiration. We therefore selected the final value for this parameter based on calibration of the simulated mean ring width against observations, constrained by the published range of values for sapwood respiration rate.

2.3 Model application

We applied the model to simulate the growth of 46 individual *Pinus koraiensis* trees from the study site between 1958 and 2006. The 46 trees were of different ages (ranging from < 50 to ca. 200 years at the time of sampling in 2006) and diameters (the diameter was at breast height from 10 to 70 cm at the time of sampling). Environmental conditions (e.g. soil depth and light availability) were relatively uniform across the sampling plot. The start date for the simulations was determined by the availability of local climate data. Site latitude, elevation, and observed monthly temperature, precipitation, and fractions of cloud cover were used as input for the P model. Each tree was initialised at its actual diameter at 1958, calculated from the measured diameter in 2007 and measured ra-

dial growth between 1958 and 2007. The model was initially run with a fixed CO₂ concentration of 360 ppm. To examine the impact of changing atmospheric CO₂ levels on tree growth, we made a second simulation using the observed monthly CO₂ concentration between 1958 and 2006 (310–390 ppm: data from the National Oceanic and Atmospheric Administration (NOAA) Earth System Research Laboratory (ESRL) (www.esrl.noaa.gov/gmd/ccgg/trends/)).

2.4 Statistical methods

For statistical analyses and comparison with observations, the individual trees were grouped into three cohorts, based on their age in 1958: young (0–49 years); mature (50–99 years); old (> 100 years). Individual trees within each cohort exhibit a range of diameters (young: ca. 20–37 cm; mature: 9–59 cm; old: 25–40 cm). These differences in size will affect the expression of ontogeny within each cohort. The mean and standard deviation (SD) of year-by-year diameter growth was calculated for each age cohort from the observations and the simulations. The Pearson correlation coefficient and root mean squared error (RMSE) were used to evaluate the degree of agreement between the observations and simulations. We used generalised linear modelling (GLM) (McCullagh, 1984) to analyse the response of tree growth to the major climate factors and age. The GLM approach is helpful for separating the independent influence of individual factors on tree growth, given the inevitable existence of correlations between these factors.

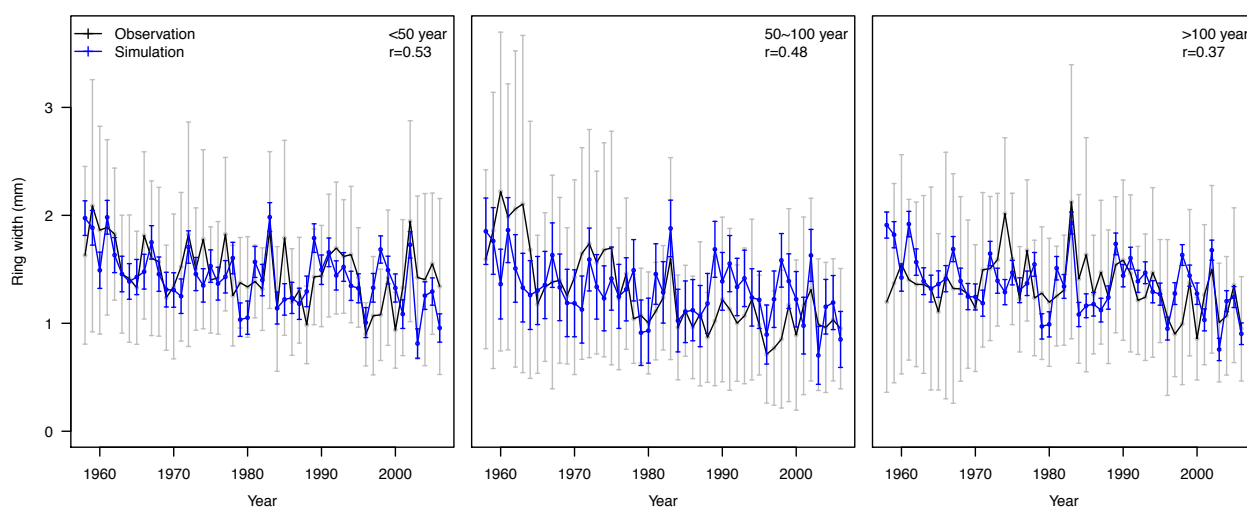


Figure 3. Comparison between simulations and observations for the three age cohorts (young: 0–49 years; mature: 50–99 years; old > 100 years). Each tree was initialised at its actual diameter at 1958, calculated from the measured diameter in 2007, and measured radial growth between 1958 and 2007. The black line is the mean of observations within each age cohort, and grey bars are the standard deviation (SD) of individuals within each age cohort. The blue lines and bars are the mean and standard deviation from the simulations.

3 Results

3.1 Simulated ring width versus observation

There are only small differences between different age cohorts in the mean simulated ring width, with a mean value of 1.43 mm for young trees, 1.31 mm for mature trees, and 1.37 for older trees. These values are comparable to the mean value obtained from the observations (1.48, 1.29, and 1.34 mm, respectively). However, the general impact of ageing is evident in the decreasing trend in ring widths between 1958 and 2007 within any one cohort (Fig. 3). The slope is stronger in the observations than in the simulations, indicating that the model somewhat underestimates the effects of ontogeny.

There is considerable year-to-year variability in tree growth. The simulated interannual variability (standard deviation) in simulated ring width is similar in all the age cohorts (0.265 mm in the young, 0.265 mm in the mature, and 0.264 mm in the old trees). This variability is somewhat less than shown by the observations, where interannual variability is 0.274, 0.367, and 0.245 mm, respectively in the young, mature, and old cohorts. The RMSE is 0.263, 0.332, and 0.284 mm, respectively for young, mature, and old age cohorts. The correlation between the observed and simulated sequence in each cohort is statistically significant ($P = 0.000$, 0.001 , and 0.009 , respectively for young, mature, and old age cohorts).

Despite the fact that the model reproduces both the mean ring width and the interannual variability in tree growth reasonably well, the range of ring widths simulated for individual trees within any one cohort is much less than the range

seen in the observations. This is to be expected, given that individual tree growth is affected by local factors (e.g. spatial variability in soil moisture) and may also be influenced by ecosystem dynamics (e.g. opening up of the canopy through the death of adjacent trees). These effects are not taken into account in the model.

3.2 Parameter sensitivity analysis

To evaluate the sensitivity of the model to specification of individual parameters, we ran a series of simulations in which individual parameter values were increased or decreased by 50 % of their reference value. For each of these simulations, the T model was run for 500 years using constant potential GPP (the mean GPP during the period 1958–2006).

The model simulates a rapid initial increase in ring width, with peak ring widths occurring after ca. 10 years, followed by a gradual and continuous decrease with age (Fig. 4). The model is comparatively insensitive to uncertainties in the specification of fine-root specific respiration rate (r_r), fine-root turnover time (τ_r), and specific leaf area (σ), while leaf area index within the crown (L), ratio of fine-root mass to foliage area (ζ), and fine-root turnover time (τ_r) only have a moderate effect on the simulated amplitude of ring width. The largest impacts on the amplitude of the simulated ring width are from the initial slope of the height–diameter relationship (a), initial ratio of crown area to stem cross-sectional area (c), and sapwood density (ρ_s). Maximum tree height (H_m) and sapwood-specific respiration rate (r_s) have the greatest influence on the shape of the simulated ageing curve. These two parameters also have a large impact on the amplitude of the growth of old trees. The parameter

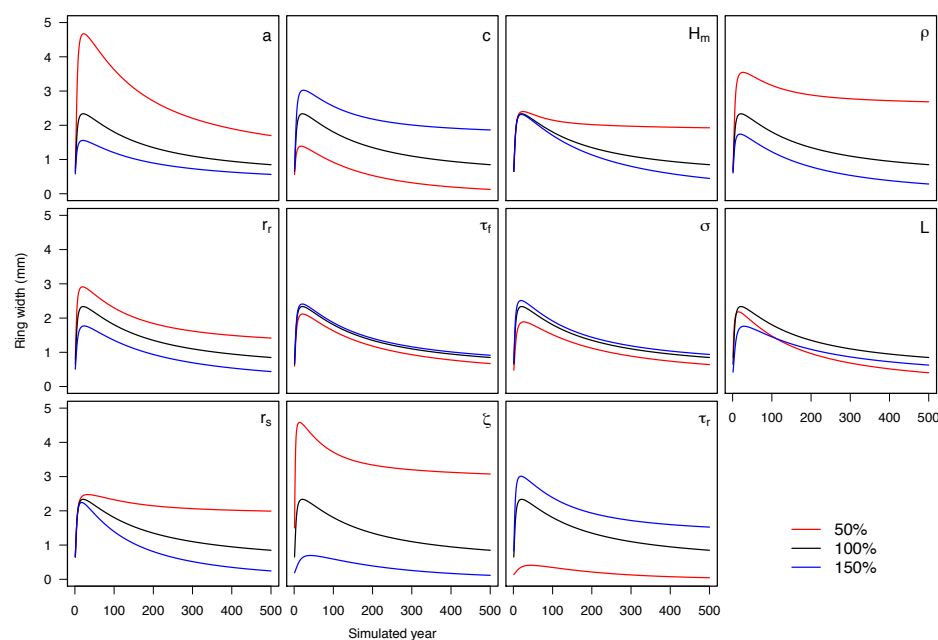


Figure 4. Parameter sensitivity analyses for the T model. A constant input of gross primary productivity (GPP) (mean during the period 1958–2006) was used to drive the T model to simulate tree growth for 500 years following establishment. The black line was obtained with the reference value of each parameter. The effects of an increase (150 % of reference value; blue line) and a decrease (50 % of reference value; red line) are also shown.

Table 2. GLM analysis of tree-growth response to the climatic factors and age, based on simulations and observations. The dependent variable is mean ring width series (1958–2006) for each age cohort (young, mature, and old). The independent variables are the growing-season total annual photosynthetically active radiation (PAR_0), mean annual temperature (MAT), and the ratio of actual to potential evapotranspiration (α), with age cohort treated as a factor.

		Intercept (mm)	PAR_0 (mm (kmol photon m^{-2}) $^{-1}$)	MAT (mm $^{\circ}C^{-1}$)	α (mm)
Observation	Estimation	−3.123	0.625	−0.180	0.702
	Error	± 0.784	± 0.093	± 0.042	± 0.301
	p value	0.004	0.000	0.000	0.021
Simulation	Estimation	−7.139	1.056	−0.078	1.142
	Error	± 0.169	± 0.020	± 0.009	± 0.065
	p value	0.000	0.000	0.000	0.000

values for a , c , H_m , and ρ_s are derived from observations, with uncertainties much less than 50 % (Fig. 2). Thus, the sensitivity of the model to these parameters is not important. However, model sensitivity to sapwood respiration (r_s), both in terms of the shape of the ageing curve and the amplitude, is of greater concern, given the large range of values in the literature. Although some part of the uncertainty in the specification of sapwood respiration may be due to differences between species, the difficulty of measuring this trait accurately also contributes to the problem. For the final model, we tuned r_s against the ring-width observations. The best match with the observations was obtained with a

value of $1.4 \text{ nmol mol}^{-1} \text{ s}^{-1}$, which is within the range of published values for pines (see summary in Landsberg and Sands, 2010). r_s is the only parameter that was tuned.

3.3 Controls on tree growth

The GLM analysis revealed a strong positive relationship between PAR_0 and tree growth, while moisture stress (as measured by α , an estimate of the ratio of actual to potential evapotranspiration) was shown to have a less steep but still positive effect (Fig. 5 and Table 2). The observed partial relationship between mean annual temperature and tree growth is negative. The Changbai Mountains are at the southern end of

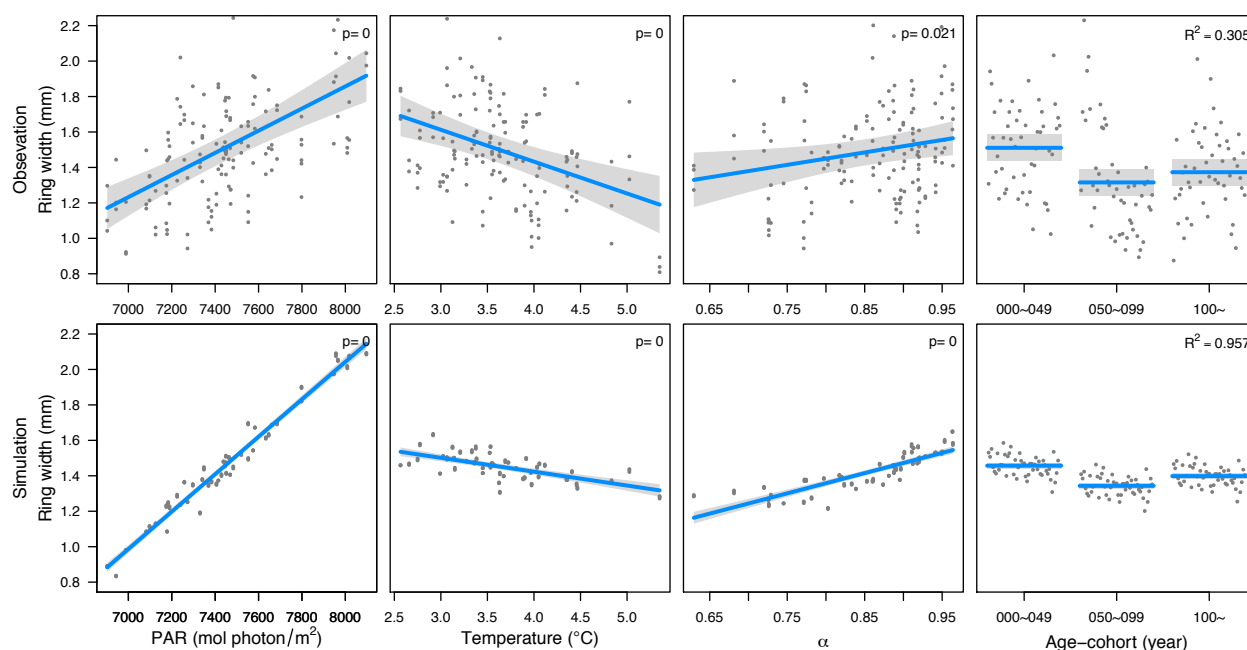


Figure 5. Tree-growth response to climate and tree age: partial residual plots based on the GLM analysis (Table 2), obtained using the visreg package in R, are shown.

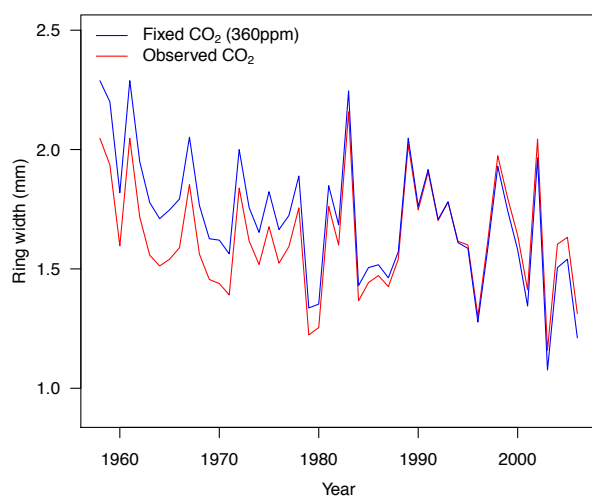


Figure 6. CO₂ effect on tree growth. Two runs, one with a fixed 360 ppm [CO₂] (blue line), the other with observed monthly [CO₂] (red line), are compared to show the simulated effect of [CO₂] on tree growth during the period 1958–2006.

the distribution of *Pinus koraiensis* in China, which makes it plausible that tree growth would be inhibited during warmer years.

The model reproduces these observed relationships between climate factors and tree growth. The slope of the observed positive relationship with α is statistically indistinguishable from the modelled slope, but the observed positive

relationship with PAR₀ is weaker, and the negative correlation with mean annual temperature is stronger in the observations than in the simulations. These differences between observations and simulations could reflect the influence of an additional climate control, related to both PAR₀ and temperature (e.g. cloud cover). The difference between observed and simulated effects of temperature may also be because, although simulated growth is inhibited by low temperatures (through the computation of PAR₀), the current model does not include any mechanism for inhibition due to heat stress at high air and leaf temperatures.

The GLM analysis also showed that age, as represented by the three age cohorts, has an impact on ring width: young trees have greater ring widths than mature trees, while old trees have somewhat greater ring widths than mature trees. This pattern is seen in both the observations and simulations, although the differences between the young and mature cohorts are slightly greater in the observations.

The overall similarity in the observed and simulated relationships between growth rates and environmental factors confirms that the *T* model performs realistically. The observed relationships are considerably noisier than the simulated relationships (Fig. 5, Table 2), reflecting the fact that growth rates are affected by small-scale variability in environmental conditions, as well as time-varying competition for light.

3.4 Simulated CO₂ effect on tree growth

Elevated levels of CO₂ are expected to have a positive impact on tree growth (Hyvönen et al., 2007; Donohue et al., 2013; Hickler et al., 2008; Boucher et al., 2014). This positive response to [CO₂] is seen in the comparison of the fixed [CO₂] and real [CO₂] simulations (Fig. 6). In the first part of the simulation, prior to 1980, the actual [CO₂] is lower than the level of 360 ppm used in the fixed [CO₂] experiment. This results in lower growth rates. The 50 ppm difference between the two experiments at the beginning of the simulation results in a difference in ring width of 0.242 mm. After 1980, when the actual [CO₂] was higher than 360 ppm, the tree growth in the simulation with realistic [CO₂] is enhanced. The 30 ppm difference at the end of the simulation results in a difference in ring width of 0.101 mm. Overall, the change in [CO₂] between 1958 and 2006 results in a positive enhancement of tree growth of ca. 0.343 mm yr⁻¹. However, this difference is very small compared to the impact of ageing (> 1 mm from observations) or to the differences resulting from the interannual variability of climate (1.212 mm) on tree growth.

4 Discussion

We have shown that radial growth (ring width) can be realistically simulated by coupling a simple generic model of GPP with a model of carbon allocation and functional geometric tree growth with species-specific values. The model is responsive to changes in climate variables, and can account for the impact of changing CO₂ and ontogeny on tree growth. Although several models draw on basic physiological and/or geometric constraints in order to simulate tree-ring indices (Fritts, 2012; Vaganov et al., 2006; Rathgeber et al., 2005; Misson, 2004), and indeed the two approaches have been combined to simulate between-site differences in ecosystem productivity and tree growth (Härkönen et al., 2010, 2013), this is the first time, to our knowledge, that the two approaches have been combined to yield an explicit treatment of individual tree-growth processes, tested against an extensive ring-width data set.

Our simulations suggest that, after a brief but rapid increase for young plants, there is a general and continuous decrease in radial growth with age (Fig. 4). This pattern is apparent in individual tree-ring series, and is evident in the decreasing trend in ring widths shown when the series are grouped into age cohorts (Fig. 3). It is a necessary consequence of the geometric relationship between the stem diameter increment and cross-sectional area; more biomass is required to produce the same increase in diameter in thicker, taller trees than thinner, shorter ones. However, we find that ring widths in old trees in our study region are consistently wider than those in mature trees, and this property is reproduced in the simulations (Fig. 5). This situation arises because the old trees are, on average, smaller than the mature

trees at the start of the simulation (in 1958). Thus, while the difference between average ring widths in the mature and old cohorts conforms to the geometric relationship between stem diameter increment and cross-sectional area, it is a response that also reflects differences in the history of tree growth at this site, which determined the initial size of the trees in 1958. Lack of climate data prior to 1958 or detailed information about stand dynamics precludes diagnosis of the cause of the growth history differences between mature and old trees.

Studies attempting to isolate the impact of climate variability on tree growth, including attempts to reconstruct historical climate changes using tree-ring series, often describe the impact of ageing as a negative exponential curve (Fritts, 2012). However, our analyses suggest that this is not a good representation of the actual effect of ageing on tree growth, and would result in the masking of the impact of climate-induced variability in mature and old trees. The simulated NPP of individual trees always increases with size (or age). This is consistent with the observation that carbon sequestration increases continuously with individual tree size (Stephenson et al., 2014).

We have shown that total PAR during the growing season is positively correlated with tree growth at this site. This is not surprising given that PAR is the primary driver of photosynthetic carbon fixation. However, none of the empirical or semi-empirical models of tree growth uses PAR directly as a predictor variable; most use some measure of seasonal or annual temperature as a surrogate. PAR is determined by latitude and cloudiness. Although temperature varies with latitude and cloudiness, it is also influenced by other factors, including heat advection. Temperature changes can impact the length of the growing season, and hence have an impact on total growing-season PAR, but this is a trivial effect over recent decades. In fact, we show that mean annual temperature is negatively correlated with tree growth at this site. Given this decoupling, and the potential that longer-term changes in cloudiness will not necessarily be correlated with changes in temperature (Charman et al., 2013), we strongly advocate the use of growing-season PAR for empirical modelling, as well as in process-based modelling.

We found no age-related sensitivity to interannual variability in climate; the interannual variability in ring width is virtually identical between age cohorts. The strength of the relationship with individual climate variables is also similar between the three age cohorts. It is generally assumed that juvenile and old trees are at greater risk of mortality from environmental stress than mature trees are (e.g. Lines et al., 2010; McDowell et al., 2008). This may be true in the case of extreme events, such as wildfires, windthrow, or pest attacks. Our results suggest that, although climate variability has an important effect on tree growth, it is not an important influence on mortality.

We have assumed that the period contributing to growth (i.e. the effective growing season) in any year includes carbon stores generated during the second half of the previous

year. The total foliage area determines the radial area of the stem, and, once this is achieved, NPP is allocated either to fine-root production or stored as carbohydrate for use in stem growth in the early part of the subsequent year. This is consistent with observations that radial growth begins before leaf-out (Michelot et al., 2012) and that maximum leaf area is generally achieved by mid-summer (Rautiainen et al., 2012). The MAIDEN model also allows tree growth to be influenced by a fixed contribution from the previous year's growth (Misson, 2004). Defining the effective growing season as being only the current growth year had no impact on the influence of climate on ring widths, or the shape of the ageing curve. It did, however, produce a considerably lower correlation between simulated and observed interannual variability in growth. Since tree-ring width reflects the integrated climate over the "effective growing season", reconstructions of climate variables reflect conditions during that season, not only during the current calendar year.

The high degree of autocorrelation present in tree-ring series is often seen as a problem requiring pretreatment of the series in order to derive realistic reconstructions of climate variables (e.g. Cook et al., 2012; Anchukaitis et al., 2013; Wiles et al., 2014). However, spatial or temporal autocorrelation is a reflection of the causal mechanism underpinning the observed patterning. Here, we postulate that the mechanism that gives rise to the temporal autocorrelation in tree-ring series is the existence of carbon reserves that are created in one year and fuel early growth in the next. If a large reserve of carbon is created in the second half of the growing season, because of favourable conditions, this will offset poor conditions in the following year. However, large reserves may not be necessary if conditions during the subsequent growing year are very favourable. The fact that the relative influence of one year on the next can vary explains why the measured autocorrelation strength in a given tree-ring series varies through time.

The T model is sensitive to the values adopted for some parameters, specifically the initial slope of the height–diameter relationship (a), the initial ratio of crown area to stem cross-sectional area (c), maximum tree height (H_m), sapwood density (ρ_s), sapwood-specific respiration rate (r_s), leaf area index within the crown (L), ratio of fine-root mass to foliage area (ζ), and fine-root turnover time (τ_r). Several of these parameters are easily derived from observations (e.g. a , c , H_m , ρ_s , and L) and, provided that sufficient site-based observations are available, they should not pose a problem for applications of the model. However, the model is also sensitive to less easily measured parameters, including sapwood respiration, root respiration, and the ratio of fine roots to leaves. Estimates of values for root respiration and root mass to foliage area in the literature do not show substantial differences, and we therefore used an average value to parameterise our model. This approach could be used for other applications. We parameterised fine-root turnover rates based on observations on *Pinus koraiensis* from Changbai. While

this obviated the need for tuning in the current application, lack of data on fine-root turnover rates in other regions (or for other species) could pose problems for future applications of the model. The model is also highly sensitive to the parameter value used for sapwood respiration, and the range of reported values is large (Table 1). Because of this, we derived a value for sapwood respiration by tuning the model to obtain a good representation of average ring width. This is the only parameter that requires tuning in the current version of the T model. Although sapwood respiration is difficult to measure, it would certainly be better if more measurements of sapwood respiration were available, as this would remove the need for model tuning.

Our modelling approach integrates the influence of climate, $[\text{CO}_2]$, and ontogeny on individual tree growth. Such a model is useful to explore the response of tree growth to potential future changes in climate, and the impact of changes in tree growth on carbon sequestration. We also envisage that it could also be used to investigate the impact of past climate changes on tree growth. Reconstructions of temperature changes beyond the recent observational period, used as a baseline for the detection of anthropogenic influences on the climate system, are largely derived from statistical reconstructions based on tree-ring series (Jones et al., 1998; Esper et al., 2002; Hegerl et al., 2006; Mann et al., 2008; Ahmed et al., 2013). However, as we show here, temperature is neither the only nor the most important influence on tree growth. This may help to explain why correlations between ring widths and climate at individual sites appear to have broken down in recent decades (the so-called "divergence problem"; D'Arrigo et al., 2008). The availability of a robust model to investigate tree growth could help to provide better reconstructions of past climate changes (see Boucher et al., 2014, for example), as well as more plausible projections of the response of tree growth to continuing climate change in the future.

Acknowledgements. We thank Wang Han for assistance with the P model. G. Li is supported by an International Postgraduate Research Scholarship at Macquarie University. The work is a contribution to the AXA Chair programme on Biosphere and Climate Impacts and the Imperial College initiative Grand Challenges in Ecosystems and the Environment.

Edited by: U. Seibt

References

- Ahmed, M., Anchukaitis, K. J., Asrat, A., Borgaonkar, H. P., Braid, M., Buckley, B. M., Büntgen, U., Chase, B. M., Christie, D. A., and Cook, E. R.: Continental-scale temperature variability during the past two millennia, *Nat. Geosci.*, 6, 339–346, 2013.
- Anchukaitis, K. J., D'Arrigo, R. D., Andreu-Hayles, L., Frank, D., Verstege, A., Curtis, A., Buckley, B. M., Jacoby, G. C.,

- and Cook, E. R. Tree-Ring-Reconstructed Summer Temperatures from Northwestern North America during the Last Nine Centuries. *J. Clim.*, 26, 3001–3012, 2013.
- Bai, F., Sang, W., Li, G., Liu, R., Chen, L., and Wang, K.: Long-term protection effects of national reserve to forest vegetation in 4 decades: biodiversity change analysis of major forest types in Changbai Mountain Nature Reserve, China, *Sci. China Ser. C*, 51, 948–958, 2008.
- Bauerle, W. L., Oren, R., Way, D. A., Qian, S. S., Stoy, P. C., Thornton, P. E., Bowden, J. D., Hoffman, F. M., and Reynolds, R. F.: Photoperiodic regulation of the seasonal pattern of photosynthetic capacity and the implications for carbon cycling, *P. Natl. Acad. Sci.*, 109, 8612–8617, 2012.
- Bernacchi, C., Pimentel, C., and Long, S.: In vivo temperature response functions of parameters required to model RuBP-limited photosynthesis, *Plant Cell Environ.*, 26, 1419–1430, 2003.
- Bonan, G. B.: Forests and climate change: forcings, feedbacks, and the climate benefits of forests, *Science*, 320, 1444–1449, 2008.
- Boucher, É., Guiot, J., Hatté, C., Daux, V., Danis, P.-A., and Dusouillez, P.: An inverse modeling approach for tree-ring-based climate reconstructions under changing atmospheric CO₂ concentrations, *Biogeosciences*, 11, 3245–3258, doi:10.5194/bg-11-3245-2014, 2014.
- Caspersen, J. P., Vanderwel, M. C., Cole, W. G., and Purves, D. W.: How stand productivity results from size- and competition-dependent growth and mortality, *PLoS One*, 6, e28660, 2011.
- Charman, D. J., Beilman, D. W., Blaauw, M., Booth, R. K., Brewer, S., Chambers, F. M., Christen, J. A., Gallego-Sala, A., Harrison, S. P., Hughes, P. D. M., Jackson, S. T., Korhola, A., Mauquoy, D., Mitchell, F. J. G., Prentice, I. C., van der Linden, M., de Vleeschouwer, F., Yu, Z. C., Alm, J., Bauer, I. E., Corish, Y. M. C., Garneau, M., Hohl, V., Huang, Y., Karofeld, E., Le Roux, G., Moschen, R., Nichols, J. E., Nieminen, T., McDonald, G. M., Phadtare, N. R., Rausch, N., Shotyk, W., Sillasoo, U., Swindles, G. T., Tuittila, E. S., Ukonmaanaho, L., Väliranta, M., van Bellen, S., van Geel, B., Vitt, D. H., and Zhao, Y.: Climate-driven changes in peatland carbon accumulation during the last millennium, *Biogeosciences*, 10, 929–944, doi:10.5194/bg-10-929-2013, 2013.
- Chen, G., Dai, L., and Zhou, L.: Structure of stand and canopy characteristics of disturbed communities of broadleaved *Pinus koraiensis* forest in Changbai Mountain [J], *Chin. J. Ecol.*, 23, 116–120, 2004.
- Ciais, P., Sabine, C., Bala, G., Bopp, L., Brovkin, V., Canadell, J., Chhabra, A., DeFries, R., Galloway, J., Heimann, M., Jones, C., Quéré, C. L., Myneni, R. B., Piao, S., and Thornton, P.: Carbon and Other Biogeochemical Cycles, in: *Climate Change 2013: The Physical Science Basis. Contribution of Working Group I to the Fifth Assessment Report of the Intergovernmental Panel on Climate Change*, edited by: Stocker, T. F., Qin, D., Plattner, G.-K., Tignor, M., Allen, S. K., Boschung, J., Nauels, A., Xia, Y., Bex, V., and Midgley, P. M., Cambridge University Press, Cambridge, UK and New York, NY, USA, 2013.
- Claesson, J. and Nycander, J.: Combined effect of global warming and increased CO₂-concentration on vegetation growth in water-limited conditions, *Ecol. Model.*, 256, 23–30, 2013.
- Cook, E. R., Krusic, P. J., Anchukaitis, K. J., Buckley, B. M., Nakatsuka, T., and Sano, M.: Tree-ring reconstructed summer temperature anomalies for temperate East Asia since 800 CE, *Clim. Dyn.*, 41, 2957–2972, 2012.
- Cruiziat, P., Cochard, H., and Améglio, T.: Hydraulic architecture of trees: main concepts and results, *Ann. For. Sci.*, 59, 723–752, 2002.
- Danis, P.-A., Hatté, C., Misson, L., and Guiot, J.: MAIDENiso: a multiproxy biophysical model of tree-ring width and oxygen and carbon isotopes, *Can. J. Forest Res.*, 42, 1697–1713, 2012.
- D'Arrigo, R., Wilson, R., Liepert, B., and Cherubini, P.: On the 'divergence problem' in northern forests: a review of the tree-ring evidence and possible causes, *Global Planet. Change*, 60, 289–305, 2008.
- Donohue, R. J., Roderick, M. L., McVicar, T. R., and Farquhar, G. D.: Impact of CO₂ fertilization on maximum foliage cover across the globe's warm, arid environments, *Geophys. Res. Lett.*, 40, 3031–3035, 2013.
- Duursma, R. A., Mäkelä, A., Reid, D. E., Jokela, E. J., Porté, A. J., and Roberts, S. D.: Self-shading affects allometric scaling in trees, *Funct. Ecol.*, 24, 723–730, 2010.
- Esper, J., Cook, E. R., and Schweingruber, F. H.: Low-frequency signals in long tree-ring chronologies for reconstructing past temperature variability, *Science*, 295, 2250–2253, 2002.
- Falster, D. S. and Westoby, M.: Tradeoffs between height growth rate, stem persistence and maximum height among plant species in a post-fire succession, *Oikos*, 111, 57–66, 2005.
- Falster, D. S., Brännström, Å., Dieckmann, U., and Westoby, M.: Influence of four major plant traits on average height, leaf-area cover, net primary productivity, and biomass density in single-species forests: a theoretical investigation, *J. Ecol.*, 99, 148–164, 2011.
- Friedlingstein, P. and Prentice, I.: Carbon–climate feedbacks: a review of model and observation based estimates, *Curr. Opin. Environ. Sustain.*, 2, 251–257, 2010.
- Fritts, H. C.: *Tree rings and climate*, Academic Press, London, 2012.
- Gallego-Sala, A. V., Clark, J. M., House, J. I., Orr, H. G., Prentice, I. P., Smith, P., Farewell, T., and Chapman, S. J.: Bioclimatic envelope model of climate change impacts on blanket peatland distribution in Great Britain, *Clim. Res.*, 45, 151–162, 2010.
- Givnish, T. J.: Adaptation to sun and shade: a whole-plant perspective, *Funct. Plant Biol.*, 15, 63–92, 1988.
- Häkönen, S., Pulkkinen, M., Duursma, R., and Mäkelä, A.: Estimating annual GPP, NPP and stem growth in Finland using summary models, *Forest. Ecol. Manag.*, 259, 524–533, 2010.
- Häkönen, S., Tokola, T., Packalén, P., Korhonen, L., and Mäkelä, A.: Predicting forest growth based on airborne light detection and ranging data, climate data, and a simplified process-based model, *Can. J. For. Res.*, 43, 364–375, 2013.
- Harrison, S. P., Prentice, I. C., Barboni, D., Kohfeld, K. E., Ni, J., and Sutra, J. P.: Ecophysiological and bioclimatic foundations for a global plant functional classification, *J. Veg. Sci.*, 21, 300–317, 2010.
- Hegerl, G. C., Crowley, T. J., Hyde, W. T., and Frame, D. J.: Climate sensitivity constrained by temperature reconstructions over the past seven centuries, *Nature*, 440, 1029–1032, 2006.
- Hickler, T., Smith, B., Prentice, I. C., Mjöfors, K., Miller, P., Arneth, A., and Sykes, M. T.: CO₂ fertilization in temperate FACE experiments not representative of boreal and tropical forests, *Global Change Biol.*, 14, 1531–1542, 2008.

- Huang, J., Bergeron, Y., Denneler, B., Berninger, F., and Tardif, J.: Response of forest trees to increased atmospheric CO₂, *Crit. Rev. Plant Sci.*, 26, 265–283, 2007.
- Huo, H. and Wang, C.: Effects of canopy position and leaf age on photosynthesis and transpiration of *Pinus koraiensis*, *Chin. J. Appl. Ecol.*, 18, 1181–1186, 2007.
- Hyvönen, R., Ågren, G. I., Linder, S., Persson, T., Cotrufo, M. F., Ekblad, A., Freeman, M., Grelle, A., Janssens, I. A., and Jarvis, P. G.: The likely impact of elevated [CO₂], nitrogen deposition, increased temperature and management on carbon sequestration in temperate and boreal forest ecosystems: a literature review, *New Phytol.*, 173, 463–480, 2007.
- Ishii, H., Reynolds, J. H., Ford, E. D., and Shaw, D. C.: Height growth and vertical development of an old-growth *Pseudotsuga-Tsuga* forest in southwestern Washington State, USA, *Can. J. Forest Res.*, 30, 17–24, 2000.
- Jarvis, P. G. and Leverenz, J. W.: Productivity of temperate, deciduous and evergreen forests, in: *Physiological plant ecology IV*, Springer, Berlin Heidelberg, 233–280, 1983.
- Jones, P. D., Briffa, K. R., Barnett, T. P., and Tett, S. F. B.: High-resolution palaeoclimatic records for the last millennium: interpretation, integration and comparison with General Circulation Model control-run temperatures, *Holocene*, 8, 455–471, 1998.
- Jonson, T.: Taxatoriska undersökningar om skogsträdens form: (1) granens stamform, *Skogsvardfor, Tidskrift*, 8, 285–328, 1910.
- King, D. A.: Size-related changes in tree proportions and their potential influence on the course of height growth, in: *Size- and age-related changes in tree structure and function*, Springer, Netherlands, 165–191, 2011.
- Körner, C.: Plant CO₂ responses: an issue of definition, time and resource supply, *New Phytol.*, 172, 393–411, 2006.
- Koutavas, A.: CO₂ fertilization and enhanced drought resistance in Greek firs from Cephalonia Island, Greece, *Global Change Biol.*, 19, 529–539, 2013.
- Landsberg, J. J. and Sands, P.: *Physiological ecology of forest production: principles, processes and models*, Academic Press, 2010.
- Larson, P. R.: Stem form development of forest trees, *For. Sci., Monograph*, 5, 1–42, 1963.
- Lines, E. R., Coomes, D. A., and Purves, D. W.: Influences of forest structure, climate and species composition on tree mortality across the eastern US, *PLoS One*, 5, e13212, doi:10.1371/journal.pone.0013212, 2010.
- Lloyd, J.: The CO₂ dependence of photosynthesis, plant growth responses to elevated CO₂ concentrations and their interaction with soil nutrient status, II. Temperate and boreal forest productivity and the combined effects of increasing CO₂ concentrations and increased nitrogen deposition at a global scale, *Funct. Ecol.*, 13, 439–459, 1999.
- Luo, T.: Patterns of net primary productivity for Chinese major forest types and their mathematical models, Doctor of Philosophy, Chinese Academy of Sciences, Beijing, 1996.
- Luo, Y., Su, B., Currie, W. S., Dukes, J. S., Finzi, A., Hartwig, U., Hungate, B., McMurtrie, R. E., Oren, R., and Parton, W. J.: Progressive nitrogen limitation of ecosystem responses to rising atmospheric carbon dioxide, *Bioscience*, 54, 731–739, 2004.
- Mäkelä, A., Landsberg, J., Ek, A. R., Burk, T. E., Ter-Mikaelian, M., Ågren, G. I., Oliver, C. D., and Puttonen, P.: Process-based models for forest ecosystem management: current state of the art and challenges for practical implementation, *Tree Physiol.*, 20, 289–298, 2000.
- Mann, M. E., Zhang, Z., Hughes, M. K., Bradley, R. S., Miller, S. K., Rutherford, S., and Ni, F.: Proxy-based reconstructions of hemispheric and global surface temperature variations over the past two millennia, *P. Natl. Acad. Sci. USA*, 105, 13252–13257, 2008.
- McCullagh, P.: Generalized linear models, *Eur. J. Oper. Res.*, 16, 285–292, 1984.
- McDowell, N., Pockman, W. T., Allen, C. D., Breshears, D. D., Cobb, N., Kolb, T., Plaut, J., Sperry, J., West, A., and Williams, D. G.: Mechanisms of plant survival and mortality during drought: why do some plants survive while others succumb to drought?, *New Phytol.*, 178, 719–739, 2008.
- Medvigy, D. and Moorcroft, P. R.: Predicting ecosystem dynamics at regional scales: an evaluation of a terrestrial biosphere model for the forests of northeastern North America, *Philos. T. Roy. Soc. B.*, 367, 222–235, 2012.
- Michelot, A., Simard, S., Rathgeber, C., Dufrêne, E., and Damesin, C.: Comparing the intra-annual wood formation of three European species (*Fagus sylvatica*, *Quercus petraea* and *Pinus sylvestris*) as related to leaf phenology and non-structural carbohydrate dynamics, *Tree physiol.*, 32, 1033–1045, 2012.
- Miller, H. G.: Carbon × nutrient interactions – the limitations to productivity, *Tree physiol.*, 2, 373–385, 1986.
- Misson, L.: MAIDEN: a model for analyzing ecosystem processes in dendroecology, *Can. J. Forest Res.*, 34, 874–887, 2004.
- Misson, L., Rathgeber, C., and Guiot, J.: Dendroecological analysis of climatic effects on *Quercus petraea* and *Pinus halepensis* radial growth using the process-based MAIDEN model, *Can. J. For. Res.*, 34, 888–898, 2004.
- Moorcroft, P., Hurtt, G., and Pacala, S. W.: A method for scaling vegetation dynamics: the ecosystem demography model (ED), *Ecol. Monogr.*, 71, 557–586, 2001.
- Moritz, M. A., Hurteau, M. D., Suding, K. N., and D’Antonio, C. M.: Bounded ranges of variation as a framework for future conservation and fire management, *Ann. N. Y. Acad. Sci.*, 1286, 92–107, 2013.
- Pan, Y., Birdsey, R. A., Fang, J., Houghton, R., Kauppi, P. E., Kurz, W. A., Phillips, O. L., Shvidenko, A., Lewis, S. L., and Canadell, J. G.: A large and persistent carbon sink in the world’s forests, *Science*, 333, 988–993, 2011.
- Pierce, L. L. and Running, S. W.: Rapid estimation of coniferous forest leaf area index using a portable integrating radiometer, *Ecology*, 1762–1767, 1988.
- Prentice, I. C., Dong, N., Gleason, S. M., Maire, V., and Wright, I. J.: Balancing the costs of carbon gain and water transport: testing a new theoretical framework for plant functional ecology, *Ecol. Lett.*, 17, 82–91, 2014.
- Rathgeber, C. B., Misson, L., Nicault, A., and Guiot, J.: Bioclimatic model of tree radial growth: application to the French Mediterranean Aleppo pine forests, *Trees*, 19, 162–176, 2005.
- Rautiainen, M., Heiskanen, J., and Korhonen, L.: Seasonal changes in canopy leaf area index and MODIS vegetation products for a boreal forest site in central Finland, *Boreal Environ. Res.*, 17, 72–84, 2012.
- Reich, P. B., Hobbie, S. E., Lee, T., Ellsworth, D. S., West, J. B., Tilman, D., Knops, J. M., Naeem, S., and Trost, J.: Nitrogen lim-

- itation constrains sustainability of ecosystem response to CO₂, *Nature*, 440, 922–925, 2006.
- Shan, J., Tao, D., Wang, M., and Zhao, S.: Fine roots turnover in a broad-leaved Korean pine forest of Changbai mountain, *Chin. J. Appl. Ecol.*, 4, 241–245, 1993.
- Shevliakova, E., Stouffer, R. J., Malyshev, S., Krasting, J. P., Hurtt, G. C., and Pacala, S. W.: Historical warming reduced due to enhanced land carbon uptake, *P. Natl. Acad. Sci. USA*, 110, 16730–16735, 2013.
- Shinozaki, K., Yoda, K., Hozumi, K., and Kira, T.: A quantitative analysis of plant form-the pipe model theory: I. Basic analyses, *Jap. J. Ecol.*, 14, 97–105, 1964.
- Smith, B., Prentice, I. C., and Sykes, M. T.: Representation of vegetation dynamics in the modelling of terrestrial ecosystems: comparing two contrasting approaches within European climate space, *Global Ecol. Biogeogr.*, 10, 621–637, 2001.
- Stephenson, N. L., Das, A. J., Condit, R., Russo, S. E., Baker, P. J., Beckman, N. G., Coomes, D. A., Lines, E. R., Morris, W. K., and Rüger, N.: Rate of tree carbon accumulation increases continuously with tree size, *Nature*, 507, 90–93, doi:10.1038/nature12914, 2014.
- Thomas, S. C.: Asymptotic height as a predictor of growth and allometric characteristics in Malaysian rain forest trees, *Am. J. Bot.*, 83, 556–556, 1996.
- Vaganov, E. A., Hughes, M. K., and Shashkin, A. V.: Introduction and factors influencing the seasonal growth of trees, Springer, Berlin Heidelberg, 2006.
- Wang, H., Prentice, I. C., and Davis, T. W.: Biophysical constraints on gross primary production by the terrestrial biosphere, *Biogeosciences Discuss.*, 11, 3209–3240, 2014, <http://www.biogeosciences-discuss.net/11/3209/2014/>.
- White, M. A., Thornton, P. E., Running, S. W., and Nemani, R. R.: Parameterization and sensitivity analysis of the BIOME-BGC terrestrial ecosystem model: net primary production controls, *Earth Interact.*, 4, 1–85, 2000.
- Wiles, G. C., D'Arrigo, R., Barclay, D., Wilson, R. S., Jarvis, S. K., Vargo, L., and Frank, D.: Surface air temperature variability reconstructed with tree rings for the Gulf of Alaska over the past 1200 years. *The Holocene*, 24, 198–208, 2014.
- Wright, I. J., Reich, P. B., and Westoby, M.: Least-cost input mixtures of water and nitrogen for photosynthesis, *Am. Nat.*, 161, 98–111, 2003.
- Wullschlegel, S. D., Tschaplinski, T. J., and Norby, R. J.: Plant water relations at elevated CO₂-implications for water-limited environments, *Plant Cell Environ.*, 25, 319–331, 2002.
- Yan, X. and Zhao, J.: Establishing and validating individual-based carbon budget model FORCCHN of forest ecosystems in China, *Acta Ecol. Sin.*, 27, 2684–2694, 2007.
- Yokozawa, M. and Hara, T.: Foliage profile, size structure and stem diameter-plant height relationship in crowded plant populations, *Ann. Bot.-London*, 76, 271–285, 1995.
- Zhang, Y., Xu, M., Chen, H., and Adams, J.: Global pattern of NPP to GPP ratio derived from MODIS data: effects of ecosystem type, geographical location and climate, *Global Ecol. Biogeogr.*, 18, 280–290, 2009.
- Zogg, G. P., Zak, D. R., Burton, A. J. and Pregitzer, K. S.: Fine root respiration in northern hardwood forests in relation to temperature and nitrogen availability, *Tree Physiol.*, 16, 719–725, 1996.

Chapter 6

A model analysis of climate and CO₂ controls on tree growth in a semi-arid woodland

Contribution by Co-Authors: G. L. was responsible for collecting the tree-ring data, running the model experiments, data analysis, figure and table generation; G. L. S. P. H., and I. C. P. were jointly responsible for interpretation of the data, and drafting the text.

A model analysis of climate and CO₂ controls on tree growth and carbon allocation in a semi-arid woodland

G. Li¹, S. P. Harrison^{1,2} and I. C. Prentice^{1,3}

1 Department of Biological Sciences, Macquarie University, North Ryde, NSW 2109, Australia

2 School of Archaeology, Geography and Environmental Sciences (SAGES), Reading University, Reading, UK

3 AXA Chair of Biosphere and Climate Impacts, Grand Challenges in Ecosystem and the Environment, Department of Life Sciences and Grantham Institute – Climate Change and the Environment, Imperial College London, Silwood Park Campus, Buckhurst Road, Ascot SL5 7PY, UK

Correspondence to: G. Li (guangqi.li@students.mq.edu.au)

Abstract

The absence of a signal of increasing [CO₂] has been noted in many tree-ring records, despite the enhancement of photosynthetic rates and water-use efficiency resulting from increasing [CO₂]. Detection of a [CO₂] effect should be easiest in semi-arid climates. To examine this issue, we used a light-use efficiency model of photosynthesis coupled with a dynamic carbon allocation and tree-growth model to simulate annual growth of the gymnosperm *Callitris columellaris* in the semi-arid Great Western Woodlands, Western Australia, over the past 100 years. Parameter values were derived from independent observations except for sapwood specific respiration rate, fine-root turnover time, fine-root specific respiration rate and the ratio of fine-root mass to foliage area, which were estimated by Bayesian optimization. The model reproduced the general pattern of interannual variability in radial growth (tree-ring width), including the response to the shift in precipitation regimes that occurred in the 1960s. Both simulated and observed responses to climate show a significant positive response of tree-ring width to total photosynthetically active

radiation received and to the ratio of modeled actual to equilibrium evapotranspiration, and a significant negative response to vapour pressure deficit. However, the simulations showed an enhancement of radial growth in response to increasing atmospheric CO₂ concentration (ppm) ([CO₂]) during recent decades that is not present in the observations. The discrepancy disappeared when the model was recalibrated on successive 30-year windows. Then the ratio of fine-root mass to foliage area increases by 14% (from 0.127 to 0.144 kg C m⁻²) as [CO₂] increased while the other three estimated parameters remained constant. Our simulations suggest that the absence of increased radial growth could be explained as a consequence of a shift towards below-ground carbon allocation.

Introduction

The Great Western Woodlands (GWW) in southwestern Western Australia, with an area of about 160,000 km², is the largest remaining area of intact Mediterranean woodland on Earth (Watson, 2008; Lee et al., 2013). The GWW region is unique because of the diversity of large trees that grow there, despite the dry climate and nutrient-poor sandy soils (Watson, 2008; Prober et al., 2012).

The southwest region of Western Australia has experienced a multidecadal drought since the mid-1970s (Ansell et al., 2000; Cai and Cowan, 2006; Hope et al., 2006; Cullen and Grierson, 2009; Van Ommen and Morgan, 2010), characterized by a substantial reduction in winter rainfall. This change is consistent with a poleward shift in the mid-latitude storm track (Smith et al., 2000; Frederiksen and Frederiksen, 2007) and a reduction in the frequency of synoptic events and the associated amount of winter precipitation, coupled with an increase in the intensity of individual rainfall events (Hope et al., 2006). These changes are projected to continue under global warming (Yin, 2005; Hope, 2006). They have been variously linked to changes in the Indian Ocean dipole (Smith et al., 2000; England et al., 2006), in Antarctic climate (van Ommen and Morgan, 2010) and ultimately to changes in the Southern Annular Mode (Cai and Cowan, 2006; Hendon et al., 2007; Meneghini et al., 2007; Feng et al., 2010).

Although the drought is more marked in the coastal regions of Western Australia than inland (Van Ommen and Morgan, 2010), the regional changes in climate are also reflected in the GWW. Analysis of the CRU TS v3.22 climate data (Harris et al., 2014) for the location of the GWW Supersite at Credo (30.1°S, 120.7°E; <http://www.tern-supersites.net.au/supersites/gww/>) shows that mean annual temperature has increased significantly in the last 100 years (0.139 ± 0.015 °C/decade, $p < 0.001$). There has been no trend in annual precipitation, but the number of rain days has decreased significantly since the middle of last century, especially after 1960 (-6.16 day/decade, $p < 0.001$); and the mean precipitation on rain days (i.e. precipitation intensity) has increased (0.38 mm/decade, $p < 0.001$). The interannual variability of annual precipitation has also increased (72.8 mm and 81.7 mm for the standard deviation of annual precipitation before and after 1960 respectively). These changes were expected to have had a significant impact on tree growth in the GWW.

The changes in climate in southwestern Western Australia cannot be unambiguously attributed to anthropogenic increases in [CO₂] (Pitman et al., 2004; Cai and Cowan, 2006). However, the observed increase in [CO₂] has direct impacts on photosynthesis and the water-use efficiency of trees (Drake et al., 1997). Model studies of the growth of the temperate trees *Quercus petraea* (France) and *Pinus koraiensis* (China) have suggested that the impact of [CO₂] on radial stem growth is limited (Boucher et al., 2014; Li et al., 2014) and this is supported by tree-ring measurements of trees from both temperate and tropical regions (Kienast and Luxmoore, 1988; Gedalof and Berg, 2010; van der Sleen et al., 2015). However, none of these studies were conducted in regions where tree growth is limited by moisture availability or its seasonal distribution. A stronger response to enhanced [CO₂] might be expected *a priori* in water-limited regions (Field et al., 1983; Hyvönen et al., 2007), such as the GWW, because stomatal conductance is reduced when [CO₂] is higher and thus the water loss per unit of carbon assimilation can be less (Wright et al., 2003; Prentice et al., 2014).

In this study, we demonstrate that the radial growth of the gymnosperm *Callitris columellaris* in the GWW can be simulated using a light-use efficiency model of

photosynthesis coupled with a dynamic allocation and tree-growth model. We then use this model to explore the impact of changes in climate and [CO₂] on tree growth under water-limited conditions, and specifically to test whether we can detect an impact of [CO₂] on ring width under these conditions.

2 Methods

2.1 The study area

The vegetation of the GWW is dominated by open eucalypt woodlands, with patches of heathland, mallee and grassland. The climate is characterized by winter rainfall and summer drought, although storms associated with the monsoonal penetration into the continental interior can also bring occasional rains in summer (Sturman et al., 1996). The sampling site (GWW Super Site, Credo, 30.1°S, 120.7°E, 400m a.s.l.) lies in the northernmost and driest part of the GWW (Fig. 2), with a mean annual rainfall of ca 270 mm. This area is dominated by naturally regenerating eucalypts (*Eucalyptus salmonophloia* and *E. salubris*), associated with *Acacia* and the multi-stemmed gymnosperm *Callitris columellaris*, with *Atriplex* in the understorey. Human impact on the landscape is minimal.

2.2 Tree ring data

The genus *Callitris* has been shown to provide a good record of annual tree growth in a wide variety of climates across Australia (Ash, 1983; Cullen and Grierson, 2007; Baker et al., 2008; Cullen et al., 2008; Cullen and Grierson, 2009). Tree-ring cores were obtained from ten multi-stemmed *Callitris columellaris* trees (Fig. 1) from a 500 x 500 m plot at the Credo Super Site in August 2013. The selected trees were canopy trees, with a mean height of 4.2 meters, and not overshadowed by other individuals. The sampling plot was considered relatively undisturbed. Other environmental conditions (e.g. soil type, soil depth) showed no obvious variation between the sampled trees. Multiple cores were obtained from each tree, taking care to sample each of the individual stems of each tree. A total of 32 tree ring cores were obtained.

Measurements of annual growth were made on each core. The cores were cross-dated visually, based on pointing-year identification and ring-width pattern matching, and the final measuring accuracy was checked with the cross-dating software COFECHA (Holmes, 1983). The basic tree ring-width statistics are summarized in Table 1. The measurements of tree growth on individual stems were aggregated to produce an estimate of the total radial growth of each tree for comparison with model outputs. The “effective” single-stemmed basal diameter (D) and “effective” single-stemmed diameter increment (dD/dt) were obtained from observed multi-stemmed basal diameter (δ_i) and individual-stem diameter increments ($d(\delta_i)/dt$) by:

$$D = \sqrt{\sum_{i=1}^n \delta_i^2}, \text{ and } dD/dt = \frac{1}{D} \sum_{i=1}^n (\delta_i \cdot d\delta_i/dt)$$

The effective annual growth measured at the study site is shown in Figure 3. Note that, in contrast with traditional tree-ring studies, the ring-width series were not detrended to account for aging effects because these are explicitly simulated by the model. Furthermore, we simulate each of the 10 sampled trees individually rather than creating a composite series.

Tree-ring series from the Southern Hemisphere are conventionally presented with annual increments attributed to the calendar year in which tree growth was initiated (Schulman, 1956). Although the longest tree-ring record obtained dates from 1870 (Fig. 3), only three trees have pre-1920 records. Some of the changes in the early part of the record, such as the step-like decrease and increase before 1920, are likely to be artefacts because of the low number of tree records. For this reason, and because the climate data are also less reliable in the early part of the century, we focus on the interval post-1920 for analyses.

2.3 The tree growth model

We used a light-use efficiency model (the P model: Wang et al., 2014) to simulate gross primary production (GPP), which is then used as input to a species-based carbon allocation and functional geometric tree-growth model (the T model: Li et al., 2014) to simulate tree growth. The P model simulates GPP per unit of absorbed PAR using data on latitude, elevation, [CO₂] and monthly temperature, precipitation, and fractional cloud cover (Wang et al., 2014). The P model has been shown to

reproduce observed geographic patterning in the magnitudes of observed GPP reasonably well (Wang et al., 2014).

The potential GPP per unit of absorbed PAR as predicted by the P model depends on the PAR incident on the vegetation canopy during the growing season (temperature above 0°C), the intrinsic quantum efficiency of photosynthesis (taken as 0.085: Collatz et al., 1998; Wang et al., 2014), and the effects of photorespiration and substrate limitation at subsaturating [CO₂] represented as a function of the leaf-internal [CO₂] and the photorespiratory compensation point. Leaf-internal [CO₂] is estimated from ambient [CO₂] via the least-cost hypothesis (Wright et al., 2003; Prentice et al., 2014) as a function of atmospheric aridity (expressed as ΔE , the climatic moisture deficit: difference between annual (estimated) actual evapotranspiration (E_a) and equilibrium evapotranspiration (E_q)), air temperature and elevation. In the version used here, GPP is further modified by a factor $\alpha^{1/4}$ (α is the ratio of modelled actual to potential evapotranspiration (Cramer and Prentice, 1988)) to account for the reduction in GPP at very low soil moisture content, which has been observed in flux measurements in arid regions.

In the T model, the fraction of incident PAR absorbed by the canopy (fAPAR) is estimated from the leaf area index within the canopy and used to convert potential to actual GPP with the help of Beer's law (Jarvis and Leverenz, 1983). Annual net primary production (NPP) is derived from annual GPP, corrected for foliage respiration, by deducting growth respiration (assumed to be proportional to NPP) and the maintenance respiration of sapwood and fine roots. NPP is allocated to stem, foliage and fine-root increments, foliage turnover and fine-root turnover. Carbon is allocated to different tissues within the constraint of the basic functional or geometric relationships between different dimensions of the tree, including asymptotic height-diameter trajectories (Thomas, 1996; Ishii et al., 2000; Falster and Westoby, 2005).

A full description of the coupled model is given in Li et al. (2014). The model has previously been used to simulate the growth of *Pinus koraiensis* in a temperate and relatively moist site in the Changbai Mountains, China. Tree growth in the Changbai Mountains is primarily constrained by growing-season PAR, which in turn is strongly influenced by cloud cover. When driven by local climate data and changing

atmospheric [CO₂], the model produced a good representation of interannual variability in *Pinus koraiensis* growth over the past 50 years.

2.4 Derivation of model parameter values

The P model is generic for all C₃ plants and has no free parameters. The T model requires 15 parameters to be specified. Most of these could be obtained from measurements made at the sampling site, or from the literature (Table 2). Stem basal diameter, tree height and crown area were measured on 150 trees at the sampling site. The measurements were made on all *Callitris* trees within a 1 km² plot. Parameter values for the initial slope of the height–diameter relationship (a : 41.35), the initial ratio of crown area to stem cross-sectional area (c : 626.92), and maximum tree height (H_m : 9.58 m) were estimated using non-linear regression applied to the effective basal diameter (D), tree height (H), and crown area (A_c) measurements on these trees. Values for sapwood density (ρ_s) and specific leaf area (σ) were derived from five measurements made at the sampling site (Table 2).

We used generic values for the quantum efficiency of photosynthesis (ϵ), PAR extinction coefficient (k) and yield factor (y), from the literature (Table 2). We used estimates of leaf area index within the crown (L) and foliage turnover time (τ_f) measured on *Callitris* species in other regions of Australia. Previous analyses show that the T model is relatively insensitive to these five parameters (Li et al., 2014).

There are no estimates of fine-root turnover time (τ_r), fine-root specific respiration rate (r_r), sapwood-specific respiration rate (r_s), and ratio of fine-root mass to foliage area (ζ) for *Callitris* in the literature and these parameters were not measured in the field. However, these parameters have been shown to have a substantial impact on simulated radial growth and the shape of the ontogenetic ageing curve (Li et al., 2014). We used neural-network Bayesian parameter optimization (Jaakkola and Jordan, 2000; Pelikan, 2005) to derive mutually consistent values of these four parameters. In Bayesian data analysis and estimation methods, the uncertain quantities are modelled in terms of their joint probability distribution in order to obtain

a joint posterior distribution of the parameters. This can be done using a single variable target or involve multiple targets (Gelman et al., 2003; Rougier and Goldstein, 2014). The method has been widely applied to calibrate climate and carbon-cycle model parameters (Knutti et al., 2002; Murphy et al., 2004; Stainforth et al., 2005; Ricciuto et al., 2008; Smith et al., 2009; Klocke et al., 2011; Kaminski et al., 2013). In the case of the carbon-cycle calibration, multiple plant physiological parameters were estimated from time-varying CO₂ concentration (Kaminski et al., 2013). In a similar fashion, Bayesian parameter calibration using tree-ring series as a target has also been used to optimise a tree growth model (Tolwinski-Ward et al., 2013). In the present study, the calibration target is mean ring-width during the period 1950-2012, and the posterior is constructed based on sampling the joint parameter distribution 100,000 times and retaining the values of the 100 samples that most closely match the calibration target (van der Vaart et al., 2015).

We examined the correlation between the posterior parameter values, using both Pearson correlation coefficients and principal components analysis. These analyses show that there is no correlation between estimates of fine-root turnover time (τ_r), fine-root specific respiration rate (r_r), and sapwood-specific respiration rate (r_s). The ratio of fine-root mass to foliage area (ζ) is only weakly correlated with fine root turnover time (0.25) and fine root respiration rate (-0.35). The calibration procedure produces a shift in the median value and a reduction in the uncertainty for all four parameters (Fig. 4). However, the largest reduction in uncertainty is found for ζ . The final optimized parameter values for all four variables lie within the range of measurements that have been made on other gymnosperms (Table 2).

2.5 Climate inputs

The P model requires daily temperature, precipitation, and fractional cloud cover as an input, which are generally obtained from linear interpolation of monthly values of these variables (Wang et al., 2014). Although three meteorological stations (Credo, Kalgoorlie, Ora Banda, Menzies; Fig. 2) are near to the GWW site, none has records for all three variables covering the whole interval sampled by the tree-ring series (i.e. 1920-2013). We therefore used monthly temperature, precipitation, and cloud cover fraction for the interval 1920 onwards from the CRU TS v3.22 data set (Harris et al.,

2014), using values of these variables for the single grid cell (30.25°S, 120.75°E) from CRU TS v3.22 in which the sampling site lies (Fig. 5). We examined the reliability of this approach by comparing the gridded climate values with observed values from the three meteorological stations for all overlapping intervals for each variable; in the case of solar radiation/cloud cover this was very short (post-1990 only). There is generally good agreement between the gridded monthly (and annual) temperature and precipitation data and meteorological station data with respect to long-term means, interannual variability and trends. The correlation between the gridded and observed values of interannual variability in temperature at Kalgoorlie post 1911 is 0.907 ($p < 0.001$). Similarly, the correlation between the gridded and observed values of interannual variability in precipitation at Menzies between 1901 and 2008 is 0.905 ($p < 0.001$).

2.6 Definition of the effective growing season

The GWW is characterized by strong precipitation seasonality, while temperature variations are relatively modest. In climates with cold winters there is always a distinct growing season even for evergreen trees. Carbon that is assimilated after maximum leaf-out in any year is normally stored and contributes to tree growth in the subsequent growing season (Michelot et al., 2012). Thus the effective growing season for tree growth in seasonally cold climates can be defined as from mid-summer in one year until mid-summer in the subsequent year (Li et al., 2014). It is less obvious how to define the effective growing season in moisture-limited regions. However, several studies have indicated that radial growth in *Callitris* is affected not only by seasonal precipitation during the year when tree-ring growth is initialized but also by precipitation during the wet season in previous years (Baker et al., 2008; Cullen and Grierson, 2009), suggesting that it is necessary to consider an effective growing season for carbon accumulation that is longer than the current growth year.

We investigated the optimal interval influencing carbon accumulation and tree growth using ordinary least-squares multiple linear regression. We used total annual photosynthetically active radiation (PAR₀), mean annual temperature (MAT), and the ratio of actual to potential evapotranspiration (α) as independent variables in the

regression and mean tree-ring width during the period from 1950-2013 as the dependent variable. (PAR_0 is globally defined as total incident PAR during periods with temperatures $> 0^{\circ}\text{C}$, but note that for GWW this is the same as the total incident PAR; we use the notation PAR_0 for consistency with other work using the P and T models.) The post-1950 interval was used for this analysis in order to use all ten tree-ring records to derive the target mean tree-ring width. We defined the effective growing season as the period from January to December in the current growth year, and then extended the interval by six-month steps for a period up to three years. In these latter analyses, each six-month period contributes equally to the carbon available for growth. The goodness-of-fit of each model was judged based on the significance of the slope coefficient of each independent variable (p value) and the R^2 of the overall model.

The results from the ordinary least-squares multiple linear regression analysis ([Table 3](#)) show that the best overall prediction of tree-ring width ($R^2 = 0.308$) was obtained using an effective growing season of two years (from January in the previous year to December in the year of the tree-ring formation). This interval also produced significant p values for each of the predictor variables ([Table 3](#)). The overall relationship, and the significance of each climate variable, deteriorated when the effective growing season was defined as any longer than two years. Thus, in the subsequent application of the model, we used a carbon-accumulation period of two years to simulate growth rates. This is consistent with the general observation that radial growth of *Callitris* is also influenced by precipitation in the previous rainy season (Baker et al., 2008; Cullen and Grierson, 2009).

2.7 Application of the Model

Each tree was initialized with its actual effective single-stemmed basal diameter in the first year of growth, except that trees that started growing before 1901 were initialised using the actual effective single-stemmed basal diameter in 1901. The availability of climate data determined the earliest start date of the simulations (1901). The initial basal diameter was calculated from the measured diameter in August 2013 (which varied between 11.9 and 28.2 cm) and measured radial growth between the starting date and sampling date.

The model was initially run with a fixed [CO₂] of 360 ppm. To examine the impact of changing [CO₂] on tree growth, we made a second simulation with the same parameter values but using the observed annual [CO₂] between 1901 and 2013 (296–389 ppm: Fig. 5). The CO₂ observations are based on merging ice-core records for the interval from 1901 to 1957 (Etheridge et al., 1996; MacFarling Meure et al., 2006) and the yearly average of direct atmospheric measurements from Mauna Loa and the South Pole stations from 1958 to 2013 (http://scrippsco2.ucsd.edu/data/merged_ice_core/merged_ice_core_yearly.csv).

3 Results

3.1 Simulated ring width versus observations

The T model captured the amplitude and interannual variability of *Callitris* tree growth in the GWW realistically (Fig. 6). The mean simulated ring width for the period 1950–2012 was 0.722 mm, compared to an observed value of 0.718 mm. There was a highly significant positive correlation ($r = 0.37$, $p < 0.01$) between the simulated and observed mean tree-ring time series. The model underestimated the standard deviation (SD) of the mean ring width series (0.122 mm) compared to the observed SD (0.190 mm). This difference probably reflects the impact of local variability in environmental conditions on individual tree growth, which is not accounted for in our modelling approach.

Regression analysis (Fig. 7, Table 4) showed that observed tree growth has a strongly positive, independent response to both PAR₀ and soil moisture availability (as measured by α) and a negative response to VPD ($p < 0.1$). There is no response to MAT. These relationships can also be shown in the simulations. Although there is more scatter in the observations, the slopes of the observed and simulated response to PAR₀, α and VPD are similar in the model and the observation. The positive relationship with PAR₀ reflects the universal control of photosynthesis by light availability, and the positive relationship with α is consistent with observations that the growth of *Callitris* is determined by precipitation variability (Ash, 1983; Cullen and Grierson, 2009). VPD affects stomatal conductance such that increasing VPD leads

to stomatal closure, with a correspondingly negative impact on photosynthesis and hence carbon assimilation.

3.2 Simulations with varying [CO₂]

Comparison of the fixed and varying [CO₂] simulations (Fig. 8) shows a positive response of tree ring width to [CO₂]: simulated ring widths were smaller in the varying [CO₂] simulation than in the fixed [CO₂] simulation prior to ca 1990 (i.e. when the actual [CO₂] was less than 360 ppm) and larger thereafter. The average difference in simulated ring width in the last decade of the simulation is 0.228 mm. But the positive impact of enhanced [CO₂] is not apparent in the observations. Regression analysis (Fig. 9, Table 4) shows that there is no relationship between [CO₂] and observed tree ring width (slope = -0.001 ± 0.001 mm ppm⁻¹, $p = 0.687$). As a result, the simulations using realistic time-varying [CO₂] did not satisfactorily reproduce the observed pattern of variability in ring widths.

While enhanced [CO₂] is expected to have a positive effect on tree growth (Huang et al., 2007; Hyvönen et al., 2007; Donohue et al., 2013) the absence of a response in tree radial growth to elevated [CO₂] has been noted previously (Kienast and Luxmoore, 1988; Gedalof and Berg, 2010). Possible explanations for this are that either the additional carbon is consumed through enhanced respiration or allocated to other parts of the tree – effects that are not taken into account when fixed parameter values are used for respiration and allocation between different pools. As a test of whether parameter values might plausibly have changed in response to varying [CO₂], we re-ran the Bayesian parameter optimization of fine-root turnover time (τ_r), fine-root specific respiration rate (r_r), sapwood specific respiration rate (r_s) and ratio of fine-root mass to foliage area (ζ) for 30-year moving windows since 1920 using appropriate [CO₂] and climate for each window. This resulted in no change in the estimated values for fine-root turnover time, fine-root specific respiration rate, and sapwood-specific respiration rate (Fig. 10). However, the estimated value of the ratio of fine-root mass to foliage area (ζ) increased by about 14% from 1950 to the end of the period. Variance partitioning (Chevan and Sutherland, 1991; analyses made using the hier.part package in R) shows that ca 80% of the variability in ζ can be

explained as a consequence of changes in CO₂ and ca 20% as a consequence of changes in soil moisture availability, as indexed by α .

A simulation with observed [CO₂] and time-varying values of ζ produced a better agreement ($r = 0.27$) with the tree-ring observations (Fig. 11). In particular, this simulation does not produce the large systematic overestimation of ring widths in recent years compared to observations that is seen in the simulation with observed [CO₂] and fixed ζ . The regression analysis shows that the impact of the CO₂ effect on simulated tree growth is very much weakened (Fig. 12) compared to simulations in which ζ is not allowed to vary (Fig. 9).

4 Discussion and Conclusions

We have shown that the radial growth (ring width) of the gymnosperm *Callitris columellaris* over the last century in the seasonally dry environment of the GWW can be realistically simulated by coupling a generic model of GPP with a model of carbon allocation and functional geometric tree growth using species-specific parameter values. Model performance was not adversely affected by the reduction in winter precipitation and the shift towards more variable precipitation that occurred in the mid-1970s, indicating that it successfully captured the climate controls on tree growth during the whole period considered. This conclusion was borne out by regression analyses, which show that the simulated and observed responses to key climate variables were similar.

The radial growth of *Callitris columellaris* in the GWW is positively correlated with PAR₀ and α , and negatively correlated VPD. These relationships are seen in observations and reproduced by the model. The response to VPD can be explained as a consequence of the atmospheric control on stomatal conductance and hence photosynthesis. Thus, both atmospheric and soil moisture deficits (the former represented by VPD, the latter by α) apparently exert independent controls on radial stem growth. Previous studies have shown that the growth of *Callitris* in southwestern Australia is controlled by precipitation (Sgherza et al., 2010), but that there is only a weak correlation between stable carbon isotope measurements and

precipitation of the current year because *Callitris* has a strong water-conservation strategy (Sgherza et al., 2010). These findings are consistent with the observed response to VPD and also support the use of a 2-year period contributing to carbon accumulation and growth in our model.

We have shown that the radial growth of *Callitris columellaris* in the GWW has not responded to increasing $[\text{CO}_2]$ in recent decades. The lack of a response to $[\text{CO}_2]$ has been a feature of several other tree-ring studies (Kienast and Luxmoore, 1988; Archer et al., 1995; Gedalof and Berg, 2010; van der Sleen et al., 2015). Our model experiments suggest that the lack of response in radial growth could be because of changes in allocation to different components of the tree, specifically increased allocation to fine roots. This is consistent with analyses of stable carbon isotopes and growth rings of tropical trees (van der Sleen et al., 2015), which found an increase in water-use efficiency but no stimulation of radial growth from CO_2 fertilisation during the recent 150 years.

Results from free-air carbon enrichment (FACE) experiments are equivocal about the impact of enhanced $[\text{CO}_2]$ on tree growth and the allocation to fine roots. However, the majority of sites (Oak Ridge FACE: Norby et al., 2004; DUKE-FACE: DeLucia et al., 1999; Pritchard et al., 2008; Rhineland ASPEN-FACE: King et al., 2001; EUROFACE: Calfapietra et al., 2003; Lukac et al., 2003; Bangor FACE: Smith et al., 2013) have shown increased allocation to fine roots as a consequence of enhanced $[\text{CO}_2]$. The Swiss Canopy Crane site is the outlier, with decreased below-ground allocation (Bader et al., 2009). We might expect *a priori* that trees at sites experiencing strong nutrient limitation would show this kind of response because of the need to increase root mass to extract more nutrients to support increased above-ground production, whereas trees at sites experiencing strong water limitation might show the opposite response due to enhanced water use efficiency at high $[\text{CO}_2]$ such that the plants have less need to increase root mass to ensure an adequate supply of water to maintain increased above-ground production. Our results do not support this reasoning, suggesting instead that the trees are allocating more below ground as $[\text{CO}_2]$ increases even in the strongly water limited environment of the GWW. It is possible that this belowground allocation could in part represent increased carbon

export to mycorrhiza or the rhizosphere (Godbold et al., 2015), in order to maximize nutrient uptake.

Appropriately analyzed, tree-ring records worldwide should yield consistent information about the diverse responses of tree growth and allocation to environmental change. A noteworthy feature of our study is that a relatively slight change in the allocation of carbon to fine roots *versus* leaves provides a quantitatively consistent explanation of the apparent absence of a growth response to [CO₂]. If this explanation is correct, it does not support the interpretation that tree NPP is not responsive to [CO₂] (whether through nutrient limitation, sink limitation or any other reason). It does however support the idea that above-ground NPP and radial growth are sensitive to environmental effects on the allocation of assimilates to different plant compartments.

Acknowledgements

We thank Henrique Togashi for assistance in making the SLA and wood density measurements in GWW. GL is supported by International Postgraduate Research Scholarship at Macquarie University. The work is a contribution to the AXA Chair programme on Biosphere and Climate Impacts and the Imperial College initiative “Grand Challenges in Ecosystems and the Environment”. The GWW Supersite is a node in the Terrestrial Ecosystem Research Network (TERN), supported by the Australian Supersites facility.

References

- Ansell, T., Reason, C., Smith, I., and Keay, K.: Evidence for decadal variability in southern Australian rainfall and relationships with regional pressure and sea surface temperature, *Int. J. Climatol.*, 20, 1113-1129, 2000.
- Archer, S., Schimel, D. S., and Holland, E. A.: Mechanisms of shrubland expansion: land use, climate or CO₂?, *Climatic Change*, 29, 91-99, 1995.
- Ash, J.: Tree rings in tropical *Callitris macleayana* F. Muell, *Aust. J. Bot.*, 31, 277-281, 1983.

- Bader, M., Hiltbrunner, E., and Körner, C.: Fine root responses of mature deciduous forest trees to free air carbon dioxide enrichment (FACE), *Funct. Ecol.*, 23, 913-921, 2009.
- Baker, P. J., Palmer, J. G., and D'Arrigo, R.: The dendrochronology of *Callitris intratropica* in northern Australia: annual ring structure, chronology development and climate correlations, *Aust. J. Bot.*, 56, 311-320, 2008.
- Boucher, É., Guiot, J., Hatté, C., Daux, V., Danis, P.-A., and Dussouillez, P.: An inverse modeling approach for tree-ring-based climate reconstructions under changing atmospheric CO₂ concentrations, *Biogeosciences*, 11, 3245-3258, 2014.
- Burrows, W., Hoffman, M., Compton, J., and Back, P.: Allometric relationship and community stocks in white cypress pine (*Callitris glaucophylla*) and associated eucalypts in the Carnarvon area-south central Queensland, Australian Greenhouse Office, Canberra, 2001.
- Burton, A. J., and Pregitzer, K. S.: Measurement carbon dioxide concentration does not affect root respiration of nine tree species in the field, *Tree Physiol.*, 22, 67-72, 2002.
- Cai, W., and Cowan, T.: SAM and regional rainfall in IPCC AR4 models: Can anthropogenic forcing account for southwest Western Australian winter rainfall reduction?, *Geophys. Res. Lett.*, 33, 2006.
- Calfapietra, C., Gielen, B., Galema, A., Lukac, M., De Angelis, P., Moscatelli, M., Ceulemans, R., and Scarascia-Mugnozza, G.: Free-air CO₂ enrichment (FACE) enhances biomass production in a short-rotation poplar plantation, *Tree Physiol.*, 23, 805-814, 2003.
- Collatz, G. J., Berry, J. A., and Clark, J. S.: Effects of climate and atmospheric CO₂ partial pressure on the global distribution of C4 grasses: present, past, and future, *Oecologia*, 114, 441-454, 1998.
- Cramer, W. and Prentice, I. C.: Simulation of regional soil moisture deficits on a European scale, *Norsk Geografisk Tidsskrift – Norwegian Journal of Geography*, 42, 149–151, 1988.
- Cullen, L. E., Adams, M. A., Anderson, M. J., and Grierson, P. F.: Analyses of $\delta^{13}\text{C}$ and $\delta^{18}\text{O}$ in tree rings of *Callitris columellaris* provide evidence of a change in stomatal control of photosynthesis in response to regional changes in climate, *Tree Physiol.*, 28, 1525-1533, 2008.
- Cullen, L. E., and Grierson, P. F.: Multi-decadal scale variability in autumn-winter rainfall in south-western Australia since 1655 AD as reconstructed from tree rings of *Callitris columellaris*, *Clim. Dynam.*, 33, 433-444, 2009.

- DeLucia, E. H., Hamilton, J. G., Naidu, S. L., Thomas, R. B., Andrews, J. A., Finzi, A., Lavine, M., Matamala, R., Mohan, J. E., and Hendrey, G. R.: Net primary production of a forest ecosystem with experimental CO₂ enrichment, *Science*, 284, 1177-1179, 1999.
- Donohue, R. J., Roderick, M. L., McVicar, T. R., and Farquhar, G. D.: Impact of CO₂ fertilization on maximum foliage cover across the globe's warm, arid environments, *Geophys. Res. Lett.*, 40, 3031-3035, 2013.
- Drake, B. G., González-Meler, M. A., and Long, S. P.: More efficient plants: a consequence of rising atmospheric CO₂?, *Annu. Rev. Plant. Biol.*, 48, 609-639, 1997.
- England, M. H., Ummenhofer, C. C., and Santoso, A.: Interannual rainfall extremes over southwest Western Australia linked to Indian Ocean climate variability, *J. Clim.*, 19, 1948-1969, 2006.
- Etheridge, D., Steele, L., Langenfelds, R., Francey, R., Barnola, J. M., and Morgan, V.: Natural and anthropogenic changes in atmospheric CO₂ over the last 1000 years from air in Antarctic ice and firn, *J. Geophys. Res.*, 101, 4115-4128, 1996.
- Falster, D. S., and Westoby, M.: Tradeoffs between height growth rate, stem persistence and maximum height among plant species in a post-fire succession, *Oikos*, 111, 57-66, 2005.
- Feng, J., Li, J., and Li, Y.: Is there a relationship between the SAM and southwest Western Australian winter rainfall?, *J. Clim.*, 23, 6082-6089, 2010.
- Fieber, K. D., Davenport, I. J., Tanase, M. A., Ferryman, J. M., Gurney, R. J., Walker, J. P., and Hacker, J. M.: Effective LAI and CHP of a single tree from small-footprint full-waveform LiDAR, *IEEE Geosci. Remote Sens. Lett.*, 11, 1634-1638, 2014.
- Field, C., Merino, J., and Mooney, H. A.: Compromises between water-use efficiency and nitrogen-use efficiency in five species of California evergreens, *Oecologia*, 60, 384-389, 1983.
- Frederiksen, J. S., and Frederiksen, C. S.: Interdecadal changes in southern hemisphere winter storm track modes, *Tellus Ser. A*, 59, 599-617, 2007.
- Gedalof, Z. e., and Berg, A. A.: Tree ring evidence for limited direct CO₂ fertilization of forests over the 20th century, *Glob. Biogeochem. Cycles*, 24, 2010.
- Gelman, A., Carlin, J. B., Stern, H. S., and Rubin, D. B.: Bayesian data analysis, Taylor & Francis, Boca Raton, London, New York, Washington, D.C., 2014.
- Godbold, D.L., Vašutová, M., Wilkinson, A., Edwards-Jonášová, M., Bambrick, M., Smith, A.R., Pavelka, M., Cudlin, P.: Elevated Atmospheric CO₂ affects ectomycorrhizal

- species abundance and increases sporocarp production under field conditions. *Forests*, 6, 1256-1273, 2015.
- Harris, I., Jones, P.D., Osborn, T.J. and Lister, D.H.: Updated high-resolution grids of monthly climatic observations - the CRU TS3.10 Dataset, *Int. J. Climatol.*, 34, 623-642, 2014.
- Hendon, H. H., Thompson, D. W., and Wheeler, M. C.: Australian rainfall and surface temperature variations associated with the Southern Hemisphere annular mode, *J. Clim.*, 20, 2452-2467, 2007.
- Holmes, R. L.: Computer-assisted quality control in tree-ring dating and measurement, *Tree-ring Bull.*, 43, 69-78, 1983.
- Hope, P. K.: Projected future changes in synoptic systems influencing southwest Western Australia, *Clim. Dynam.*, 26, 765-780, 2006.
- Hope, P. K., Drosowsky, W., and Nicholls, N.: Shifts in the synoptic systems influencing southwest Western Australia, *Clim. Dynam.*, 26, 751-764, 2006.
- Huang, J.-G., Bergeron, Y., Denneler, B., Berninger, F., and Tardif, J.: Response of forest trees to increased atmospheric CO₂, *Crit. Rev. Plant Sci.*, 26, 265-283, 2007.
- Hyvönen, R., Ågren, G. I., Linder, S., Persson, T., Cotrufo, M. F., Ekblad, A., Freeman, M., Grelle, A., Janssens, I. A., and Jarvis, P. G.: The likely impact of elevated [CO₂], nitrogen deposition, increased temperature and management on carbon sequestration in temperate and boreal forest ecosystems: a literature review, *New Phytol.*, 173, 463-480, 2007.
- Ishii, H., Reynolds, J. H., Ford, E. D., and Shaw, D. C.: Height growth and vertical development of an old-growth *Pseudotsuga-Tsuga* forest in southwestern Washington State, USA, *Can. J. Forest Res.*, 30, 17-24, 2000.
- Jaakkola, T. S., and Jordan, M. I.: Bayesian parameter estimation via variational methods, *Stat. Comput.*, 10, 25-37, 2000.
- Jarvis, P., and Leverenz, J.: Productivity of temperate, deciduous and evergreen forests, in: *Physiological plant ecology IV*, Springer, Berlin Heidelberg, 233-280, 1983.
- Kaminski, T., Knorr, W., Schürmann, G., Scholze, M., Rayner, P., Zaehle, S., Blessing, S., Dorigo, W., Gayler, V., and Giering, R.: The BETHY/JSBACH carbon cycle data assimilation system: experiences and challenges, *J. Geophys. Res.: Biogeophys.*, 118, 1414-1426, 2013.

- Kienast, F., and Luxmoore, R. J.: Tree-ring analysis and conifer growth responses to increased atmospheric CO₂ levels, *Oecologia*, 76, 487-495, 1988.
- King, J., Pregitzer, K., Zak, D., Sober, J., Isebrands, J., Dickson, R., Hendrey, G., and Karnosky, D.: Fine-root biomass and fluxes of soil carbon in young stands of paper birch and trembling aspen as affected by elevated atmospheric CO₂ and tropospheric O₃, *Oecologia*, 128, 237-250, 2001.
- Klocke, D., Pincus, R., and Quaas, J.: On constraining estimates of climate sensitivity with present-day observations through model weighting, *J. Climate*, 24, 6092-6099, 2011.
- Körner, C., Asshoff, R., Bignucolo, O., Hättenschwiler, S., Keel, S. G., Peláez-Riedl, S., Pepin, S., Siegwolf, R. T., and Zotz, G.: Carbon flux and growth in mature deciduous forest trees exposed to elevated CO₂, *Science*, 309, 1360-1362, 2005.
- Knutti, R., Stocker, T. F., Joos, F., and Plattner, G.-K.: Constraints on radiative forcing and future climate change from observations and climate model ensembles, *Nature*, 416, 719-723, 2002.
- Landsberg, J. J., and Sands, P.: *Physiological ecology of forest production: principles, processes and models*, Academic Press, 2010.
- Lee, P. S., Mackey, B. G., and Berry, S. L.: Modelling vegetation structure-based bird habitat resources in Australian temperate woodlands, using multi-sensors, *Eur. J. Remote Sens.*, 46, 641-674, 2013.
- Li, G., Harrison, S., Prentice, I., and Falster, D.: Simulation of tree-ring widths with a model for primary production, carbon allocation, and growth, *Biogeosciences*, 11, 6711-6724, 2014.
- Lukac, M., Calfapietra, C., and Godbold, D. L.: Production, turnover and mycorrhizal colonization of root systems of three *Populus* species grown under elevated CO₂ (POPFACE), *Glob. Change Biol.*, 9, 838-848, 2003.
- MacFarling Meure, C., Etheridge, D., Trudinger, C., Steele, P., Langenfelds, R., Van Ommen, T., Smith, A., and Elkins, J.: Law Dome CO₂, CH₄ and N₂O ice core records extended to 2000 years BP, *Geophys. Res. Lett.*, 33, 2006.
- McCullagh, P., Nelder, J. A., and McCullagh, P.: *Generalized linear models*, Chapman and Hall, London, 1989.
- Meneghini, B., Simmonds, I., and Smith, I. N.: Association between Australian rainfall and the southern annular mode, *Int. J. Climatol.*, 27, 109-121, 2007.

- Michelot, A., Simard, S., Rathgeber, C., Dufrêne, E., and Damesin, C.: Comparing the intra-annual wood formation of three European species (*Fagus sylvatica*, *Quercus petraea* and *Pinus sylvestris*) as related to leaf phenology and non-structural carbohydrate dynamics, *Tree physiol.*, 32, 1033–1045, 2012.
- Murphy, J. M., Sexton, D. M., Barnett, D. N., Jones, G. S., Webb, M. J., Collins, M., and Stainforth, D. A.: Quantification of modelling uncertainties in a large ensemble of climate change simulations, *Nature*, 430, 768-772, 2004.
- Norby, R. J., Ledford, J., Reilly, C. D., Miller, N. E., and O'Neill, E. G.: Fine-root production dominates response of a deciduous forest to atmospheric CO₂ enrichment, *Proc. Natl. Acad. Sci. U.S.A.*, 101, 9689-9693, 2004.
- Pelikan, M.: Bayesian optimization algorithm, in: *Hierarchical Bayesian Optimization Algorithm*, Springer, Berlin Heidelberg, 31-48, 2005.
- Pierce, L. L., and Running, S. W.: Rapid estimation of coniferous forest leaf area index using a portable integrating radiometer, *Ecology*, 1762-1767, 1988.
- Pitman, A. J., Narisma, G. T., Pielke, R., and Holbrook, N.: Impact of land cover change on the climate of southwest Western Australia, *J. Geophys. Res.*, 109, 2004.
- Prentice, I. C., Dong, N., Gleason, S. M., Maire, V., and Wright, I. J.: Balancing the costs of carbon gain and water transport: testing a new theoretical framework for plant functional ecology, *Ecol. Lett.*, 17, 82-91, 2014.
- Pritchard, S. G., Strand, A. E., McCormack, M., Davis, M. A., Finzi, A. C., Jackson, R. B., Matamala, R., Rogers, H. H., and Oren, R.: Fine root dynamics in a loblolly pine forest are influenced by free-air-CO₂-enrichment: A six-year-minirhizotron study, *Glob. Change Biol.*, 14, 588-602, 2008.
- Prober, S. M., Thiele, K. R., Rundel, P. W., Yates, C. J., Berry, S. L., Byrne, M., Christidis, L., Gosper, C. R., Grierson, P. F., and Lemson, K.: Facilitating adaptation of biodiversity to climate change: a conceptual framework applied to the world's largest Mediterranean-climate woodland, *Clim. Change*, 110, 227-248, 2012.
- Ricciuto, D. M., Davis, K. J., and Keller, K.: A Bayesian calibration of a simple carbon cycle model: The role of observations in estimating and reducing uncertainty, *Global. Biogeochem. Cy.*, 22, doi: 10.1029/2006GB002908, 2008.
- Rogers, H. H., Runion, G. B., and Krupa, S. V.: Plant responses to atmospheric CO₂ enrichment with emphasis on roots and the rhizosphere, *Environ. Pollut.*, 83, 155-189, 1994.

- Rougier, J., and Goldstein, M.: Climate simulators and climate projections, *Annu. Rev. Stat. Appl.*, 1, 103-123, 2014.
- Sgherza, C., Cullen, L. E., and Grierson, P. F.: Climate relationships with tree-ring width and $\delta^{13}\text{C}$ of three *Callitris* species from semiarid woodlands in south-western Australia. *Aust. J. Bot.*, 58, 175-187, 2010.
- Smith, I., McIntosh, P., Ansell, T., Reason, C., and McInnes, K.: Southwest Western Australian winter rainfall and its association with Indian Ocean climate variability, *Int. J. Climatol.*, 20, 1913-1930, 2000.
- Smith, A. R., Lukac, M., Bambrick, M., Miglietta, F., and Godbold, D. L.: Tree species diversity interacts with elevated CO₂ to induce a greater root system response, *Glob. Change Biol.*, 19, 217-228, 2013.
- Smith, R. L., Tebaldi, C., Nychka, D., and Mearns, L. O.: Bayesian modeling of uncertainty in ensembles of climate models, *J. Am. Stat. Assoc.*, 104, 97-116, 2009.
- Stainforth, D. A., Aina, T., Christensen, C., Collins, M., Faull, N., Frame, D. J., Kettleborough, J. A., Knight, S., Martin, A., and Murphy, J.: Uncertainty in predictions of the climate response to rising levels of greenhouse gases, *Nature*, 433, 403-406, 2005.
- Sturman, A. P., Tapper, N. J., Sturman, A., and Sturman, A.: The weather and climate of Australia and New Zealand, Oxford University Press Melbourne, 1996.
- Thomas, S. C.: Asymptotic height as a predictor of growth and allometric characteristics in Malaysian rain forest trees, *Am. J. Bot.*, 556-566, 1996.
- Tolwinski-Ward, S., Anchukaitis, K. J., and Evans, M. N.: Bayesian parameter estimation and interpretation for an intermediate model of tree-ring width, *Clim. Past*, 9, 1481-1493, 2013.
- van der Sleen, P., Groenendijk, P., Vlam, M., Anten, N. P., Boom, A., Bongers, F., Pons, T. L., Terburg, G., and Zuidema, P. A.: No growth stimulation of tropical trees by 150 years of CO₂ fertilization but water-use efficiency increased, *Nat. Geosci.*, 8, 24-28, 2015.
- van der Vaart, E., Johnston, A. S., & Sibly, R. M.: Predicting how many animals will be where: How to build, calibrate and evaluate individual-based models. *Ecol. Model.*, doi: <http://dx.doi.org/10.1016/j.ecolmodel.2015.08.012>, 2015
- van Ommen, T. D., and Morgan, V.: Snowfall increase in coastal East Antarctica linked with southwest Western Australian drought, *Nat. Geosci.*, 3, 267-272, 2010.

- Wang, H., Prentice, I., and Davis, T.: Biophysical constraints on gross primary production by the terrestrial biosphere, *Biogeosciences*, 11, 5987-6001, 2014.
- Watson, A.: The extraordinary nature of the Great Western Woodlands, Wilderness Society of WA, 2008.
- White, M. A., Thornton, P. E., Running, S. W., and Nemani, R. R.: Parameterization and sensitivity analysis of the BIOME-BGC terrestrial ecosystem model: net primary production controls, *Earth Interact.*, 4, 1-85, 2000.
- Wright, I. J., and Westoby, M.: Leaves at low versus high rainfall: coordination of structure, lifespan and physiology, *New Phytol.*, 155, 403-416, 2002.
- Wright, I. J., Reich, P. B., and Westoby, M.: Least-cost input mixtures of water and nitrogen for photosynthesis, *Amer. Nat.*, 161, 98-111, 2003.
- Yin, J. H.: A consistent poleward shift of the storm tracks in simulations of 21st century climate, *Geophys. Res. Lett.*, 32, 2005.
- Yuan, Z., and Chen, H. Y.: Fine root biomass, production, turnover rates, and nutrient contents in boreal forest ecosystems in relation to species, climate, fertility, and stand age: literature review and meta-analyses, *Crit. Rev. Plant Sci.*, 29, 204-221, 2010.
- Zhang, Y., Xu, M., Chen, H., and Adams, J.: Global pattern of NPP to GPP ratio derived from MODIS data: effects of ecosystem type, geographical location and climate, *Glob. Ecol. Biogeogr. Lett.*, 18, 280-290, 2009.

Table and Figure Captions

Table 1. Statistics for *Callitris columellaris* tree ring-width series sampled in the Great Western Woodlands, Western Australia.

Table 2. Definition of T model parameters and derivation of parameter values. Most of the values were obtained from field measurements or are generic. For those values estimated using Bayesian calibration, we show the range of values given for *Callitris* (or related species) in the literature, the prior values used in the calibration, the posterior values and uncertainties, and the value used in the final model. The units are defined in the parameter column, except in the case of sapwood specific respiration where the measurements are in a different unit from the model parameter (and therefore specified explicitly).

Table 3. Regression analysis of relationship between ring width and climate parameters using different definitions of the effective growing season, based on the interval from 1950 to present. The dependent variable is mean ring width. The independent variables are the total incident photosynthetically active radiation (PAR₀), mean annual temperature (MAT), and the ratio of actual to potential evapotranspiration (α). This analysis indicates that the optimum period contributing to tree growth is two years.

Table 4. Regression analyses of simulated and observed response of tree growth to climate variables and CO₂. The dependent variable is mean radial growth series of the 10 trees (from 1950 to 2012). The independent variables are the total incident photosynthetically active radiation (PAR₀), mean annual temperature (MAT), the ratio of actual to potential evapotranspiration (α), vapour pressure deficit (VPD) and monthly [CO₂].

Figure 1. An example of *Callitris collumelaris* sampled for tree-ring cores in the Great Western Woodlands, Western Australia.

Figure 2. Location of the Great Western Woodlands sampling site, Western Australia. The underlying map shows mean annual precipitation (MAP). We also show the location of other sites across Australia where *Callitris* have been sampled (data from International Tree-Ring Data Bank), and the locations of the nearest meteorological stations to the sampling site.

Figure 3. Interannual variability in tree-ring widths of *Callitris columellaris* from the Great Western Woodlands, Western Australia. In the top panel, the black line is the mean of the observations, and the grey bars show the standard deviation (SD) of the individual sampled trees. The blue line in the bottom panel shows the number of trees sampled for each interval.

Figure 4. Prior (gray) and posterior (red) probability distribution function for fine-root turnover time (τ_r), fine-root specific respiration rate (r_r), sapwood-specific respiration rate (r_s); ratio of fine-root mass to foliage area (ζ).

Figure 5. Climate at the Great Western Woodlands site. The plot shows mean annual temperature, precipitation, total incident photosynthetically active radiation (PAR_0), and the ratio of actual to equilibrium evapotranspiration (α). The observed changes in $[CO_2]$ are shown for comparison.

Figure 6. Comparison between simulated and observed tree ring widths, for the period 1920 to the present, with $[CO_2]$ set at 360 ppm. The black line is the mean of the observations, and the grey bars are the standard deviation (SD) among the ten individual trees sampled. The blue line and bars are the mean and standard deviation for the ten simulated individual trees.

Figure 7. Simulated and observed responses of tree growth to climate: partial residual plots based on the regression analysis, obtained using the visreg package in R, are shown. The predictor variables are (a) total incident photosynthetically active radiation (PAR_0), mean annual temperature (MAT), the ratio of actual to potential evapotranspiration (α) and vapour pressure deficit (VPD).

Figure 8. Comparison of simulated ring width in simulations with fixed (blue line) and time-varying (red line) $[CO_2]$. The black line is the mean of the observed ring widths,

and the grey bars are the standard deviation (SD) among the ten individual trees sampled.

Figure 9. Simulated and observed response of tree radial growth to [CO₂]: partial residual plots based on the regression analysis, obtained using the visreg package in R, are shown. The dependent variable is mean ring width (from 1950 to 2012). The predictor variables are total incident photosynthetically active radiation (PAR₀), vapour pressure deficit (VPD), the ratio of actual to potential evapotranspiration (α), and monthly [CO₂].

Figure 10. Time variation of the values of parameters estimated by Bayesian optimization. The graph shows the percentage change to the mean value of fine-root turnover time (τ_r), fine-root specific respiration rate (r_r), sapwood specific respiration rate (r_s) and the ratio of fine-root mass to foliage area (ζ) for 30-year moving windows since 1920, using the appropriate [CO₂] and α for each window. Values on the X-axis are plotted against the first year of each 30-year window. The uncertainty estimates (bars) for the ratio of fine-root mass to foliage area (ζ) are the standard deviation of six 5-year sub-windows within each 30-year window.

Figure 11. Simulation of radial growth in response to changing climate and observed [CO₂], allowing for the effect of changing allocation to fine roots. The black line is the mean of the observations, and the grey bars are the standard deviation (SD) among the ten individual trees sampled. The blue line and bars are the mean and standard deviation for the ten simulated individual trees.

Figure 12. Simulated and observed response of tree radial growth to climate and [CO₂] based on the simulations in which the ratio of fine-root mass to foliage area (ζ) is allowed to vary. Partial residual plots based on the regression analysis, obtained using the visreg package in R, are shown. The dependent variable is mean ring width (from 1950 to 2012). The predictor variables are total incident photosynthetically active radiation (PAR₀), vapour pressure deficit (VPD), the ratio of actual to potential evapotranspiration (α), and monthly [CO₂].

Table 1. Statistics for *Callitris columellaris* tree ring-width series sampled in the Great Western Woodlands, Western Australia.

Species	<i>Callitris columellaris</i>
Elevation	400
Total number of sampled trees	10
Total number of sampled cores	33
Full chronology interval	1870-2013
Mean	0.3988
Mean sensitivity	0.2626
Standard deviation	0.1344
First order autocorrelation	0.5633
Mean correlations among all radii	0.106
Mean correlations between trees	0.096
Mean correlations within trees	0.217
Mean correlations Radii vs mean	0.361
Signal-to-noise ratio	1.061
Express population signal	0.515
Variance in first eigenvector	16.94%

Table 2. Definition of T model parameters and derivation of parameter values. Most of the values were obtained from field measurements or are generic. For those values estimated using Bayesian calibration, we show the range of values given for *Callitris* (or related species) in the literature, the prior values used in the calibration, the posterior values and uncertainties, and the value used in the final model. The units are defined in the parameter column, except in the case of sapwood specific respiration where the measurements are in a different unit from the model parameter (and therefore specified explicitly).

Parameter	Symbol	Uncertainty or range of values from literature	Source of information	Prior value	Posterior value	Accepted value	Reference
initial slope of height-diameter relationship (–)	a	41.35 ± 2.58	observation	-	-	41.35	-
initial ratio of crown area to stem cross-sectional area (–)	c	626.92 ± 20.03	observation	-	-	626.92	-
maximum tree height (m)	H_m	9.58 ± 1.11	observation	-	-	9.58	-
sapwood density (kg C m ⁻³)	ρ_s	406 ± 32	observation	-	-	406	-
specific leaf area (m ² kg ⁻¹ C)	σ	5.16 ± 0.32	observation	-	-	5.16	-
leaf area index within the crown (–)	L	1.87 ± 0.18	species-specific literature value	-	-	1.87	Fieber et al., 2014
foliage turnover time (yr)	τ_l	2.58	species-specific literature value	-	-	2.58	Wright and Westoby, 2002
PAR extinction coefficient (–)	k	0.48-0.58	generic value	-	-	0.5	Pierce and Running, 1988
yield factor (–)	Y	0.5-0.7	generic value	-	-	0.6	Zhang et al., 2009
fine-root turnover time (yr)	τ_r	0.76 ± 0.06	Bayesian parameter optimization	0.75 ± 0.5	0.96 ± 0.50	0.96	Yuan and Chen, 2010 (estimation for evergreen needleleaf trees)
fine-root specific respiration rate (yr ⁻¹)	r_r	1.36	Bayesian parameter optimization	1.36 ± 1	1.23 ± 0.80	1.23	Burton and Prigitzler, 2002 (estimation from one-seeded Juniper)
sapwood specific respiration rate (yr ⁻¹)	r_s	$0.5-10, 20$ nmol mol ⁻¹ s ⁻¹	Bayesian parameter optimization	1 ± 0.75 nmol mol ⁻¹ s ⁻¹	1.09 ± 0.61 nmol mol ⁻¹ s ⁻¹	1.09 nmol mol ⁻¹ s ⁻¹ (0.034 yr ⁻¹)	Landsberg and Sands, 2010
ratio of fine-root mass to foliage area (kgC m ⁻²)	ζ	1.0; 0.17	Bayesian parameter optimization	0.6 ± 0.5	0.150 ± 0.071	0.150	Burrows et al., 2001 (estimation for <i>Callitris</i>); White et al. (2000) (estimation for evergreen needleleaf tree)

Table 3. Regression analysis of relationship between ring width and climate parameters using different definitions of the effective growing season, based on the interval from 1950 to present. The dependent variable is mean ring width. The independent variables are the total incident photosynthetically active radiation (PAR_0), mean annual temperature (MAT), and the ratio of actual to potential evapotranspiration (α). This analysis indicates that the optimum period contributing to tree growth is two years.

		PAR_0 (mm (kmol photon m^{-2}) $^{-1}$)	MAT (mm $^{\circ}C^{-1}$)	α (–)	R^2
Formation year	Estimation	0.347	–0.052	0.746	0.076
	Standard error	± 0.186	± 0.054	± 0.558	
	<i>p</i> value	0.068	0.340	0.187	
Calendar year	Estimation	0.335	–0.093	0.930	0.141
	Standard error	± 0.185	± 0.051	± 0.436	
	<i>p</i> value	0.076	0.074	0.038	
1.5 Calendar years	Estimation	0.557	–0.148	1.640	0.270
	Standard error	± 0.207	± 0.057	± 0.510	
	<i>p</i> value	0.010	0.013	0.002	
2 Calendar years	Estimation	0.527	–0.177	2.003	0.308
	Standard error	± 0.229	± 0.065	± 0.539	
	<i>p</i> value	0.025	0.008	0.000	
2.5 Calendar years	Estimation	0.530	–0.158	2.092	0.236
	Standard error	± 0.262	± 0.074	± 0.634	
	<i>p</i> value	0.048	0.037	0.002	
3 Calendar years	Estimation	0.774	–0.192	2.434	0.252
	Standard error	± 0.282	± 0.081	± 0.685	
	<i>p</i> value	0.008	0.022	0.001	

Table 4. Regression analyses of simulated and observed response of tree growth to climate variables and CO₂. The dependent variable is mean radial growth series of the 10 trees (from 1950 to 2012). The independent variables are the total incident photosynthetically active radiation (PAR₀), mean annual temperature (MAT), the ratio of actual to potential evapotranspiration (α), vapour pressure deficit (VPD) and monthly [CO₂].

		PAR ₀ (mm (kmol photon m ⁻²) ⁻¹)	MAT (mm ° C ⁻¹)	α (mm)	VPD (mm hPa ⁻¹)	CO ₂ (mm ppm ⁻¹)
Observation	Estimation	0.713	0.057	1.574	-0.217	
	Standard error	±0.248	±0.148	±0.583	±0.125	
	<i>p</i> value	0.006	0.704	0.009	0.088	
Simulation with 360 ppm CO ₂	Estimation	0.827	-0.010	2.576	-0.065	
	Standard error	±0.069	±0.041	±0.161	±0.035	
	<i>p</i> value	<0.001	0.793	<0.001	0.058	
Observation	Estimation	0.729	0.060	1.649	-0.209	-0.001
	Standard error	±0.246	±0.150	±0.614	±0.127	±0.002
	<i>p</i> value	0.006	0.401	0.010	0.107	0.674
Simulation with actual CO ₂	Estimation	0.777	-0.005	2.329	-0.095	0.008
	Standard error	±0.060	±0.035	±0.144	±0.030	±0.000
	<i>p</i> value	<0.001	0.887	<0.001	0.003	<0.001
Time- dependent simulation with actual CO ₂	Estimation	0.868	0.120	2.317	-0.185	0.003
	Standard error	±0.078	±0.046	±0.189	±0.039	±0.000
	<i>p</i> value	<0.001	0.012	<0.001	<0.001	<0.001



Figure 1. An example of *Callitris collumellaris* sampled for tree-ring cores in the Great Western Woodlands, Western Australia.

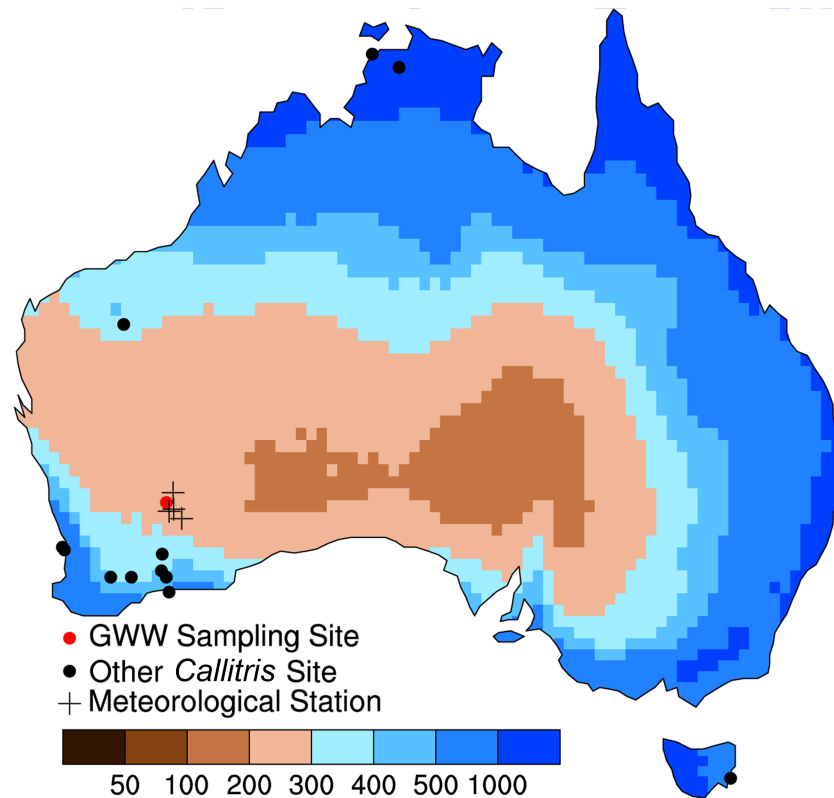


Figure 2. Location of the Great Western Woodlands sampling site, Western Australia. The underlying map shows mean annual precipitation (MAP). We also show the location of other sites across Australia where *Callitris* have been sampled (data from International Tree-Ring Data Bank), and the locations of the nearest meteorological stations to the sampling site.

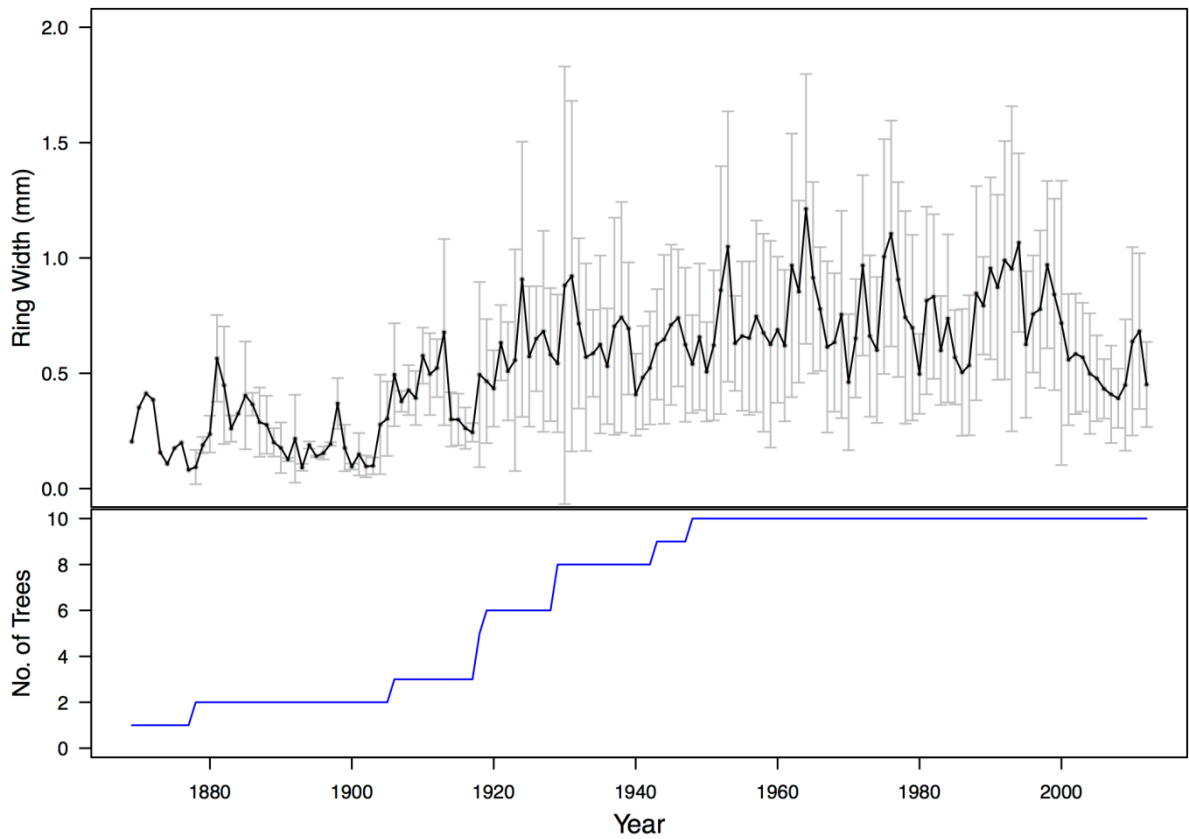


Figure 3. Interannual variability in tree-ring widths of *Callitris columellaris* from the Great Western Woodlands, Western Australia. In the top panel, the black line is the mean of the observations, and the grey bars show the standard deviation (SD) of the individual sampled trees. The blue line in the bottom panel shows the number of trees sampled for each interval.

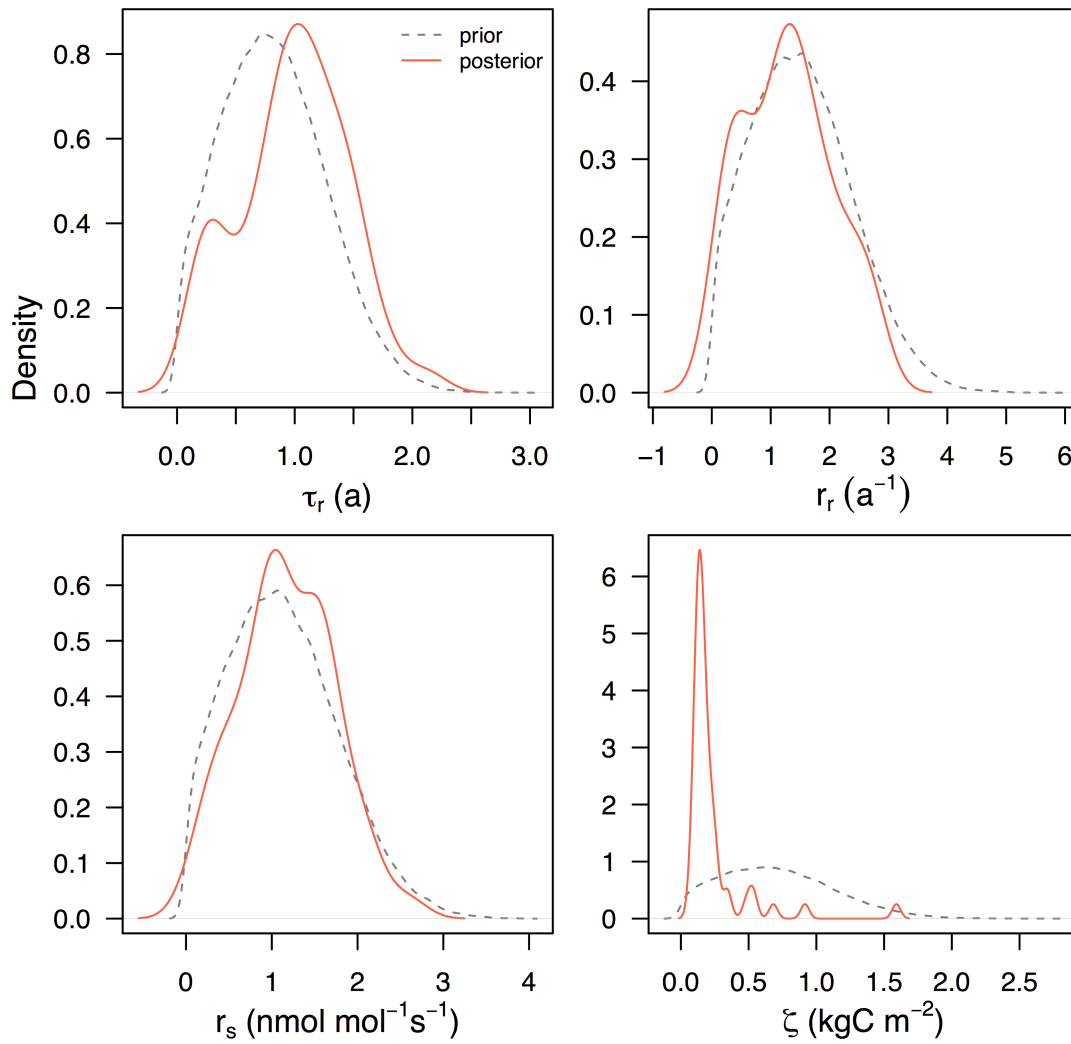


Figure 4. Prior (gray) and posterior (red) probability distribution function for fine-root turnover time (τ_r), fine-root specific respiration rate (r_r), sapwood-specific respiration rate (r_s); ratio of fine-root mass to foliage area (ζ).

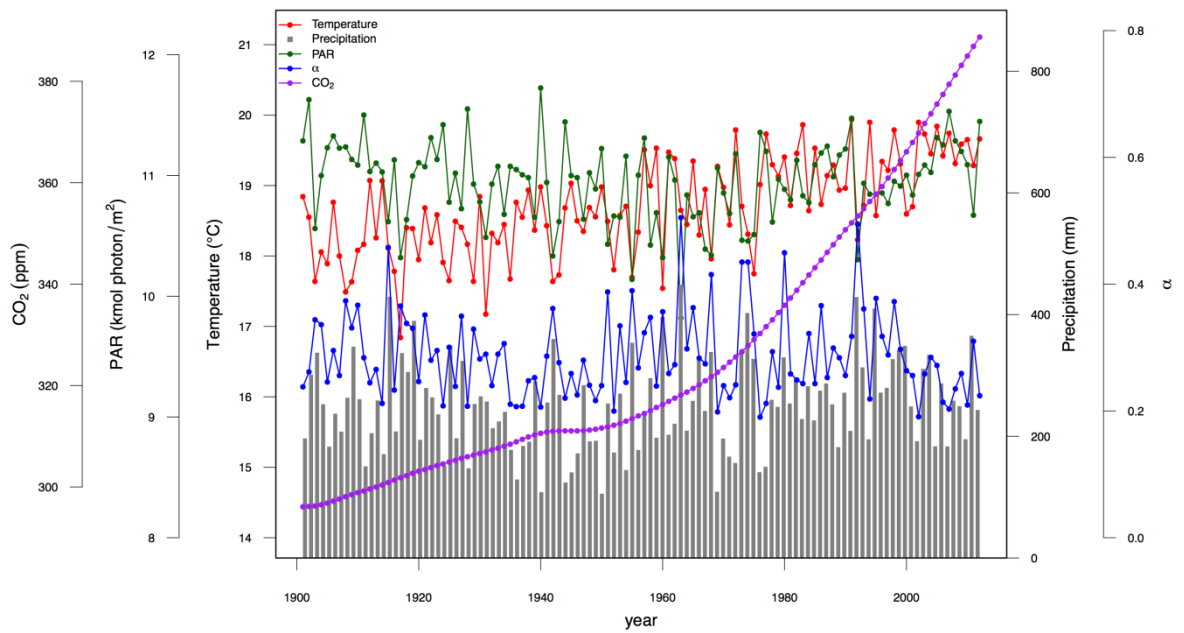


Figure 5. Climate at the Great Western Woodlands site. The plot shows mean annual temperature, precipitation, total incident photosynthetically active radiation (PAR_0), and the ratio of actual to equilibrium evapotranspiration (α). The observed changes in $[CO_2]$ are shown for comparison.

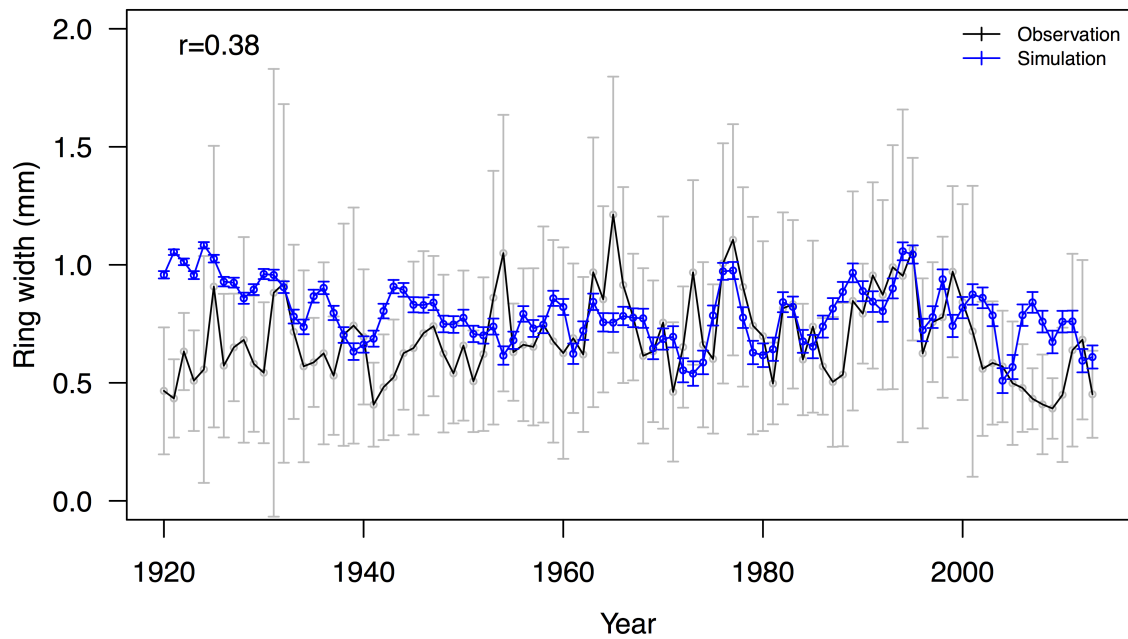


Figure 6. Comparison between simulated and observed tree ring widths, for the period 1920 to the present, with [CO₂] set at 360 ppm. The black line is the mean of the observations, and the grey bars are the standard deviation (SD) among the ten individual trees sampled. The blue line and bars are the mean and standard deviation for the ten simulated individual trees.

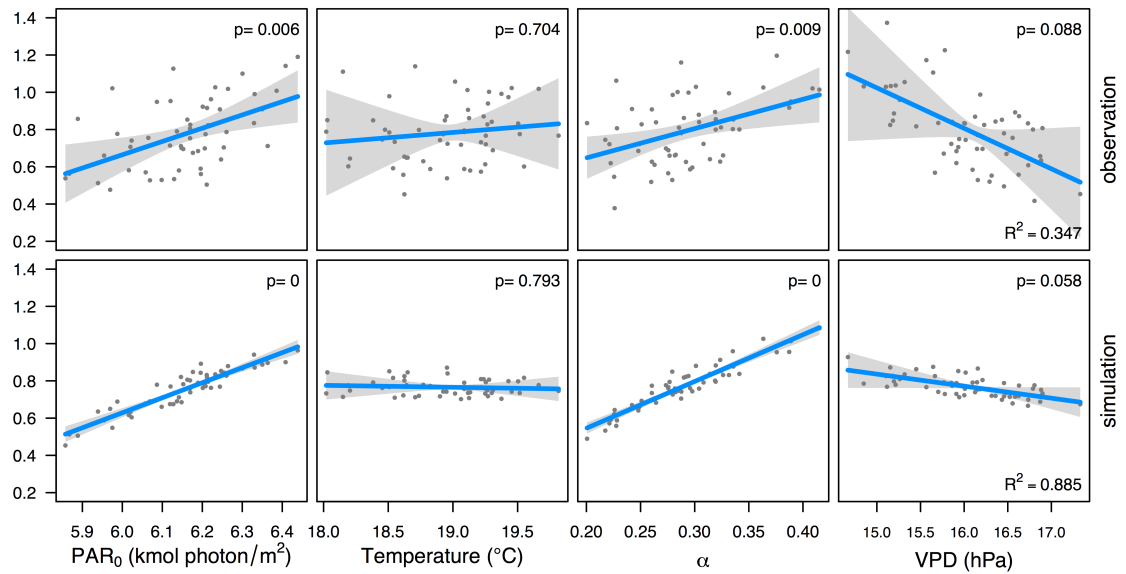


Figure 7. Simulated and observed responses of tree growth to climate: partial residual plots based on the regression analysis, obtained using the visreg package in R, are shown. The predictor variables are (a) total incident photosynthetically active radiation (PAR_0), mean annual temperature (MAT), the ratio of actual to potential evapotranspiration (α) and vapour pressure deficit (VPD).

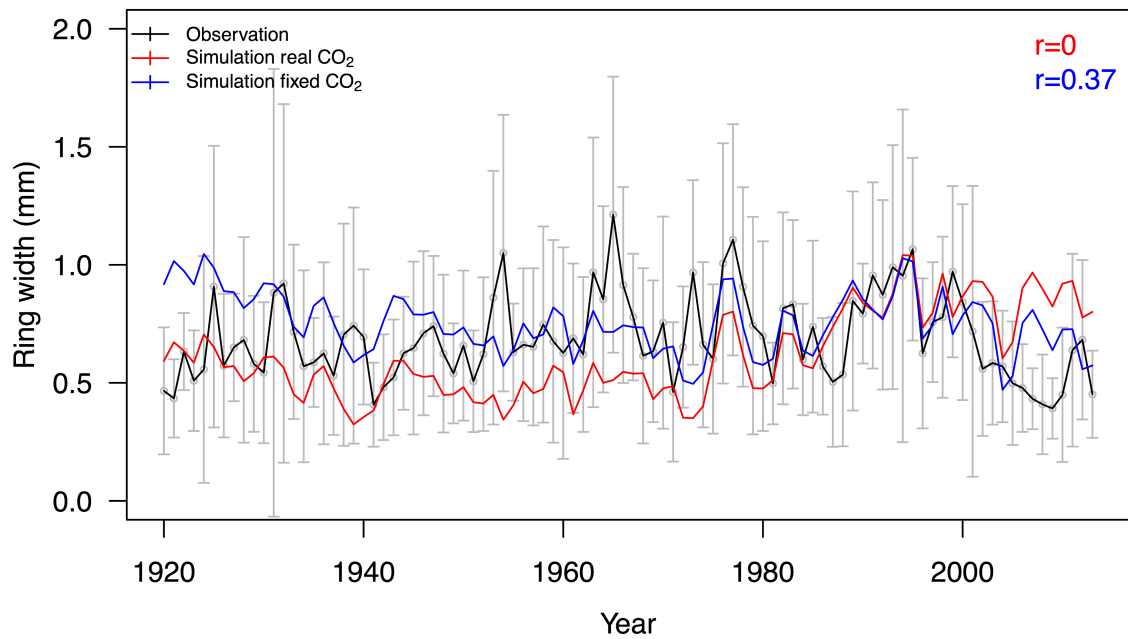


Figure 8. Comparison of simulated ring width in simulations with fixed (blue line) and time-varying (red line) [CO₂]. The black line is the mean of the observed ring widths, and the grey bars are the standard deviation (SD) among the ten individual trees sampled.

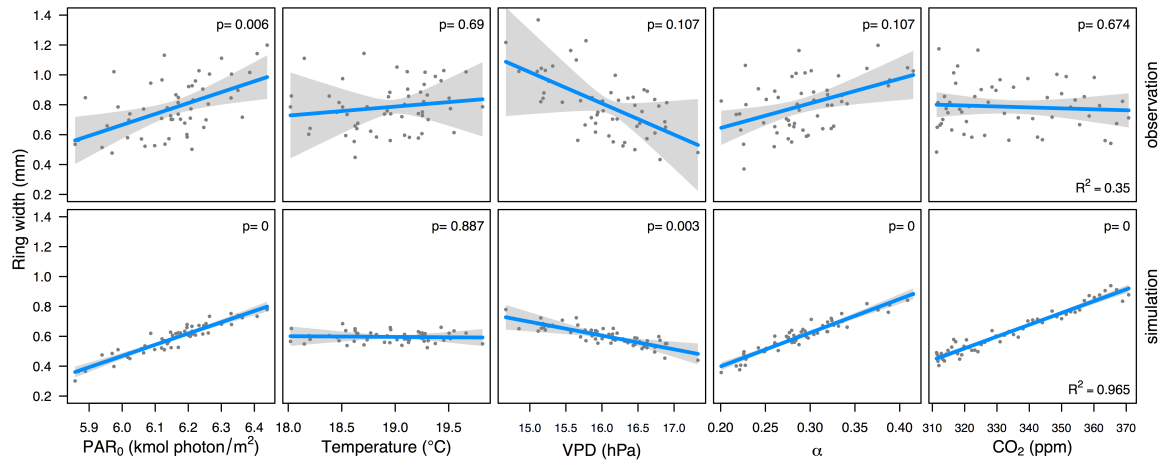


Figure 9. Simulated and observed response of tree radial growth to $[CO_2]$: partial residual plots based on the regression analysis, obtained using the visreg package in R, are shown. The dependent variable is mean ring width (from 1950 to 2012). The predictor variables are total incident photosynthetically active radiation (PAR_0), vapour pressure deficit (VPD), the ratio of actual to potential evapotranspiration (α), and monthly $[CO_2]$.

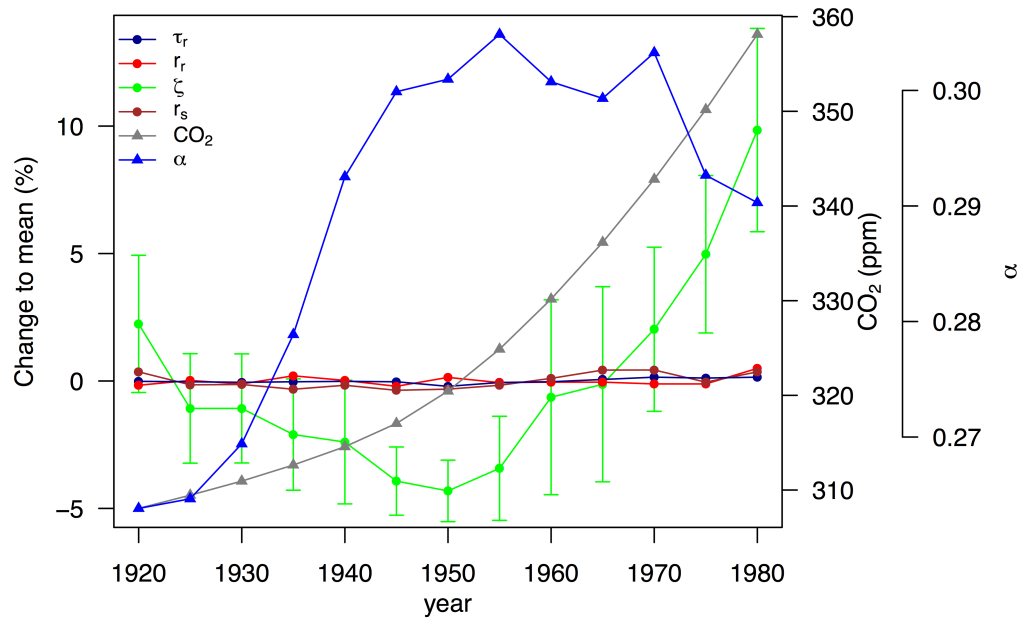


Figure 10. Time variation of the values of parameters estimated by Bayesian optimization. The graph shows the percentage change to the mean value of each of the parameters fine-root turnover time (τ_r), fine-root specific respiration rate (r_r), sapwood specific respiration rate (r_s) and the ratio of fine-root mass to foliage area (ζ) for 30-year moving windows since 1920, using the appropriate [CO₂] and α for each window. Values on the x-axis are plotted against the middle year of each 30-year moving window. The uncertainty estimates (bars) for the ratio of fine-root mass to foliage area (ζ) are the standard deviation of six 5-year sub-windows within each 30-year window.

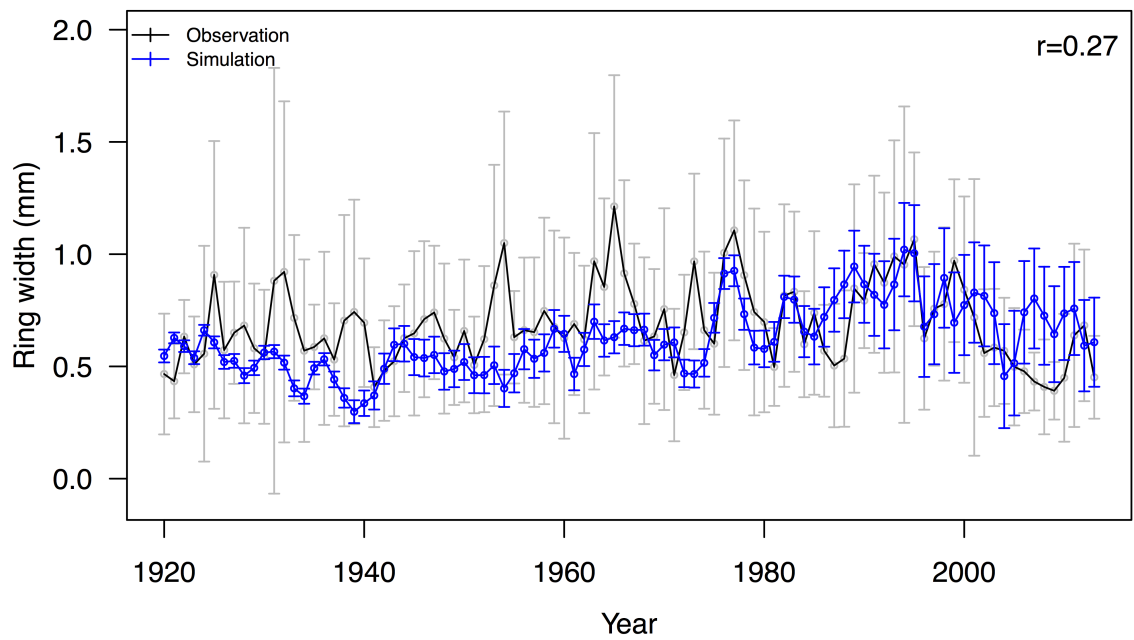


Figure 11. Simulation of radial growth in response to changing climate and observed [CO₂], allowing for the effect of changing allocation to fine roots. The black line is the mean of the observations, and the grey bars are the standard deviation (SD) among the ten individual trees sampled. The blue line and bars are the mean and standard deviation for the ten simulated individual trees.

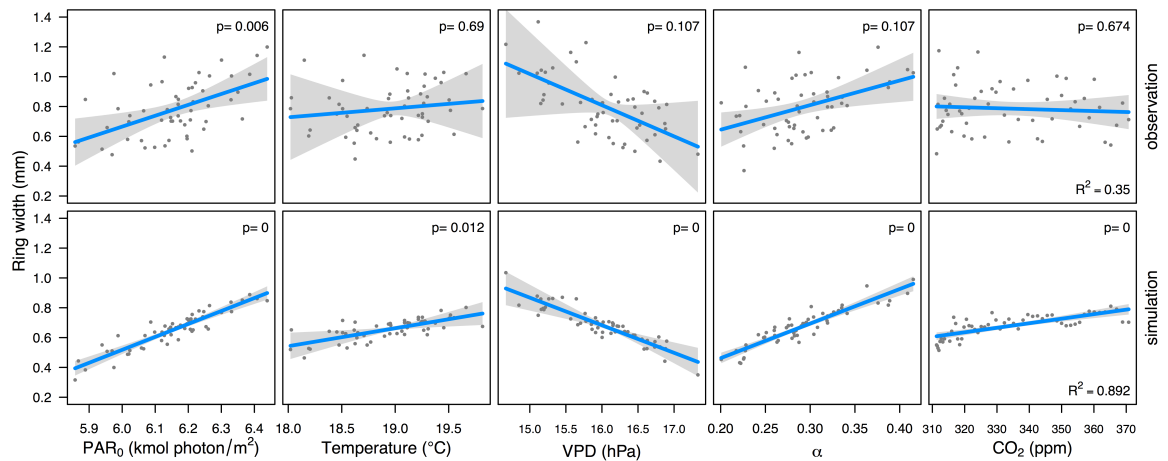


Figure 12. Simulated and observed response of tree radial growth to climate and [CO₂] based on the simulations in which the ratio of fine-root mass to foliage area (ζ) is allowed to vary. Partial residual plots based on the regression analysis, obtained using the visreg package in R, are shown. The dependent variable is mean ring width (from 1950 to 2012). The predictor variables are total incident photosynthetically active radiation (PAR₀), vapour pressure deficit (VPD), the ratio of actual to potential evapotranspiration (α), and monthly [CO₂].

Chapter 7

Allocation changes buffer CO₂ effect on tree growth since the last ice age

Contribution by Co-Authors: the plan for the research originated with I.C.P. and S.P.H; L. M. G. , and J. W. supplied the observations; G. L. was responsible for running the model experiments, data analysis, figure and table generation; G. L., S. P. H., I. C. P. were jointly responsible for interpretation of the data, G.L. and S.P.H. drafted the first version of the text and all authors contributed to the final version.

Allocation changes buffer CO₂ effect on tree growth since the last ice age

Guangqi Li¹, Laci M. Gerhart², Sandy P. Harrison^{1,3}, Joy Ward⁴ & I. Colin Prentice^{1,5}

- 1 Department of Biological Sciences, Macquarie University, North Ryde, NSW 2109, Australia
- 2 Biology Department, University of Hawai'i, West O'ahu, Kapolei, HI 96707, USA
- 3 School of Archaeology, Geography and Environmental Sciences (SAGES), Reading University, Reading, UK
- 4 Department of Ecology and Evolutionary Biology, University of Kansas, Lawrence, KS 66045, USA
- 5 AXA Chair of Biosphere and Climate Impacts, Grand Challenges in Ecosystem and the Environment, Department of Life Sciences and Grantham Institute – Climate Change and the Environment, Imperial College London, Silwood Park Campus, Buckhurst Road, Ascot SL5 7PY, UK

Correspondence to: G. Li (guangqi.li@students.mq.edu.au)

Ms for Nature Communication

Abstract

Isotopic measurements on junipers growing in southern California during the last glacial, when the ambient atmospheric [CO₂] (c_a) was ~180 ppm, show the leaf-internal [CO₂] (c_i) was close to the modern CO₂ compensation point for C₃ plants. Despite this, stem growth rates were similar to today. Using a coupled light-use efficiency and tree growth model, we show that the c_i/c_a ratio was stable because both vapor pressure deficit and temperature were decreased with compensating effects. Reduced photorespiration at lower temperatures partly mitigated the effect of low c_i on gross primary production, but maintenance of present-day radial growth also required a ~25% reduction in below-ground carbon allocation. Such a shift was possible due to reduced drought stress. This finding is consistent with increased

below-ground allocation, and the apparent homeostasis of radial growth, as c_a increases today.

Introduction

Fossil *Juniperus* spp wood specimens from the La Brea Tar Pits (34.06°N, 118.36°W, 80 m.a.s.l.) have been radiocarbon-dated to the second half of the last glaciation, between 55-22 kyr BP, an interval when the climate was globally ca 5-8° C colder than today¹ and CO₂ concentration was between 180-220 ppm². The fossil *Juniperus* samples from La Brea cannot be identified to species level³, but are assumed to be either *J. californica* or *J. occidentalis* based on modern species distribution⁴. Stable carbon isotope measurements on these specimens were used to estimate the ratio of leaf intercellular [CO₂] (c_i) to ambient [CO₂] (c_a) at the time of growth³. The c_i/c_a ratio during glacial times was similar to that found today^{3,4}, resulting in c_i values of only 100-120 ppm (i.e. close to the modern compensation point for C₃ plants, ~ 40-70 ppm). The low c_i values should imply a strong reduction in gross primary production (GPP). Nevertheless, remarkably, measurements of annual growth rate of these trees (as shown by the width of the annual rings) show that stem growth was similar to today.

Palaeoenvironmental evidence indicates that the climate of this region was both cooler and wetter than today^{5,6}. Pollen-based reconstructions show a cooling of 2-6° C in both summer and winter⁷. Mean annual precipitation was 100-300 mm more than today, as a result of circulation changes due to southward deflection of the Westerlies by the Laurentide Ice Sheet⁸⁻¹⁰. These changes in climate could potentially have compensated for the impact of low leaf-internal [CO₂] on GPP and growth, through the effect of lower temperature in reducing photorespiration (thus lowering the compensation point), and/or through reducing the potential loss of photosynthetic activity due to drought stress. However, it is not immediately clear whether these effects would have been sufficient to compensate for the reduction in GPP due to low c_i .

A growing body of evidence suggests that changing [CO₂] results in changes in carbon allocation between aboveground (leaf, stem) and underground (root) biomass

pools. Observations of the response to artificially high [CO₂] conditions in Free-Air Carbon Enrichment (FACE) experiments show that trees typically allocate more carbon below ground, in the form of increased root mass and increased exudates¹¹⁻¹⁷, often at the expense of stem growth¹⁸ (Battipaglia et al., 2013). The widespread failure to detect a response to increasing [CO₂] during the 20th century in many tree-ring records¹⁹⁻²¹ is consistent with the idea that increased productivity due to increased [CO₂] does not necessarily lead to increased stem growth and may be reflected in changes in allocation. Unfortunately, there are no observations of the allocation response to low [CO₂] in trees.

Here we use a generic light-use efficiency model, 'P'²² coupled to a species-specific carbon allocation model, 'T'²³ that has been shown to reproduce the observed growth response to climate and [CO₂] changes during the historic period in both cold, humid and warm semi-arid conditions^{23,24}, to investigate whether climate conditions and/or changes in allocation strategy facilitated the growth of junipers during the glacial at the La Brea site. Specifically, we investigate whether:

- (a) the growth of *Juniperus* at La Brea during the LGM necessitated a change in carbon allocation between leaves, stem and roots;
- (b) changes in allocation were facilitated by the known changes in regional climate.

Results

The c_i/c_a ratio of the fossil wood samples from La Brea dated to the glacial *sensu stricto* (55 – 22 kyr) is 0.51 ± 0.02 compared to values of 0.53 ± 0.05 for modern samples from six southern Californian sites^{3,4}. The modern sites are at higher elevations (630 to 2830 m a.s.l), because junipers do not grow at the elevation of La Brea today. The average ring width for the fossil specimens is 1.39 mm compared to 1.16 mm for the modern trees⁴. However, the range of individual values of both c_i/c_a and ring width is much larger than the range for the fossil specimens.

The modern records of *Juniperus* from sites near La Brea were primarily collected for isotopic measurements; some of these records are very short (< 50 years) and there are too few replicates to provide a well-founded record of the response of stem

growth to climate variability. We therefore used a record of *Juniperus occidentalis* from site CA640 (36.95°N, 118.92°W, 2630 m a.s.l.), which provides a cross-dated record of tree ring widths for the period 1903 to 1985²⁵, to test the performance of the coupled light-use efficiency and carbon allocation model (hereafter called PT). We use the age model for site CA640 provided by the original author²⁵. The PT model captures the observed amplitude and interannual variability of radial growth during this period (Figure 1). The simulated mean ring width is 0.73 mm compared to the observed average width of 0.79 mm, and the correlation between simulated and observed interannual variability is significant ($r = 0.50$, $p < 0.001$). The simulations and observations show consistent responses to different climate drivers (Appendix Figure 1). These include a significant positive correlation with photosynthetically active radiation (PAR) and [CO₂], a positive response to soil moisture (as measured by the ratio of actual to equilibrium evapotranspiration: α), a positive (though non-significant) response to temperature, and a negative response to vapour pressure deficit (VPD). The response to α and VPD is significant in the simulations but not in the observations, probably because these relationships are obscured by local factors in the real environment.

Simulated c_i is obtained from ambient [CO₂] via the “least-cost hypothesis”^{26,27}. The simulated c_i/c_a ratio decreases with elevation under modern conditions (Figure 2). This decline is partly a result of elevational changes in temperature, which decreases from 16.6° C at the lowest elevation to 6.7° C at the highest elevation, and partly due to the effect of decreasing air pressure on enzyme reaction rates and on the vapour pressure of water. The elevational effect is also apparent in the observations ($p < 0.001$), despite considerable noise in the data set (Figure 2). However, the similarity between observed glacial and modern c_i/c_a values is not because of differences in elevation. The glacial c_i/c_a ratio at La Brea and each of the modern sites, simulated using climate variables for the last glacial maximum (LGM, ca 21,000 years ago) from the Community Climate System Model Version 4 (CCSM4) climate model^{28,29} adjusted to account for the bias in the modern control simulation and interpolated to the appropriate elevation, is the same as today (Figure 2). The LGM c_i/c_a simulated at La Brea is 0.57 ± 0.01 , close to the value of 0.53 ± 0.01 obtained for the glacial sample closest to the LGM (22 kyr).

The known changes in regional climate at the LGM, specifically the year-round reduction in temperature and the decrease in aridity, would have opposite effects on c_i/c_a . According to the least-cost hypothesis (supported by field measurements in contrasting climates²⁷), the ‘pure’ effect of a decrease in temperature should be to decrease c_i/c_a while a wetter climate would imply reduced VPD, which should tend to increase c_i/c_a . Sensitivity tests, using either modern temperature with glacial VPD or glacial temperature with modern VPD, show that these two effects are of roughly equal magnitude and thus compensate for one another, resulting in almost no change in c_i/c_a compared to present (Figure 3). Thus, the similarity between c_i/c_a under modern and glacial conditions at La Brea appears to be a response to the relatively unusual combination of LGM changes in regional climate.

The low glacial c_i values (simulated values ~ 90 -110 ppm) result in simulated values of GPP under continuous vegetation cover of $3.8 \text{ kg C m}^{-2} \text{ a}^{-1}$. The simulated GPP at La Brea under modern climate is $4.3 \text{ kg C m}^{-2} \text{ a}^{-1}$, while simulated GPP under modern climate at the six higher-elevation sites ranges from 4.4 to $5.2 \text{ kg C m}^{-2} \text{ a}^{-1}$. The reduced GPP under glacial conditions would necessarily lead to a reduction in radial growth unless there was a shift in carbon allocation to the stem from some other pool. We used approximate Bayesian computation³⁰⁻³² to calibrate the T model for glacial climate conditions and lower [CO₂], using [CO₂] values between 320 to 160 ppm, and taking the observed glacial ring width of 1.83 mm as a target. These simulations (Figure 4) show that ring width can only be maintained by decreasing allocation both to leaves (as represented by leaf area index within the crown, L) and by decreasing root mass (as represented by the ratio of fine root mass to foliage area, ζ). At 180 ppm (i.e. the approximate level of CO₂ at 22 ka BP), the reduction in L is ca 7% and the reduction in ζ is ca 25% compared to values obtained with [CO₂] levels corresponding of the mean during the 20th century (320 ppm).

The simulated reduction in GPP already takes account of one impact of the colder glacial climate on primary production through the reduction of photorespiration at lower temperatures: the carbon cost through photorespiration would be $\sim 20\%$ more without this reduction. However, temperature also affects moisture supply through reducing saturated atmospheric vapour pressure and hence evapotranspiration. The reduction in temperature and increase in precipitation, and the implied increase in relative humidity, at the LGM in this region all have favourable impacts on moisture

supply – which could be of importance given the very large simulated reduction in root mass at the LGM. To examine the relative importance of each of these factors on radial growth at the LGM, we ran a series of sensitivity tests in which we substituted modern values of these variables separately and in combination (Figure 5) holding all other variables (including $[\text{CO}_2]$) at glacial values. When temperature is set to modern values, ring widths decrease by 46%. The effect of precipitation changes alone is smaller, leading to a reduction of ring widths by 17%. The combined impact of colder temperature, more precipitation and increased humidity is equivalent to a 67% increase in ring width. Although tree growth does not cease in these simulations, these experiments suggest that the regional changes in climate during the LGM played an important role in the maintenance of tree growth under low $[\text{CO}_2]$.

Discussion

Natural changes in radiative forcing and climate since the Last Glacial Maximum were as large as those projected to occur over the 21st century as a result of anthropogenic changes in greenhouse gas concentrations³³. Measurements on glacial fossil *Juniperus* wood provides a direct picture of tree growth after long-term adaptation to low $[\text{CO}_2]$ and glacial climate. The low temperature and low $[\text{CO}_2]$ during the glacial climate is the converse of modern changes towards high $[\text{CO}_2]$ and temperature and so we would expect biotic responses also to be opposite to those taking place today. Free-air Carbon dioxide Enrichment (FACE) experiments have shown increased root system biomass as a response to enhanced $[\text{CO}_2]$ (Oak Ridge FACE¹¹, DUKE-FACE^{12,13}, Rhinelander ASPEN-FACE¹⁴, EUROFACE^{15,16}, Bangor FACE³⁴). Increased carbon export to mycorrhiza or the rhizosphere could also be responsible for the increasing belowground allocation¹⁷. Either way, the response is presumably adaptive, reflecting the need for plants to acquire additional nutrients, most notably nitrogen, to support increased total net primary production that is made possible by higher photosynthetic rates under enhanced $[\text{CO}_2]$.

$[\text{CO}_2]$ has increased greatly since pre-industrial time (from 280 to 400 ppm). Increased photosynthesis is a universal response to enhanced $[\text{CO}_2]$ in C_3 plants; as is the enhancement of water use efficiency, due to increased photosynthesis

combined with reduced stomatal conductance, which has been identified through stable carbon isotope measurements in tropical forests²¹ and elsewhere²⁰. However, several studies including that of van der Sleen et al.²¹ have failed to show any concomitant increase in stem radial growth. A possible explanation mooted by van der Sleen et al. is increased below-ground carbon allocation²¹. The lack of a [CO₂] signal in the radial growth of trees has also been noted consistently in mid- to high-latitude regions^{19,35}. Model simulations for *Callitris* in the Great Western Woodland, Western Australia, where the trees also show no increase in ring width with increasing [CO₂], showed that a modest increase in the ratio of root mass to foliage area (ζ) is sufficient to account for the lack of a [CO₂] signal in ring widths²⁴. The phenomenon could not be explained by variation in any other parameter of the T model. Thus, it is plausible that allocation shifts – consistent with the increased nutrient requirements for growth under high [CO₂] and reduced requirements under low [CO₂] – could be causing an apparent homeostasis in the radial growth rates of trees with respect to [CO₂].

Methods

The PT model

Potential gross primary production (GPP) was simulated by a generic light-use-efficiency model (a modified version of the P model²²). The resulting GPP is allocated to foliage, transport tissue, and fine-root production and turnover via a geometric tree-growth model (T model²³) that has a limited number of species-specific parameters influencing the allocation of carbon to different compartments. Tree growth (including stem radial growth) is simulated on an annual basis.

Potential GPP is determined by the photosynthetically active radiation (PAR) incident on the vegetation canopy during the growing season (here defined as the period with temperatures above -1° C, consistent with observations that photosynthesis can occur at temperatures below 0° C in temperate climates: Larcher, 2003) controlled by the maximum quantum efficiency of photosynthesis (Φ_0), and CO₂ limitation effect ($c_i - \Gamma^*$)/($c_i + 2\Gamma^*$) via Equation 1:

$$\text{GPP} = \Phi_0 (\text{PAR} \times \text{fAPAR}) (c_i - \Gamma^*) / (c_i + 2\Gamma^*) \quad (1)$$

where Φ_0 is set to $0.816 \text{ g C mol}^{-1} \text{ photon}$, equivalent to a quantum efficiency of $0.085 \text{ mol C mol}^{-1} \text{ photon}^{22,36}$ and a leaf absorptance of 0.8. PAR is calculated based on solar geometry and is subsequently modified by atmosphere transmission, depending on elevation and cloud cover. The fraction of absorbed PAR (fAPAR) is set to 1 (complete vegetation cover) in the P model.

In the modified version of the P model, the effects of photorespiration and substrate limitation at subsaturating $[\text{CO}_2]$ are represented as a function of the leaf-internal $[\text{CO}_2]$ (c_i) and the photorespiratory compensation point (Γ^*). c_i is obtained from

$$c_i/c_a = \xi / (\xi + \sqrt{D}), \quad (2)$$

where D is a measure of atmospheric moisture (represented by the vapour pressure deficit, VPD) and ξ is the stomatal sensitivity. ξ is obtained from:

$$\xi = \sqrt{(\beta K / (1.6\eta^*))}, \quad (3)$$

where β is the ratio of unit costs for carboxylation and transpiration at 25°C ; K is the effective Michaelis–Menten coefficient for Rubisco-limited photosynthesis, depending on temperature, atmospheric pressure and oxygen concentration; η^* is the viscosity correction factor (the ratio of the viscosity of water at current temperature to that at 25°C).

The photorespiratory compensation point (Γ^*) is controlled by temperature, and described by an exponential closely approximating an Arrhenius function:

$$\Gamma^* = \Gamma_{25}^* \exp(0.0512\Delta T) \quad (4)$$

where Γ_{25}^* is the value of Γ^* at 25°C (4.331 Pa), and ΔT is the temperature difference from 25°C .

GPP is further modified by a factor $(\alpha/1.26)^{1/4}$ (α is the ratio of actual to equilibrium evapotranspiration) to account for GPP reduction due to drought.

GPP from the modified P model is used as input to the T model. In this model, the fraction of incident PAR absorbed by the canopy (fAPAR) is estimated from the leaf area index within the canopy and used to convert potential to actual GPP using Beer's law. Annual net primary production (NPP) is derived from annual GPP, corrected for foliage respiration, by deducting growth respiration (assumed to be proportional to NPP) and the maintenance respiration of sapwood and fine roots. NPP is allocated to stem, foliage and fine-root increments, foliage turnover and fine-root turnover. Carbon is allocated to different tissues within the constraint of the basic functional or geometric relationships between different dimensions of the tree, including asymptotic height-diameter trajectories. A full description of the T model is given in Li et al. (2014)²³.

The T model requires 11 species-specific parameters to be specified. Appropriate values for *Juniperus* were originally derived from the literature (appendix Table 1). Parameters for which there were no observations on *Juniperus* were optimized using neural-network Bayesian parameter optimization^{30,31}. The calibration objective was to minimize the absolute difference between modelled and observed mean tree-ring width at site CA640 (36.95°N, 118.92°W, 2630 m a.s.l.) during the period 1930-1980, constrained by ensuring that there were no negative growth rates of any model component, and the criterion for convergence was a difference of no more than $\pm 2.5\%$ of the mean value. The prior of each parameter was based on the median of the published values for *Juniperus* (where available) or evergreen needle-leaved trees (where no values for *Juniperus* were available), and the standard deviation was set to half of the median value.

The T model accumulates carbon over an effective growing season, here set to 2 years commencing from the middle of the year two years before the year of tree-ring formation (July of -2 year to June of current year) following the treatment for water-limited species described in Li et al. (2015)²⁴. We checked that this treatment was appropriate for juniper in this region using an ordinary least-squares multiple linear regression of driving climate variables (total annual photosynthetically active radiation: PAR, mean annual temperature: MAT, the ratio of actual to potential evapotranspiration: α , vapour pressure deficit: VPD, and [CO₂]) accumulated over varying periods of time against mean tree-ring width from CA640 during the period

from 1930-1980. This analysis confirmed that the 2-year accumulation period was appropriate and correlations were significantly worse for either longer or shorter intervals.

Climate and CO₂ input: modern

Climate data for the CA640 site was obtained from 0.5° CRU TS v3.22 data set³⁷, which provides time series of mean monthly temperature, diurnal temperature range, precipitation, vapour pressure and cloudiness. It is not possible to discriminate the elevations of the modern southern Californian sites at this resolution. We therefore derived an elevational correction factor for each monthly climate variable using the modern climatology data from the 10' CRU CL 2.0³⁸ and applied this to the times series data to derive interannually-varying climate values at the appropriate elevation of each site. Modern [CO₂] observations are based on merging ice-core records for the interval from 1901 to 1957^{39,40} and the yearly average of direct atmospheric measurements from Mauna Loa and the South Pole stations from 1958 to 2013 (http://scrippsco2.ucsd.edu/data/merged_ice_core/merged_ice_core_yearly.csv).

Climate and CO₂ input: LGM

We used model outputs from a Last Glacial Maximum (LGM, 21,000 years ago) and a control simulation (piControl) run with the The Community Climate System Model Version 4 (CCSM4) following the PMIP3/CMIP5 protocol (<https://pmip3.lsce.ipsl.fr/>). This is an equilibrium simulation with fixed values of CO₂ throughout (180 ppm) and thus the interannual variability is not forced but reflects internal variability. The simulated times series of LGM monthly climate was corrected, to remove the potential difference between the piControl and the modern climate at each site, by adding the difference between the longterm mean of the last 100 years of the piControl and the elevation-adjusted climatology between 1961-1990 at each site to the LGM times series. Glacial [CO₂] are from the Taylor Dome ice-core records⁴¹.

Simulations

The PT model was run using inputs of monthly climate and annual changes in CO₂. The simulations were run with varying climate and CO₂ from 1903-1985. Information about the diameter of the modern trees used to construct the CA640 record at the time of sampling is not available. However, all of the sampled tree used to construct the chronology were at least 200 years old in 1985, and thus over 100 years old in 1903. We therefore initialized the T model component of the simulations with a diameter of 0.3 m, corresponding to a reasonable diameter for a mature tree of this genus.

The calculations of simulated c_i/c_a under modern day conditions, at the elevation of the La Brea Tar Pit and for each of the southern Californian sites, were made for the period of 1951-2000. This interval was chosen to maximize comparability with the observed values of c_i/c_a at the southern Californian sites. The calculation of simulated c_i/c_a under glacial conditions was made using the last 100 years of the LGM simulation. Given that this is an equilibrium simulation, the different length of the averaging period between LGM and modern makes no difference to the comparison. In addition to the LGM simulation, we ran two sensitivity tests in which we used (a) modern monthly temperatures with glacial monthly VPD and (b) glacial monthly temperatures with modern monthly VPD. These are the only two climate variables that impact the calculation of c_i/c_a in the P model. The impact of the small change in elevation between LGM and present (~ 120 m) is negligible for these calculations.

The simulations to test the sensitivity of radial growth to individual climate variables were run by perturbing monthly temperature, precipitation and relative humidity singly and in combination. In each test, the modern values of the variable were substituted for the glacial values, holding all other variables including [CO₂] at glacial values.

References

- 1 Members, N. P. High-resolution record of Northern Hemisphere climate extending into the last interglacial period. *Nature* **431**, 147-151 (2004).
- 2 members, E. c. Eight glacial cycles from an Antarctic ice core. *Nature* **429**, 623-628 (2004).

- 3 Ward, J. K. *et al.* Carbon starvation in glacial trees recovered from the La Brea tar pits, southern California. *Proceedings of the National Academy of Sciences of the United States of America* **102**, 690-694 (2005).
- 4 Gerhart, L. M., Harris, J. M., Nippert, J. B., Sandquist, D. R. & Ward, J. K. Glacial trees from the La Brea tar pits show physiological constraints of low CO₂. *New Phytologist* **194**, 63-69 (2012).
- 5 Thompson, R. S., Whitlock, C., Bartlein, P. J., Harrison, S. P. & Spaulding, W. G. Climate changes in the western United States since 18,000 yr BP, in *Global Climates since the Last Glacial Maximum*, 468-513 (University of Minnesota Press, Minneapolis, 1993).
- 6 Clark, P. U. *et al.* The Last Glacial Maximum. *Science* **325**, 710-714 (2009).
- 7 Bartlein, P. J. *et al.* Pollen-based continental climate reconstructions at 6 and 21 ka: a global synthesis. *Climate Dynamics* **37**, 775-802 (2011).
- 8 Members, C. Climatic changes of the last 18,000 years: observations and model simulations. *Science* **241**, 1043-1052 (1988).
- 9 Kageyama, M. & Valdes, P. J. Impact of the North American ice-sheet orography on the Last Glacial Maximum eddies and snowfall. *Geophysical Research Letters* **27**, 1515-1518 (2000).
- 10 Ullman, D. J., LeGrande, A. N., Carlson, A. E., Anslow, F. S. & Licciardi, J. M. Assessing the impact of Laurentide Ice Sheet topography on glacial climate. *Climate of the Past* **10**, 487-507 (2014).
- 11 Norby, R. J., Ledford, J., Reilly, C. D., Miller, N. E. & O'Neill, E. G. Fine-root production dominates response of a deciduous forest to atmospheric CO₂ enrichment. *Proceedings of the National Academy of Sciences of the United States of America* **101**, 9689-9693 (2004).
- 12 DeLucia, E. H. *et al.* Net primary production of a forest ecosystem with experimental CO₂ enrichment. *Science* **284**, 1177-1179 (1999).
- 13 Pritchard, S. G. *et al.* Fine root dynamics in a loblolly pine forest are influenced by free-air-CO₂-enrichment: A six-year-minirhizotron study. *Global Change Biology* **14**, 588-602 (2008).
- 14 King, J. *et al.* Fine-root biomass and fluxes of soil carbon in young stands of paper birch and trembling aspen as affected by elevated atmospheric CO₂ and tropospheric O₃. *Oecologia* **128**, 237-250 (2001).

- 15 Calfapietra, C. *et al.* Free-air CO₂ enrichment (FACE) enhances biomass production in a short-rotation poplar plantation. *Tree Physiology* **23**, 805-814 (2003).
- 16 Lukac, M., Calfapietra, C. & Godbold, D. L. Production, turnover and mycorrhizal colonization of root systems of three *Populus* species grown under elevated CO₂ (POPFACE). *Global Change Biology* **9**, 838-848 (2003).
- 17 Godbold, D. L. *et al.* Elevated atmospheric CO₂ affects ectomycorrhizal species abundance and increases sporocarp production under field conditions. *Forests* **6**, 1256-1273 (2015).
- 18 Battipaglia, G. *et al.* Elevated CO₂ increases tree-level intrinsic water use efficiency: insights from carbon and oxygen isotope analyses in tree rings across three forest FACE sites. *New Phytologist* **197**, 544-554 (2013).
- 19 Gedalof, Z. & Berg, A. A. Tree ring evidence for limited direct CO₂ fertilization of forests over the 20th century. *Global Biogeochemical Cycles* **24** (2010).
- 20 Andreu-Hayles, L. *et al.* Long tree-ring chronologies reveal 20th century increases in water-use efficiency but no enhancement of tree growth at five Iberian pine forests. *Global Change Biology* **17**, 2095-2112 (2011).
- 21 van der Sleen, P. *et al.* No growth stimulation of tropical trees by 150 years of CO₂ fertilization but water-use efficiency increased. *Nature Geoscience* **8**, 24-28 (2015).
- 22 Wang, H., Prentice, I. & Davis, T. Biophysical constraints on gross primary production by the terrestrial biosphere. *Biogeosciences* **11**, 5987-6001 (2014).
- 23 Li, G., Harrison, S., Prentice, I. & Falster, D. Simulation of tree-ring widths with a model for primary production, carbon allocation, and growth. *Biogeosciences* **11**, 6711-6724 (2014).
- 24 Li, G., Harrison, S. P. & Prentice, I. C. A model analysis of climate and CO₂ controls on tree growth in a semi-arid woodland. *Biogeosciences Discussions* **12**, 4769-4800 (2015).
- 25 Graumlich, L. J. A 1000-year record of temperature and precipitation in the Sierra Nevada. *Quaternary Research* **39**, 249-255 (1993).
- 26 Wright, I. J. & Westoby, M. Leaves at low versus high rainfall: coordination of structure, lifespan and physiology. *New Phytologist* **155**, 403-416 (2002).
- 27 Prentice, I. C., Dong, N., Gleason, S. M., Maire, V. & Wright, I. J. Balancing the costs of carbon gain and water transport: testing a new theoretical framework for plant functional ecology. *Ecology Letters* **17**, 82-91 (2014).
- 28 Gent, P. R. *et al.* The community climate system model version 4. *Journal of Climate* **24**, 4973-4991 (2011).

- 29 Brady, E. C., Otto-Bliesner, B. L., Kay, J. E. & Rosenbloom, N. Sensitivity to glacial forcing in the CCSM4. *Journal of Climate* **26**, 1901-1925 (2013).
- 30 Jaakkola, T. S. & Jordan, M. I. Bayesian parameter estimation via variational methods. *Statistics and Computing* **10**, 25-37 (2000).
- 31 Pelikan, M. Bayesian optimization algorithm, in *Hierarchical Bayesian Optimization Algorithm*, 31-48 (Springer, Berlin, Heidelberg, 2005).
- 32 van der Vaart, E., Beaumont, M. A., Johnston, A. S. & Sibly, R. M. Calibration and evaluation of individual-based models using Approximate Bayesian Computation. *Ecological Modelling* **312**, 182-190 (2015).
- 33 Braconnot, P. *et al.* Evaluation of climate models using palaeoclimatic data. *Nature Climate Change* **2**, 417-424 (2012).
- 34 Smith, A. R., Lukac, M., Bambrick, M., Miglietta, F. & Godbold, D. L. Tree species diversity interacts with elevated CO₂ to induce a greater root system response. *Global change biology* **19**, 217-228 (2013).
- 35 Kienast, F. & Luxmoore, R. J. Tree-ring analysis and conifer growth responses to increased atmospheric CO₂ levels. *Oecologia* **76**, 487-495 (1988).
- 36 Collatz, G. J., Berry, J. A. & Clark, J. S. Effects of climate and atmospheric CO₂ partial pressure on the global distribution of C₄ grasses: present, past, and future. *Oecologia* **114**, 441-454 (1998).
- 37 Harris, I., Jones, P., Osborn, T. & Lister, D. Updated high-resolution grids of monthly climatic observations—the CRU TS3. 10 Dataset. *International Journal of Climatology* **34**, 623-642 (2014).
- 38 New, M., Lister, D., Hulme, M. & Makin, I. A high-resolution data set of surface climate over global land areas. *Climate Research* **21**, 1-25 (2002).
- 39 Etheridge, D. *et al.* Natural and anthropogenic changes in atmospheric CO₂ over the last 1000 years from air in Antarctic ice and firn. *Journal of Geophysical Research: Atmospheres* **101**, 4115-4128 (1996).
- 40 MacFarling Meure, C. *et al.* Law Dome CO₂, CH₄ and N₂O ice core records extended to 2000 years BP. *Geophysical Research Letters* **33** (2006).
- 41 Indermühle, A., Monnin, E., Stauffer, B., Stocker, T. F. & Wahlen, M. Atmospheric CO₂ concentration from 60 to 20 kyr BP from the Taylor Dome ice core, Antarctica. *Geophysics Research Letter* **27**, 735-738 (2000).

Figure captions

Figure 1. Comparison between simulated and observed *Juniperus occidentalis* ring widths, for the period 1903 to 1987, from site CA640 (36.95°N, 118.92°W, 2630 m. a.s.l.). The black line is the mean of observations and the grey bars are the standard deviation (SD) between trees. The red line is the mean from the simulations.

Figure 2. Changes in c_i/c_a with elevation. The left panel show the simulated c_i/c_a at La Brea and the southern Californian sites under modern (red) and glacial (blue) conditions. The bar shows the two standard deviations for each site during the simulation period (50 years for modern, 100 years for glacial). Lower right panel shows the observed c_i/c_a from modern trees (all values for the period 1951-2000, red) and the 22 ka BP fossil sample from La Brea (blue). The red line shows the linear regression between observed modern c_i/c_a and elevation.

Figure 3. Simulated impact of the separate effects of temperature and vapour pressure deficit (VPD) on c_i/c_a under glacial conditions.

Figure 4. The impact of [CO₂] on carbon allocation. The results show the impact of Bayesian tuning using glacial climate variables and different levels of [CO₂] between 320 and 160 ppm. ζ is the ratio of fine-root mass to foliage area; L is leaf area index within the crown.

Figure 5. Impact of individual climate variables on simulated glacial ring widths, where each experiment is run by imposing modern values for a variable or combination of variables and all other variables (including CO₂) are held at glacial values. The bars show the percentage change in simulated ring width between each experiment and the baseline glacial simulation. H has modern relative humidity; P has modern precipitation; T has modern temperature; TP has both modern temperature and precipitation; TPH has modern temperature, precipitation and relative humidity. In the final experiment (Full) all of the climate variables are modern and only CO₂ is set to glacial levels.

Figure 1. Comparison between simulated and observed *Juniperus occidentalis* ring widths, for the period 1903 to 1987, from site CA640 (36.95°N, 118.92°W, 2630 m. a.s.l.). The black line is the mean of observations and the grey bars are the standard deviation (SD) between trees. The red line is the mean from the simulations.

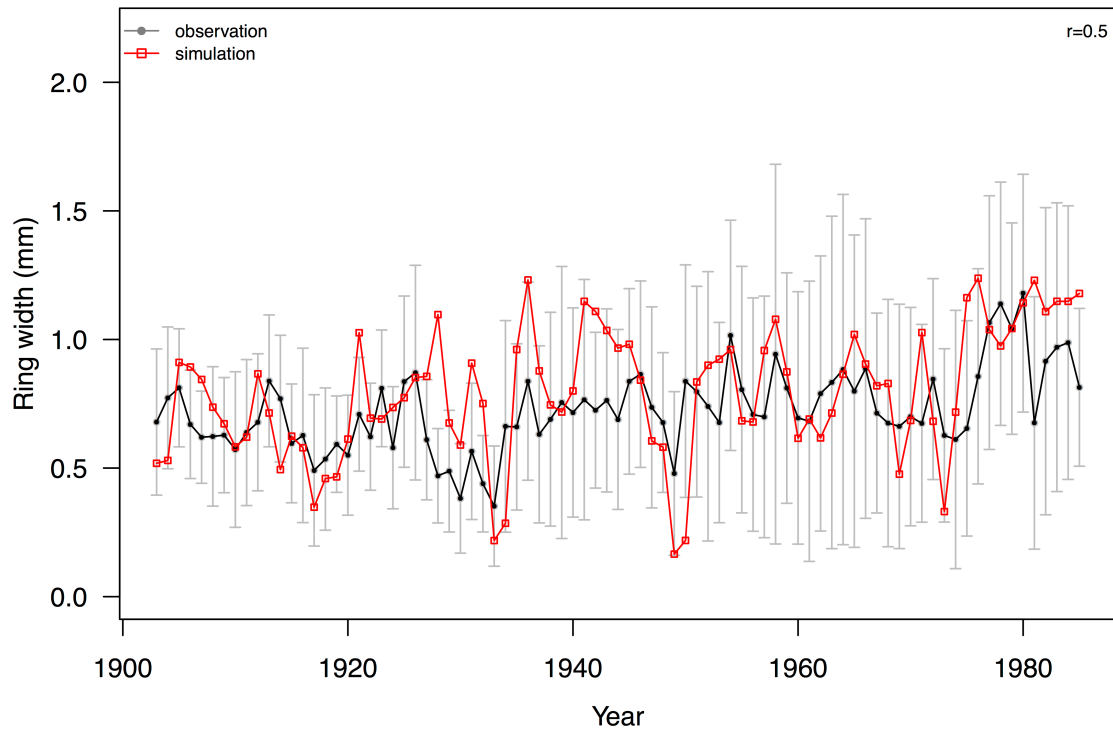


Figure 2. Elevational distribution of $c_i:c_a$. Upper panel is the model simulated mean $c_i:c_a$ along elevation gradient both in the modern (1951-2000, red), and in the Last Glacial Maximum (100 year, blue). The bar is the range of 2 SD for each site during the simulation period (1951-2000 for modern, last 100 year of LGM). Lower panel is the observed $c_i:c_a$ from 15 modern trees (value for period of 1951-2000) and 1 fossil tree (~22.0 ka BP). Red line is the linear regression line between observed modern $c_i:c_a$ and elevation.

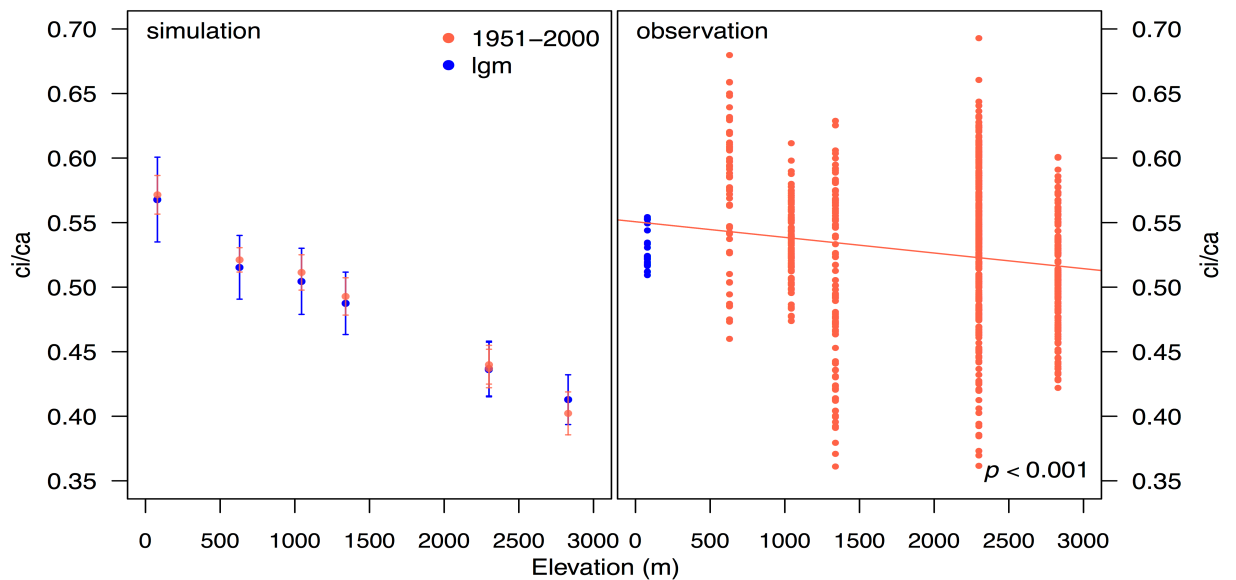


Figure 3. Simulated impact of the separate effects of temperature and vapour pressure deficit (VPD) on c_i/c_a under glacial conditions.

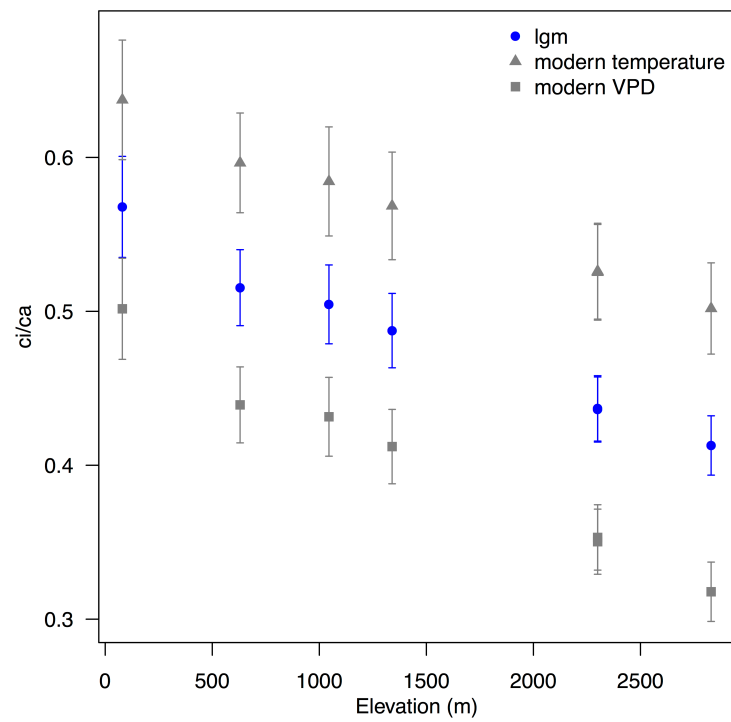


Figure 4. The impact of [CO₂] on carbon allocation. The results show the impact of Bayesian tuning using glacial climate variables and different levels of [CO₂] between 320 and 160 ppm. ζ is the ratio of fine-root mass to foliage area; L is leaf area index within the crown.

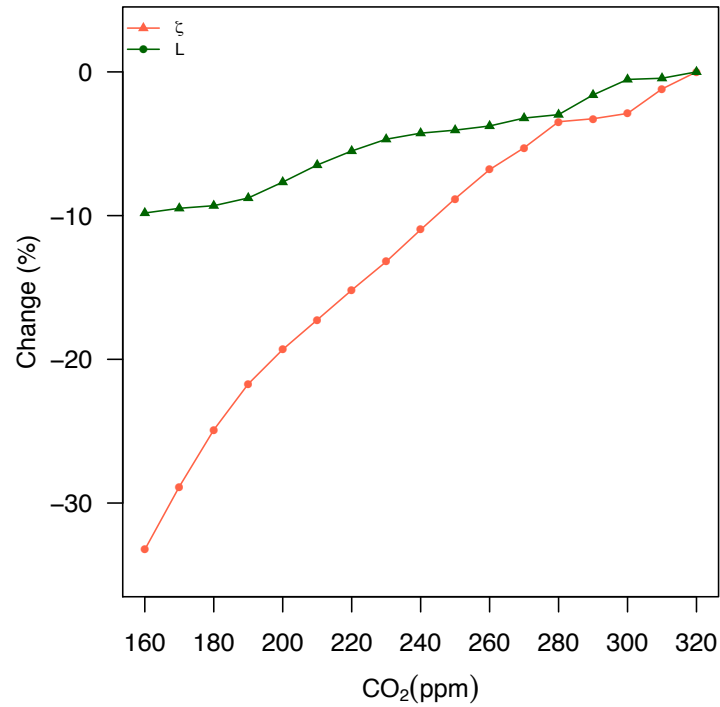
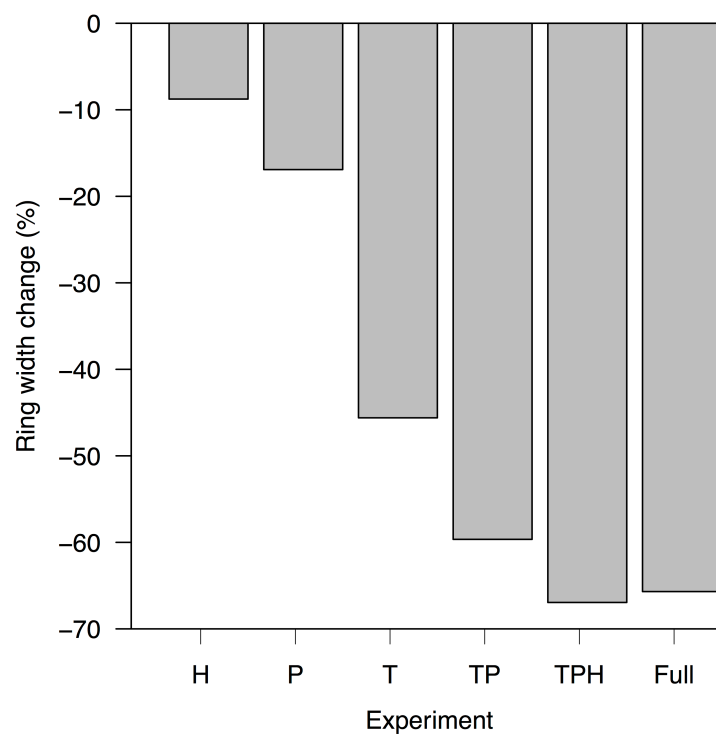


Figure 5. Impact of individual climate variables on simulated glacial ring widths, where each experiment is run by imposing modern values for a variable or combination of variables and all other variables (including CO₂) are held at glacial values. The bars show the percentage change in simulated ring width between each experiment and the baseline glacial simulation. H has modern relative humidity; P has modern precipitation; T has modern temperature; TP has both modern temperature and precipitation; TPH has modern temperature, precipitation and relative humidity. In the final experiment (Full) all of the climate variables are modern and only CO₂ is set to glacial levels.



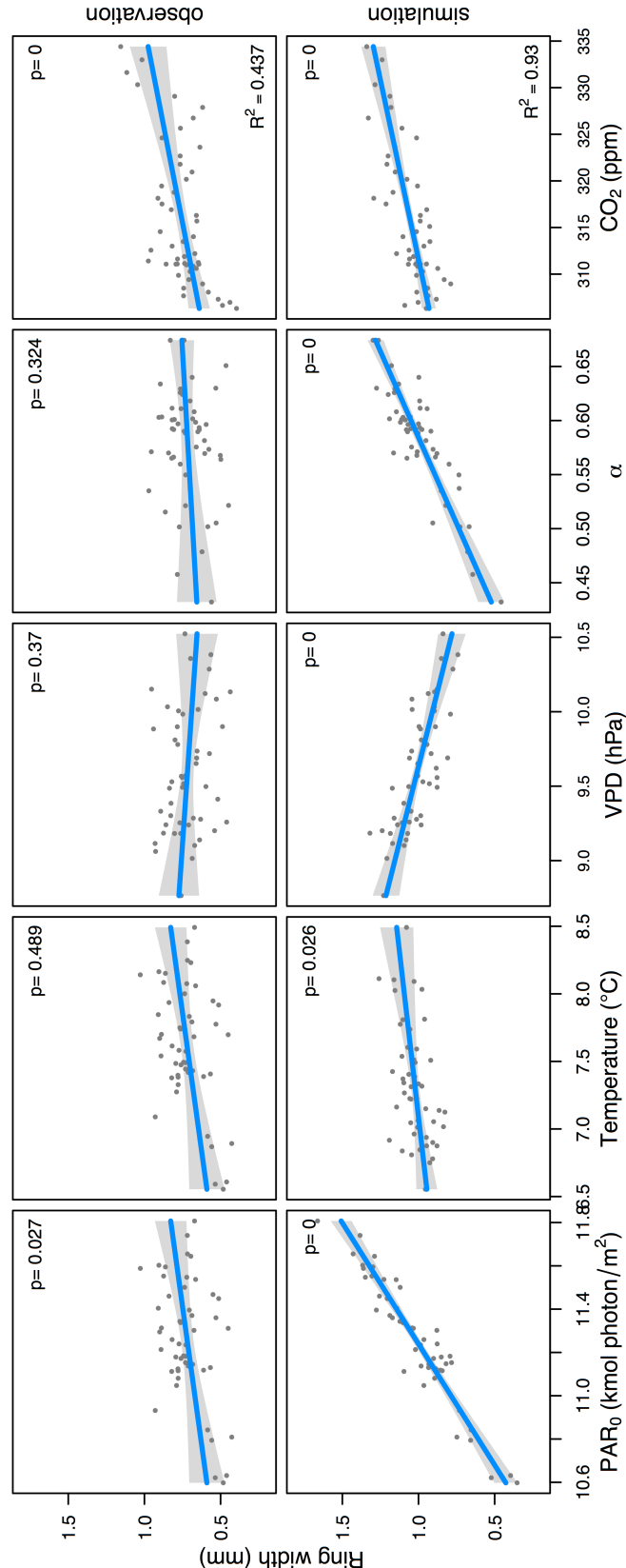
Appendix:

Table1 Bayesian parameter optimization for *Juniperus* in site CA640 (36.95°N, 118.92°W, 2630 m a.s.l.)

Parameter	Code	Value from literature	Species	Prior value	Posterior value	Accepted value
initial slope of height-diameter relationship (–)	a	–	–	60±30	72.24±25.27	72.24
initial ratio of crown area to stem cross-sectional area (–)	c	–	–	500±250	467.10±213.80	467.1
maximum tree height (m)	H _m	–	–	12±6	12.03±4.68	12.03
sapwood density (kgC m ⁻³)	ρ _s	250	<i>Juniperus</i> spp.	–	–	250
specific leaf area (m ² kg ⁻¹ C)	σ	6.54 ~ 7.76 ¹ , 5.6 ~ 6.54 ¹	<i>Juniperus ashei</i> , <i>Juniperus erythrocarpa</i>	–	–	6.54
leaf area index within the crown (–)	L	1.5~12.5 ¹	<i>Juniperus erythrocarpa</i>	–	–	6
foliage turnover time (year)	τ _f	6.5, 8.23 ²	<i>Juniperus monosperma</i>	–	–	7
fine-root turnover time (year)	τ _r	0.76±0.063 ³	<i>Juniperus osteosperma</i>	–	–	1
fine-root specific respiration rate (yea ⁻¹)	r _r	1.364 ⁴	<i>Juniperus monosperma</i>	–	–	1.364
sapwood specific respiration rate (nmol mol ⁻¹ s ⁻¹)	r _s	0.5~10 (20) ⁵	Evergreen needle-leaved tree	1±0.5	1.013±0.471	1.013
ratio of fine-root mass to foliage area (kgC m ⁻²)	ζ	0.17 ⁶	Evergreen needle-leaved tree	0.1±0.15	0.171±0.017	0.171

- Owens, M. & Ansley, J. Ecophysiology and growth of Ashe and redberry juniper. in *Juniper Symposium*, 19-31 (Texas A&M University, San Angelo, Texas, 1997).
- Reich, P. B. *et al.* Generality of leaf trait relationships: a test across six biomes. *Ecology* **80**, 1955-1969 (1999).
- Peek, M. S. *et al.* Root turnover and relocation in the soil profile in response to seasonal soil water variation in a natural stand of Utah juniper (*Juniperus osteosperma*). *Tree Physiology* **26**, 1469-1476 (2006).
- Burton, A., Pregitzer, K., Ruess, R., Hendrick, R. & Allen, M. Root respiration in North American forests: effects of nitrogen concentration and temperature across biomes. *Oecologia* **131**, 559-568 (2002).
- Landsberg, J. J. & Sands, P. *Physiological Ecology of Forest Production: Principles, Processes and Models*. (Academic Press, London, 2010).
- White, M. A., Thornton, P. E., Running, S. W. & Nemani, R. R. Parameterization and sensitivity analysis of the BIOME-BGC terrestrial ecosystem model: net primary production controls. *Earth Interactions* **4**, 1-85 (2000).

Figure 1. Simulated and observed response of tree radial growth to climate and [CO₂]: partial residual plots based on the regression analysis, obtained using the visreg package in R, are shown. The dependent variable is time series mean ring width of *Juniperus occidentalis* from site CA640 (36.95°N, 118.92°W, 2630 m a.s.l.) from 1903 to 1985. The predictor variables are total incident photosynthetically active radiation (PAR₀), mean annual temperature, vapour pressure deficit (VPD), the ratio of actual to potential evapotranspiration (α), and [CO₂] during the growing season.



Conclusions and Directions for Future Work

Conclusions and Directions for Future Work

Simulations of the historic period and future climate projections all show that precipitation increases with increasing temperature, though at less than the rate prediction by the Clausius-Clapeyron relationship for the change in atmospheric water vapour with temperature. Although some analyses of meteorological data have shown a similar scaling relationship, there are large uncertainties associated with the observations because of the limited temperature change that has occurred during the instrumental period and the short length of the reliable records. The palaeorecord provides an opportunity to determine whether the simulated scaling of precipitation with temperature is realistic, because it is possible to sample a larger range of climate change. I have shown (in Chapter 2: Li et al., 2013) that state-of-art climate models from CMIP5 produce a similar scaling in cold (LGM) and warm (increased CO₂) climates (global: 2.06%/°C, land: 1.75%/°C; ocean: 2.42%/°C). By comparing the LGM and 20th century simulations with palaeoclimate and instrumental observations, I have shown that the models can reproduce the large-scale patterns of precipitation scaling with temperature in a realistic way. The scaling of precipitation to temperature is 1-3%, which is the same range as changes in evaporation with temperature under equilibrium conditions. These analyses therefore indicate that energetic constraints on evaporation are the major reason why precipitation sensitivity to temperature is less than would be expected from the Clausius-Clapeyron relationship. The reduced sensitivity of precipitation to temperature over land compared to that over the ocean reflects an additional constraint imposed by moisture availability. Seasonal changes of tropical precipitation in a warmer world also reflect the constraint by moisture availability, or so called “rich get richer” syndrome (Trenberth, 2011) where wet climates become wetter and dry climates become drier. This pattern is robust between models and also between cold past (LGM) and warm future (abrupt4xCO₂) simulations.

Thus, my analyses (Chapter 2: Li et al., 2013) confirm that state-of-the-art climate models are able to simulate the large-scale (continental to hemispheric) changes in precipitation realistically, and indicate that we can have some confidence in future projections of large-scale precipitation changes. A similar conclusion was reached Izumi et al. (2013, 2015) in relation to large-scale temperature changes. They

showed that features such as the ratio of land-sea contrast or of high-latitude to low-latitude temperature changes were similar cold past (LGM) and warm future (abrupt4xCO₂) simulations, arose through similar energy-balance mechanisms in both climate states, and that the palaeoclimate changes were realistic (see also Chapter 4: Harrison et al., 2015). Thus, palaeoclimate analysis has confirmed that the broad-scale patterns of temperature and precipitation changes projected for the future are likely to be robust and realistic.

However, it is also important to evaluate whether state-of-the-art models are capable of simulating regional climate changes realistically. Previous generations of models (PMIP and PMIP2) had difficulty in simulating regional climates, such as the insolation-induced expansion of the northern African monsoon, changes in precipitation seasonality in the Mediterranean, and the extent of drying in mid-continental Eurasia during the MH. I have shown that these problems still exist in the latest generation of models (Chapter 3: Perez-Sanz et al., 2014, and Chapter 4: Harrison et al., 2015). The CMIP5 models simulate an enhancement of the monsoon in northern Africa in the MH, but fail to simulate the observed increase in magnitude or the spatial expansion (Chapter 3: Perez-Sanz et al., 2014). The discrepancy between observed and simulated changes in the amount of MH precipitation over northern Africa in the latitude band from 15°-30° N is at least 50% (Chapter 3: Perez-Sanz et al., 2014). Monsoon enhancement is a feature of future projections (Collins et al., 2013; Kirtmann et al., 2013). Although the ultimate cause is different (increased greenhouse gases rather than changes in insolation), the mechanism (enhanced land-sea contrast) is the same in these future simulations and in the MH simulations. Thus, the failure to simulate the magnitude and extent of the MH monsoon in northern Africa suggests that future changes in the monsoon may be seriously underestimated in the projections.

The mismatch between observed and simulated monsoon climates in the MH is one of magnitude; the mismatch between observed and simulated climate in mid-continental Eurasia (between 45° and 60° N) is one of sign (Chapter 4: Harrison et al., 2015). State-of-the-art climate models simulate increased aridity as a consequence of the increase in summer insolation, and the increased aridity leads in turn to an increase in summer temperatures in the simulations. In contrast, the observations show somewhat wetter conditions and cooler summers. Increased mid-continental aridity is a feature of the future projections, and again the fact that this is

unrealistic in the MH simulations suggests that this prediction should be viewed with caution.

I have shown that the failure to simulate the MH monsoon expansion in northern Africa is not a result of biases in the modern control simulation (Chapter 3: Perez-Sanz et al., 2014). However, the mismatch between simulated and observed climates in mid-continental Eurasia could be due to biases in the control simulation, specifically biases in evapotranspiration (see e.g. Mueller and Seneviratne, 2014). Whether the failure of state-of-the-art climate models to reproduce known regional climate changes is due to biases or not, it indicates that there is an urgent need to improve process-representation in these models.

Model-data disagreements are not only caused by problems in the models; they could also arise because the experimental design is inappropriate or because of poor data quality. In CMIP5/PMIP3 palaeoclimate simulations are simplified experiments: the LGM experiment is driven by changes in ice sheet extent and height, land-sea geography and changes in greenhouse gas concentrations, while the MH experiment is driven by orbital changes and a small change in greenhouse gas concentrations (Braconnot et al., 2012). In both experiments the non-ice covered land is prescribed to be the same as in the control pre-industrial simulation, which itself uses modern vegetation distributions. However, as reconstructions of past vegetation cover show, the distribution of vegetation was very different from today both at the LGM and during the MH (Prentice et al., 2000). The land-surface changes in northern Africa were particularly marked: this now desertic region was characterized by abundant large lakes and wetlands, and grass and shrubland vegetation (Hoelzmann et al., 1998; Elenga et al., 2000; Watrin et al., 2009; Lezine et al., 2011). Climate model simulations with prescribed changes in land-surface conditions over northern Africa produce a significant enhancement of the monsoon during the MH (e.g. Kutzbach et al., 1996; Claussen and Gaylor, 1997; Brostrom et al., 1998). Thus, the failure to include land-surface changes in the CMIP5/PMIP3 MH simulations could be one cause of the observed mismatch between the simulations and observations. However, the response of the monsoon to land-surface feedbacks in fully coupled models varies, and in many cases the amplification is still smaller than observed (Levis et al., 2004; Braconnot et al., 2007; Wang et al., 2008). Again, this indicates the need to improve process-representation in these models.

Another reason for disagreement between simulations and observations could be poor data quality. My evaluation of the regional climates of northern Africa (Chapter 3: Perez-Sanz et al., 2014) and mid-continental Eurasia (Chapter 4: Harrison et al., 2015) was based on quantitative climate reconstructions from Bartlein et al. (2011). The number of data points from both regions is limited. There are only 75 precipitation records from northern Africa, for example, and only 133 records of summer temperature for mid-continental Eurasia. Despite this, we have confidence that these records provide a reliable picture of the regional climate change because they are supported by a much larger number of qualitative records (see discussion in Chapter 4: Harrison et al., 2015). Thus, there is abundant evidence for wetter conditions in the Sahara during the MH, as shown by the presence of large lakes, shrubland vegetation, archaeological settlements and the presence of large, water-demanding animals (Hoelzmann et al., 1998; Elenga et al., 2000; Kuper and Kröpelin, 2006; Watrin et al., 2009). Similarly, lake and pollen evidence from mid-continental Eurasia confirm that it was wetter than today during the MH (Yu and Harrison, 1996; Harrison et al., 1996; Tarasov et al., 1998; Li and Morrill, 2010). Nevertheless, an increase in the number of quantitative reconstructions available from both regions would improve our ability to evaluate model simulations and could allow a better discrimination between models.

The Bartlein et al. (2011) reconstructions are based on a synthesis of all of the available reconstructions for each region. This involves combining statistically-based reconstructions and reconstructions obtained by model inversion. Although Bartlein et al. (2011) show that the results obtained using different methods are not significantly different, other studies have suggested that there may be significant differences between the reconstructions obtained by these two methods during glacial intervals of low CO₂ (see e.g. Brewer et al., 2008). Changes in CO₂ have a direct impact on plant growth through changing water-use efficiency (Prentice and Harrison, 2009), and statistically-based reconstructions cannot take this into account and hence will tend to overestimate the degree of aridity compared to model-inversion reconstructions. Given that the focus of model evaluations using LGM reconstructions has been on large-scale features, and not on regional climates in semi-arid regions where the water-use efficiency issue would be most crucial (see discussion in Chapter 7: Li et al., 2015b), partial reliance on statistical reconstructions in the current LGM benchmarking data

set is probably not an issue. However, it would be useful to re-examine this question and in particular to ensure that model-inversion techniques are more widely applied for palaeoclimate reconstruction.

One further source of uncertainty in data-model comparisons is the practice of using the preindustrial control simulation (pi Control) as the basis for calculating model anomalies. Thus simulated changes in the MH and LGM as expressed relative to the climate of ca 1850 CE. This poses problems in evaluating the control simulations because of the lack of reliable observations for the preindustrial period (~1850 AD). In Chapter 3 of this thesis (Perez-Sanz et al., 2014), we used modern day precipitation data to evaluate the simulation of pre-industrial precipitation regimes, on the assumption that the changes between 1850 CE and today were relatively small. A similar issue could affect the climate reconstructions. Pollen-based reconstructions generally use analogues drawn from the late half of the 20th century. Again, the assumption is that the difference between the climate of the preindustrial period and the last half of 20th century (in Bartlein et al. (2011) is 1961-1990) is relatively small, and certainly smaller than the simulated anomaly between the preindustrial control and either the MH or LGM. Nevertheless, it could be important to investigate the degree to which use of the pre-industrial as a baseline affects data-model comparisons. One possible way of doing this would be to run an equilibrium simulation for the modern period (e.g. 1961-1990) and thus quantify the impact of using the pre-industrial state as a baseline for data-model comparisons.

The LGM and MH are good targets for model evaluation, but the palaeorecord provides many other opportunities for evaluation. Two new palaeo-experiments will be included in the next phase of the Coupled Model Intercomparison Project (CMIP6): the Last Interglacial (LIG, ca 128,000 years ago) and the mid-Pliocene (ca 3.2M years ago). The LIG provides an opportunity to examine the response to orbital changes when the ice sheets were smaller and sea-level was between 5-10m higher than today (Masson-Delmotte et al., 2013). The mid-Pliocene provides an opportunity to examine model responses in an interval when CO₂ was somewhat higher than today (ca 400 ppm) (Haywood et al., 2010; Haywood et al., 2013). Both these experiments will provide opportunities for model evaluation.

Palaeo-evaluations have shown that state-of-art climate models from CMIP5 can simulate large scale climate patterns realistically, including the scaling of precipitation to temperature change (Li et al., 2013), and global/ or hemispheric long-term mean temperature and energy balance (Izumi et al., 2013 and 2015). These findings support the idea that model projections of large-scale temperature and precipitation changes are reliable. However, the underestimation of MH monsoon change in North Africa (Pérez Sanz et al., 2014), and overestimation of MH drought in the Eurasian midcontinent (Harrison et al., 2015), shows these models are poor at simulating regional climate changes realistically, casting doubt on the reliability of future projections of the monsoons and other circulation patterns.

In order to be able to examine how well state-of-the-art models simulate short-term (annual to decadal) climate variability, I have developed a model that simulates tree growth and hence ring widths (Chapter 5: Li et al., 2014). I have shown that the model works for three different tree species in three very different climate settings: *Pinus koraiensis* in the temperate and humid forests of the Changbai Mountains, China (Chapter 5: Li et al., 2014); the multi-stem gymnosperm *Callitris columellaris* in the warm and dry Great Western Woodland (GWW), Western Australia (Chapter 6: Li et al., 2015a); and *Juniperus occidentalis* in the cool montane forests in California, USA (Chapter 7: Li et al., 2015b). In all three sites, the PT model captures the mean magnitude and interannual variability in observed ring widths. The simulated ring width shows the same response as observed ring width to specific climate variables: a significant positive response to photosynthetically active radiation (PAR), soil moisture (α : actual to potential evapotranspiration) and air moisture (i.e. a negative response to vapour pressure deficit, VPD).

The PT model is a powerful tool to investigate climate and CO₂ impacts on tree growth under past and future climates. My model results have shown that changes in carbon allocation are an important response of tree growth to changing CO₂, and that this helps to explain why ring widths do not necessarily increase with increases in CO₂ (Chapter 6: Li et al., 2015a) and how trees survive in low CO₂ conditions (Chapter 7: Li et al., 2015b). My modelling results suggest that an increase in carbon allocation to the root system could explain why there is no response of radial growth to increasing CO₂ signal in recent decades in GWW (Chapter 6: Li et al., 2015a) and similarly in regions where CO₂ fertilisation appears to lead to increased water-use

efficiency but not increased radial growth (Andreu-Hayles et al., 2011; van der Sleen et al., 2015). My modelling results also suggest that decreased carbon allocation to the root system (~25%) under glacial conditions, when CO₂ was reduced to ca 180 ppm, would allow *Juniperus* trees to grow at rates similar to today (Chapter 7: Li et al., 2015b). My work suggests that changes in carbon allocation strategy could be an important response to changes in CO₂, both in the past and the present. Although I have not demonstrated changes in allocation at the GWW, and such information is not available for the LGM, the idea that carbon allocation changes in response to changes in CO₂ is supported by experimental evidence from Free-Air Carbon dioxide Enrichment (FACE) experiments. A significant increase in root biomass has been observed at FACE sites in different forest ecosystems around the world, e.g. Duke Forest FACE (Herrick and Thomas, 2001), AspenFACE (Karnosky et al., 2003), Oak Ridge National Laboratory (ORNL) FACE (Norby et al., 2002). These FACE results are consistent with the model results that increasing CO₂ would cause increasing carbon allocation to root.

The possibility that there might be changes in carbon allocation in response to changes in CO₂, and potentially to other environmental stressors such as nutrients limitation (see discussion in Chapter 7: Li et al., 2015b) is not normally taken into account when using tree-rings to make climate reconstructions – but may, for example, be an explanation for the divergence problem. The possibility that increases in CO₂ in the future would lead to increased productivity but not necessarily increased radial growth also has important implications for forestry management.

The PT model provides a robust tool which can be used to examine the impact of changes in short-term climate variability on tree growth. The P-T model simulates tree growth (and tree ring width) based on the first principles of photosynthesis and carbon allocation. The carbon allocation component of the model has only 13 parameters, most of which are specified using observed values from the literature. Parameter-tuning has been used in this thesis for some parameters that are less well-known (e.g. sapwood respiration rate and root parameters from some species) but the tuned values all fall within the range of published values from similar species or genera.

By running the model in forward mode, driven by climate model outputs, it will be possible to derive a simulated ring-width series that could be directly compared with

observed ring-width series at specific sites. This approach could be used to examine how well models can capture past changes in climate phenomena such as the North Atlantic Oscillation (NAO; see e.g. Gladstone et al., 2005) or the El Niño-Southern Oscillation (see e.g. Braconnot et al., 2012). Understanding how short-term variability is likely to change with changes in mean climate is a key gap in our current understanding of climate change (Meehl et al., 2000; Kirtman et al., 2013). The PT model is comparatively simple, and has only 13 free parameters (Chapter 4: Li et al., 2014). This opens up the possibility that it could be inverted to provide reconstructions of annual climate, reconstructions that are likely to be more robust than current tree-ring based reconstructions (see e.g. PAGES 2k Consortium, 2013) because they will account for the influence of multiple climate and environmental variables on tree growth.

Conventional climate reconstructions based on tree rings often allow conditions in previous years to influence growth in any given year (see e.g. Baker et al., 2008; Cullen and Grierson, 2009). Although this lag effect is established by statistical analysis, it reflects the fact that some carbon is stored as non-structural carbohydrates (NSC) and used for growth in the early part of the growing season when leaf area has not reached its optimum (Michelot et al., 2012; Rautiainen et al., 2012). The PT model also assumes that carbon is stored and used in subsequent years, and statistical methods are used to determine the optimal period of storage. In the Changbai application, carbon fixed last half of the previous growing season contributed to growth in the following year (Chapter 5: Li et al., 2014). In the drought-limited areas of GWW (Chapter 6: Li et al., 2015a) and La Brea (Chapter 7: Li et al., 2015b), an interval of 2 years was found to provide the best match between simulated GPP and observed growth and so was used as the effective carbon accumulation period. It would be useful to model the accumulation of NSC explicitly in order to avoid the necessity for this statistical optimization. However, this would require a better understanding of the temporal dynamics of NSC pools (Richardson et al., 2013) and the controls on NSC formation and use (Simard et al., 2013).

Stable isotopes (e.g. ^{13}C and ^{18}O) provide information about changes in water-use efficiency (Farquhar and Richards, 1984; Ehleringer and Dawson, 1992; Prentice et al., 2011; Prentice et al., 2014) and hence can provide an additional constraint in modelling tree growth responses to climate change. The MAIDENiso model (Danis et

al., 2012) explicitly simulates both ^{13}C and ^{18}O . Stable isotopes are also used to reconstruct climate, particularly hydroclimate, from tree rings (Anderson et al., 1998; Barber et al., 2004; Cullen and Grierson, 2007) and there is an abundance of long-term isotopic records available. A future goal for development of the PT model is to include explicit simulation of ^{13}C and ^{18}O , both because it will provide a wider range of targets for climate-model evaluation using forward modelling and because it will facilitate inversion of the model to produce climate reconstructions by increasing the number of constraints.

In my thesis, I have demonstrated the usefulness of palaeo-evaluation to measure the reliability (or otherwise) of climate models in simulating mean climate changes, provided a model-based framework for evaluating short-term climate variability through developing the PT model, applied the PT model to simulate tree growth in both the modern and palaeo climates, and analysed the CO_2 effect on tree growth and carbon allocation. The methods and tools that I have developed will be useful for the evaluation of palaeoclimate simulations in CMIP6.

References

- Anderson, W. T., Bernasconi, S. M., McKenzie, J. A., and Saurer, M.: Oxygen and carbon isotopic record of climatic variability in tree ring cellulose (*Picea abies*): an example from central Switzerland (1913–1995), *Journal of Geophysical Research: Atmospheres*, 103, 31625–31636, 1998.
- Andreu-Hayles, L., Planells, O., Gutierrez, E., Muntan, E., Helle, G., Anchukaitis, K. J., and Schleser, G. H.: Long tree-ring chronologies reveal 20th century increases in water-use efficiency but no enhancement of tree growth at five Iberian pine forests, *Global Change Biology*, 17, 2095–2112, 2011.
- Baker, P. J., Palmer, J. G., and D'Arrigo, R.: The dendrochronology of *Callitris intratropica* in northern Australia: annual ring structure, chronology development and climate correlations, *Australian Journal of Botany*, 56, 311–320, 2008.
- Barber, V. A., Juday, G. P., Finney, B. P., and Wilmking, M.: Reconstruction of summer temperatures in interior Alaska from tree-ring proxies: evidence for changing synoptic climate regimes, *Climatic Change*, 63, 91–120, 2004.
- Bartlein, P. J., Harrison, S. P., Brewer, S., Connor, S., Davis, B. A. S., Gajewski, K., Guiot, J., Harrison-Prentice, T. I., Henderson, A., Peyron, O., Prentice, I. C., Scholze, M.,

- Seppä, H., Shuman, B., Sugita, S., Thompson, R. S., Viau, A. E., Williams, J., and Wu, H.: Pollen-based continental climate reconstructions at 6 and 21 ka: a global synthesis, *Climate Dynamics*, 37, 775-802, 2011.
- Braconnot, P., Harrison, S. P., Kageyama, M., Bartlein, P. J., Masson-Delmotte, V., Abe-Ouchi, A., Otto-Bliesner, B., and Zhao, Y.: Evaluation of climate models using palaeo-climatic data, *Nature Climate Change*, 2, 417-424, 2012.
- Brewer, S., Guiot, J., Sánchez-Gómez, M., and Klotz, S.: The climate in Europe during the Eemian: a multi-method approach using pollen data, *Quaternary Science Reviews*, 27, 2303-2315, 2008.
- Collins, M., Knutti, R., Arblaster, J., Dufresne, J. L., Fichet, T., Friedlingstein, P., Gao, X., Gutowski, W. J., Johns, T., Krinner, G., Shongwe, M., Tebaldi, C., Weaver, A. J., and Wehner, M.: Long-term climate change: Projections, commitments and irreversibility, in: *Climate Change 2013: The Physical Science Basis. Contribution of Working Group I to the Fifth Assessment Report of the Intergovernmental Panel on Climate Change*, edited by: Stocker, T. F., Qin, D., Plattner, G. K., Tignor, M., Allen, S. K., Boschung, J., Nauels, A., Xia, Y., Bex, V., and Midgley, P. M., Cambridge University Press, Cambridge, United Kingdom and New York, NY, USA., 2013.
- Cullen, L. E., and Grierson, P. F.: A stable oxygen, but not carbon, isotope chronology of *Callitris columellaris* reflects recent climate change in north-western Australia, *Climatic Change*, 85, 213-229, 2007.
- Cullen, L. E., and Grierson, P. F.: Multi-decadal scale variability in autumn-winter rainfall in south-western Australia since 1655 AD as reconstructed from tree rings of *Callitris columellaris*, *Climate Dynamics*, 33, 433-444, 2009.
- Ehleringer, J. R., and Dawson, T. E.: Water uptake by plants: perspectives from stable isotope composition, *Plant, Cell & Environment*, 15, 1073-1082, 1992.
- Elenga, H., Peyron, O., Bonnefille, R., Jolly, D., Cheddadi, R., Guiot, J., Andrieu, V., Bottema, S., Buchet, G., and De Beaulieu, J. L.: Pollen-based biome reconstruction for southern Europe and Africa 18,000 yr bp, *Journal of Biogeography*, 27, 621-634, 2000.
- Farquhar, G. D., and Richards, R. A.: Isotopic composition of plant carbon correlates with water-use efficiency of wheat genotypes, *Functional Plant Biology*, 11, 539-552, 1984.
- Gladstone, R. M., Ross, I., Valdes, P. J., Abe-Ouchi, A., Braconnot, P., Brewer, S., Kageyama, M., Kitoh, A., Legrande, A., and Marti, O.: Mid-Holocene NAO: A PMIP2 model intercomparison, *Geophysical Research Letters*, 32, 2005.

- Harrison, S. P., Bartlein, P. J., Izumi, K., Li, G., Annan, J., Hargreaves, J., Braconnot, P., and Kageyama, M.: Implications of evaluation of CMIP5/PMIP3 palaeosimulations for climate projections, *Nature Climate Change*, (in press), August 2015.
- Harrison, S. P., Yu, G., and Tarasov, P. E.: Late Quaternary lake-level record from northern Eurasia, *Quaternary Research*, 45, 138-159, 1996.
- Haywood, A., Dowsett, H., Otto-Bliesner, B., Chandler, M., Dolan, A., Hill, D., Lunt, D., Robinson, M., Rosenbloom, N., and Salzmann, U.: Pliocene Model Intercomparison Project (PlioMIP): experimental design and boundary conditions (experiment 1), *Geoscientific Model Development*, 3, 227-242, 2010.
- Haywood, A. M., Hill, D. J., Dolan, A. M., Otto-Bliesner, B. L., Bragg, F., Chan, W., Chandler, M. A., Contoux, C., Dowsett, H. J., and Jost, A.: Large-scale features of Pliocene climate: results from the Pliocene Model Intercomparison Project, *Climate of the Past*, 9, 191-209, 2013.
- Herrick, J. D., and Thomas, R. B.: No photosynthetic down-regulation in sweetgum trees (*Liquidambar styraciflua* L.) after three years of CO₂ enrichment at the Duke Forest FACE experiment, *Plant, Cell & Environment*, 24, 53-64, 2001.
- Hoelzmann, P. H., Jolly, D., Harrison, S. P., Laarif, F., Bonnefille, R., and Pachur, H. J.: Mid-Holocene land-surface conditions in northern Africa and the Arabian Peninsula: A data set for the analysis of biogeophysical feedbacks in the climate system, *Global Biogeochemical Cycles*, 12, 35-51, 1998.
- Izumi, K., Bartlein, P. J., and Harrison, S. P.: Consistent large-scale temperature responses in warm and cold climates, *Geophysical Research Letters*, 40, 1817-1823, 2013.
- Izumi, K., Bartlein, P. J., and Harrison, S. P.: Energy-balance mechanisms underlying consistent large-scale temperature responses in warm and cold climates, *Climate Dynamics*, 44, 3111-3127, 2015.
- Karnosky, D. F., Zak, D. R., Pregitzer, K. S., Awmack, C. S., Bockheim, J. G., Dickson, R. E., Hendrey, G. R., Host, G. E., King, J. S., and Kopper, B. J.: Tropospheric O₃ moderates responses of temperate hardwood forests to elevated CO₂: a synthesis of molecular to ecosystem results from the Aspen FACE project, *Functional Ecology*, 17, 289-304, 2003.
- Kirtman, B., Power, S. B., Adedoyin, J. A., Boer, G. J., Bojariu, R., Camilloni, I., Doblas-Reyes, F. J., Fiore, A. M., Kimoto, M., and Meehl, G. A.: Near-term climate change: Projections and predictability, in: *Climate Change 2013: The Physical Science Basis. Contribution of Working Group I to the Fifth Assessment Report of the Intergovernmental Panel on Climate Change*, edited by: Stocker, T. F., Qin, D., Plattner, G.-K.,

- Tignor, M., Allen, S. K., Boschung, J., Nauels, A., Xia, Y., Bex, V., and Midgley, P. M., Cambridge University Press, Cambridge, UK, and New York, 953-1028, 2013.
- Kuper, R., and Kröpelin, S.: Climate-controlled Holocene occupation in the Sahara: motor of Africa's evolution, *Science*, 313, 803-807, 2006.
- Li, G., Harrison, S., Prentice, I., and Falster, D.: Simulation of tree-ring widths with a model for primary production, carbon allocation, and growth, *Biogeosciences*, 11, 6711-6724, 2014.
- Li, G., Harrison, S. P., Bartlein, P. J., Izumi, K., and Prentice, I. C.: Precipitation scaling with temperature in warm and cold climates: An analysis of CMIP5 simulations, *Geophysical Research Letters*, 40, 4018-4024, 2013.
- Li, G., Harrison, S. P., and Prentice, I. C.: A model analysis of climate and CO₂ controls on tree growth in a semi-arid woodland, *Biogeosciences Discussions*, 12, 4769-4800, 2015a.
- Li, G., Gerhart, L. M., Harrison, S. P., Ward, J., and Prentice, I. C.: Allocation changes buffer CO₂ effect on tree growth since the last ice age, *Nature Communication*, (submitted), 2015b.
- Li, Y., and Morrill, C.: Multiple factors causing Holocene lake-level change in monsoonal and arid central Asia as identified by model experiments, *Climate Dynamics*, 35, 1119-1132, 2010.
- Masson-Delmotte, V., Schulz, M., Abe-Ouchi, A., Beer, J., Ganopolski, A., Rouco, J. F. G., Jansen, E., Lambeck, K., Luterbacher, J., Naish, T., Osborn, T., Otto-Bliesner, B., Quinn, T., Ramesh, R., Rojas, M., Shao, X., and Timmermann, A.: Information from Paleoclimate Archives, in: *Climate Change 2013: The Physical Science Basis. Contribution of Working Group I to the Fifth Assessment Report of the Intergovernmental Panel on Climate Change*, edited by: Stocker, T. F., Qin, D., Plattner, G.-K., Tignor, M., Allen, S. K., Boschung, J., Nauels, A., Xia, Y., Bex, V., and Midgley, P. M., Cambridge University Press, Cambridge University Press, Cambridge, United Kingdom and New York, NY, USA, 2013.
- Meehl, G. A., Zwiers, F., Evans, J., Knutson, T., Mearns, L., and Whetton, P.: Trends in extreme weather and climate events: Issues related to modeling extremes in projections of future climate change, *Bulletin of the American Meteorological Society*, 81, 427-436, 2000.
- Michelot, A., Simard, S., Rathgeber, C., Dufrêne, E., and Damesin, C.: Comparing the intra-annual wood formation of three European species (*Fagus sylvatica*, *Quercus petraea* and *Pinus sylvestris*) as related to leaf phenology and non-structural carbohydrate dynamics, *Tree Physiology*, 32, 1033-1045, 2012.

- Mueller, B., and Seneviratne, S. I.: Systematic land climate and evapotranspiration biases in CMIP5 simulations, *Geophysical Research Letters*, 41, 128-134, 2014.
- Norby, R. J., Hanson, P. J., O'Neill, E. G., Tschaplinski, T. J., Weltzin, J. F., Hansen, R. A., Cheng, W., Wullschleger, S. D., Gunderson, C. A., and Edwards, N. T.: Net primary productivity of a CO₂-enriched deciduous forest and the implications for carbon storage, *Ecological Applications*, 12, 1261-1266, 2002.
- PAGES 2k Consortium: Continental-scale temperature variability during the past two millennia, *Nature Geoscience*, 6, 339-346, 2013.
- Pérez Sanz, A., Li, G., González-Sampériz, P., and Harrison, S. P.: Evaluation of modern and mid-Holocene seasonal precipitation of the Mediterranean and northern Africa in the CMIP5 simulations, *Climate of the Past*, 10, 551-568, 2014.
- Prentice, I.C., Meng, T., Wang, H., Harrison, S.P., Ni, J., Wang, G. : Evidence for a universal scaling relationship of leaf CO₂ drawdown along a moisture gradient, *New Phytologist*, 190, 169–180, 2011.
- Prentice, I. C., Dong, N., Gleason, S. M., Maire, V., and Wright, I. J.: Balancing the costs of carbon gain and water transport: testing a new theoretical framework for plant functional ecology, *Ecology Letters*, 17, 82-91, 2014.
- Prentice, I. C., and Harrison, S. P.: Ecosystem effects of CO₂ concentration: evidence from past climates, *Climate of the Past*, 5, 297-307, 2009.
- Prentice, I.C., Jolly D. and BIOME 6000 participants: Mid-Holocene and glacial-maximum vegetation geography of the northern continents and Africa, *Journal of Biogeography* 27, 507-519, 2000
- Rautiainen, M., Heiskanen, J., and Korhonen, L.: Seasonal changes in canopy leaf area index and MODIS vegetation products for a boreal forest site in central Finland, *Boreal Environment Research*, 17, 71-84, 2012.
- Richardson, A. D., Carbone, M. S., Keenan, T. F., Czimczik, C. I., Hollinger, D. Y., Murakami, P., Schaberg, P. G., and Xu, X.: Seasonal dynamics and age of stemwood nonstructural carbohydrates in temperate forest trees, *New Phytologist*, 197, 850-861, 2013.
- Simard, S., Giovannelli, A., Treydte, K., Traversi, M. L., King, G. M., Frank, D., and Fonti, P.: Intra-annual dynamics of non-structural carbohydrates in the cambium of mature conifer trees reflects radial growth demands, *Tree Physiology*, 33, 913-923, 2013.
- Tarasov, P. E., Webb III, T., Andreev, A. A., Afanas'eva, N. B., Berezina, N. A., Bezusko, L. G., Blyakharchuk, T. A., Bolikhovskaya, N. S., Cheddadi, R., and Chernavskaya, M. M.: Present-day and mid-Holocene biomes reconstructed from pollen and plant macro-

- fossil data from the former Soviet Union and Mongolia, *Journal of Biogeography*, 1029-1053, 1998.
- Trenberth, K. E.: Changes in precipitation with climate change, *Climate Research*, 47, 123, 2011.
- van der Sleen, P., Groenendijk, P., Vlam, M., Anten, N. P., Boom, A., Bongers, F., Pons, T. L., Terburg, G., and Zuidema, P. A.: No growth stimulation of tropical trees by 150 years of CO₂ fertilization but water-use efficiency increased, *Nature Geoscience*, 8, 24-28, 2015.
- Watrin, J., Lézine, A.-M., and Hély, C.: Plant migration and plant communities at the time of the “green Sahara”, *Comptes Rendus Geoscience*, 341, 656-670, 2009.
- Yu, G., and Harrison, S. P.: An evaluation of the simulated water balance of Eurasia and northern Africa at 6000 y BP using lake status data, *Climate Dynamics*, 12, 723-735, 1996.